THE UNIVERSITY OF QUEENSLAND

AUSTRALIA

The Cellular and Molecular Mechanisms of Axonal Maintenance and Regeneration

Sean Coakley

BSc (Hons)

A thesis submitted for the degree of Doctor of Philosophy at

The University of Queensland in 2014

Queensland Brain Institute

Abstract

How a neuron responds to and withstands injury is a central question in neurobiology. Neuronal injury can be caused mechanically with force, chemically with toxic insults, or genetically with mutations in genes that lead to damage. The axon, the neuron's longest compartment, is often the focal point of degeneration due to traumatic injury, toxic insults, or neurodegenerative diseases. Damage to the axon can have drastic functional consequences for the organism. In some cases axonal injury can lead to death of the neuron, while in others repair mechanisms are triggered that promote regeneration of the injured axon. Important discoveries during the last decade have uncovered many components of the molecular machinery that regulate axonal degeneration and regeneration. However, the precise ways in which these pathways converge and respond to different insults remains largely unknown. Here, using the nematode *Caenorhabditis elegans* as an experimental model system, we present important discoveries outlining the cellular and molecular mechanisms underpinning axonal maintenance and regeneration. Using forward and reverse genetic approaches, combined with optogenetic, genetic, and laser-injury tools, we identify critical components of these biological processes. We demonstrate how genes functioning during axon development also have roles in mature axons, regulating both degeneration and regeneration. Firstly, we discover a role for MEC-7/β-tubulin in regulating both axon development and regeneration. Second, we develop and characterize an optogenetic method to induce cell ablation and neurodegeneration using the genetically encoded photosensitizer KillerRed. Third, we identify novel mutants with defects in axonal maintenance and describe a new phenomenon of neuronal fusion following genetically induced damage. Finally, we demonstrate a role for conserved components of the apoptotic machinery in the recognition of damaged neurons during regeneration. These findings both extend our understanding of the molecular mechanisms of axonal degeneration and regeneration, as well as provide new paradigms in which these processes can be investigated.

Declaration by author

This thesis is composed of my original work, and contains no material previously published or written by another person except where due reference has been made in the text. I have clearly stated the contribution by others to jointly-authored works that I have included in my thesis.

I have clearly stated the contribution of others to my thesis as a whole, including statistical assistance, survey design, data analysis, significant technical procedures, professional editorial advice, and any other original research work used or reported in my thesis. The content of my thesis is the result of work I have carried out since the commencement of my research higher degree candidature and does not include a substantial part of work that has been submitted to qualify for the award of any other degree or diploma in any university or other tertiary institution. I have clearly stated which parts of my thesis, if any, have been submitted to qualify for another award.

I acknowledge that an electronic copy of my thesis must be lodged with the University Library and, subject to the General Award Rules of The University of Queensland, immediately made available for research and study in accordance with the *Copyright Act 1968*.

I acknowledge that copyright of all material contained in my thesis resides with the copyright holder(s) of that material. Where appropriate I have obtained copyright permission from the copyright holder to reproduce material in this thesis.

Publications during candidature

Refereed research publications

Williams, D.C.*, El Bejjani, R.*, Mugno Ramirez, P.*, Coakley, S.* , Kim, S.A., Lee, H., Wen, Q., Samuel, A., Lu, H., Hilliard, M.A. and Hammarlund, M. (2013) Rapid and permanent neuronal inactivation in vivo via subcellular generation of reactive oxygen with the use of KillerRed. *Cell Reports 5*, 552-563.

*These authors contributed equally.

Kirszenblat, L., Neumann, B., Coakley, S. and Hilliard M.A. (2012) A dominant mutation in *mec-7/β-tubulin* affects axon development and regeneration in *Caenorhabditis elegans* neurons. *Mol Biol Cell 24*, 285-96.

Conference abstracts

Presenting author:

Coakley, S., Neumann, B., Yang, H., Xue, D. and Hilliard, M.A. Neuronal fusion induced by *unc-70/β-spectrin* dependent axonal injury requires components important for clearance of apoptotic cells. International *C. elegans* Meeting, Los Angeles, June 2013 (Poster).

Coakley, S. and Hilliard, M.A. Axonal looping: a gateway to study axonal fusion during regeneration. EMBO Conference Series *C. elegans* Neurobiology, Heidelberg, June 2012 (Talk).

Coakley, S. and Hilliard M.A. Exploring alternative means to induce axonal injury in *C. elegans* neurons. International *C. elegans* Meeting, Los Angeles, June 2011 (Poster).

Co-author:

Neumann, B., **Coakley, S.**, Giordano-Santini, R., Linton, C., Zhang, Y., Yang, H., Xue, D. and Hilliard, M.A. Axonal fusion in regenerating axons shares molecular components with the apoptotic cell recognition pathway. Australasian Neuroscience Society meeting, Adelaide, January 2014 (Poster).

Neumann, B., **Coakley, S.**, Giordano-Santini, R., Linton, C., Zhang, Y., Yang, H., Xue, D. and Hilliard, M.A. Axonal fusion in regenerating axons shares molecular components with the apoptotic cell recognition pathway. EMBO Workshop on Cell-Cell Fusion, Ein Gedi, November, 2013 (Talk)

Neumann, B., **Coakley, S.**, Yang, H., Xue, D. and Hilliard, M.A. Axonal fusion in regenerating axons shares molecular components with the apoptotic cell recognition pathway. International *C. elegans* Meeting, Los Angeles, June 2013 (Talk).

Publications included in this thesis

Section 2.2

Kirszenblat, L., Neumann, B., Coakley, S. and Hilliard M.A. (2012) A dominant mutation in *mec-7/β-tubulin* affects axon development and regeneration in *Caenorhabditis elegans* neurons. *Mol Biol Cell 24*, 285-96.

Contributor	Statement of contribution
Leonie Kirszenblat	Conceived and designed experiments (40%) Wrote paper (50%) Performed experiments (50%)
Brent Neumann	Conceived and designed experiments (10%) Wrote paper (10%) Performed experiments (25%)
Sean Coakley (Candidate)	Conceived and designed experiments (10%) Wrote paper (10%) Performed experiments (25%)
Massimo A. Hilliard	Conceived and designed experiments (40%) Wrote paper (30%)

Section 3.2

Williams, D.C.*, El Bejjani, R.*, Mugno Ramirez, P.*, Coakley, S.* , Kim, SA., Lee, H., Wen, Q., Samuel, A., Lu, H., Hilliard, M.A. and Hammarlund, M. (2013) Rapid and permanent neuronal inactivation in vivo via subcellular generation of reactive oxygen with the use of KillerRed. *Cell Reports 5*, 552-563.

*These authors contributed equally.

Contributor	Statement of contribution
Daniel C. Williams	Conceived and designed experiments (5%) Performed experiments (20%)
Rachid El Bejjani	Conceived and designed experiments (5%) Wrote paper (15%) Performed experiments (20%)
Paula Mugno Ramirez	Conceived and designed experiments (5%) Wrote paper (15%) Performed experiments (20%)
Sean Coakley (Candidate)	Conceived and designed experiments (5%) Wrote paper (15%) Performed experiments (20%)
Shinae A Kim	Conceived and designed experiments (5%) Performed experiments (7.5%)
Hyewon Lee	Conceived and designed experiments (5%) Performed experiments (7.5%)
Quan Wen	Conceived and designed experiments (5%) Performed experiments (5%)
Aravi Samuel	Conceived and designed experiments (10%)
Hang Lu	Conceived and designed experiments (15%) Wrote paper (20%)
Massimo A. Hilliard	Conceived and designed experiments (20%) Wrote paper (20%)
Marc Hammarlund	Conceived and designed experiments (20%) Wrote paper (20%)

Contributions by others to the thesis

In addition to the contributions listed for publications included in this thesis, work contained in chapters 4 and 5 will be published with multiple authors and includes key contributions from others.

Section 4.2

The work presented in this section will be published with the candidate Sean Coakley as the first author. The candidate conceived and designed the experiments, wrote the manuscript and performed the experiments. Alessandra Donato and Paula Mugno Ramirez assisted with designing and performing the experiments. Shinae Kim and Hyewon Lee performed all experiments using selective illumination. Hang Lu and Massimo Hilliard conceived and designed experiments and wrote the manuscript.

Section 5.2

The work presented in this section will be published with Dr. Brent Neumann as the first author. Dr. Neumann conceived and designed experiments, performed experiments and wrote the manuscript. The candidate Sean Coakley conceived and designed experiments, performed experiments and wrote the manuscript. Dr. Rosina Giordano-Santini conceived and designed experiments, performed experiments and wrote the manuscript. Casey Linton performed experiments. Yi Zhang, Hengwen Yang, and Ding Xue provided strains and reagents. Massimo A. Hilliard conceived and designed experiments and wrote the manuscript.

Statement of parts of the thesis submitted to qualify for the award of another degree

None.

Acknowledgements

I would like to firstly acknowledge the guidance and support of my PhD supervisor Dr. Massimo Hilliard. Throughout my candidature you have been a fantastic mentor. You have given me incredible opportunities and offered me valuable advice along the way that I will cherish forever. Thank you for the trust, loyalty and care you have shown me.

I would like to thank the past and present members of the Hilliard laboratory for making every day of my candidature such fun: Annika Nichols, Rhianna Knable, Leonie Kirszenblat, Divya Pattabiraman, Dr. Nick Valmas, Paula Mugno Ramirez, Casey Linton, Justin Chaplin, Alessandra Donato, Fiona Ritchie, Dr. Rosina Giordano-Santini, Dr. Ellen Meelkop and Dr. Brent Neumann. Your intelligence, energy, humour and work ethic provided the perfect environment for me to work.

I would like to thank my associate supervisor Dr. Sean Millard for support and feedback during my candidature, Rowan Tweedale for invaluable feedback with manuscripts and my thesis, Luke Hammond and Daniel Matthews for microscopy support, Judy Bracefield and Donna Martin for their support and kinds words, Maria Caldeira and Janette Zlamal for keeping my worms happy, as well as the QBI students (especially Oressia Zalucki and Simmy Poonian) for their support and perseverance.
I also would like to acknowledge the scientists whose laboratories I have been fortunate enough to collaborate with during my candidature: Marc Hammarlund (Yale University), Hang Lu (Georgia Institute of Technology), Aravi Samuel (Harvard University) and Ding Xue (University of Colorado).

To my family, thank you for your love and support and for always being there when I need you.
To my friends, thank you for your encouragement, distraction, food and beer.

Claudia, we did it! Thank you. You are still the best discovery I have made in a lab.

Keywords

axonal degeneration, axonal regeneration, axonal fusion, reactive oxygen species, apoptosis, KillerRed, Wallerian degeneration, optogenetic.

Australian and New Zealand Standard Research Classifications (ANZSRC)

110902: Cellular Nervous System (100%)

Fields of Research (FoR) Classification

1109: Neurosciences (100%)

Table of contents

List of figures

List of tables

List of abbreviations used

ALS	amyotrophic lateral sclerosis
DNA	deoxyribonucleic acid
GABA	gamma-aminobutyric acid
GFP	green fluorescent protein
JNK	c-Jun N-terminal kinase
Wld^S	wallerian degeneration slow
MAP3K	mitogen-activated protein triple kinase
MAPK	mitogen-activated protein kinase
MS	multiple sclerosis
PNS	peripheral nervous system
PS	phosphatidylserine
RFP	red fluorescent protein
RNA	ribonucleic acid
ROS	reactive oxygen species
WT	wild-type

Chapter 1:
Literature review

1.1 Axonal injury – finding the balance between destruction and repair

Abstract

Maintenance of neuronal circuitry is critical for the preservation of correct neuronal function. Injury to the axon can trigger degeneration of this neuronal compartment as well as, in some cases, the initiation of axonal regeneration. A balancing act between these two seemingly opposite biological events can be critical for the rescue of the disrupted neuronal circuit. Axonal degeneration is a key pathological hallmark of nearly all neurodegenerative conditions; however the molecular mechanisms underlying axonal degeneration remain poorly understood. In contrast to degenerative mechanisms, axonal regeneration represents the quickest and most efficient means of re-establishing neuronal circuitry following injury to the axon. Evidence suggests that specific molecular mechanisms regulate both these processes, and that competency for either is determined by a variety of intrinsic and extrinsic factors that decline with age. Studies in vertebrates have suggested that axonal degeneration following injury is required for efficient regeneration. We outline what is currently understood about each of these processes and discuss recent observations from invertebrate studies where declining capacities for both degeneration and regeneration coincide to facilitate rapid reconnection of damaged nerves.

Introduction

Connectivity of neural networks is fundamental for the correct functioning of the nervous system. The integrity of the axon, the primary efferent signalling component of every neuron, is essential to maintain circuitry. Disruption of these connections can have catastrophic consequences for the organism. This can occur as a result of vascular accidents, physical traumas, toxic insults, and neurodegenerative conditions. Axons are also removed as part of normal development through axonal pruning. A large body of knowledge has come from the study of axonal degeneration following physical transection, due to the commonality of axonal degeneration from multiple injury models and the underlying shared molecular machinery (Coleman, 2005). Injury that results in transection of the axon splits the neuron into two distinct compartments: a distal axonal fragment that is separated from the neuronal cell body, and a proximal axonal fragment that remains connected with the soma (Figure 1.1a). Following separation from the cell body the distal axonal fragment undergoes a stereotypical process of degeneration classically referred to as Wallerian degeneration (Figure 1.1b), characterized by a thinning and beading of the axonal process, followed

by fragmentation and clearance of axonal debris (Waller, 1850). A complementary process of regeneration occurs in the proximal axonal fragment that is still connected to the neuronal cell body, whereby a growth cone forms at the distal tip of the axonal stump and regrows towards its distal target (Figure 1.1c).

The events that take place in both the distal and proximal axonal fragments are now understood to be active mechanisms that require the exquisite coordination of intrinsic and extrinsic mechanisms. Here we will outline and highlight some of the critical components of these distinct processes and the cell-intrinsic pathways that are activated in response to axonal injury. We will give a special focus to recent evidence that suggests it is possible to reverse degeneration of the distal axonal compartment by inducing reconnection of the regrowing proximal fragment during regeneration.

Initial neuronal response to axonal injury

Ca^{2+} influx is critical for injury signalling in both degenerative and regenerative responses (Kerschensteiner et al., 2005; Knoferle et al., 2010; Ziv and Spira, 1995). In the distal fragment the degeneration-promoting effect of Ca^{2+} is dependent upon calpain proteases and acts to initiate cytoskeletal breakdown (Billger et al., 1988; Johnson et al., 1991). Preventing either Ca^{2+} influx or activation of calpain proteases is sufficient to protect axons from degeneration (Coleman, 2005). An increase in intracellular Ca^{2+} levels has been shown to promote regeneration in a variety of systems (Bhatt et al., 2004; Ghosh-Roy et al., 2010; Neumann et al., 2002; Pichichero et al., 1973; Ziv and Spira, 1995). This is thought to be the result of a combination of Ca^{2+} influx through the site of injury, the activation of voltage-gated calcium channels, as well as release via intracellular stores (Knoferle et al., 2010; Kulbatski et al., 2004; Ziv and Spira, 1993). Increased intracellular Ca^{2+} has been demonstrated to activate cAMP signalling to promote regeneration (Bhatt et al., 2004; Ghosh-Roy et al., 2010; Neumann et al., 2002). In *C. elegans* this occurs via adenylyl cyclase in a protein kinase A-dependent manner (Ghosh-Roy et al., 2010). Importantly, in these experiments, it was total $[Ca^{2+}]$ that determined the regenerative response and not the magnitude of the transient. This raises the possibility that the type of injury to the axon and the amount of Ca^{2+} influx triggered by it may be determining factors in regeneration. Similarly the excitability of the neuron is able to modulate the regenerative response in a Ca^{2+}-dependent manner. It has been observed in invertebrate neurons that regenerative ability is affected by mutations in neurotransmitter-synthesizing enzymes, neurotransmitter receptors, and ion channels, all of which are components that alter the excitability of the neuron (Chen et al., 2011). A higher excitability

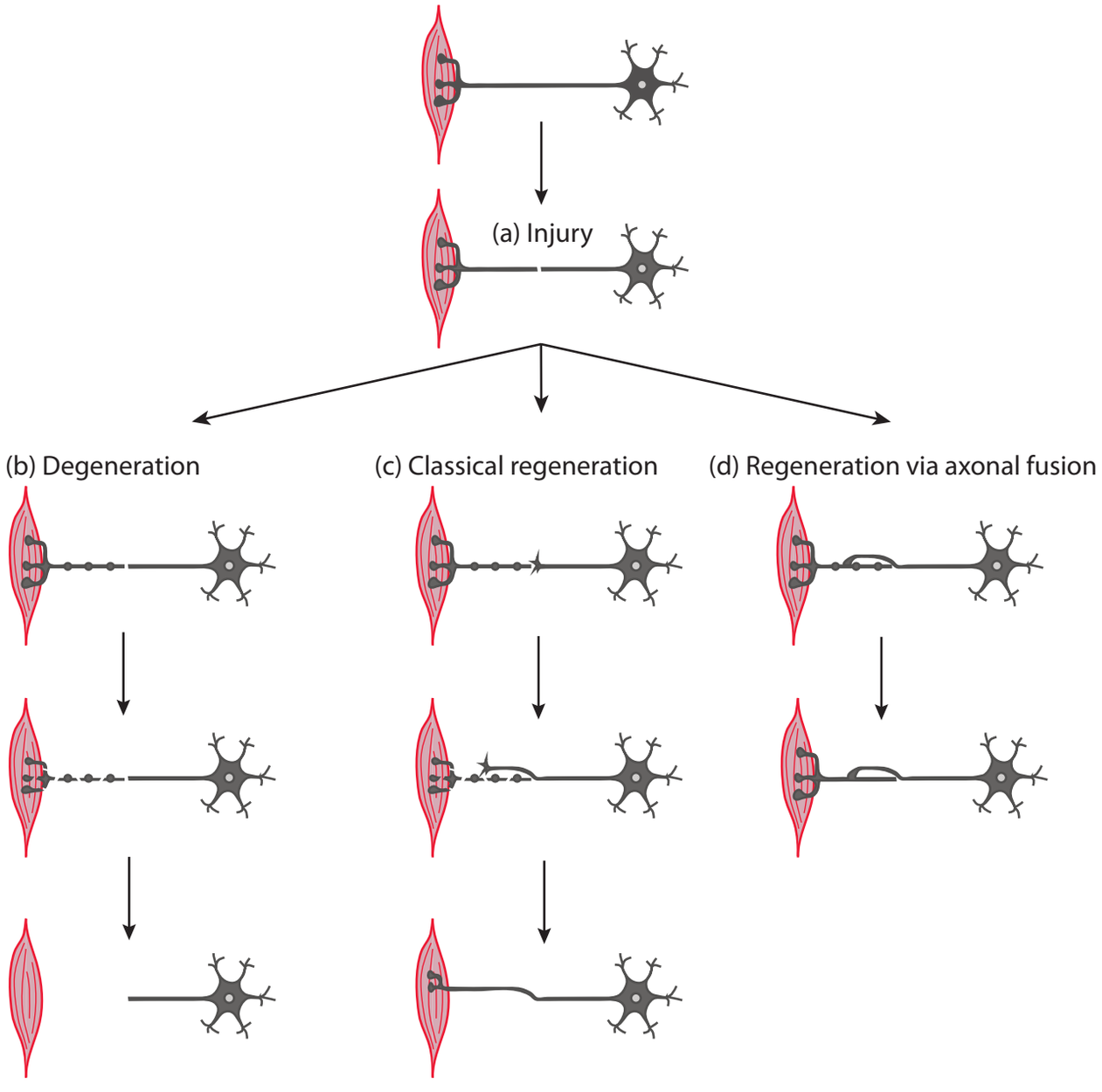

Figure 1.1. Axonal injury triggers axonal degeneration and regeneration pathways. A schematic diagram depicting a neuron connected to its distal target. Axonal injury can trigger both degenerative and regenerative pathways. **a**, injury to the axon that results in transection splits the axon into two compartments, a proximal fragment that is still connected to the cell body, and a distal fragment that is disconnected from the cell body. **b**, the distal axonal fragment undergoes stereotypical Wallerian degeneration characterized by beading, thinning, and clearance. **c**, in parallel with degeneration of the distal axonal fragment, injury can trigger regeneration of the proximal fragment. Classically this proceeds via the generation of a growth cone from the proximal axonal fragment, followed by extension and regrowth which can directly, or indirectly, re-innervate the distal target tissue. **d**, invertebrate neurons are capable of rapidly re-establishing neuronal circuitry via axonal fusion. The proximal axonal fragment generates a growth cone, which extends towards the distal axonal fragment and is able to reconnect and re-establish membrane and cytoplasmic continuity.

results in a better regenerative response, whereas the opposite is true for a neuron with decreased excitability. Taken together, these findings demonstrate that Ca^{2+} is a critical early injury signal that acts to promote axonal degeneration and regeneration in the respective axonal compartments following axonal damage. Once triggered, these specific programs coordinate the destruction and removal of the separated distal axonal fragment and the remodelling of the proximal axonal fragment into a regrowing axon.

Degeneration of the distal axonal compartment: an active process

Discovery of Wlds, Sarm, and DLK

The initial debate surrounding the active or passive nature of axonal degeneration was mostly settled with the discovery and isolation of the Wallerian degeneration slow mutant (*Wld*^{S}) mouse, which presented with heavily delayed (two - three weeks instead of a few days) axonal degeneration pattern following transection (Lunn et al., 1989); this strongly suggested that Wallerian degeneration is an active event, rather than simply occurring passively due to lack of trophic support from the cell body. Several successive studies in different model organisms have confirmed this notion, with one of the strongest examples being the recent discovery that loss of functions mutations in the gene encoding Sarm1 (sterile α/Armadillo/Toll-interleukin receptor homology domain protein) in *Drosophila* and mice strongly suppress Wallerian degeneration for weeks after axotomy (Osterloh et al., 2012). The second important aspect of axonal degeneration is its distinction from neuronal cell death. In humans, axonal degeneration is a pathological hallmark of many neurodegenerative diseases and conditions, including motor neuron disease, glaucoma, and Parkinson's, Alzheimer's and Huntington's diseases (Coleman, 2005). These are also characterized by neuronal cell death, and in many cases it is not clear in which neuronal compartment the pathological condition starts. However, several lines of evidence in different model organisms suggest that the axon is a major component of neurodegenerative conditions. First, the degeneration of the axonal compartment correlates well with the onset and progression of the disease (Conforti et al., 2007). Second, Wld^S is able to delay axonal degeneration in mouse models of neurodegenerative diseases including progressive motor neuropathy (pmn mice; Ferri et al., 2003), Charcot-Marie-Tooth disease (myelin protein zero mutants; Samsam et al., 2003), and gracile axonal dystrophy (gad mutant mice; Mi et al., 2005). Finally, blocking cell death by overexpression of the apoptotic protective gene *bcl-2* did indeed reduce apoptosis but not axonal degeneration and the pathological symptoms (Sagot et al., 1995). In summary, the serendipitous discovery of the *Wld*^{S} mutant mouse has prompted a different level of detail in the study of axonal degeneration.

The protective effect of the *Wld*^{S} gene product against axonal degeneration induced by physical traumas, chemical insults, and a number of neurodegenerative conditions in both vertebrates and invertebrates has allowed its use in a variety of different paradigms, and revealed axonal degeneration to be an active mechanism that is largely universal and conserved across neuronal subtype and species.

A candidate molecule as an early sensor of axonal damage is the dual leucine zipper kinase DLK. DLK is a conserved mitogen-activated protein triple kinase (MAP3K) shown to regulate both axonal degeneration and regeneration following injury (Tedeschi and Bradke, 2013). Loss of DLK has been demonstrated to protect against axonal degeneration in mice and *Drosophila* (Ghosh et al., 2011; Miller et al., 2009). DLK activates both c-Jun N-terminal kinase (JNK) and p38 mitogen-activated protein kinase (MAPK) pathways to promote axonal degeneration (Miller et al., 2009). Moreover, the loss of DLK in *Drosophila* neurons is protective against degeneration induced by both axotomy and toxic insults (Miller et al., 2009). Together this supports a conserved role for DLK in promoting a general intrinsic mechanism of axonal degeneration following injury. The degeneration-promoting targets of DLK activation are still unclear, but there is an emerging picture of converging downstream axonal degeneration mechanisms, which may act together or in parallel to eliminate the distal axonal compartment. Elucidating the molecular elements of axonal degeneration programs is considered central to understanding the pathogenesis of neurodegenerative diseases. The key effectors of this degenerative program are likely to be targets for the prevention of axonal degeneration caused by trauma, toxin exposure, ageing, and genetic predisposition.

Functional axonal transport in axonal maintenance

Normal axonal transport is required to maintain neuronal activity as well as to remove proteins targeted for degradation. The morphology of axons, thin processes that are often projected over large distances, makes them particularly susceptible to trafficking defects, with disruption of normal axonal transport a causative event in axonal degeneration (Perlson et al., 2010). The most extreme example of this occurrence is a physical transection of the axon, leading to degeneration of the distal fragment. Disruption of components of the axonal transport machinery is also sufficient to cause degeneration. Mutations in the retrograde motor complex of dynein-dynactin have been directly shown to induce death of the cell body of motor neurons in mice (Chen et al., 2007; Hafezparast et al., 2003; LaMonte et al., 2002), while defects in anterograde transport have been demonstrated to specifically cause axonal degeneration (Reid et al., 2002; Zhao et al., 2001). In addition to motor proteins, disruption to the cytoskeletal network can in turn disrupt transport and

lead to degenerative phenotypes. Alterations to microtubule stability, either pharmacologically or genetically, can induce axonal degeneration. For example, microtubule destabilization with the chemotherapeutic drugs vincristine or colchicine is able to trigger axonal degeneration (Singer et al., 1956; Wang et al., 2000). In *C. elegans* sensory neurons, loss of the acetyl-transferase *mec-17/αTAT1* leads to altered stability of microtubules, which causes axonal transport defects, and loss of synaptic material, and leads to spontaneous degeneration of axons in aged animals (Neumann and Hilliard, 2014). Consistent with the hypothesis that axonal transport is essential for axonal maintenance, axonal transport defects have been implicated in the pathology of Parkinson's, Huntington's, Alzheimer's, and motor neuron diseases (Morfini et al., 2009; Perlson et al., 2010). However, it is still not clear if axonal transport defects are a primary or secondary deficit in disease pathology.

The role of mitochondria in axonal maintenance

The trafficking of mitochondria is one example of a specific organelle whose trafficking is critical for axonal maintenance. Although axons are capable of generating mitochondria (Calkins and Reddy, 2011), a significant proportion (10-30%) of axonal mitochondria are trafficked large distances (Misgeld et al., 2007) and some axonal mitochondria are generated in the cell body (Amiri and Hollenbeck, 2008). Altered mitochondrial transport has been observed in some neurodegenerative conditions and it is proposed that normal trafficking of mitochondria is a mechanism by which neurons are able to maintain a functional population of mitochondria in the axon (Court and Coleman, 2012). The unique morphology of neurons places extreme demands on the function of axonal mitochondria. Mitochondria are responsible for supplying adenosine triphosphate as well as buffering Ca^{2+} in the axon. In some cases, preventing mitochondria from entering the axon is sufficient to induce spontaneous axonal degeneration (Fang et al., 2012; Rawson et al., 2014). Mitochondrial dysfunction is an almost ubiquitous feature of neurodegenerative diseases with an axonal degeneration component, with disruptions of mitochondrial quality-control mechanisms being the major source of mitochondrial dysfunction (Court and Coleman, 2012; Rugarli and Langer, 2012). Mitochondrial fusion and fission are highly regulated dynamic processes that act to maintain a healthy mitochondrial population and confer protection against apoptosis (Westermann, 2010). Fusion of healthy mitochondria with dysfunctional mitochondria facilitates the replenishment of damaged materials, while fission of dysfunctional mitochondria into fragments enables their destruction via mitophagy and prevents the release of pro-apoptotic molecules. Both mitochondrial fusion and fission have been associated with axonal degeneration in human disease. The outer mitochondrial membrane protein Mitofusin 2, which mediates mitochondrial fusion (Chen et al., 2003), and GDAP1, which mediates

mitochondrial fission (Niemann et al., 2005), are both mutated in patients with Charcot-Marie-Tooth disease (Baxter et al., 2002; Zuchner et al., 2004). Due to their multiple roles in energy production, buffering intracellular Ca^{2+}, generation and detoxification of reactive oxygen species (ROS), as well as their dependence upon axonal trafficking, mitochondria represent an important convergence point in the molecular mechanisms of axonal degeneration.

The function of ROS

A byproduct of mitochondrial respiration is the production of ROS. In addition to their important physiological signalling functions such as the activation of kinases and transcription factors (Bartosz, 2009; Corcoran and Cotter, 2013), ROS accumulation causes irreversible damage to cellular components (DiMauro and Schon, 2008; Uttara et al., 2009). Neurons are particularly susceptible to this damage and increased ROS has been shown to induce Wallerian degeneration in axons (Press and Milbrandt, 2008). As a consequence, there are several cellular mechanisms in place to detoxify ROS that, when disrupted, result in a damaging oxidative cellular environment. For example, deletion of the super oxide dismutase enzyme SOD1, which is part of the endogenous ROS detoxification system, causes spontaneous axonal degeneration in cultured rat dorsal root ganglia (Fischer and Glass, 2010). Further evidence for the involvement of ROS in axonal degeneration can be found in many neurodegenerative diseases. The biggest risk factor for neurodegenerative diseases is age, which is characterized by accumulation of mitochondrial mutations and oxidative damage (Lin and Beal, 2006). Oxidative damage has been linked to Alzheimer's and Parkinson's diseases, amyotrophic lateral sclerosis (ALS), and multiple sclerosis (MS) (Uttara et al., 2009). Since the first linkage of mutations in SOD1 with ALS in humans (Rosen, 1993), a large number of mutations have been identified, representing one of the largest causes of familial ALS (Andersen and Al-Chalabi, 2011). The close link between the generation and detoxification of ROS and mitochondrial dysfunction, in both ageing and neurodegenerative disorders, suggests a pathological role for oxidative stress in axonal degeneration. Recently it has been demonstrated that exposure to ROS is sufficient to inhibit axonal transport in cultured neurons (Fang et al., 2012), illustrating the close association and convergence of multiple mechanisms which, when disrupted, lead to the elimination of the axon.

Regeneration of the proximal axonal compartment

Following injury of regeneration-competent neurons, the proximal fragment that is still connected to the cell body undergoes a transformation into a developmental-like state, generating a growth

cone and extending it in an attempt to recover the functional circuitry lost through injury. This process has been observed in invertebrate and vertebrate neurons of the peripheral nervous system (PNS) (Liu et al., 2011), and is able to restore function (Bhatt et al., 2004; Yanik et al., 2004). It has also been established that extrinsic molecules, such as those derived from myelin, are able to inhibit axonal regeneration (Yiu and He, 2006). However, the emerging theme from the growing body of work in both invertebrates and vertebrates is that the main determinant of regenerative potential is intrinsic. Much is now known about the regulation of specific regenerative events, including retrograde injury signals, initiation of growth cone formation, and pro-regenerative pathways; however a complete picture of how this process proceeds and how it can be controlled is still lacking.

MAP kinases – the master regulators

Axonal injury, and the subsequent production of Ca^{2+} transients, result in retrograde signals that are transported to the neuronal cell body and function as positive injury signals to regulate a regenerative response (Abe and Cavalli, 2008). These injury signals include MAPKs, which are activated by axonal injury and retrogradely transported to the neuronal cell body (Perlson et al., 2005). Elegant genetic studies in *C. elegans*, utilizing a mutant with spontaneous axonal breakage followed by regeneration, have led to the identification of an entire regulatory pathway of MAPK signalling that is essential for axonal regeneration (Figure 1.2; Hammarlund et al., 2009; Nix et al., 2011). Intriguingly, the MAP3K DLK (DLK-1 in *C. elegans*) functions as an early injury signal for axonal regeneration in motor and sensory neurons in *C. elegans* (Hammarlund et al., 2009; Yan et al., 2009), a key role that matches the central function of this molecule in regulating degeneration of the distal axonal fragment, as discussed above (Ghosh et al., 2011; Miller et al., 2009). In contrast to its role in promoting degeneration, DLK-1 functions in the proximal axonal compartment to promote regeneration together with a parallel pathway containing the MAP3K MLK-1 (Nix et al., 2011). These pathways share several common regulators and act at the time of injury, via downstream kinases, to regulate growth cone formation and axon extension. Activation of the DLK-1 pathway results in the stabilization of the mRNA transcript of the CCAAT/enhancer binding factor homologue CEBP-1 (Yan et al., 2009). Precisely how either of these pathways regulate regeneration is unknown. Importantly, DLK-1 has been demonstrated to promote regeneration in *Drosophila* and mice, suggesting that this pathway represents a major conserved mechanism of axonal regeneration (Itoh et al., 2009; Xiong et al., 2010).

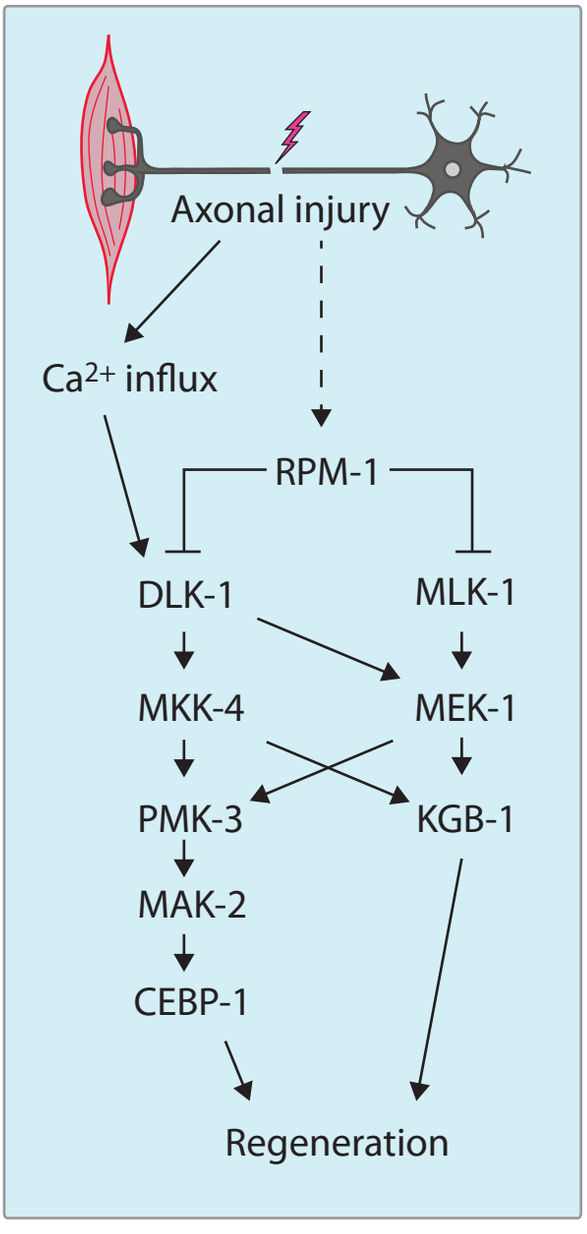

Figure 1.2. The *C. elegans* mitogen-activated kinase cascade in regeneration. Axonal injury triggers a rise in intracellular Ca^{2+} which activates DLK-1 and the DLK-1–MKK-4–PMK-3 pathway. In parallel the MLK-1–MEK-1–KBG-1 pathway is also activated in response to injury. RPM-1 coordinates the regulation of both regenerative pathways. DLK-1, dual leucine zipper kinase 1; MKK-4, MAP kinase kinase ; PMK-3, p38-like MAP kinase; MAK-2, MAP kinase-activated protein kinase; CEBP-1, CCAAT/enhancer-binding protein 1; MLK-1, MAP kinase kinase kinase; MEK-1, MAP kinase kinase; KGB-1, c-Jun N-terminal-like MAP kinase; RPM-1, regulator of presynaptic morphology 1. Diagram adapted from Nix et al. (2011).

Cytoskeletal dynamics

Successful axonal regeneration requires large-scale changes to the state of the injured axon such that it is converted from a stable mature axon into a dynamic regrowing one. Axonal injury triggers alterations to actin and microtubule networks which are intimately linked to injury signalling, growth cone formation, and axon extension (Chisholm, 2013). Microtubules are polarized in axons, with polymers organized in a plus-end out orientation. Studies in *Aplysia*, *Drosophila,* and *C. elegans* have examined the dynamics of microtubules following axonal injury. Axotomy triggers local microtubule severing and depolymerization followed by the growth of polymers with mixed polarity (Erez and Spira, 2008; Ghosh-Roy et al., 2010; Stone et al., 2010). Microtubule disassembly is likely triggered by a combination of the injury itself as well as a local Ca^{2+} influx triggering severing of microtubules by Ca^{2+}-dependent enzymes (Gitler and Spira, 1998; Spira et al., 2003). In addition to Ca^{2+}, there is also evidence to suggest that microtubules are regulated by DLK. In *C. elegans* sensory neurons, overexpression of DLK-1 increases the number of growing microtubules in un-injured axons, and the absence of DLK-1 reduces the number of dynamic microtubules following axonal injury (Ghosh-Roy et al., 2012). Promoting catastrophe of microtubule polymers by overexpression of the Arf6 guanine nucleotide exchange factor EFA-6 in *C. elegans* inhibits regeneration, whereas loss-of-function mutants have enhanced regeneration (Chen et al., 2011). Recently, two studies demonstrated that loss of PTRN-1, a *C. elegans* homologue of the microtubule minus-end binding calmodulin-regulated spectrin-associated family, reduces microtubule stability and triggers a repair-like mechanism, dependent on DLK-1 (Marcette et al., 2014; Richardson et al., 2014). This supports a mechanism whereby DLK is downstream of microtubule destabilization in regeneration signalling. Although the direct relationship between DLK, Ca^{2+} transients, and microtubule dynamics is not understood, there is much evidence to support the requirement of a dynamic microtubule network for successful initiation of axonal regeneration. Much less is known about the requirement of microtubules at later stages of axonal regeneration, such as target reconnection.

Regeneration via axonal fusion

Successful regeneration requires re-innervation the target tissue following axonal injury. This is generally considered as regrowth of the proximal axonal fragment along the entire length of the separated distal fragment, followed by innervation, either directly or indirectly through other neurons, of the distal target. This regrowth can be initiated from the tip of the proximal axonal stump, or through sprouting from another axonal region, and can progress along the original axonal path, or via an ectopic route (Harel and Strittmatter, 2006; Yiu and He, 2006). In axons of the vertebrate PNS, degeneration of the distal axonal fragment is required for efficient regrowth of the

proximal fragment (Bisby and Chen, 1990; Brown et al., 1992; Brown et al., 1994). An alternative mode of axonal regeneration has been observed in invertebrate neurons. Here, the regrowing proximal axonal fragment generates a growth cone, which extends towards the distal axonal fragment and reconnects with it via a membrane fusion event, preventing degeneration of the distal axonal fragment and re-establishing the original axon. This type of regeneration, termed regeneration via axonal fusion, has been observed in the axons of earthworms, leeches, crayfish, *Aplysia*, and most recently *C. elegans* (Bedi and Glanzman, 2001; Birse and Bittner, 1976; Deriemer et al., 1983; Ghosh-Roy et al., 2010; Hoy et al., 1967; Neumann et al., 2011). In *C. elegans* sensory neurons, regenerative fusion events have been demonstrated to re-establish membrane and cytoplasmic continuity between the proximal and distal axonal fragments (Ghosh-Roy et al., 2010; Neumann et al., 2011). Axonal fusion between the proximal and distal fragments prevents Wallerian degeneration of the distal fragment, and halts regrowth of the proximal fragment through unknown signals. This process is also highly specific, with regrowing axons selectively fusing with the correct distal axonal fragment despite the presence of associated axons from other neurons, suggesting the existence of a regulatory mechanism of recognition involved in repair (Neumann et al., 2011). The *C. elegans* fusogen EFF-1, which mediates multiple developmental membrane fusion events, is required for axonal fusion during regeneration (Ghosh-Roy et al., 2010). Elevated Ca^{2+}/cAMP levels have been demonstrated to increase axonal fusion rates, although it is unclear if this is a direct effect on fusion mechanisms or an indirect effect on regeneration/degeneration rates (Ghosh-Roy et al., 2010). The mechanism by which fusion machinery is activated in regrowing neurons and the mechanisms of recognition between the distal and proximal fragments are currently unknown and are a major focus of this thesis.

Age-related decline

The rate of both axonal degeneration and axonal regeneration following injury has been observed to decline with age in *C. elegans* neurons (Annika Nichols and Massimo Hilliard, personal communication; Byrne et al., 2014; Gabel et al., 2008; Hammarlund et al., 2009; Nix et al., 2011; Wu et al., 2007; Zou et al., 2013). A similar decline in regeneration rates has been observed in vertebrate neurons (Pestronk et al., 1980; Tanaka et al., 1992; Verdu et al., 1995; Verdu et al., 2000). In *C. elegans* motorneurons this decline in regenerative ability has been demonstrated to be regulated intrinsically by the insulin/IGF-1 receptor DAF-2 and the transcription factor DAF-16/FOXO (Byrne et al., 2014). A similar decline has been observed in the rate of degeneration of *C. elegans* sensory neurons, through unknown mechanisms (Annika Nichols and Massimo Hilliard,

personal communication). Interestingly, this decline in degeneration and regeneration rates overlaps with the appearance of axonal fusion during regeneration, which is observed at a lower rate in early larval stages compared to adult animals (Brent Neumann and Massimo Hilliard, *personal communication*). It is unknown if there is a direct link between regenerative capacity and axonal fusion during regeneration.

Research directions

Here we have outlined how following axonal injury, the neuron is split into two distinct compartments, the proximal and distal axonal fragments. Fascinatingly, injury-triggered Ca^{2+} influx disrupting microtubule stability and activation of the DLK pathway initiate completely opposing responses in each axonal compartment (Figure 1.3). The execution of axonal degeneration in the distal axonal fragment involves the convergence of injury signals, cytoskeletal disassembly, axonal transport defects, and mitochondrial dysfunction. On the contrary, the regrowth of the proximal axonal fragment requires the transition of a mature, stable axon into a labile dynamic structure more similar to a developing neuron, which requires injury-triggered changes to microtubule dynamics and the transmission of retrograde injury signals that cause alterations to gene expression. We have also highlighted the phenomenon of axonal fusion during regeneration described in invertebrate neurons, where degeneration and regeneration are coordinated to facilitate rapid reconnection of axonal compartments. To date axonal fusion during regeneration is the only scenario in which Wallerian degeneration cannot only be delayed, but also reversed. It is tempting to speculate that the ability of a neuron to undergo axonal fusion during regeneration represents a fine balance between the rates of axonal degeneration and regeneration. If this is the case it may be possible to manipulate these rates *in vivo* to facilitate axonal fusion in cases where it does not spontaneously occur. It is unknown if axonal fusion is a normal occurrence in vertebrate neurons at the level of a single axon. So far all studies have focused on surgical methods of fusion combined with the use of high molecular weight compounds to facilitate fusion between proximal and distal nerve bundles (Bittner et al., 2012; Britt et al., 2010; Dong et al., 2013; Silva et al., 2010; Spaeth et al., 2012). These methods have delivered extremely promising results, but at this stage it is unclear of the specificity of this process and if it represents a method of indirect re-innervation or something more similar to axonal fusion observed in invertebrates. In fact, axonal fusion in *C. elegans* has not yet been demonstrated to restore function to the axon. It is conceivable that although axonal fusion during regeneration may reverse Wallerian degeneration of the distal axonal fragment and restore cytoplasmic continuity between the neuronal cell body and its distal axon, function may remain

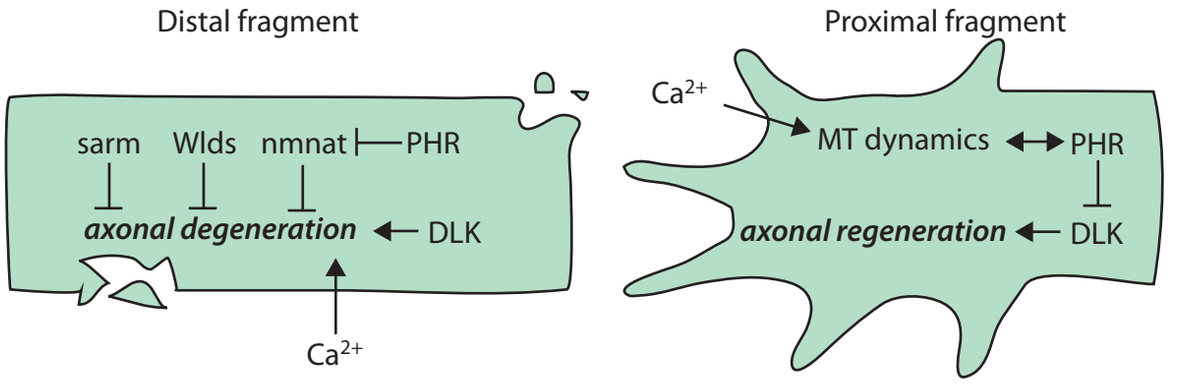

Figure 1.3. Overlapping injury signals promote axonal degeneration and regeneration mechanisms. A simplified diagram of known upstream regulators of axonal degeneration and regeneration. Similar components in each axonal compartment activate completely opposing responses. Ca^{2+}, PHR (RPM-1 in *C. elegans*), and DLK (DLK-1 in *C. elegans*) represent key convergance points of axonal degeneration and regeneration mechanisms.

disrupted. In this case, axonal fusion may not be the optimal method of repairing injury. There is much evidence from PNS regeneration in vertebrate models that supports a model in which degeneration and regeneration rates are proportional, whereby delaying degeneration of the distal axonal fragment inhibits regeneration of the proximal axonal fragment. Degeneration of the distal fragment prevents axonal fusion and therefore, *a priori,* one would assume that delaying degeneration of the distal fragment might increase the likelihood of axonal fusion with the proximal fragment. In this sense, axonal fusion during regeneration may represent an alternative to complete regeneration towards the distal target, with the preserved distal axonal fragment offering a shortcut to an ageing and slowly regrowing axon. Given the obvious limitations to the regenerative capacity of vertebrate neurons, particularly those of the central nervous system, axonal fusion in any form represents a unique opportunity to repair functional circuitry with minimal regeneration.

1.2 Summary and aims

The review of literature presented as section 1.1 outlined what is currently known about the cellular mechanisms of axonal degeneration and regeneration following injury. The emerging picture from these studies is that active mechanisms are present that regulate these two seemingly contradictory phenomena. This section highlighted how both axonal degeneration and regeneration share components of the initial stages of injury signalling which lead to the activation of two distinct non-developmental programs. The main aim of this thesis was to develop novel injury strategies for use in *C. elegans* that would facilitate forward and reverse genetic approaches to discover the mechanisms of axonal degeneration and regeneration.

Aim 1: Develop genetic methods of axonal damage to study degeneration and regeneration.

Aim 2: Discover molecules that regulate degeneration and regeneration with forward and reverse genetic approaches.

Chapter 2:
Developmental control of axonal morphology and regeneration

2.1 Introduction

A critical event in neuronal development is neuronal polarization. Neurons typically comprise two distinct processes: an axon, which sends signals to other neurons, and dendrites, which receive inputs from other neurons. The establishment of these two neuronal compartments is essential for correct neuronal function, and occurs soon after the neuron is born. Growing evidence, primarily from *in vitro* studies, suggests that regulation of the microtubule cytoskeleton provides key instructive signals to specify axon and dendrite identity (Polleux and Snider, 2010). In addition to their role in neuronal polarity during development, microtubule dynamics have been recently implicated in axonal regeneration and degeneration (reviewed in chapter 1). The emerging picture is that early developmental events can not only result in defects in axon and dendrite specification and development, but can also lead to deficits in axonal maintenance and regeneration after injury over the lifetime of the organism.

The *C. elegans* anterior lateral mechanosensory neurons (ALM right and ALM left) are located symmetrically on the lateral sides of the animal's body and are responsible for sensing anterior light mechanical stimulation (touch) to initiate a reversal response (Chalfie et al., 1985). Each ALM is a highly polarized neuron with a single axon that extends anteriorly from the mid body of the animal, where the soma is located, into the head of the animal. In the present study, together with two colleagues, we address how early defects in neuronal polarity affect both axonal morphology and specification, as well post-developmental events such as axonal regeneration. We show that mutations in the gene *mec-7/β-tubulin* cause the extension of an ectopic neurite with axon-like properties. We demonstrate that these defects are due to changes in the dynamics of microtubules, and that in addition to defects in neurite specification during development these animals have defects in axonal regeneration following injury.

The critical aspect of this study relevant to this thesis is the demonstration that the regulation of microtubule dynamics is essential for axon outgrowth, maintenance, and repair. This work was published in the peer-reviewed journal *Molecular Biology of the Cell*. A copy of this article is presented as section 2.2 of this thesis.

2.2 A dominant mutation in *mec-7/β-tubulin* affects axon development and regeneration in Caenorhabditis elegans neurons

Kirszenblat, L., Neumann, B., **Coakley, S.** and Hilliard M.A. (2012) A dominant mutation in *mec-7/β-tubulin* affects axon development and regeneration in *Caenorhabditis elegans* neurons. ***Mol Biol Cell*** *24*, 285-96.

A dominant mutation in *mec-7/β-tubulin* affects axon development and regeneration in *Caenorhabditis elegans* neurons

Leonie Kirszenblat, Brent Neumann, Sean Coakley, and Massimo A. Hilliard
Queensland Brain Institute, The University of Queensland, Brisbane 4072, Australia

ABSTRACT **Microtubules have been known for decades to be basic elements of the cytoskeleton. They form long, dynamic, rope-like structures within the cell that are essential for mitosis, maintenance of cell shape, and intracellular transport. More recently, in vitro studies have implicated microtubules as signaling molecules that, through changes in their stability, have the potential to trigger growth of axons and dendrites in developing neurons. In this study, we show that specific mutations in the *Caenorhabditis elegans mec-7/β-tubulin* gene cause ectopic axon formation in mechanosensory neurons in vivo. In *mec-7* mutants, the ALM mechanosensory neuron forms a long ectopic neurite that extends posteriorly, a phenotype that can be mimicked in wild-type worms with a microtubule-stabilizing drug (paclitaxel), and suppressed by mutations in *unc-33/CRMP2* and the kinesin-related gene, *vab-8*. Our results also reveal that these ectopic neurites contain RAB-3, a marker for presynaptic loci, suggesting that they have axon-like properties. Interestingly, in contrast with the excessive axonal growth observed during development, *mec-7* mutants are inhibited in axonal regrowth and remodeling following axonal injury. Together our results suggest that MEC-7/β-tubulin integrity is necessary for the correct number of neurites a neuron generates in vivo and for the capacity of an axon to regenerate.**

Monitoring Editor
David G. Drubin
University of California, Berkeley

Received: Jun 11, 2012
Revised: Nov 28, 2012
Accepted: Nov 29, 2012

INTRODUCTION

A neuron becomes polarized early in its development, when it breaks its symmetry by extending an axon and dendrites. The polarity of a neuron is defined by its orientation within the animal, the number of processes it extends, and the specification of neurite identity. In the nematode *Caenorhabditis elegans*, alterations to neuronal polarity have been detected by changes in cell orientation in the body of the worm, leading to the discovery of several molecules in the Wnt/Frizzled and Netrin/DCC pathway that are critical for this process in vivo (Adler *et al.*, 2006; Chang *et al.*, 2006; Hilliard and Bargmann, 2006; Prasad and Clark, 2006; Quinn *et al.*, 2008). In parallel, studies using cultured hippocampal neurons have provided insights into the molecules that specify neurite identity, thereby establishing whether a neuronal process develops into an axon or a dendrite (Polleux and Snider, 2010). Local destabilization of the actin network at the tip of a neurite has been shown to act as an early signal within the cell for axon specification (Bradke and Dotti, 1999; Witte and Bradke, 2008; Neukirchen and Bradke, 2011). However, several studies have identified molecules, such as collapsin response–mediated protein 2 (CRMP2), synapses of amphids defective (SAD) kinases, and glycogen synthase kinase-3β (GSK3β), that trigger axon specification independently of actin through microtubule dynamics (Jiang *et al.*, 2005; Kishi *et al.*, 2005; Yoshimura *et al.*, 2005; Maniar *et al.*, 2012). Furthermore, growing evidence from in vitro experiments suggests that microtubules do not merely act as simple building blocks or cargo tracks in this process, but may provide instructive signals for axon specification (Baas, 2002; Witte *et al.*, 2008; Hoogenraad and Bradke, 2009; Stiess and Bradke, 2011). Interestingly, microtubule dynamics have also been implicated in axonal regeneration, indicating microtubules are important

This article was published online ahead of print in MBoC in Press (http://www.molbiolcell.org/cgi/doi/10.1091/mbc.E12-06-0441) on December 5, 2012.

The authors declare no conflict of interest.

Address correspondence to: Massimo A. Hilliard (m.hilliard@uq.edu.au).

Abbreviations used: CRMP, collapsin response–mediated protein; GFP, green fluorescent protein; MAP, microtubule-associated protein; SNP, single-nucleotide polymorphism.

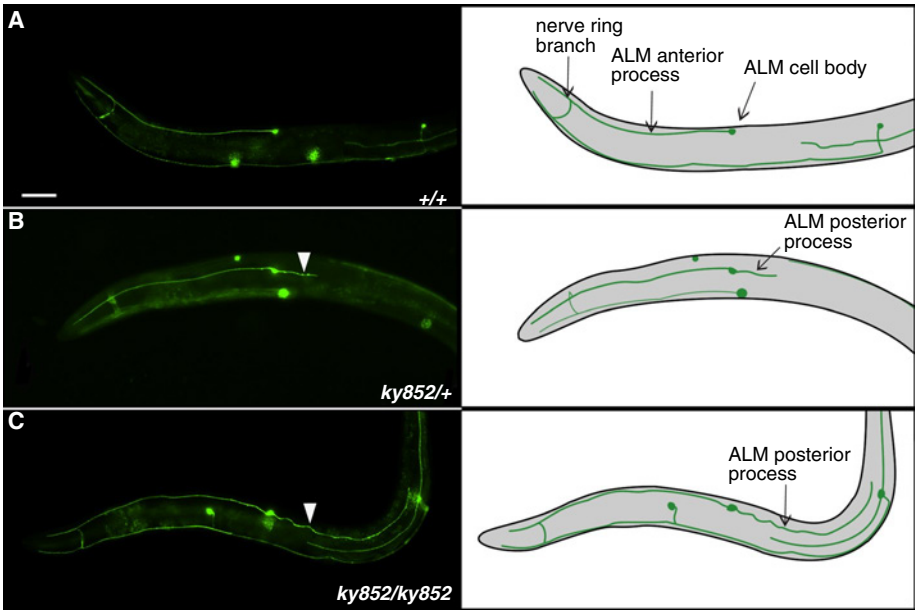

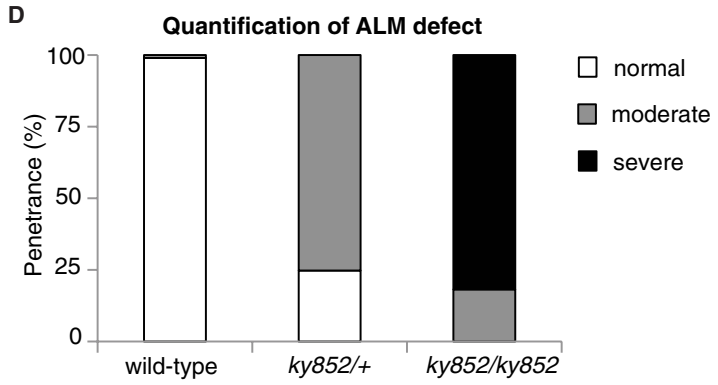

FIGURE 1: Posterior neurite outgrowth defects in ALM neurons of *ky852* mutants. Morphology of ALM in wild type (A), *ky852* heterozygotes (B), and *ky852* homozygotes (C). White arrowheads indicate the ectopic posterior process. (D) Quantification of ALM phenotypes, classified as normal (no posterior process), moderate (medium length posterior process), and severe (long posterior process). Each data set is based on an *n* of at least 100 animals. Scale bar: 25 μm.

not only during axon development but also for regrowth following injury (Erturk *et al.*, 2007; Stone *et al.*, 2010; Chen *et al.*, 2011; Hellal *et al.*, 2011; Sengottuvel and Fischer, 2011).

Although significant advances have been made in understanding the molecular mechanisms of neuronal polarization governed by neuron orientation and neurite identity, we know much less about how a neuron is able to control the number of neurites it forms in vivo. Recent results have shown the planar cell polarity molecules VANG-1 and PRKL-1 are involved in this process (Sanchez-Alvarez *et al.*, 2011).

In this study, we performed an unbiased genetic screen in *C. elegans* mechanosensory neurons to identify mutations affecting the number of neurites that a neuron generates. We show that a mutation in *mec-7*, which encodes β-tubulin, causes ALM mechanosensory neurons to develop long, ectopic neurites containing presynaptic loci, in addition to their normal axons. Time-lapse morphological characterization suggests that this defect results from a disruption in the maintenance of neuronal polarity, with pharmacological experiments revealing that similar defects arise from hyperstable microtubules. Converse to the excessive axon growth observed during development, we also demonstrate that axons of *mec-7* animals display a reduced capacity for regeneration following laser-induced injury. Our results reveal that β-tubulin mutations can alter the number of axons generated in vivo and inhibit multiple stages of axonal regeneration.

RESULTS

Semidominant mutations in MEC-7/β-tubulin induce neurite outgrowth in vivo

The *C. elegans* ALM mechanosensory neuron is bilaterally symmetrical and has a single process that extends anteriorly, with a ventral branch of this process forming synaptic connections in the nerve ring (Figure 1A). Occasionally, a short posterior neurite that is less than twice the length of the cell body is observed, although this is regarded as a protrusion, rather than a full process (White, 1986; Watari-Goshima *et al.*, 2007). The ALM neuron was visualized using the *zdIs5(Pmec-4::GFP)* transgene, which expresses green fluorescent protein (GFP) in the ALM, AVM, PVM, and PLM mechanosensory neurons. In an unbiased, forward genetic screen aimed at finding mutants with ectopic neurite outgrowth in the ALM neuron, we isolated a mutation, *ky852*, in which both the left and right ALM neurons extended a long posterior neurite, essentially converting them into bipolar neurons (Figure 1, C and D). This phenotype was fully penetrant and semidominant, with heterozygotes (*ky852/+*) displaying a less severe phenotype with shorter posterior processes than those of homozygotes (Figure 1, B and D). Interestingly, we never observed a reversed ALM phenotype in which the anterior process was misrouted posteriorly, a common occurrence in other known ALM polarity mutants (Wolf *et al.*, 1998; Hilliard and Bargmann, 2006; Prasad and Clark, 2006; Levy-Strumpf and Culotti, 2007; Watari-Goshima *et al.*, 2007; Pan *et al.*, 2008). This suggests that the *ky852* phenotype might result from disruption of a different molecular process that, rather than affecting orientation of a neuron within the animal, specifically regulates the number of neurites it develops. Moreover, unlike other polarity mutants, the *ky852* mutant also exhibited ectopic neurite formation in the mechanosensory neurons AVM and PVM, and overextension of the posterior neurite in the PLM neuron (Figure S1). Behavioral analysis of *ky852* mutants with the light-touch assay (Chalfie and Sulston, 1981) revealed a mild touch insensitivity compared with wild-type animals, suggesting that the functional integrity of the mechanosensory neurons had been affected (Figure S2). To determine whether the mutation affected other classes of neurons, we visualized the D-type GABAergic motor neurons (*Punc-25::GFP* transgene) and the oxygen sensory neurons, AQR, PQR, and URX (*Pgcy-36::GFP* transgene) in the *ky852* mutants. The morphology of these motor and oxygen sensory neurons appeared unaltered (unpublished

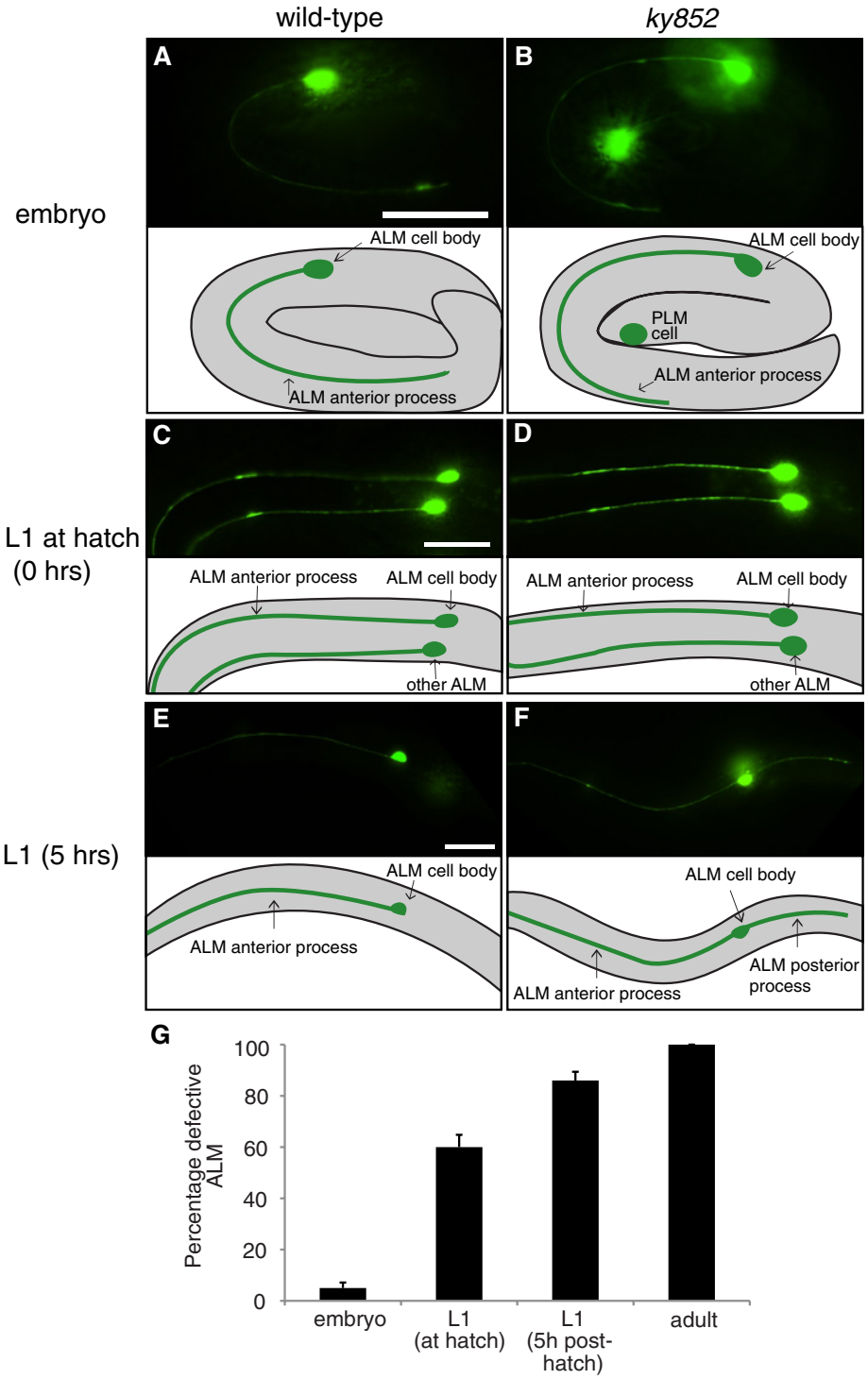

FIGURE 2: Ectopic neurites in *ky852* mutants develop following embryogenesis. Morphology of ALM neurons in wild type and *ky852* mutants in the embryo (A and B), at hatching (C and D), and 5 h after hatching (E and F). (G) Quantification of ALM neurons with posterior neurite defects in *ky852* mutants during developmental stages corresponding to the images in (A–F). Each data set is based on an *n* of at least 100 animals. Error bars represent the SE of proportion. Scale bars: 20 μm.

data), suggesting that the *ky852* mutation specifically affected the mechanosensory neurons.

The ALM mechanosensory neurons develop during embryogenesis, a time at which *mec-7* also begins to be expressed (Hamelin *et al.*, 1992), and are fully extended to the head of the animal at hatching. We reasoned that the ectopic ALM process in *ky852* mutants could either emerge during early development, which would suggest a disruption in the establishment of neuronal polarity, or arise after the development of the anterior neurite, which would indicate a defect in the maintenance of the neuronal polarity. To investigate this, we performed time-lapse analysis of ALM development and found that the ectopic neurite emerged during the L1 stage, after the normal anterior neurite had already extended to the head of the animal (Figure 2). This supports the notion that the *ky852* phenotype differs from other neuronal polarity mutants, in which polarity defects are already seen in the embryo when the cell first begins to develop asymmetry (Hilliard and Bargmann, 2006), and therefore indicates the *ky852* mutation affects signaling processes occurring later in development.

Using single-nucleotide polymorphism (SNP) analysis (Wicks *et al.*, 2001; Davis *et al.*, 2005; Davis and Hammarlund, 2006), we mapped the *ky852* mutation to an interval of chromosome X including the *mec-7* gene, which encodes a β-tubulin that is specifically expressed in the six mechanosensory neurons of *C. elegans* and forms a component of the 15 protofilament microtubules unique to these neurons (Chalfie and Thomson, 1982). Several lines of evidence indicated the *ky852* phenotype was due to a mutation in the *mec-7* gene. First, sequence analysis of the *ky852* mutant revealed a single base-pair change (ccg to tcg) in the *mec-7* gene that generated a missense mutation (proline to serine at amino acid position 220) in the encoded protein (Figure 3A). Second, when we introduced a wild-type copy of *mec-7* under the control of the *mec-4* promoter *(Pmec-4::mec-7)* into *ky852* mutant animals, we found that this transgene could partially rescue the ALM defect, with the length of the ectopic process being reduced or returned to wild-type length in the majority of animals (Figure 3B). This partial rescue was consistent with the mutation being semidominant, as heterozygous animals showed ectopic processes of intermediate lengths (Figure 1, B and D), due to the presence of both wild type and mutant copies of the gene. Third, expression of the *mec-7(ky852)* mutant allele in wild-type animals induced ectopic posterior outgrowth in some ALM neurons (Figure 3C), further supporting the semidominant role of this gene. Finally, the *mec-7* gene has been extensively characterized for mutations that affect the touch sensitivity of *C. elegans*, with more than 50 alleles identified (Savage *et al.*, 1989, 1994). Although visualization in these studies of MEC-7 with antibodies indicated that the vast

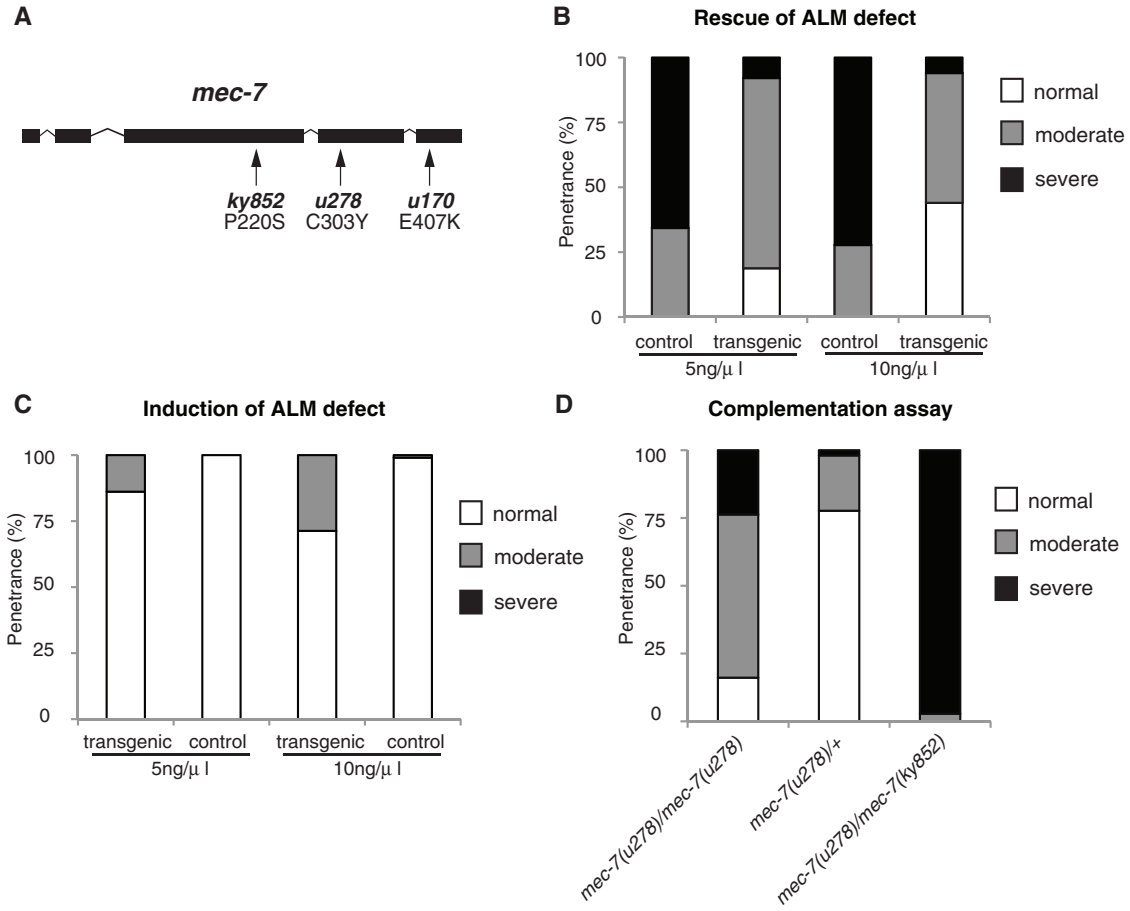

FIGURE 3: The *ky852* phenotype is caused by a mutation in the *mec-7* gene. (A) Diagram of the *mec-7* gene. Solid bars represent exons and connecting lines represent introns. The *ky852* mutation and two other alleles that cause similar ALM neurite outgrowth phenotypes are indicated. (B) Rescue of ALM defects by insertion of wild-type *mec-7* into *mec-7(ky852)* mutants. Two independent lines that were generated with different concentrations of injected transgene are shown. Phenotypic distributions between transgenics and nontransgenic controls were significantly different in both cases (chi-square test: $p < 0.0001$). (C) Induction of *mec-7(ky852)* phenotype by insertion of mutant *mec-7* into wild-type animals. Two independent lines that were generated with different concentrations of injected transgene are shown. In both cases, transgenics had a reduced percentage of normal ALMs and an increased percentage of ALMs with intermediate length posterior process defects (Fisher's exact test: $p < 0.0001$). (D) ALM phenotype of *mec-7(u278)* homozygotes, *mec-7(u278)* heterozygotes, and *mec-7(u278)/mec-7(ky852)* double heterozygotes. Data sets for (B–D) are based on an *n* of at least 100 animals.

majority of these alleles cause degenerative phenotypes in ALM, two alleles, *u278* and *u170*, presented posterior outgrowth in ALM similar to that observed in the *ky852* mutant animals (Savage *et al.*, 1994). We visualized and quantified the phenotypes of the *mec-7(u278)* allele in the *zdIs5(Pmec-4::GFP)* background and found it had a qualitatively similar but less severe phenotype compared with the *ky852* mutant, with a lower penetrance of the ALM defect (Figure 3D). Complementation analysis between the *ky852* and *mec-7(u278)* alleles revealed a significant worsening of the defect in the double heterozygotes (noncomplementation) compared with either individual heterozygote (Figure 3D), confirming *ky852* to be a novel allele of *mec-7*.

Ectopic neurite outgrowth is triggered by hyperstable microtubules

Local stabilization of microtubules in immature neurites of dissociated neurons is sufficient to trigger axon formation (Witte *et al.*, 2008). To investigate whether the ectopic processes in *mec-7(ky852)* animals were a result of hyperstable microtubules, we treated animals with a microtubule-destabilizing agent, colchicine, or a microtubule-stabilizing agent, paclitaxel. Colchicine is known to inhibit the assembly of microtubules by binding to tubulin, thereby disrupting microtubule dynamics (Fojo, 2008). Treatment of *mec-7(ky852)* animals with colchicine prevented outgrowth of the ectopic posterior process in the ALM neuron, leaving the anterior process intact (Figure 4A). To determine the developmental period during which colchicine produces its effect, we restricted treatment to the first 24 h after hatching (when the animals are largely in the L1/L2 stages) or to the following 24 h (during L3/L4). Approximately 70% of ALM neurons formed normally in *mec-7(ky852)* animals treated with colchicine during the first 24 h following hatching; in contrast, no rescue of the ALM posterior neurite was observed when the colchicine treatment was started 24 h after hatching (Figure 4B). The ability to specifically block development of the ALM ectopic process during the early L1 stage supports our observation that the defect emerges later than the normal ALM process, which is formed during embryogenesis. Notably, concentrations of colchicine that blocked development of the ALM ectopic process also affected neurite

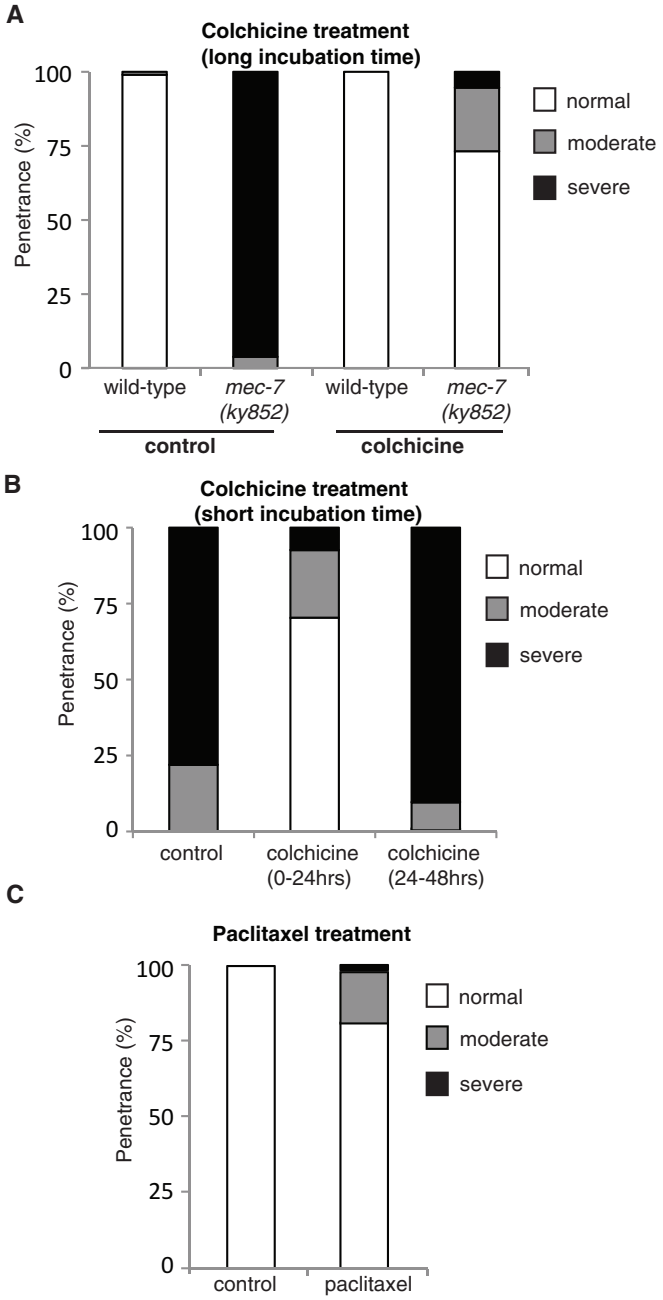

FIGURE 4: Manipulation of microtubule stability using colchicine and paclitaxel affects development of ectopic ALM neurites. (A) Rescue of ALM posterior neurite defects in *mec-7(ky852)* animals grown on colchicine throughout development. The distribution of ALM phenotypes in *mec-7(ky852)* animals grown on colchicine was significantly different from that of control *mec-7(ky852)* animals (chi-square test: $p < 0.0001$). (B) Rescue of ALM defects in *mec-7(ky852)* animals when treated with colchicine during the first 24 h but not the second 24 h after hatching. Animals treated with colchicine from 0 to 24 h were significantly different than controls (chi-square test: $p < 0.0001$). (C) Ectopic neurites generated in ALM neurons of wild-type (*bus-17; zdIs5*) animals grown on paclitaxel. ALM phenotypes of animals treated with paclitaxel were significantly different than controls (Fisher's exact test: $p < 0.03$). Each data set is based on an *n* of at least 50 animals in (A) and (B) and 59 and 24 animals for paclitaxel-treated and control animals, respectively, in (C).

outgrowth of the AVM and PVM mechanosensory neurons in wild-type animals, both of which develop within the first 24 h after hatching, suggesting that the microtubules in *mec-7(ky852)* animals have similar sensitivity to colchicine to those of wild-type animals (i.e., the mutation does not appear to affect the ability of colchicine to bind to β-tubulin).

We next tested the effect of a microtubule-stabilizing agent, paclitaxel, on development of the mechanosensory neurons. Paclitaxel binds to microtubule polymers, stabilizing them by suppressing microtubule dynamics (Fojo, 2008). We hypothesized that pharmacological stabilization of microtubules would produce a similar phenotype to that of *mec-7(ky852)* mutants. *bus-17(e2800)* mutant animals were used for this experiment due to their thinner cuticles, which enhance the permeability of drugs (Bounoutas *et al.*, 2009). In the absence of paclitaxel treatment, the mechanosensory neurons were normal in these animals, as visualized using the *Pmec-4::GFP* transgene (*zdIs5*; *bus-17)*. However, treatment with paclitaxel during development induced the formation of ectopic processes, producing a phenotype that was similar to that of the *mec-7(ky852)* mutants, albeit to a lower penetrance (Figure 4C). This demonstrates that microtubule-stabilizing agents can induce ectopic neurite formation in vivo. Moreover, it suggests that the *mec-7(ky852)* phenotype could arise from excessive stabilization of microtubules, providing a dosage effect of hyperstable β-tubulin consistent with the semidominant nature of the mutation.

Ectopic outgrowth in *mec-7(ky852)* is suppressed by *unc-33* and *vab-8* mutations

Microtubule growth and stability is regulated by a variety of tubulin-binding molecules. To investigate whether β-tubulin could interact with such molecules to produce ectopic neurite outgrowth, we searched for suppressors of the *mec-7(ky852)* ALM phenotype. We first investigated the *ptl-1* gene, which is the sole *C. elegans* homologue of the Tau/MAP2/MAP4 family of microtubule-associated proteins (MAPs) and promotes microtubule assembly (Goedert *et al.*, 1996). A deletion mutation of the *ptl-1* gene had no effect on the ALM outgrowth defects of *mec-7(ky852)* animals (Figure 5A and Table S1), suggesting that PTL-1 does not contribute to the mutant phenotype.

Next we analyzed the *C. elegans* member of the collapsin response–mediated protein (CRMP) family, UNC-33. UNC-33 binds tubulin, promoting its assembly into microtubules, and has been shown to be necessary for axon outgrowth, microtubule structure, and polarized axonal transport (Hedgecock *et al.*, 1985; Inagaki *et al.*, 2001; Tsuboi *et al.*, 2005; Maniar *et al.*, 2012). We found that the *unc-33(e204)* mutation could partially suppress the *mec-7(ky852)* ALM outgrowth phenotype, as double mutants displayed a significant number of normal ALMs (never seen in *mec-7(ky852)* single mutants) and a dramatic reduction in the length of the ectopic process outgrowth (Figure 5A and Table S1). In contrast, the normal anterior process remained unaffected by the *unc-33* mutation. This suggests that the ectopic outgrowth phenotype caused by the mutant MEC-7/β-tubulin could be caused by an enhanced or altered interaction with UNC-33, which may contribute to excessive growth of microtubules in these mutants.

An intriguing question is how a single mutation in MEC-7/β-tubulin can produce such precise, posterior outgrowth of a neuronal process. We hypothesized that this phenotype may be caused by interaction with VAB-8, a novel kinesin-like protein of *C. elegans* that is specifically required for posterior migration of both cells and growth

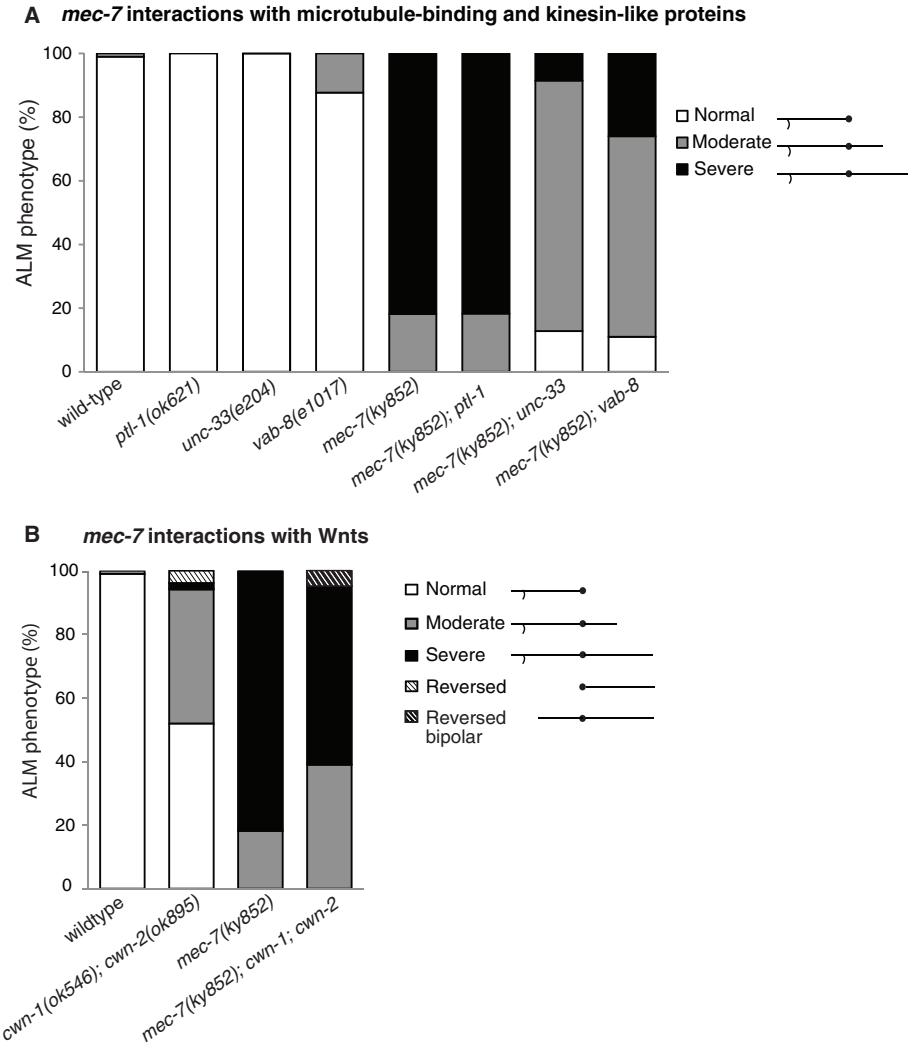

FIGURE 5: Genetic interactions of *mec-7(ky852)* with MAPs and Wnts. (A) ALM phenotypes in double mutants of the microtubule-binding proteins, PTL-1/Tau and UNC-33/CRMP2, and the kinesin-like molecule VAB-8. *mec-7(ky852); unc-33(e204)* and *mec-7(ky852); vab-8(e1017)* double mutants have significantly more wild-type ALMs and less severe ALM defects compared with the *mec-7(ky852)* mutant (chi-square test: $p < 0.001$). (B) ALM phenotypes in *mec-7(ky852)*; *cwn-1; cwn-2* triple mutants. The *mec-7(ky852)* mutation converts the reversed unipolar neurons generated in *cwn-1; cwn-2* double mutant animals into bipolar neurons. Each data set is based on an *n* of at least 100 animals.

cones (Wightman *et al.*, 1996; Wolf *et al.*, 1998; Lai and Garriga, 2004). Indeed, mutations in *vab-8* could partially suppress the *mec-7(ky852)* ALM phenotype (Figure 5A and Table S1). Furthermore, several molecules that have been proposed to act downstream of VAB-8 in axon outgrowth, such as UNC-40 and UNC-73 (Levy-Strumpf and Culotti, 2007; Watari-Goshima *et al.*, 2007) with its interacting partner CED-10/Rac (Steven *et al.*, 1998; Spencer *et al.*, 2001), could also partially suppress the ALM outgrowth phenotype (Table S1). Together these results suggest that VAB-8 and other downstream molecules interact with mutant MEC-7/β-tubulin to coordinate posterior neurite outgrowth.

Finally, we examined interactions with Wnt molecules, which act redundantly in ALM polarity (Hilliard and Bargmann, 2006; Prasad and Clark, 2006). Loss of specific combinations of Wnt molecules, such as in *cwn-1 cwn-2* double mutants, results in the development of bipolar and reversed ALMs. Reversed ALMs remain monopolar but have an opposite orientation within the animal's body, with their single process extending posteriorly toward the tail. We asked whether the *mec-7(ky852)* mutation was able to transform a reversed unipolar ALM into a bipolar ALM, thus indicating an independent mechanism of action. We found that in triple mutants *mec-7(ky852) cwn-1 cwn-2*, 100% of the reversed ALM neurons extended an ectopic anterior process (Figure 5B and Table S1), distinguishable from a normal ALM process, because it had not extended in the L1 and did not reach the nerve ring (unpublished data). This suggests that the function of *mec-7(ky852)* is preserved regardless of the orientation of the neuron, and is independent from this polarity effect of the Wnt mutations.

Mutant β-tubulin alters synaptic localization and axonal transport

Presynaptic loci are important elements that define the axonal identity of a neurite (Nonet, 1999; Hilliard and Bargmann, 2006; Mahoney *et al.*, 2006; Ou *et al.*, 2011). We investigated whether the ectopic posterior neurite in the ALM neuron of *mec-7(ky852)* mutants had axon-like properties, and whether the mutation could alter the normal distribution of presynaptic loci in the anterior process. In wild-type animals, ALM neurons have presynaptic sites located on a short branch of the anterior process that enters the nerve ring (Figure 6, A and E). Presynaptic densities can be labeled by the vesicle-associated Ras GTPase, RAB-3 (Nonet *et al.*, 1997; Nonet, 1999; Mahoney *et al.*, 2006). We used a *Pmec-4::mCherry::rab-3* transgene to visualize the presynaptic sites specifically in the mechanosensory neurons of wild type and *mec-7(ky852)* mutants. A high percentage of *mec-7(ky852)* animals displayed mCherry::RAB-3 expression on the ectopic posterior process of the ALM neurons (Figure 6, B and E). The presence of the presynaptic marker on the ectopic process indicates that it has acquired an axon-like identity, indicating that the ALM neuron in the *mec-7(ky852)* animals has been changed from a cell with a single axon to a cell with two axon-like neurites. However, among those animals that ectopically expressed mCherry::RAB-3 on the posterior ALM process, approximately half also showed a loss of synapses from the normal anterior process of ALM, suggesting that the *ky852* mutation might compromise the normal transport of vesicles to the anterior neurite. To determine whether this could occur in other neurons, we investigated the presynaptic distribution in the bipolar PLM neuron of *mec-7(ky852)* mutants. Interestingly, we found that, similar to ALM, the transport of presynaptic vesicles in PLM was altered in the mutants. In the PLM neurons of mutant animals, the RAB-3 presynaptic marker was mislocalized to the posterior neurite, with only a small percentage of selective localization on the anterior neurite, as in wild-type animals (Figure S3).

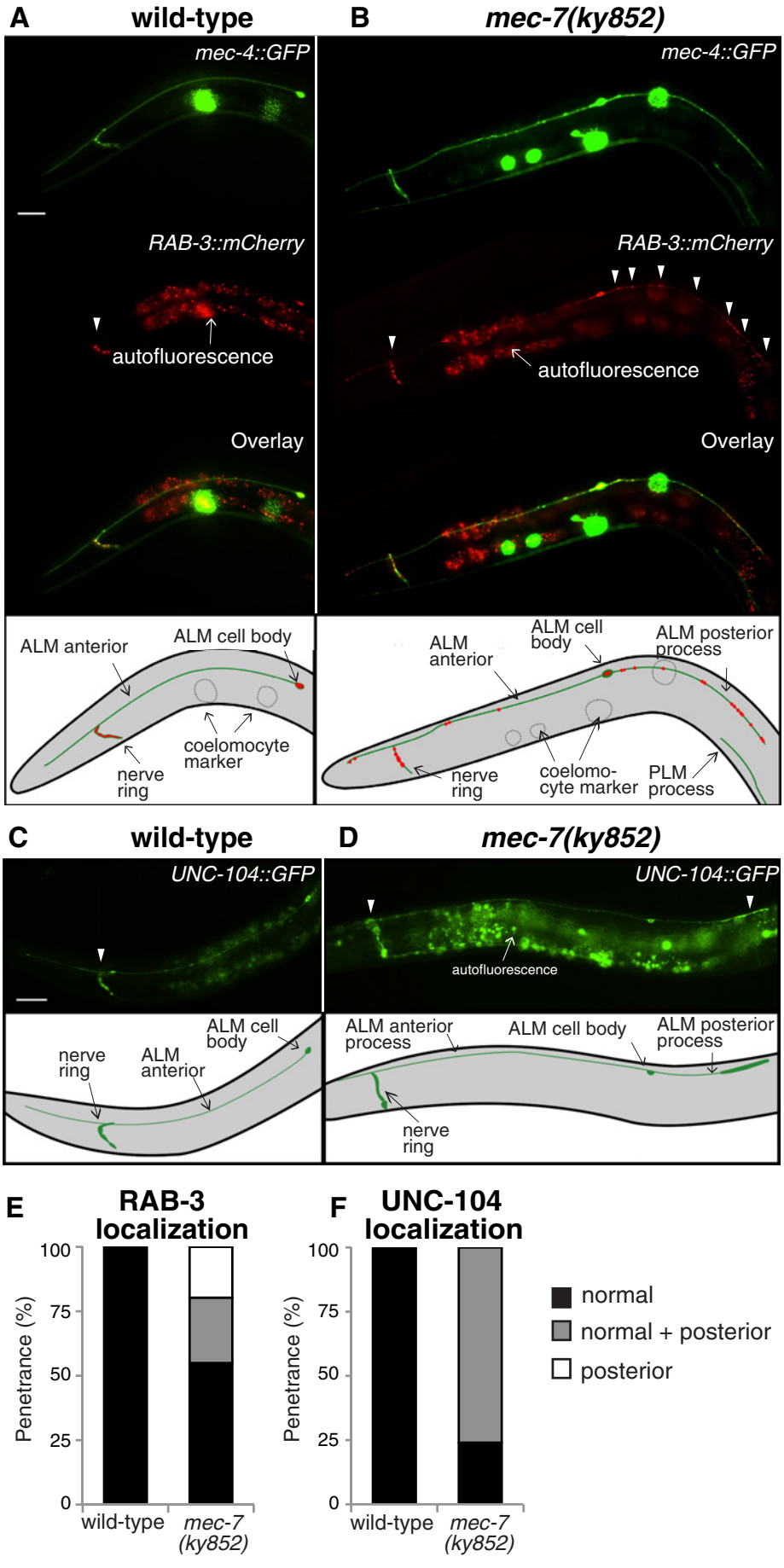

Anterograde transport of synaptic vesicles along axonal microtubules is mediated by the UNC-104/KIF1A motor protein (Hall and Hedgecock, 1991). To investigate whether this machinery was compromised in the *mec-7(ky852)* animals, we examined its localization in the ALM mechanosensory neurons of wild-type animals and *mec-7(ky852)* mutants using a *Pmec-4::unc-104::GFP* transgene. In wild-type mechanosensory neurons, UNC-104::GFP is expressed throughout the cell body and axon and is strongly localized to presynaptic sites (Kumar *et al.*, 2011; Figure 6C). In *mec-7(ky852)* mutants, UNC-104::GFP appeared to localize normally in the anterior ALM process; however, it was also enriched in the terminals of the ectopic posterior processes (Figure 6, D and F), indicating a failure to restrict transport to the anterior process. As expected, the ectopic UNC-104::GFP appeared to colocalize with RAB-3 (unpublished data). Together these results suggest that *mec-7(ky852)* animals have mislocalized transport of synaptic vesicles into the ectopic posterior processes, which gives them an axon-like identity.

Axonal regeneration is inhibited in *mec-7(ky852)* mutants

The likelihood that an axon will regrow following injury has been closely linked to the presence of presynaptic loci, as axons regenerate poorly when they are severed distally from presynaptic sites (Wu *et al.*, 2007).

FIGURE 6: Distribution of RAB-3 and UNC-104/kinesin in ALM neurons of *mec-7(ky852)* mutants. (A) Normal localization of the RAB-3::mCherry presynaptic marker in ALM neurons of wild-type animals. White arrowheads indicate RAB-3 in the nerve ring branch of ALM. Gray dashed circles represent coelomocytes expressing GFP that were used as a transgenic marker. (B) RAB-3::mCherry localizes to the posterior processes of ALM neurons in *mec-7(ky852)* mutants. White arrowheads indicate RAB-3 in the nerve ring branch and ectopic posterior process of ALM. (C) UNC-104::GFP localization in ALM neurons of wild-type animals. Localization of UNC-104 is indicated (white arrowheads). (D) UNC-104::GFP localizes to the posterior processes of ALM neurons in *mec-7(ky852)* mutants. (E) Quantification of RAB-3::mCherry localization on the anterior processes and on the posterior processes of ALM neurons. (F) Quantification of UNC-104::GFP localization on the anterior and posterior processes of ALM neurons. Each data set is based on an *n* of at least 50 animals. Scale bar: 25 μm.

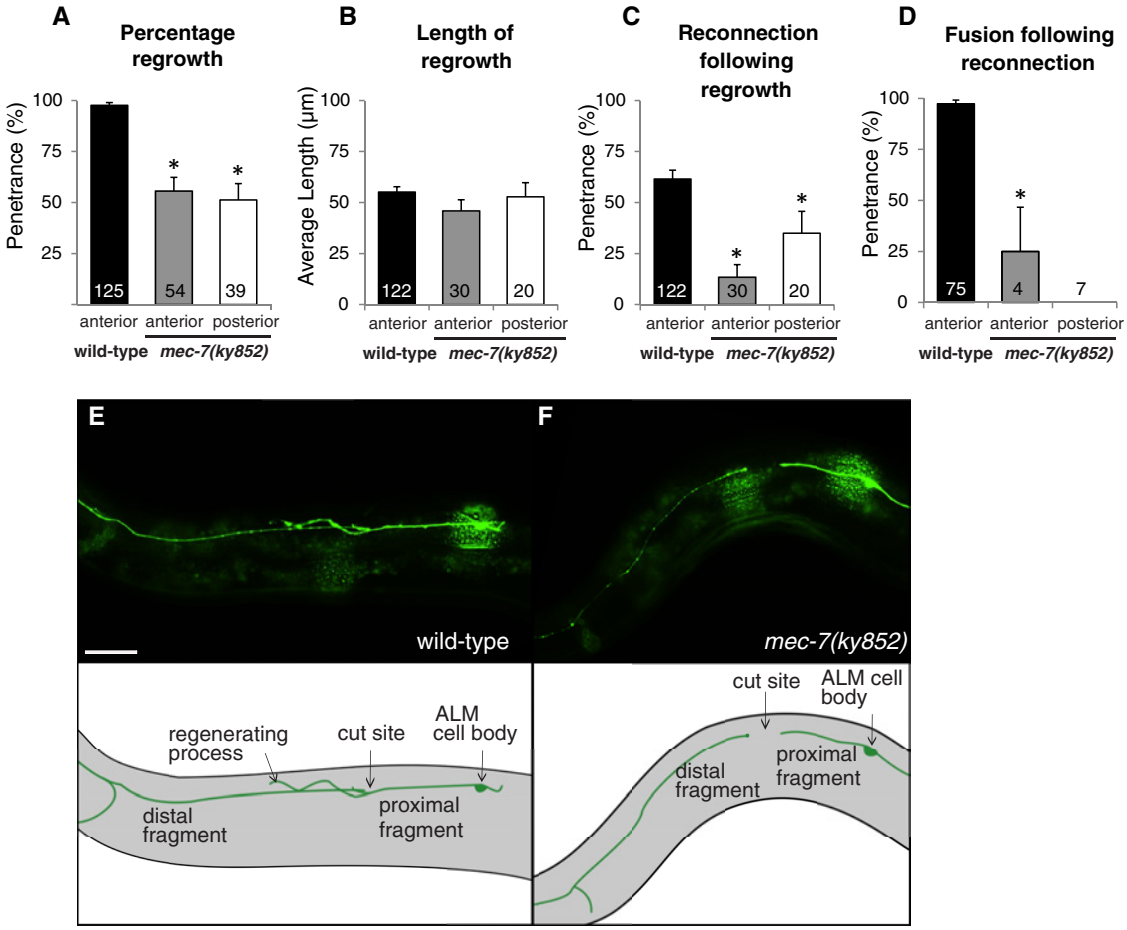

FIGURE 7: Axonal regeneration defects in *mec-7(ky852)* mutants. Regeneration of the anterior ALM process in wild-type animals and both the anterior and posterior ALM processes in mutants is shown in each graph. (A) Percentage of ALM neurons showing regrowth following axotomy in wild-type and *mec-7(ky852)* animals. (B) Quantification of the average length of regrowth of regenerating axons shown in (A). (C and D) Percentage of ALM neurons showing reconnection of the regenerating process to the distal fragment, and of these reconnected axons, the percentage showing maintenance of the connection (fusion). (E and F) Images showing axonal regeneration in a wild-type animal (E) and defective axonal regeneration a *mec-7(ky852)* mutant (F). In wild-type animals, the regenerating axon regrows from the proximal fragment (closest to the cell body) to the distal fragment of the ALM neuron. *n* for each data set is indicated on the bars of the graph. Error bars represent the SE of proportion. *, significant difference between wild-type and mutant animals (Student's *t* test: $p < 0.05$).

Our observation that *mec-7(ky852)* animals displayed mislocalization of the RAB-3 presynaptic marker suggested that this might influence their capacity for axonal regeneration. To test whether this was the case, we used laser axotomy to sever the axons of ALM neurons in wild-type and mutant animals and then quantified the level of regeneration. As previously shown by us and by others, ALM presents a high rate of regeneration following injury, with the regrowing proximal axon extending toward the distal fragment and often reconnecting with it by means of axonal fusion, which restores the axonal tract (Yanik *et al.*, 2006; Wu *et al.*, 2007; Ghosh-Roy *et al.*, 2011; Neumann *et al.*, 2011). Interestingly, regeneration of both the anterior and posterior neurites was reduced in *mec-7(ky852)* mutants (Figure 7). *mec-7(ky852)* animals displayed a reduced capacity to initiate axon regrowth (Figure 7A); however, axon extension was normal, as the average length of regrowth in animals that could initiate regeneration was similar to that of wild-type animals (Figure 7B). Furthermore, regrowing ALM neurites in *mec-7(ky852)* mutants displayed a reduced rate of axonal reconnection and fusion compared with wild-type animals (Figure 7, C and D). To determine whether these defects also extended to other neurons, we tested the regenerative capacity of PLM. Neurite regeneration was also altered in this cell, similar to ALM, with strongly reduced initiation of regrowth and reduced fusion (Figure S4). These results suggest that the *mec-7(ky852)* mutation causes defects in multiple aspects of axonal regeneration, including regrowth initiation and reconnection with separated distal fragments.

DISCUSSION

Studies in cultured neurons have demonstrated that regulation of microtubule dynamics plays a crucial role in determining whether an immature neurite develops into an axon. Nevertheless, evidence that this can occur in vivo has been lacking. Witte *et al.* (2008) recently demonstrated that local stabilization of microtubules in cultured hippocampal neurons is sufficient to induce axon formation, and suggested that microtubules play an active, instructive role in specifying axonal identity. Our study provides evidence that a single point mutation in the *mec-7/β-tubulin* gene can lead to outgrowth of secondary axon-like neurites. Interestingly, we find that the same

mutation inhibits axonal regeneration in these neurons. Together our results indicate that the mutant form of β-tubulin affects multiple aspects of neuronal development and repair, and suggest that there are critical differences between axonal growth and regeneration.

We have identified a novel allele of *mec-7/β-tubulin* that causes an unusual polarity phenotype in the ALM mechanosensory neurons, inducing the outgrowth of an additional neurite, which transforms them into bipolar neurons. The precision of this phenotype is remarkable: the neurons in the mutant animals are consistently bipolar (rather than multipolar), and the long ectopic processes always grow in the posterior direction. Such precise ectopic neurite outgrowth along the anterior–posterior axis has also been observed in the six *C. elegans* VC motor neurons (VC1–6), suggesting the involvement of common factors (Sanchez-Alvarez *et al.*, 2011). These phenotypes may be explained by the presence of extracellular factors, or intrinsic cell signals, that bias the direction of outgrowth. A number of studies have identified mutations in guidance cues, receptors, and intracellular proteins that cause ALM polarity defects (Wolf *et al.*, 1998; Hilliard and Bargmann, 2006; Levy-Strumpf and Culotti, 2007; Watari-Goshima *et al.*, 2007; Pan *et al.*, 2008). However, the phenotypes observed in these studies differed from those in the *mec-7(ky852)* animals, as they predominantly showed complete inversion of ALM polarity and were generated during the embryonic development of the ALM neuroblast (Hilliard and Bargmann, 2006), rather than postembryonically. Finally, our finding that inverted ALM neurons caused by Wnt mutations were transformed into bipolar neurons in a *mec-7(ky852)* mutant background suggests that the outgrowth of the *mec-7(ky852)* ectopic process is mediated by an intrinsic cell bias, which may operate independently of neuronal polarity established by Wnts. Our study suggests that the kinesin-like protein,VAB-8, recruits molecules required for the posterior neurite outgrowth seen in the *mec-7(ky852)* mutants. Whether VAB-8 binds directly to tubulin remains to be investigated.

In cultured cells, neuronal polarization is considered to occur when a preexisting immature neurite transforms into an axon (Polleux and Snider, 2010; Namba *et al.*, 2011). In such cases, the number of potential axons and their directions of outgrowth are dependent on the location and number of immature neurites. In contrast, *C. elegans* ALM neurons usually lack secondary neurites, with only a small proportion of animals presenting a short posterior protrusion, which may be indicative of a preexisting intrinsic cell bias. Thus the ALM ectopic posterior process observed in the *mec-7(ky852)* mutants usually emerges directly from the cell body. This suggests that mutations in *mec-7/β-tubulin* can alter the entire process of axon formation in vivo, from the initial emergence of the neurite to its full extension into an axon-like process containing presynaptic sites.

Our results suggest that microtubule stabilization contributes to the regulation of axon outgrowth in vivo. First, application of paclitaxel to wild-type animals was sufficient to trigger the outgrowth of ectopic processes. Second, colchicine treatment could rescue the ectopic ALM outgrowth in *mec-7(ky852)* mutants, suggesting that microtubules could mitigate the effect of the mutation. Whether the *ky852* mutation can specifically confer microtubule hyperstability remains unclear. One possibility is that it might alter the structure of tubulin polymers, such that they interfere with normal microtubule dynamics, slowing or preventing microtubule breakdown. Alternatively, the mutation may alter the binding or transport of molecules that regulate microtubule stability. Our finding that UNC-33/CRMP could suppress the *mec-7(ky852)* ALM phenotype suggests that the binding of this molecule, which has been shown to regulate microtubule structure, dynamics, and transport (Fukata *et al.*, 2002; Maniar *et al.*, 2012), may contribute to excessive axon outgrowth, consistent with the results of overexpression studies in hippocampal neurons (Inagaki *et al.*, 2001).

The ectopic localization of the RAB-3 presynaptic marker and the UNC-104/KIF1A motor protein in the posterior ALM processes of *mec-7(ky852)* animals suggests that the mutant microtubules affect normal intracellular transport. Notably, defects in synapse and axon outgrowth have recently been observed in *C. elegans* mutants of other tubulin subunits (Baran *et al.*, 2010), further indicating that the nature of microtubules and their potential interactions with motor proteins is crucial for normal axonal transport. Intracellular transport of proteins is dependent on the intrinsic polarity of microtubules, which have dynamic plus ends that undergo rapid growth or collapse, and more stable minus ends (Howard and Hyman, 2003). These polarized polymers serve as one-way conduits for intracellular trafficking by plus end–directed or minus end–directed motor proteins (Baas and Lin, 2011) and are thus crucial for axon development and maintenance. Interestingly, UNC-33 is required for polarization of microtubule subunits and directed transport of synaptic proteins into the axon of PVD neurons (Maniar *et al.*, 2012). Polarized transport has also been shown to be essential for correct synapse localization to the axon of the *C. elegans* DA9 motor neuron and for transport of polarity proteins into the axon in cultured neurons (Nishimura *et al.*, 2004; Shi *et al.*, 2004; Ou *et al.*, 2011). The plus end–directed kinesin-1 motor domain has been reported to selectively accumulate in a neurite prior to its specification as an axon (Jacobson *et al.*, 2006). Therefore it is possible that intrinsic microtubule polarity could provide an initial cue for axon formation by promoting movement of cargo by axon-specific kinesins into the developing axon.

The altered transport of synaptic proteins in *mec-7(ky852)* mutants may also be a cause of their axonal regeneration defects. Following injury, rapid signaling must occur between the site of injury and the cell body in order to initiate regeneration (Abe and Cavalli, 2008). This is reliant on the transport of proteins, as impairment of axonal transport mechanisms has been found to affect regrowth of PLM in *C. elegans* (Chen *et al.*, 2011). Therefore it is possible that *mec-7(ky852)* regeneration defects are partly due to a failure of axonal transport following injury. Another possible explanation is that regeneration may be triggered only when the cell body detects a loss of synapses. This hypothesis is consistent with the findings of Wu *et al.* (2007), who showed that axons of *C. elegans* mechanosensory neurons severed distally to the presynaptic sites (i.e., with presynaptic sites still connected to the cell body) fail to regenerate and, furthermore, that regeneration can be rescued by severing the branch containing presynaptic sites. Thus, it is possible that in *mec-7(ky852)* mutants, which often lack presynaptic sites in the axons, the cell fails to detect a loss of synapses following severing of its axon and consequently fails to signal for regeneration to occur. Future studies are required to determine whether the defects in axonal regeneration observed in these mutants are caused by impairment of axonal transport or by alterations to the synaptic sites, or whether an alternative mechanism is in place.

Although emerging evidence suggests that the regulation of microtubule dynamics is a crucial determinant of axonal regenerative capacity (Erturk *et al.*, 2007; Stone *et al.*, 2010; Chen *et al.*, 2011; Hellal *et al.*, 2011; Sengottuvel and Fischer, 2011), a direct role for β-tubulin in regeneration has not been shown. Regeneration of an axon requires drastic remodeling of cell shape, which relies on dynamic instability of the cytoskeleton. An axon must first sprout a new process with a growth cone at its tip; this must then extend in the correct direction to reconnect with its target tissue. Interestingly, although regrowth initiation and reconnection to the distal process

are inhibited in the *mec-7(ky852)* mutants, there are no apparent deficits in extension of regrowing axons. It is therefore likely that regrowth initiation and reconnection by axonal fusion require comparatively greater structural changes to the cytoskeleton than axon extension. Thus *mec-7(ky852)* mutations may differentially affect distinct stages of regeneration, depending on their specific requirements for dynamic microtubules.

This study of a *C. elegans* β-tubulin mutant has revealed a central role for microtubules in axon outgrowth and regeneration in vivo. Our findings contribute to growing evidence that precise microtubule dynamics are essential for neuronal development, maintenance, and repair. Mutations in human tubulin have been found to cause neurodevelopmental and neurodegenerative diseases (Kuijpers and Hoogenraad, 2011; Tischfield *et al.*, 2011). As β-tubulin is highly conserved across species, understanding its function in model organisms has the potential to provide important insights into microtubule-related neuropathies in humans.

MATERIALS AND METHODS

Strains

Nematodes were cultured under standard conditions (Brenner, 1974). All experiments were performed at 22°C on hermaphrodite animals. The Hawaiian CB4856 strain was used for SNP mapping of the *mec-7(ky852)* mutation (Wicks *et al.*, 2001; Davis *et al.*, 2005; Davis and Hammarlund, 2006). The wild-type Bristol N2 strain and the following mutations were used: LGX: *mec-7(ky852), mec-7(u278)*; LGI: *unc-73(e936), mig-2(mu28), unc-40(e1430)*; LGII: *cwn-1(ok546)*; LGIII: *mig-10(ct41), ptl-1(ok621)*; LGIV: *ced-10(n3246), unc-33(e204), cwn-2(ok895)*; and LGV: *vab-8(e1017)*. Transgenes used were: *zdIs5*[*Pmec-4::GFP*]; *juIs76*[*Punc-25::GFP*]; *vdEx262*[*Pmec-4::mCherry::rab-3 (0.5 ng/μl), Punc-122::GFP (25 ng/μl)*]; *vdEx309*[*Pmec-4::mec-7 (5 ng/μl), Podr-1::dsRed (30 ng/μl)*]; *vdEx312*[*Pmec-4::mec-7 (10 ng/μl), Podr-1::dsRed (30 ng/μl)*]; *jsIs1111*[*Pmec-4::unc-104::GFP*]; *vdEx263*[*(Pmec-4::mCherry (5 ng/μl), Podr-1::dsRed (30 ng/μl)*]; *vdEx326* [*Pmec-4::mec-7(ky852) (5 ng/μl), Podr-1::dsRed (30 ng/μl)*]; *vdEx329*[*Pmec-4::mec-7(ky852)(10 ng/μl), Podr-1::dsRed (30 ng/μl)*]. The *jsIs1111* strain was a kind gift from Sandhya Koushika (Tata Institute of Fundamental Research, Bangalore, India).

Molecular biology

Standard molecular biology techniques were used (Sambrook and Russell, 2001). The *Pmec-4::mec-7::unc-54* 3′UTR plasmid was generated through excision of the GFP coding sequences from the *Pmec-4::GFP* plasmid and subsequent insertion of the entire *mec-7* coding sequence (amplified from N2 DNA, with the following primers: forward, 5′-tcagtgggatccaagcaacatgcgcgagatcg-3′; reverse, 5′-tcagtggatccatttactctccgtcgaacgc-3′). The *Pmec-4::mec-7(ky852)::unc-54* 3′UTR plasmid was generated by QuikChange Site-Directed Mutagenesis (Agilent, Santa Clara, CA) using the *Pmec-4::mec-7::unc-54* 3′UTR as template DNA and the following primers to introduce the *ky852* mutation: sense, 5′-cactctgaaactgacgacatcgacatatggagacc-3′; antisense, 5′-ggtctccatatgtcgatgtcgtcagtttcagagtg-3′. The *Pmec-4::mCherry::RAB-3::unc-54* 3′UTR plasmid was created through modification of the *Pmec-4::GFP* plasmid. First, the coding sequence for GFP was excised and replaced with that of mCherry. Next the *rab-3* coding sequence, which was amplified from the *Prab-3::eGFP::RAB-3::rim-3* 3′UTR plasmid (a kind gift from Michael Nonet, St. Louis, MO), was inserted downstream from mCherry.

Phenotypic analyses

ALM morphology was analyzed at the L4 or adult stage in a *zdIs5(Pmec-4::GFP)* background. Although ALM neurons in wild-type *zdIs5* animals are usually monopolar, some have a small posterior protrusion that is less than two cell bodies in length. The ALM posterior process defect in *mec-7(ky852)* animals was considered to be moderate when the process was between 2 and 15 cell bodies in length, and severe when greater than 15 cell bodies in length. AVM, PVM, and PLM mechanosensory neurons were also analyzed for axon outgrowth and overextension phenotypes in L4 and adult animals.

Developmental analysis of ALM morphology in the *mec-7(ky852)* mutant was performed in embryos and in synchronized populations of hatched animals. Animals were synchronized by collecting newly hatched larvae from a plate containing only eggs. Newly hatched L1 animals were either scored immediately or transferred to new plates and grown on food for 5 h or until adulthood before scoring. In embryos and L1 animals, ALM neurons were scored as defective if a posterior process was observed (in wild-type animals, posterior processes were never observed at these early stages).

Microscopy and laser axotomy

Animals were immobilized in 0.01–0.05% tetramisole hydrochloride on 4% agar pads and visualized using Zeiss Axioimager Z1 and Zeiss Axioimager A1 microscopes (Jena, Germany). Images were taken using a Photometrics camera (Cool Snap HQ^2; Tucson, AZ) and analyzed with MetaMorph software (Molecular Devices, Sunnyvale, CA). Individual planes from Z-stacks were combined in Adobe Photoshop (San Jose, CA). Axotomies were performed as previously described (Neumann *et al.*, 2011). A MicroPoint laser system basic unit (Andor, Belfast, UK) was used to perform axonal transection on L4 animals at a point ~50 μm anterior to the ALM and PLM cell bodies. For analysis of regeneration in the posterior ALM axon in *mec-7(ky852)* animals, axotomy was performed ~50 μm posterior to the cell body. Axonal regrowth was quantified by measuring the length of the longest neurite beyond the cut site 24 h postaxotomy; neurons that underwent axonal fusion were excluded from these quantifications.

Colchicine and paclitaxel treatment

Animals were grown on nematode growth medium agar plates containing colchicine (Sigma-Aldrich, St. Louis, MO) or paclitaxel (Sigma-Aldrich) with dimethyl sulfoxide, as previously described (Chalfie and Thomson, 1982).

Statistical analyses

Primer of Biostatistics 3.01 and GraphPad Prism (La Jolla, CA) were used for statistical analyses. Error of proportions was used to estimate variation within a single population. The Student's *t* test or Mann-Whitney rank sum test were used as indicated. The chi-square test was performed to estimate variance in the distribution of phenotypes between wild-type and mutant populations.

ACKNOWLEDGMENTS

We thank Cori Bargmann, in whose lab this work started; Martin Chalfie, Sandhya Koushika, Michael Nonet, Nick Valmas, and Casey Linton for sharing reagents; Paolo Bazzicalupo, Rowan Tweedale, Helen Cooper, and members of the Hilliard Lab for helpful discussion and comments on the manuscript; and Luke Hammond and Paula Mugno for technical assistance. Nematode strains used in this work were provided by the *Caenorhabditis* Genetics Center, which is funded by the National Institutes of Health (NIH) National Center for Research Resources, and the International *C. elegans* Gene Knockout Consortium. This work was funded by the National Health and Medical Research Council of Australia (NHMRC) and the NIH and was supported by the Queensland Brain Institute.

REFERENCES

Abe N, Cavalli V (2008). Nerve injury signaling. Curr Opin Neurobiol 18, 276–283.

Adler CE, Fetter RD, Bargmann CI (2006). UNC-6/Netrin induces neuronal asymmetry and defines the site of axon formation. Nat Neurosci 9, 511–518.

Baas PW (2002). Neuronal polarity: microtubules strike back. Nat Cell Biol 4, E194–E195.

Baas PW, Lin S (2011). Hooks and comets: the story of microtubule polarity orientation in the neuron. Dev Neurobiol 71, 403–418.

Baran R, Castelblanco L, Tang G, Shapiro I, Goncharov A, Jin Y (2010). Motor neuron synapse and axon defects in a *C. elegans* alpha-tubulin mutant. PLoS One 5, e9655.

Bounoutas A, O'Hagan R, Chalfie M (2009). The multipurpose 15-protofilament microtubules in *C. elegans* have specific roles in mechanosensation. Curr Biol 19, 1362–1367.

Bradke F, Dotti CG (1999). The role of local actin instability in axon formation. Science 283, 1931–1934.

Brenner S (1974). The genetics of *Caenorhabditis elegans*. Genetics 77, 71–94.

Chalfie M, Sulston J (1981). Developmental genetics of the mechanosensory neurons of *Caenorhabditis elegans*. Dev Biol 82, 358–370.

Chalfie M, Thomson JN (1982). Structural and functional diversity in the neuronal microtubules of *Caenorhabditis elegans*. J Cell Biol 93, 15–23.

Chang C, Adler CE, Krause M, Clark SG, Gertler FB, Tessier-Lavigne M, Bargmann CI (2006). MIG-10/lamellipodin and AGE-1/PI3K promote axon guidance and outgrowth in response to slit and netrin. Curr Biol 16, 854–862.

Chen L, Wang Z, Ghosh-Roy A, Hubert T, Yan D, O'Rourke S, Bowerman B, Wu Z, Jin Y, Chisholm AD (2011). Axon regeneration pathways identified by systematic genetic screening in *C. elegans*. Neuron 71, 1043–1057.

Davis MW, Hammarlund M (2006). Single-nucleotide polymorphism mapping. Methods Mol Biol 351, 75–92.

Davis MW, Hammarlund M, Harrach T, Hullett P, Olsen S, Jorgensen EM (2005). Rapid single nucleotide polymorphism mapping in *C. elegans*. BMC Genomics 6, 118.

Erturk A, Hellal F, Enes J, Bradke F (2007). Disorganized microtubules underlie the formation of retraction bulbs and the failure of axonal regeneration. J Neurosci 27, 9169–9180.

Fojo T (2008). The Role of Microtubules in Cell Biology, Neurobiology, and Oncology, Totowa, NJ: Humana.

Fukata Y *et al.* (2002). CRMP-2 binds to tubulin heterodimers to promote microtubule assembly. Nat Cell Biol 4, 583–591.

Ghosh-Roy A, Wu Z, Goncharov A, Jin Y, Chisholm AD (2011). Calcium and cyclic AMP promote axonal regeneration in *Caenorhabditis elegans* and require DLK-1 kinase. J Neurosci 30, 3175–3183.

Goedert M, Baur CP, Ahringer J, Jakes R, Hasegawa M, Spillantini MG, Smith MJ, Hill F (1996). PTL-1, a microtubule-associated protein with tau-like repeats from the nematode *Caenorhabditis elegans*. J Cell Sci 109, 2661–2672.

Hall DH, Hedgecock EM (1991). Kinesin-related gene *unc-104* is required for axonal transport of synaptic vesicles in *C. elegans*. Cell 65, 837–847.

Hamelin M, Scott IM, Way JC, Culotti JG (1992). The *mec-7* β-tubulin gene of *Caenorhabditis elegans* is expressed primarily in the touch receptor neurons. EMBO J 11, 2885–2893.

Hedgecock EM, Culotti JG, Thomson JN, Perkins LA (1985). Axonal guidance mutants of *Caenorhabditis elegans* identified by filling sensory neurons with fluorescein dyes. Dev Biol 111, 158–170.

Hellal F *et al.* (2011). Microtubule stabilization reduces scarring and causes axon regeneration after spinal cord injury. Science 331, 928–931.

Hilliard MA, Bargmann CI (2006). Wnt signals and frizzled activity orient anterior-posterior axon outgrowth in *C. elegans*. Dev Cell 10, 379–390.

Hoogenraad CC, Bradke F (2009). Control of neuronal polarity and plasticity—a renaissance for microtubules. Trends Cell Biol 19, 669–676.

Howard J, Hyman AA (2003). Dynamics and mechanics of the microtubule plus end. Nature 422, 753–758.

Inagaki N, Chihara K, Arimura N, Menager C, Kawano Y, Matsuo N, Nishimura T, Amano M, Kaibuchi K (2001). CRMP-2 induces axons in cultured hippocampal neurons. Nat Neurosci 4, 781–782.

Jacobson C, Schnapp B, Banker GA (2006). A change in the selective translocation of the kinesin-1 motor domain marks the initial specification of the axon. Neuron 49, 797–804.

Jiang H, Guo W, Liang X, Rao Y (2005). Both the establishment and the maintenance of neuronal polarity require active mechanisms: critical roles of GSK-3β and its upstream regulators. Cell 120, 123–135.

Kishi M, Pan YA, Crump JG, Sanes JR (2005). Mammalian SAD kinases are required for neuronal polarization. Science 307, 929–932.

Kuijpers M, Hoogenraad CC (2011). Centrosomes, microtubules and neuronal development. Mol Cell Neurosci 48, 349–358.

Kumar J, Choudhary BC, Metpally R, Zheng Q, Nonet ML, Ramanathan S, Klopfenstein DR, Koushika SP (2011). The *Caenorhabditis elegans* kinesin-3 motor UNC-104/KIF1A is degraded upon loss of specific binding to cargo. PLoS Genet 6, e1001200.

Lai T, Garriga G (2004). The conserved kinase UNC-51 acts with VAB-8 and UNC-14 to regulate axon outgrowth in *C. elegans*. Development 131, 5991–6000.

Levy-Strumpf N, Culotti JG (2007). VAB-8, UNC-73 and MIG-2 regulate axon polarity and cell migration functions of UNC-40 in *C. elegans*. Nat Neurosci 10, 161–168.

Mahoney TR, Liu Q, Itoh T, Luo S, Hadwiger G, Vincent R, Wang ZW, Fukuda M, Nonet ML (2006). Regulation of synaptic transmission by RAB-3 and RAB-27 in *Caenorhabditis elegans*. Mol Biol Cell 17, 2617–2625.

Maniar TA, Kaplan M, Wang GJ, Shen K, Wei L, Shaw JE, Koushika SP, Bargmann CI (2012). UNC-33 (CRMP) and ankyrin organize microtubules and localize kinesin to polarize axon-dendrite sorting. Nat Neurosci 15, 48–56.

Namba T, Nakamuta S, Funahashi Y, Kaibuchi K (2011). The role of selective transport in neuronal polarization. Dev Neurobiol 71, 445–457.

Neukirchen D, Bradke F (2011). Neuronal polarization and the cytoskeleton. Semin Cell Dev Biol 22, 825–833.

Neumann B, Nguyen KC, Hall DH, Ben-Yakar A, Hilliard MA (2011). Axonal regeneration proceeds through specific axonal fusion in transected *C. elegans* neurons. Dev Dyn 240, 1365–1372.

Nishimura T, Kato K, Yamaguchi T, Fukata Y, Ohno S, Kaibuchi K (2004). Role of the PAR-3-KIF3 complex in the establishment of neuronal polarity. Nat Cell Biol 6, 328–334.

Nonet ML (1999). Visualization of synaptic specializations in live *C. elegans* with synaptic vesicle protein-GFP fusions. J Neurosci Methods 89, 33–40.

Nonet ML, Staunton JE, Kilgard MP, Fergestad T, Hartwieg E, Horvitz HR, Jorgensen EM, Meyer BJ (1997). *Caenorhabditis elegans rab-3* mutant synapses exhibit impaired function and are partially depleted of vesicles. J Neurosci 17, 8061–8073.

Ou CY *et al.* (2011). Two cyclin-dependent kinase pathways are essential for polarized trafficking of presynaptic components. Cell 141, 846–858.

Pan CL, Baum PD, Gu M, Jorgensen EM, Clark SG, Garriga G (2008). AP-2 and retromer control Wnt signaling by regulating *mig-14/Wntless*. Dev Cell 14, 132–139.

Polleux F, Snider W (2010). Initiating and growing an axon. Cold Spring Harb Perspect Biol 2, a001925.

Prasad BC, Clark SG (2006). Wnt signaling establishes anteroposterior neuronal polarity and requires retromer in *C. elegans*. Development 133, 1757–1766.

Quinn CC, Pfeil DS, Wadsworth WG (2008). CED-10/Rac1 mediates axon guidance by regulating the asymmetric distribution of MIG-10/lamellipodin. Curr Biol 18, 808–813.

Sambrook J, Russell DW (2001). Molecular Cloning, 3rd ed., Cold Spring Harbor, NY: Cold Spring Harbor Laboratory.

Sanchez-Alvarez L, Visanuvimol J, McEwan A, Su A, Imai JH, Colavita A (2011). VANG-1 and PRKL-1 cooperate to negatively regulate neurite formation in *Caenorhabditis elegans*. PLoS Genet 7, e1002257.

Savage C, Hamelin M, Culotti JG, Coulson A, Albertson DG, Chalfie M (1989). *mec-7* is a β-tubulin gene required for the production of 15-protofilament microtubules in *Caenorhabditis elegans*. Genes Dev 3, 870–881.

Savage C, Xue Y, Mitani S, Hall D, Zakhary R, Chalfie M (1994). Mutations in the *Caenorhabditis elegans* β-tubulin gene *mec-7*: effects on microtubule assembly and stability and on tubulin autoregulation. J Cell Sci 107, 2165–2175.

Sengottuvel V, Fischer D (2011). Facilitating axon regeneration in the injured CNS by microtubule stabilization. Commun Integr Biol 4, 391–393.

Shi SH, Cheng T, Jan LY, Jan YN (2004). APC and GSK-3β are involved in mPar3 targeting to the nascent axon and establishment of neuronal polarity. Curr Biol 14, 2025–2032.

Spencer AG, Orita S, Malone CJ, Han M (2001). A RHO GTPase-mediated pathway is required during P cell migration in *Caenorhabditis elegans*. Proc Natl Acad Sci USA 98, 13132–13137.

Steven R, Kubiseski TJ, Zheng H, Kulkarni S, Mancillas J, Ruiz Morales A, Hogue CW, Pawson T, Culotti J (1998). UNC-73 activates the Rac GTPase and is required for cell and growth cone migrations in *C. elegans*. Cell 92, 785–795.

Stiess M, Bradke F (2011). Neuronal polarization: the cytoskeleton leads the way. Dev Neurobiol 71, 430–444.
Stone MC, Nguyen MM, Tao J, Allender DL, Rolls MM (2010). Global up-regulation of microtubule dynamics and polarity reversal during regeneration of an axon from a dendrite. Mol Biol Cell 21, 767–777.
Tischfield MA, Cederquist GY, Gupta ML Jr., Engle EC (2011). Phenotypic spectrum of the tubulin-related disorders and functional implications of disease-causing mutations. Curr Opin Genet Dev 21, 286–294.
Tsuboi D, Hikita T, Qadota H, Amano M, Kaibuchi K (2005). Regulatory machinery of UNC-33 Ce-CRMP localization in neurites during neuronal development in *Caenorhabditis elegans*. J Neurochem 95, 1629–1641.
Watari-Goshima N, Ogura K, Wolf FW, Goshima Y, Garriga G (2007). *C. elegans* VAB-8 and UNC-73 regulate the SAX-3 receptor to direct cell and growth-cone migrations. Nat Neurosci 10, 169–176.
White JG (1986). The structure of the nervous system of the nematode *C. elegans*. Philos Trans R Soc Lond B Biol Sci 314, 1–340.
Wicks SR, Yeh RT, Gish WR, Waterston RH, Plasterk RH (2001). Rapid gene mapping in *Caenorhabditis elegans* using a high density polymorphism map. Nat Genet 28, 160–164.
Wightman B, Clark SG, Taskar AM, Forrester WC, Maricq AV, Bargmann CI, Garriga G (1996). The *C. elegans* gene *vab-8* guides posteriorly directed axon outgrowth and cell migration. Development 122, 671–682.
Witte H, Bradke F (2008). The role of the cytoskeleton during neuronal polarization. Curr Opin Neurobiol 18, 479–487.
Witte H, Neukirchen D, Bradke F (2008). Microtubule stabilization specifies initial neuronal polarization. J Cell Biol 180, 619–632.
Wolf FW, Hung MS, Wightman B, Way J, Garriga G (1998). *vab-8* is a key regulator of posteriorly directed migrations in *C. elegans* and encodes a novel protein with kinesin motor similarity. Neuron 20, 655–666.
Wu Z, Ghosh-Roy A, Yanik MF, Zhang JZ, Jin Y, Chisholm AD (2007). *Caenorhabditis elegans* neuronal regeneration is influenced by life stage, ephrin signaling, and synaptic branching. Proc Natl Acad Sci USA 104, 15132–15137.
Yanik MF, Cinar H, Cinar HN, Chisholm A, Jin Y, Yakar AB (2006). Nerve regeneration in *C. elegans* after femtosecond laser axotomy. IEEE J Sel Top Quant 1283–1291.
Yoshimura T, Kawano Y, Arimura N, Kawabata S, Kikuchi A, Kaibuchi K (2005). GSK-3β regulates phosphorylation of CRMP-2 and neuronal polarity. Cell 120, 137–149.

2.3 Supplementary data

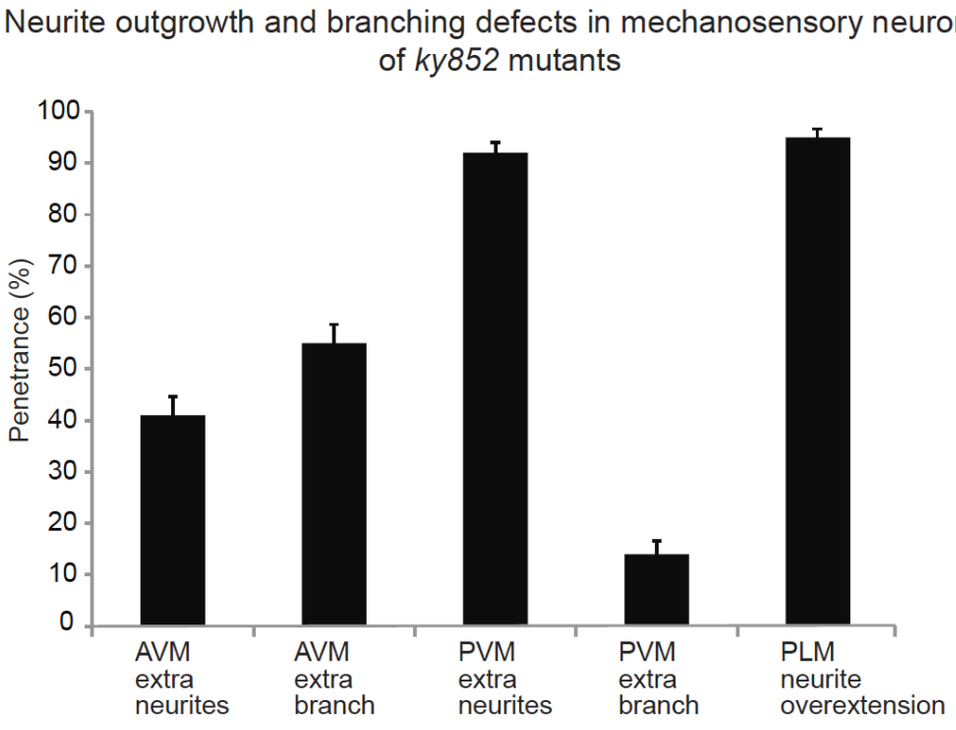

Supplemental Figure S1. Neurite outgrowth and branching defects in mechanosensory neurons of *ky852* mutants. Quantification of defects in AVM, PVM and PLM neurons. Each data set is based on an *n* of at least 100 animals. Error bars represent the s.e. of proportion.

Supplemental Table S1. Genetic analysis of ALM pheno-

	ALM Phenotype (%)					
Genotype	Normal	Moderate bipolar	Severe bipolar	Reversed	Reversed bipolar	n
wild-type *(zdIs5)*	99	1	0	0	0	210
ptl-1(ok621)	100	0	0	0	0	104
unc-33(e204)	100	0	0	0	0	102
vab-8(e1017)	88	12	0	0	0	114
mig-2(mu28)	93	7	0	0	0	100
mig-10(ct41)	94	6	0	0	0	100
unc-73(e936)	98	3	0	0	0	100
ced-10(n3246)	99	1	0	0	0	111
unc-40(e1430)	100	0	0	0	0	105
cwn-1(ok546); cwn -2(ok895)	52	42	2	4	0	102
mec-7(ky852)	0	18	82	0	0	110
mec-7(ky852); ptl-1	0	18	82	0	0	104
mec-7(ky852); unc-33	13	79	9	0	0	117
mec-7(ky852); vab-8	11	63	26	0	0	100
mec-7(ky852); mig-2	0	49	51	0	0	100
mec-7(ky852); mig-10	0	48	52	0	0	100
mec-7(ky852); unc-73	8	53	39	0	0	102
mec-7(ky852); ced-10	10	63	27	0	0	103
mec-7(ky852); unc-40	4	51	46	0	0	105
mec-7(ky852); cwn-1; cwn-2	0	39	56	0	5	105

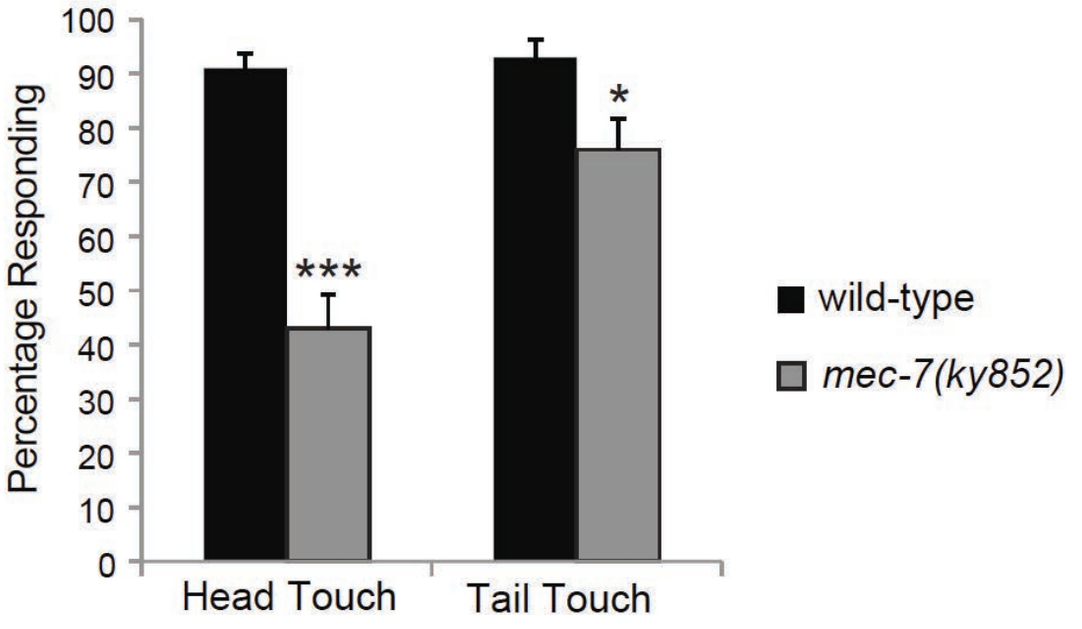

Supplementary Figure 2. *ky852* mutants have reduced touch sensitivity. Each data set is based on an *n* of 10 animals each tested 10 times. Error bars represent the s.e. of the mean. Asterisks indicate a significant difference between wild-type and mutant (Mann-Whitney *t*-test: * $p<0.05$, *** $p<0.0002$).

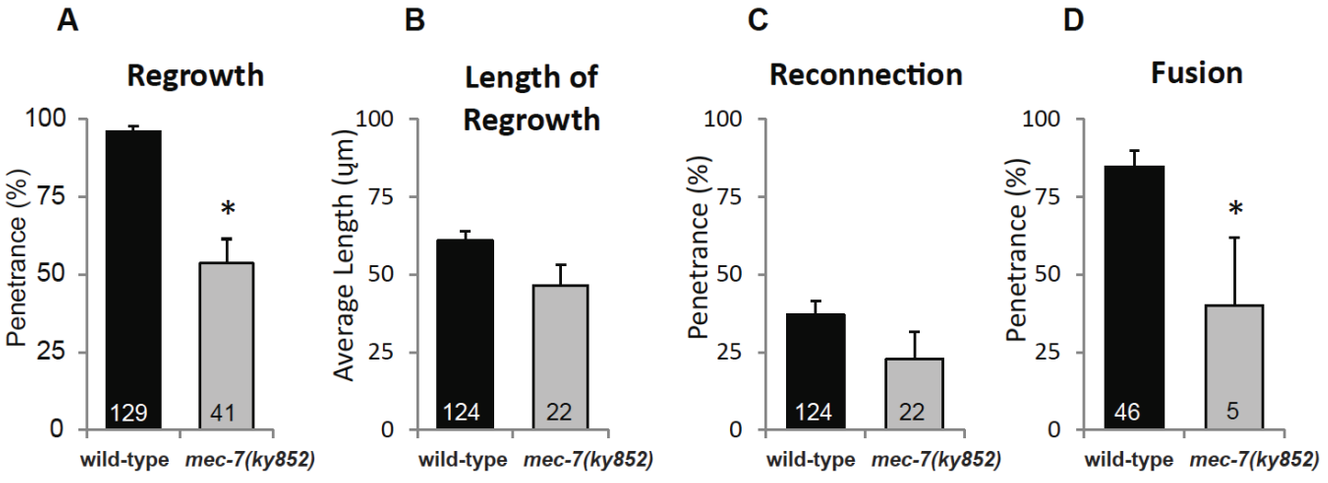

Supplementary Figure 3. Axonal regeneration defects in PLM neurons of *mec-7(ky852)* mutants. Regeneration of the anterior PLM process in wild type and *mec-7(ky852)* animals is shown in each graph. (A) Percentage of PLM neurons showing regrowth following axotomy. (B) Quantification of the average length of regrowth of regenerating axons shown in (A). (C, D) Percentage of PLM neurons showing reconnection of the regenerating process to the distal fragment, and of these reconnected axons, the percentage maintenance of the connection (fusion). *n* for each data set is indicated on the bars of the graph. Error bars represent the s.e. of proportion. Asterisks indicate a significant difference between wild-type and mutant animals (Student's *t*-test, $p<0.05$).

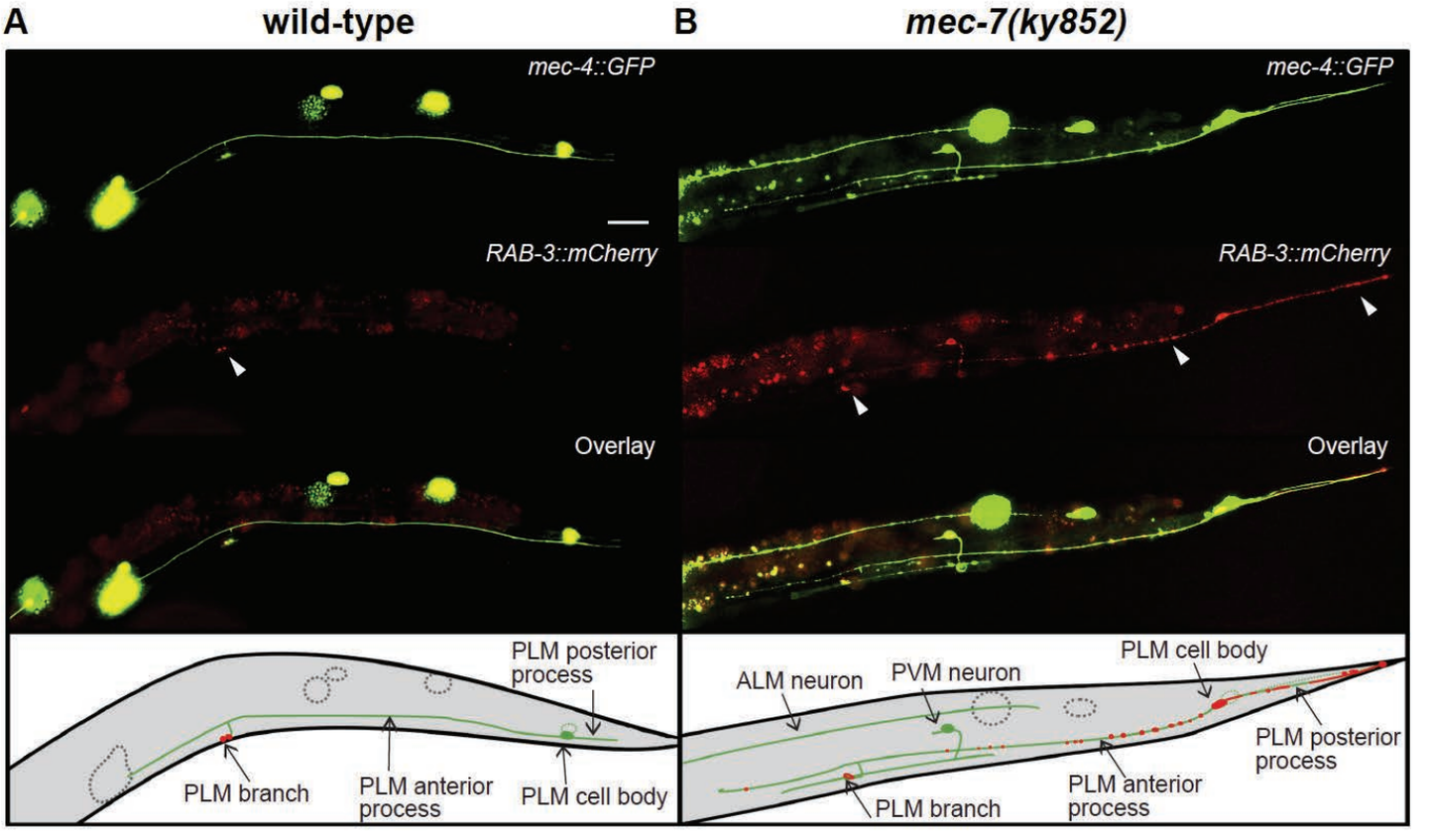

Supplementary Figure 4. RAB-3 localization in PLM neurons of *mec-7(ky852)* mutants. (A) Normal localization of the RAB-3::mCherry presynaptic marker to the synaptic branch in PLM neurons of wild-type animals. Grey dashed circles represent coelomocytes. (B) RAB-3::mCherry localizes to the posterior process of PLM neurons in *mec-7(ky852)* mutants. (C) Quantification of RAB-3::mCherry localization on the anterior processes and on the posterior processes of PLM neurons. Each data set is based on an *n* of at least 50 animals. Error bars represent the s.e. of proportion. Scale bar: 25µm

2.4 Discussion and implications of findings

The specification and outgrowth of the axonal process are critical events in the development of a mature neuron. Recent studies have identified molecules that initiate axon specification through the regulation of microtubule dynamics (Jiang et al., 2005; Kishi et al., 2005; Maniar et al., 2012; Yoshimura et al., 2005). In addition, it has been shown that pharmacological stabilization of microtubules *in vitro* is sufficient to induce axon formation (Witte et al., 2008). The present study demonstrates that a mutation increasing the stabilization of microtubules is sufficient to induce ectopic axon formation *in vivo,* and that this effect can be recapitulated with pharmacological stabilizing agents. Thus, our results *in vivo* provide strong support for the notion of a direct instructive role for microtubules in axon formation during neuronal development.

Neurons are post-mitotic cells that form connections over large distances. This requires efficient maintenance of axons and dendrites over the lifetime of the organism. There are active mechanisms in place that protect the axonal process from degeneration over time, as well as regenerative programs that are initiated after injury (reviewed in chapter 1). The present study reveals that microtubule dynamics are essential for axonal regeneration after injury induced by UV-laser axotomy. The regulation of microtubule dynamics has been demonstrated to be important for a regenerative response following injury. Our data confirm and extend these results, indicating that mutations in the gene *mec-7/β-tubulin*, which alter the microtubule dynamics, affect the regenerative capacity of the anterior axon of ALM. Although the number of axons ALM formed in *mec*-7 mutants was altered, the developmental outgrowth and guidance of the anterior axon was unaffected. Thus, our study provides an *in vivo* analysis that supports the existence of critical differences between axon outgrowth during development and regeneration. Furthermore, we show that later stages of axonal regeneration, such as reconnection and fusion with the separated distal fragment (as reviewed in chapter 1), are severely reduced in animals with mutations in *mec-7/β-tubulin*. Growth cone formation involves large scale remodelling of the microtubule cytoskelelton, which is likely responsible for the regeneration defects seen in *mec-7/β-tubulin* mutants. Similarly, axonal fusion during regeneration may also involve large-scale microtubule dynamics and as such is reduced in *mec-7/β-tubulin* mutants. Regulation of axonal fusion during regeneration will be discussed further in chapters 5 and 6.

2.5 Statement of contribution

I performed the experiments presented in Figure 3c and Figure 4. Of particular relevance are the experiments presented in Figure 4, which were performed using the microtubule affecting drugs Paclitaxel (Taxol) and Colchicine. Both these drugs have been implicated in the development of peripheral neuropathy, and were initially tested to determine their efficacy in causing axonal damage as a means to induce regeneration. My experiments indicated that this type of insult was unable to induce axonal regeneration (data not shown); instead, I used this paradigm to alter the stability of microtubules *in vivo*, in a set of critical experiments aimed at determining if this condition phenocopies the *mec-7/β-tubulin* mutant phenotype, causing ectopic neurite outgrowth.

Chapter 3:
Designing an optogenetic method of axonal injury

3.1 Introduction

Chapter 2 outlined a basic mechanism by which a neuron establishes polarity and specifies axon identity, which has implications for maintenance and regeneration following injury. Once axon identity is established and the axon has extended and formed connections with the correct distal targets (often over large distances), it must maintain these connections for the duration of the animal's lifespan. A large body of work has revealed that active mechanisms are in place to prevent degeneration of the axon during the lifetime of the animal (reviewed in chapter 1). Different axonal injury models have been used to study axonal degeneration. They include laser-induced or blade-induced axotomy, axonal damage by toxic compounds, or the use of genetic mutations that cause spontaneous damage to axons. Physical trauma (laser or blade) axotomy has the primary advantage of spatial and temporal resolution: it can target the desired axon at the desired time. In contrast, the application of toxic compounds and genetic mutations lack the specificity of injury but have the significant advantage of being applicable to high throughput forward genetic screens. In this study, together with colleagues, we combined the specificity of laser axotomy with the scalability of toxic compounds and genetic mutations, to create a *C. elegans* strain in which axonal damage can be induced *in vivo*.

Optogenetic tools are genetically encoded proteins that are activated by light. In *C. elegans* the optogenetic tools halorhodopsin (Zhang et al., 2007) and archaerhodopsin (Chow et al., 2010; Okazaki et al., 2012) have been successfully used to silence neurons *in vivo*. The aim of this study was to use the optogenetic tool KillerRed to cause axonal damage *in vivo,* to facilitate forward genetic screens for molecules that regulate axonal degeneration. KillerRed is a red fluorescent protein that produces ROS upon illumination with green light (540-580nm) (Bulina et al., 2006). Early results activating KillerRed in *C. elegans* neurons proved extremely efficient at inducing neuronal cell death *in vivo* (discussed in section 3.2). As a result this study became more focused on a method to induce neuronal cell death *in vivo* using photoactivation of KillerRed as a means of irreversibly silencing neurons.

This study was published in the peer-reviewed journal *Cell Reports* as part of an international collaboration with the laboratories of Marc Hammarlund (Yale University), Hang Lu (Georgia Institute of Technology) and Aravi Samuel (Harvard University). A copy of this article is presented in section 3.2 of this thesis.

3.2 Rapid and permanent neuronal inactivation *in vivo* via subcellular generation of reactive oxygen with the use of KillerRed

Williams, D.C.*, El Bejjani, R.*, Mugno Ramirez, P.*, **Coakley, S.*** , Kim, SA., Lee, H., Wen, Q., Samuel, A., Lu, H., Hilliard, M.A. and Hammarlund, M. (2013) Rapid and permanent neuronal inactivation *in vivo* via subcellular generation of reactive oxygen with the use of KillerRed. ***Cell Reports*** *5*, 552-563.

*These authors contributed equally.

Cell Reports
Resource

Rapid and Permanent Neuronal Inactivation In Vivo via Subcellular Generation of Reactive Oxygen with the Use of KillerRed

Daniel C. Williams,[1,5,6] Rachid El Bejjani,[1,5] Paula Mugno Ramirez,[2,5] Sean Coakley,[2,5] Shin Ae Kim,[3] Hyewon Lee,[3] Quan Wen,[4] Aravi Samuel,[4] Hang Lu,[3,*] Massimo A. Hilliard,[2,*] and Marc Hammarlund[1,*]
[1]Department of Genetics and Program in Cellular Neuroscience, Neurodegeneration and Repair, Yale University, New Haven, CT 06510, USA
[2]Queensland Brain Institute, The University of Queensland, Brisbane, QLD 4072, Australia
[3]School of Chemical & Biomolecular Engineering, Georgia Institute of Technology, Atlanta, GA 30332, USA
[4]Department of Physics and Center for Brain Science, Harvard University, Cambridge, MA 02138, USA
[5]These authors contributed equally to this work
[6]Present address: Department of Biology, Coastal Carolina University, Conway, SC 29526, USA
*Correspondence: hang.lu@gatech.edu (H.L.), m.hilliard@uq.edu.au (M.A.H.), marc.hammarlund@yale.edu (M.H.)
http://dx.doi.org/10.1016/j.celrep.2013.09.023

SUMMARY

Inactivation of selected neurons in vivo can define their contribution to specific developmental outcomes, circuit functions, and behaviors. Here, we show that the optogenetic tool KillerRed selectively, rapidly, and permanently inactivates different classes of neurons in *C. elegans* in response to a single light stimulus, through the generation of reactive oxygen species (ROS). Ablation scales from individual neurons in single animals to multiple neurons in populations and can be applied to freely behaving animals. Using spatially restricted illumination, we demonstrate that localized KillerRed activation in either the cell body or the axon triggers neuronal degeneration and death of the targeted cell. Finally, targeting KillerRed to mitochondria results in organelle fragmentation without killing the cell, in contrast to the cell death observed when KillerRed is targeted to the plasma membrane. We expect this genetic tool to have wide-ranging applications in studies of circuit function and subcellular responses to ROS.

INTRODUCTION

Optogenetic approaches to studying the function of specific neurons in vivo generally involve the use of light to acutely activate or inactivate the cells of interest. In particular, inactivation in *Caenorhabditis elegans* of specific neurons in vivo can be used to investigate their contribution to specific network functions and also to study compensation or homeostasis in the remaining cells. However, the best-described optogenetic tools for silencing neurons in *C. elegans*, halorhodopsin (Zhang et al., 2007) and archaerhodopsin (Chow et al., 2010; Okazaki et al., 2012), are light-driven ion pumps (chloride and protons, respectively) that require constant stimulation to keep neurons inactive, and may not be suitable for studying behavior, compensation, or homeostasis over longer timescales.

An alternative way to acutely and permanently inactivate specific neurons in vivo is to kill them. Investigators have utilized this approach extensively in *C. elegans* to define the function of a wide variety of cells (especially neurons), using a laser microbeam to ablate the cells (Avery and Horvitz, 1987, 1989; Fang-Yen et al., 2012). However, application of the laser-ablation approach is limited because of the difficulty of ablating multiple target cells without damaging surrounding cells or tissues, and the extensive amount of time required to perform surgery on a large number of animals. Thus, the development of optogenetic ablation tools that can be spatially and temporally controlled is highly desirable. An optimal optogenetic ablation tool should kill cells rapidly, avoid collateral damage to neighboring cells and tissues, and scale in application from single neurons to groups of cells in single animals or populations.

KillerRed is a dimeric red fluorescent protein that produces high levels of reactive oxygen species (ROS) upon illumination with green light (540–580 nm), thereby inducing cell death (Bulina et al., 2006). Structurally, KillerRed resembles other GFP-like proteins, which comprise an 11-strand antiparallel β-barrel that surrounds a centrally located chromophore (Carpentier et al., 2009; Pletnev et al., 2009). However, KillerRed is 1,000 times more toxic than other fluorescent proteins. This higher toxicity is due to the presence of a long water-filled channel in KillerRed that allows diffusion of molecular oxygen near the chromophore, and is thought to provide a path for electron transfer during the production of superoxide radicals (Roy et al., 2010; Serebrovskaya et al., 2009). Similar to the generation of GFP fluorescence, the phototoxic activity of KillerRed is effective in vivo and can be induced in mammalian and zebrafish cells without coexpression of other factors (Bulina et al., 2006; Teh et al., 2010).

Cell PRESS
Open ACCESS

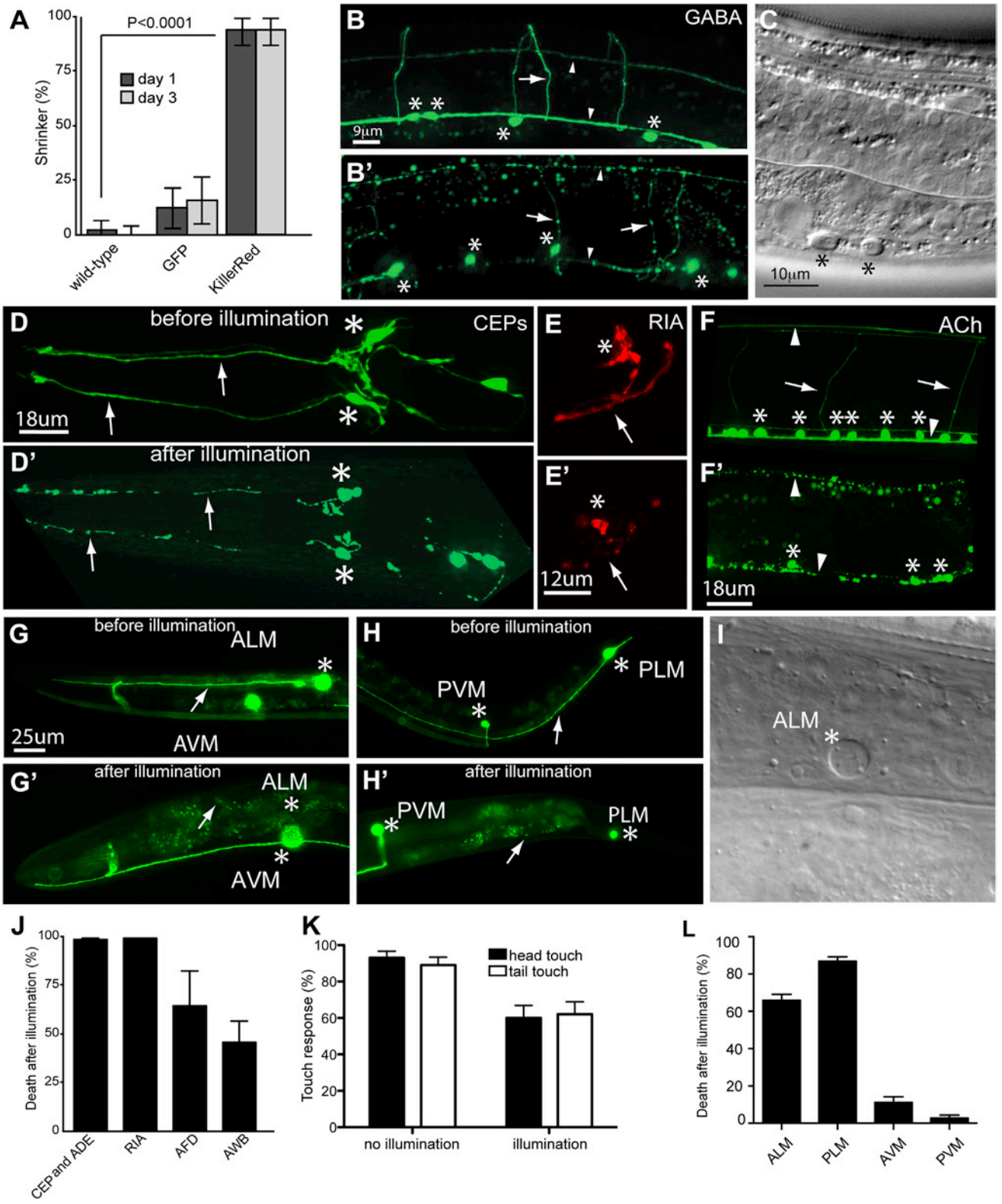

Figure 1. KillerRed Activation Disrupts the Function and Morphology of Targeted Neurons and Results in Cell Death

(A) KillerRed activation induces behavioral defects. Animals were illuminated with white light and then scored 24 and 72 hr later for the shrinker phenotype caused by GABAergic neuron dysfunction. n = 50 for KillerRed and GFP, and 100 for wild-type.

(legend continued on next page)

Here, we demonstrate that KillerRed can efficiently kill a variety of neurons in *C. elegans*, including sensory neurons, interneurons, and motor neurons. We show that the effect of KillerRed is cell-autonomous and does not spread to nearby neurons. Our results indicate that KillerRed disruption of neuronal function is rapid and can be used to alter the circuits and behavior of freely moving animals. In addition, the tool is highly modifiable, with ablation efficiency dependent upon illumination duration and intensity. We also demonstrate that certain neurons are resistant to KillerRed damage, raising the intriguing possibility that some cells possess increased intrinsic protection mechanisms against ROS. We further show that subcellular localization of KillerRed dramatically alters its function, with mitochondria localization resulting in specific disruption of organelle morphology. Finally, using selective illumination, we show that exposure of individual neuronal compartments, such as the cell body or the axon, is sufficient to induce neuronal damage and death.

RESULTS

Expressing KillerRed in *C. elegans* GABA Neurons Results in Light-Dependent Cell Death

We established the consequences of KillerRed activation in different sets of *C. elegans* neurons, including motor neurons, mechanosensory neurons, chemosensory neurons, and interneurons (details of the KillerRed constructs and illumination parameters can be found in Table S1 available online). We first generated transgenic animals expressing cytosolic KillerRed under the control of the GABAergic neuron-specific promoter *Punc-47*, which drives expression in 26 motor neurons required for coordinated movement (McIntire et al., 1997). Cytosolic KillerRed activation in GABAergic neurons caused a "shrinker" phenotype (i.e., longitudinal shortening of the body upon head touch) in the animals 24 hr after illumination, consistent with loss of GABAergic neuronal function (Figure 1A; McIntire et al., 1993). Furthermore, neuronal function remained disrupted 72 hr after KillerRed activation (Figure 1A), suggesting that the affected neurons were dead rather than merely damaged. To examine the morphology of KillerRed-expressing neurons before and after KillerRed activation, we coexpressed GFP in the targeted cells (Figure 1B). Twenty-four hours after KillerRed activation, we found that the morphology of the GABAergic neurons was severely disrupted, with axonal processes that were fragmented and broken, often with large blebs, or missing altogether (Figure 1B′). The cell bodies of the affected neurons were round and swollen, and appeared smaller than those in nonilluminated animals, consistent with neuronal death. To confirm that the morphological changes observed based on GFP fluorescence reflected cell death, we analyzed the GABAergic neurons by differential interference contrast (DIC) microscopy and found that the cell bodies of affected neurons displayed swelling, the presence of vacuole-like structures, and nuclear changes (Figure 1C), all of which are phenotypes consistent with cell death.

The observed structural and behavioral defects were specific and dependent on KillerRed expression and activation. Illumination of either wild-type animals or animals expressing only GFP in GABAergic neurons did not elicit a shrinker phenotype (Figure 1A). Moreover, expression and illumination of the spectrally similar fluorophore mCherry did not cause a detectable behavioral defect (data not shown). Furthermore, prior to illumination, neurons expressing KillerRed displayed no morphological or functional deficits, indicating that neuronal death was dependent upon KillerRed activation (Figures 1A and 1B). Thus, KillerRed activation in GABAergic neurons permanently disrupts function and results in cell death.

KillerRed Can Be Used to Efficiently Ablate Multiple Classes of Neurons

Our experiments demonstrated that KillerRed can disrupt neuronal function. Next, we asked whether we could improve the efficiency of disruption. KillerRed is dimeric (Bulina et al., 2006; Carpentier et al., 2009; Pletnev et al., 2009), and we reasoned that increased efficiency might result from expression as a tandem dimer, as previously reported for other multimeric fluorescent proteins (Campbell et al., 2002; Shaner et al., 2004). We generated a tandem-dimer version of KillerRed (tdKillerRed) and found that it was significantly more effective than monomeric KillerRed at disrupting GABA neuron function. After illumination with green light (5.1 mW/mm^2 for 5 min), 100% of tdKillerRed animals (n = 11) exhibited a shrinker phenotype, compared with only 14% for monomeric KillerRed (n = 14; $p < 0.0001$). We also localized tdKillerRed to the plasma membrane using a myristoylation tag (myr-tdKillerRed). Membrane-targeted dimeric KillerRed had efficiency similar to that of soluble dimeric KillerRed (92% shrinker, n = 13, p = 1.0). We

(B and B′) Confocal images of the GABAergic nervous system of GABA::KillerRed (*Punc-47::KillerRed*) animals before (B) and 24 hr after (B′) illumination.
(C) Nomarski image of affected GABAergic neuron cell bodies 24 hr after KillerRed activation.
(D and D′) CEPs before (D) and 24 hr after (D′) illumination. After illumination, the dendrites of CEP neurons (arrows) are fragmented and the cell bodies (asterisks) are smaller and rounded.
(E and E′) RIA interneuron before (E) and 24 hr after (E′) illumination, with the cell body and axon degenerated in (E').
(F and F′) Cholinergic nervous system before (F) and 24 hr after (F′) illumination. Activation results in fragmentation of neuronal processes as well as fewer and smaller cell bodies.
(G–H') Fluorescent images of axonal and neuronal damage in ALM and PLM before (G and H) and 24 hr after (G' and H') illumination. After illumination, ALM is completely cleared (G′) and the PLM axon has disappeared (H').
(I) Nomarski image of ablated ALM cell body 24 hr after illumination.
(J) Quantification of cell death 24 hr after illumination. n = 155 cells (CEP and ADE), 48 cells (RIA), 74 cells (AWB), and 17 cells (AFD).
(K) Light touch response 24 hr after illumination in wild-type and KillerRed-expressing animals. After KillerRed activation, there is a reduction in the response to light touch in both the head and tail of the animal. n = 50 animals.
(L) Quantification of cell death in touch neurons 24 hr after illumination. n = 107 cells (AVM and PVM) and 214 cells (ALM and PLM). In all figures, asterisks mark neuron cell bodies, arrows mark processes, and arrowheads mark dorsal and ventral nerve cords. Error bars indicate 95% confidence intervals.
See also Table S1.

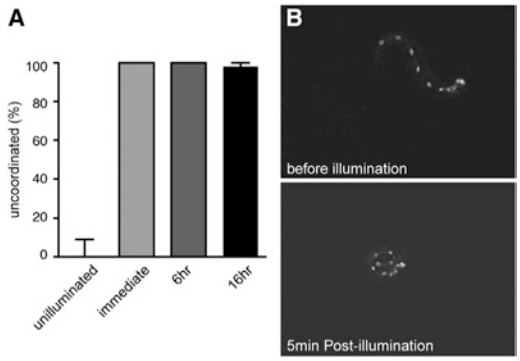

Figure 2. KillerRed Activation Results in Immediate Disruption of Neuronal Function

(A) Illumination of animals expressing KillerRed in cholinergic neurons results in immediate and permanent disruption of movement. n = 50 for unilluminated, n = 20 for immediate (just after the end of illumination) and 6 hr time points, and n = 41 for 16 hr time point. Error bars indicate 95% confidence intervals.

(B) A freely swimming L1 larva before KillerRed activation in GABAergic motor neurons (top panel). The same larva immediately following 5 min exposure to green light illumination (~40 mW/mm^2) displays uncoordinated locomotion (bottom panel).

See also Table S1.

used myr-tdKillerRed for some of the subsequent experiments (Table S1).

To determine whether other neurons could be targeted by KillerRed, we generated different transgenic strains expressing KillerRed in the dopaminergic neurons CEP, ADE, and PDE (*Pdat-1::myr-tdKillerRed*); the interneuron RIA (*Pglr-3::myr-tdKillerRed*); the cholinergic neurons (approximately 120 neurons; *Punc-17::myr-tdKillerRed*); the amphid sensory neurons AWB (*Pstr-1::myr-tdKillerRed*) and AFD (*Pgcy-8::myr-tdKillerRed*); and the mechanosensory neurons ALM (L/R), PLM(L/R), AVM, and PVM (*Pmec-4::KillerRed*). Like the GABAergic motor neurons, the dopaminergic neurons CEP and ADE and the interneuron RIA were efficiently killed after KillerRed activation (Figures 1D, 1E, and 1J). The cholinergic neurons were also efficiently killed, although the maximum efficiency could not be determined because the animals died (Figure 1F). This lethal phenotype is consistent with a requirement for cholinergic neuron function for survival of animals in early developmental stages (Alfonso et al., 1993). In comparison with these cell types, the AWB and AFD amphid neurons were killed with lower efficiency (Figure 1J). The dopaminergic PDE neurons were also killed with lower efficiency (26 out of 60 cells), even though the other dopaminergic neurons were efficiently killed in the same animals. We also tested the efficiency of KillerRed in the mechanosensory neurons, which mediate a specific behavior: response to light touch. We found that expression and activation of KillerRed in the mechanosensory neurons caused deficits in mechanosensation (Figure 1K). Consistent with this loss of touch sensitivity, KillerRed activation also caused efficient neuronal cell death in ALM and PLM neurons (Figures 1G–1I and 1L). However, the AVM and PVM neurons were refractory to axonal degeneration or cell death. Thus, KillerRed can ablate many neuronal types in *C. elegans*, and is effective at targeting single neurons as well as entire neuronal classes, with selected neurons being specifically resistant to disruption.

KillerRed Induces Immediate Inactivation of Illuminated Neurons

Although the morphological effects of KillerRed activation in neuronal cell bodies and processes are not apparent immediately after activation, it is possible that KillerRed disrupts neuronal function more rapidly than it affects neuronal morphology. To test this, we used two strategies. First, we took advantage of the profound consequence of KillerRed activation in cholinergic neurons, which triggers paralysis in a coiled posture, similar to what is observed in animals that lack cholinergic neurotransmission (Rand, 1989). To determine the time necessary for neuronal function to be disrupted by KillerRed activation, we quantified this uncoordinated behavior at various times after illumination. This revealed that functional disruption was both immediate and permanent (Figure 2A). Immediately after completion of the 5 min illumination period, the animals exhibited a robust, uncoordinated phenotype consistent with loss of cholinergic neuron function. This functional deficit persisted long after activation, suggesting that disruption was not due to temporary inactivation, but rather to permanent disruption of neuronal function followed by cell death.

Second, we used an optogenetic illumination system that allowed us to expose single, freely swimming animals to intense green laser light while monitoring their behavior before, during, and after illumination (Leifer et al., 2011). When we used this system to analyze the effect of KillerRed activation in GABAergic motor neurons of freely swimming L1 larvae, we found that activation of KillerRed caused a severe deficit in locomotion, which was observed immediately after the end of the illumination period (Figure 2B; Movies S1 and S2). Together, these experiments demonstrate that KillerRed activation can rapidly and permanently disrupt neuronal function. In addition, our inactivation experiments in the GABAergic neurons of L1 animals suggest that these neurons make a greater contribution to normal locomotion of L1 animals than was previously appreciated.

KillerRed-Dependent Neuronal Death Is Caspase Independent and Can Be Improved by Mutating ROS-Detoxifying Enzymes

KillerRed is thought to act as a type II photosensitizer, producing superoxide anion radicals rather than singlet oxygen (Pletnev et al., 2009; Shu et al., 2011). Superoxide is scavenged by superoxide dismutases (SODs), which catalyze the conversion of superoxide radicals to hydrogen peroxide and thus limit cellular damage. *C. elegans* has a total of five SODs, two of which (*sod-1* and *sod-5*) are cytoplasmic Cu/Zn SODs (the remaining three SODs are mitochondrial Fe/Mn SODs [*sod-2* and *sod-3*] and an extracellular Cu/Zn SOD [*sod-4*]) (Landis and Tower, 2005). We found that a *sod-1* mutant background, which eliminates one of the cytoplasmic SODs, increased the efficiency of ablation in AWB, a neuron that normally is refractory to KillerRed damage (Figure 3A). These data support a model in which KillerRed exerts its effect via superoxide, and demonstrate that the effect of KillerRed in normally resistant cells can be enhanced by specific genetic mutations.

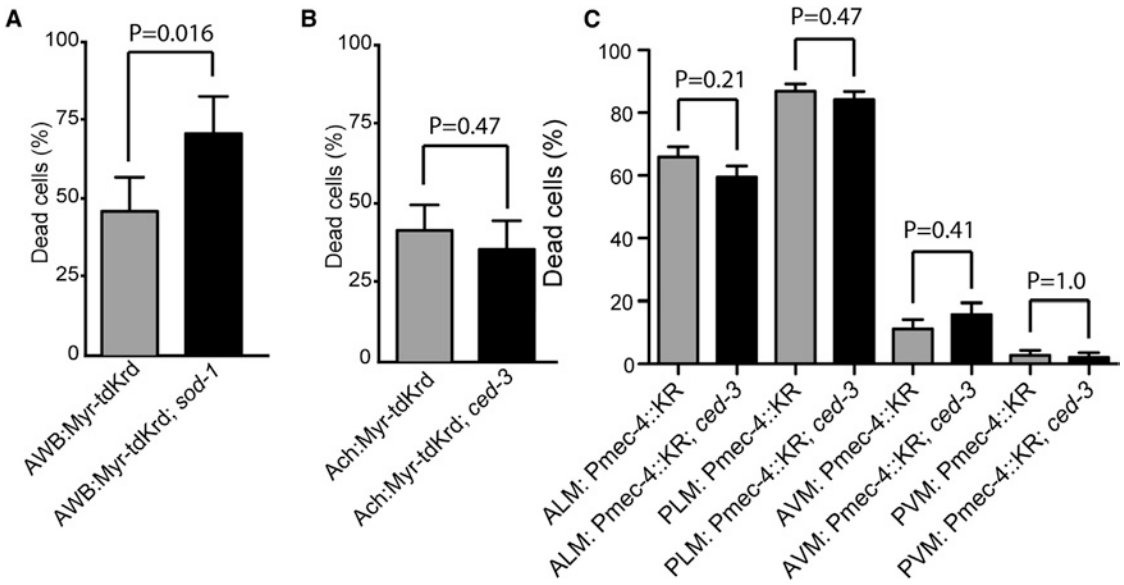

Figure 3. KillerRed Phototoxicity Is Enhanced in SOD Mutants and Does Not Require the Caspase CED-3

(A) Myr-tdKillerRed activation ablates AWB amphid neurons more effectively in *sod-1(tm776)* mutant animals. n = 74 cells (wild-type) and 38 cells (*sod-1*).

(B) Neuronal cell death induced by Myr-tdKillerRed activation in cholinergic neurons does not require *ced-3(n717)*. The illumination protocol was adjusted to avoid killing the animals (see Table S1). n = 132 cells (wild-type) and 79 cells (*ced-3*).

(C) Neuronal cell death induced by cytosolic KillerRed activation in mechanosensory neurons does not require *ced-3(n717)*. For *ced-3*, n = 95 cells (AVM, PVM) and 190 cells (ALM, PLM); for wild-type, n = 107 cells (AVM and PVM) and 214 cells (ALM and PLM; same data as Figure 1L). Phenotypes were determined 24 hr after illumination. In all panels, error bars indicate 95% confidence intervals.

See also Table S1 and Movies S1 and S2.

In *C. elegans*, apoptotic cell death requires the caspase CED-3, whereas necrotic cell death does not (Ellis and Horvitz, 1986; Hall et al., 1997). We tested whether KillerRed-mediated neuronal cell death occurred through apoptosis by examining the requirement for *ced-3*. Cell death, as well as the other morphological and behavioral consequences of KillerRed activation, was as robust in *ced-3* mutants as in the wild-type for both acetylcholine motor neurons and mechanosensory neurons (Figures 3B and 3C). Further, the pathology of neuronal cell death induced by KillerRed included cell swelling, vacuolation, and nuclear changes (Figures 1C and 1I), which is similar to previous observations of necrosis-like neuronal cell death (Hall et al., 1997) but in contrast to the compact morphology of apoptotic cells. These observations suggest that KillerRed does not act via an apoptotic pathway and may instead kill neurons through a necrotic, caspase-independent mechanism.

KillerRed's Effects Are Cell Autonomous and Do Not Spread to Adjacent Neurons

To test the cell autonomy of KillerRed's cytotoxicity, we examined the morphology of neurons located adjacent to KillerRed-targeted cells in three different experiments. First, we examined AWA and AWB, which are sensory neurons located in the head. The cell bodies of the AWA and AWB neurons are located next to each other within the lateral ganglia; their axons project into the nerve ring and their dendrites fasciculate with each other (White et al., 1986). We found that activation of KillerRed in the AWB neuron resulted in its structural disruption after illumination, but had no effect on the structure of AWA (Figures 4A and 4B). Second, we examined cholinergic and GABAergic motor neurons. These neurons are synaptic partners; their cell bodies are located near the ventral nerve cord and their processes fasciculate together in the dorsal and ventral nerve cords (White et al., 1986). We found that KillerRed activation in the GABAergic neurons did not affect the morphology of the cholinergic neurons (Figures 4C and 4D). Furthermore, KillerRed activation in GABAergic neurons caused a GABAergic-specific functional defect (Figure 1A) rather than the coiled-paralysis defect caused by activation in cholinergic neurons (Figures 1F and 2). Similar specificity was observed when GABA neurons were imaged after KillerRed activation in the cholinergic neurons, that is, activation in cholinergic neurons did not affect the GABA neurons. Finally, we tested whether KillerRed activation in the PLM mechanosensory neuron had any effect on the morphology of the nearby PLN neuron. Both PLM and PLN neurons have their cell bodies in the lumbar ganglia, and their processes run adjacent to each other for the entire posterior half of an animal's body (White et al., 1986). Activation of KillerRed in PLM had no effect on the axon or cell body of PLN (Figures 4E–4G). Together, these results indicate that KillerRed-mediated functional disruption and cell damage is cell-autonomous and does not spread beyond the targeted cell (or cells).

Selective Illumination Results in Neuronal Cell Death

We next investigated the effect of selective illumination on different regions of the animal's body or on defined regions of

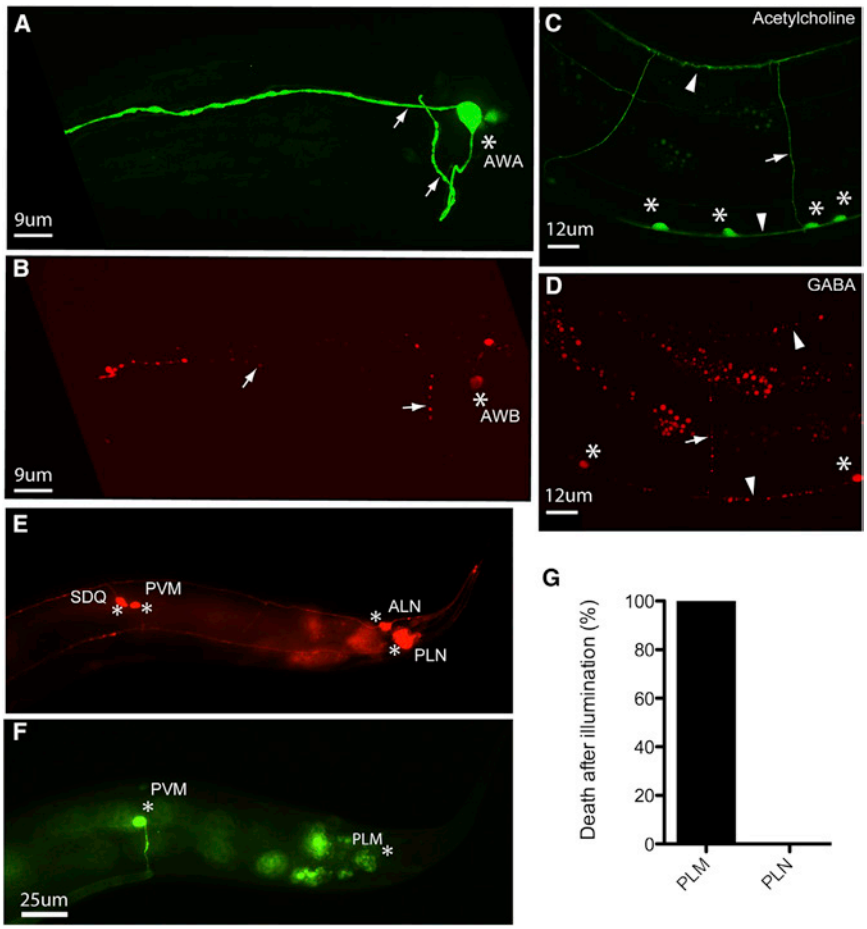

Figure 4. KillerRed Phototoxicity Does Not Spread to Neighboring Neurons

(A) AWA neuron intact after illumination (green, *Podr-10::GFP*).

(B) AWB degenerated neuron in the same animal as in (A) (red, *Pstr-1::myr-tdKillerRed*).

(C) Cholinergic neurons after illumination (green, *Punc-17::GFP*).

(D) Affected GABAergic neurons after illumination in the same animal as in (C) (red, *Punc-47::myr-tdKillerRed*).

(E) PLN neuron after illumination (red, *Plad-2::mCherry*).

(F) PLM neurons expressing KillerRed after illumination in the same animal as in (E) (green, *Pmec-4::GFP*). In all panels, asterisks mark cell bodies, arrows mark processes, and arrowheads mark dorsal (top) and ventral (bottom) nerve cords.

(G) Quantification of cell death in PLM and PLN neurons in animals expressing KillerRed in PLM only. Animals were scored for PLN death only if PLM had died; thus, PLM death is 100%. n = 25 animals in which both PLM and PLN were scored. In all panels, phenotypes were determined 24 hr after illumination.

See also Table S1.

individual neurons. For these experiments, we chose the mechanosensory neurons ALM and PLM and used a spatially restricted illumination scheme similar to that used previously for optogenetic stimulation and inhibition of neurons (Stirman et al., 2011). Specifically, we first imaged animals for GFP to locate the neurons expressing KillerRed without inducing cell damage. Then, using an LCD projector controlled by a LabVIEW program, we illuminated selected regions (such as the anterior half or posterior half of the animal's body, or the cell body or axon of a single neuron; Figure 5). Using high-magnification lenses with a small focal depth (e.g., 100×), we were able to confine illumination with precision and reproducibility. Targeting the anterior or posterior half of the animal induced cell death of specific neurons included in the respective illuminated regions (Figures 5A–5C). As was the case with the nontargeted illumination, AVM and PVM were resistant to KillerRed-induced damage. When activation was confined to a limited portion of a single neuron, we found that targeting only the cell body of the ALM mechanosensory neuron resulted in cell damage and death (Figures 5D and 5E). Similarly, when the illumination was directed selectively to the axon, we observed robust cell death (>40% of cases), with the remaining animals presenting axonal degeneration in regions beyond the irradiated sections. Thus, even though expression of KillerRed was not spatially limited, regional illumination was enough to produce KillerRed-mediated cell damage and death.

Mitochondrial Targeting Results in Organelle-Specific Effects

The experiments described above show that both membrane-targeted and cytoplasmic KillerRed can disrupt neuronal function and kill neurons. To test whether KillerRed function is dependent on subcellular localization, we targeted tandem dimeric KillerRed to mitochondria using the *tom-20* targeting sequence, which results in localization of KillerRed to the outer surface of the mitochondrion (Ichishita et al., 2008; Kanaji et al., 2000). We performed these experiments in body wall muscles because the mitochondria in these cells have a well-defined morphology, which enabled us to assess the effect of KillerRed on cell structure and function and on the mitochondria themselves. We found that KillerRed was efficiently targeted to mitochondria, and that mitochondria labeled with KillerRed (without activation) had normal morphology consisting of a reticulated network (Figure 6A). Further, animals that expressed mitochondria-targeted KillerRed (mt-tdKillerRed) in all of their body wall muscles displayed normal movement in the absence of light activation, demonstrating that muscle function was not disrupted by mt-tdKillerRed expression (data not shown). By contrast, when mt-tdKillerRed-expressing animals were exposed to green light, we observed an immediate and dramatic change in mitochondria morphology in muscle. mt-tdKillerRed activation disrupted the reticulated network of mitochondria and resulted in small, spherical mitochondria of various sizes (Figure 6B). Surprisingly, we did not observe behavioral deficits in these animals,

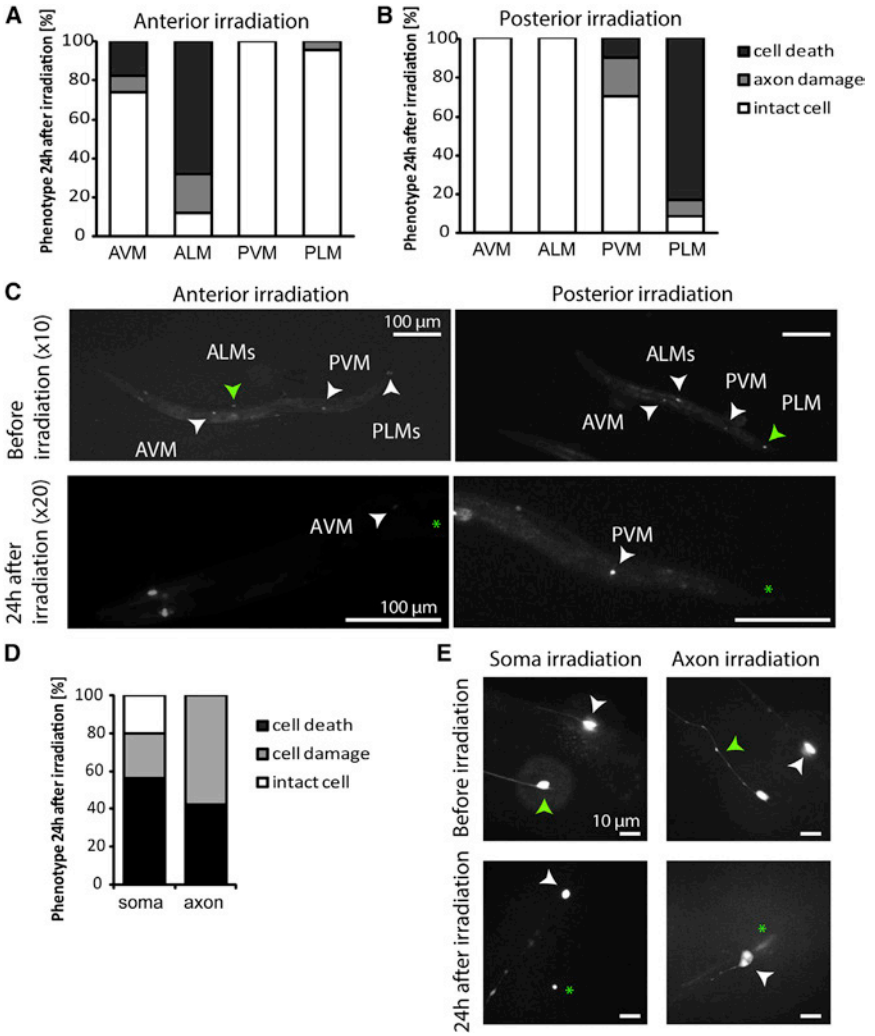

Figure 5. Selected Region Illumination Can Be Used in Combination with KillerRed to Induce Cell-Specific Killing

(A and C) Illumination of the anterior half body of the animal causes selective ablation of ALM neurons, whereas PLM neurons are intact. n = 25 animals.

(B and C) Illumination of the posterior half of the animal's body ablated PLM neurons, leaving intact ALMs. n = 24 animals.

(D and E) Selective illumination of either the soma or axon of ALM neurons can cause damage and neuronal ablation. n = 25 animals for soma and 19 animals for axon illumination. In all of the images, the green arrowhead points to the targeted neuron or axon before illumination, asterisks indicate the same cell 24 hr after illumination, and white arrowheads point to different neuronal cell bodies in the animal.

See also Table S1.

suggesting that activation of mt-tdKillerRed did not kill muscle cells (Figure 6G). By contrast, expression of plasma membrane-targeted KillerRed (myr-tdKillerRed) in the same muscle cells resulted in cell death and immediate behavioral deficits after activation (Figures 6E and 6F). Since mt-tdKillerRed did not kill muscles, we performed studies to test whether mitochondrial morphology could recover after KillerRed-mediated disruption. We found that by 48 hr after disruption, the mitochondria had recovered normal morphology (Figures 6C and 6D). Together, these results demonstrate that subcellular targeting of KillerRed enables the generation of local and specific cell-biological phenotypes.

Use of KillerRed with Other Optical Tools

A number of optical tools are currently being used in *C. elegans*, including the optogenetic tool channelrhodopsin (Nagel et al., 2005) and the reactive oxygen generator miniSOG (Qi et al., 2012). Because KillerRed is excited by green light, whereas these other tools are excited by blue light, we considered that it might be possible to address them separately in a single animal by using different illumination wavelengths. To determine the feasibility of this idea, we compared the requirements for activation of KillerRed, channelrhodopsin, and miniSOG in the cholinergic motor neurons. The activity of all three tools has been described in these cells (Figures 1F and 2; Liu et al., 2009; Qi et al., 2012; Zhang et al., 2007). First, we determined the feasibility of using KillerRed in combination with miniSOG. We irradiated animals expressing miniSOG in cholinergic motor neurons (CZ14527) using 0.57 mW/mm^2 of blue light for 30 min as previously described (Qi et al., 2012; Table S1). This treatment affected 100% of the animals: 42% were paralyzed and the remaining animals could move but were sluggish. Similarly, we irradiated animals expressing KillerRed in cholinergic neurons with the same intensity (0.57 mW/mm^2) and time of green light, and again observed 100% affected animals, with 76% paralysis and 24% sluggish movement (Figure 7A). Next, we swapped the illumination conditions, that is, we illuminated miniSOG animals with 0.57 mW/mm^2 of green light and KillerRed animals with 0.57 mW/mm^2 of blue. This treatment had little to no effect, although approximately 6% of the KillerRed animals did react to blue light illumination (Figure 7A). Finally, we asked whether higher-intensity activation could be used for miniSOG. We had previously observed that *C. elegans* can tolerate green light at 46 mW/mm^2 for 15 min with no adverse effects (other than KillerRed activation; Figure 1). However, exposing wild-type worms (n = 20) to blue light at 8 mW/mm^2 for 10 min resulted in 100% lethality, consistent with previous results (Edwards et al., 2008). Together, these data suggest that KillerRed and miniSOG can be separately addressed in vivo.

Next, we determined the feasibility of using KillerRed in conjunction with channelrhodopsin. Again, we focused on the

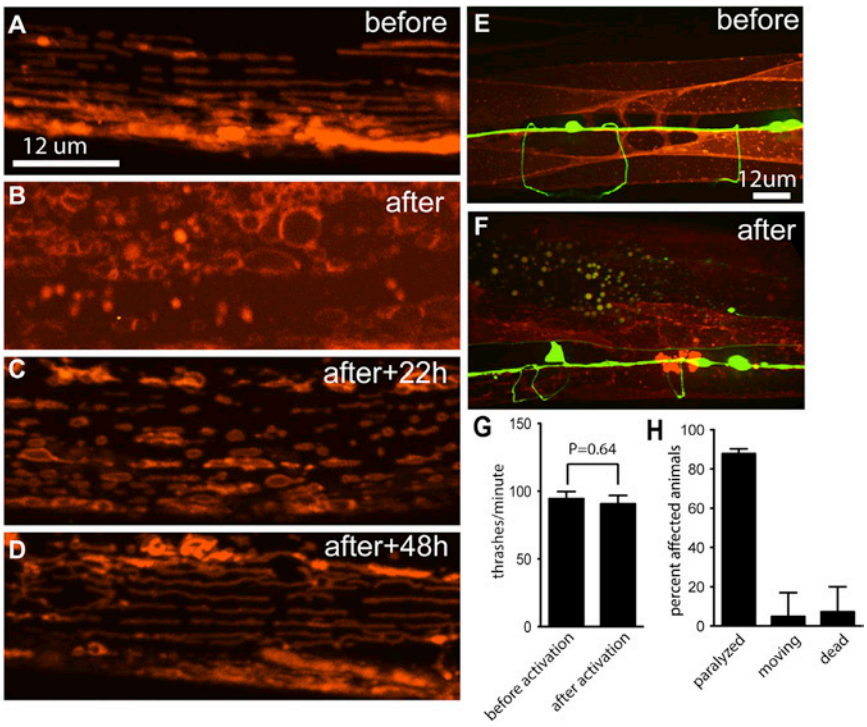

Figure 6. KillerRed Activation at Mitochondria Results in Organelle Damage but Cell Survival

(A–D) Mitochondria in body wall muscles express mt-tdKillerRed and were imaged before (A) or at various times after (B–D) illumination.

(E and F) Body wall muscles express plasma membrane KillerRed and were imaged before (E) and 16 hr after (F) illumination. GABA neurons express GFP.

(G) Average thrash rate in liquid of animals expressing mitochondria KillerRed in muscles before and after illumination, corresponding to (A) and (B). n = 9 for before illumination and 10 for after illumination; error bars indicate SEM.

(H) Phenotype distribution of animals expressing plasma membrane KillerRed in muscles after illumination, corresponding to (F). n = 41; error bars indicate 95% confidence intervals.

See also Table S1.

cholinergic motor neurons, which are a well-described site for channelrhodopsin activation (Liu et al., 2009; Zhang et al., 2007). We tested whether activation of channelrhodopsin could be performed independently of KillerRed activation. We activated channelrhodopsin in cholinergic motor neurons using 0.47 mW/mm^2 of blue light, which caused 100% of the animals to stop moving (n = 23). By contrast, 2.2 mW/mm^2 of green light had no effect on these animals (n = 22). As we previously determined that an even lower intensity of green light could be used to activate KillerRed, and a higher intensity of blue light could be used *without* activating KillerRed (Figure 7A), these experiments indicate that KillerRed can be used in multimodal experiments with channelrhodopsin. Finally, we confirmed these experiments in mechanosensory neurons. As in the cholinergic neurons, we found that prolonged illumination of KillerRed strains at the appropriate wavelength and intensity to activate channelrhodopsin had very little effect, although axon damage was observed in a small percentage of animals (Figures 7B and 7C). These data confirm that KillerRed can be used in conjunction with channelrhodopsin in *C. elegans*, as well as in conjunction with other fluorescent tools that are excited by blue or cyan light.

DISCUSSION

KillerRed is a new tool in the *C. elegans* optogenetic toolkit that can kill and inactivate cells in populations of animals with extremely high temporal and spatial control. The effect of KillerRed is immediate and cell-autonomous, with no spreading of killing, or even damage, to surrounding cells or tissues. This critical property makes KillerRed a powerful biological tool that can be applied in a wide variety of cell-perturbation studies in vivo, at scales ranging from single to multiple cells in both single animals and populations. For example, the rapidity and efficacy of this genetically encoded cell-ablation reagent will now allow investigators to examine the acute effects of disrupting specific neurons during behavioral performance. KillerRed can also be used for longer behavioral studies, since ablated neurons never recover function. For example, our data indicate that GABA neurons have an essential function in the locomotion of L1 larvae. Similarly, our data indicate that ablation of acetylcholine neurons in L4 stage animals results in relatively rapid lethality (within 24 hr of ablation), suggesting that *C. elegans* has an acute requirement for cholinergic neurotransmission for viability. One potential concern for such behavioral studies is the fact that because KillerRed damages and kills neurons, rather than merely silencing them, it is possible that secondary effects on the remaining cells in the network might complicate analysis. However, our data demonstrate that, at least for the neurons assessed here, the effects of ablation are restricted to the cells that express KillerRed.

Further, because KillerRed is excited by green light, it can be used in combination with other optogenetic tools that are excited by blue light, such as GFP, GCaMP, channelrhodopsin, and miniSOG. The green light activation of KillerRed may have some additional practical advantages in *C. elegans*, as worms tolerate high levels of green light, but actively avoid—and can be killed by—equivalent amounts of blue light (Edwards et al., 2008). The selective-illumination method we describe here may also have additional applications, such as ablating a neuron from a distance by targeting a region of its axon (this is particularly important when using KillerRed expressed in cells whose cell bodies are in very close proximity and therefore are more difficult to target individually), and investigating ROS effects in axonal sections.

Our results also indicate that subcellular localization of KillerRed can be exploited to study specific cell-biological

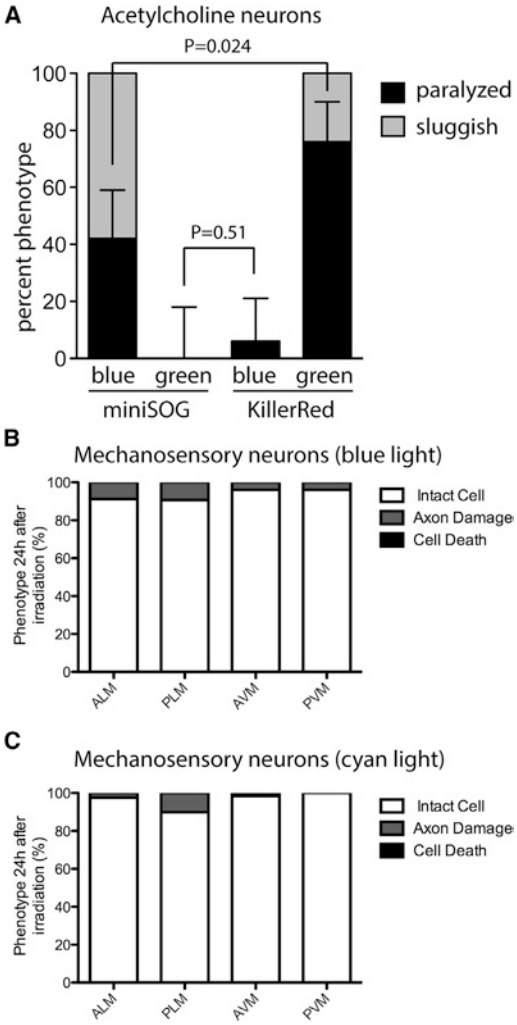

Figure 7. KillerRed Can Be Used in Multimodal Optical Experiments

(A) Comparison of the effects of KillerRed and miniSOG in acetylcholine neurons illuminated with either blue or green light. n = 33 for miniSOG/blue, n = 21 for miniSOG/green, n = 32 for KillerRed/blue, and n = 21 for KillerRed/green. Error bars show 95% confidence interval for the paralyzed phenotype. Phenotypes were determined 10 min after illumination.

(B and C) Effect of KillerRed in mechanosensory neurons illuminated with either blue (b) or cyan (c) light. n = 102 for blue light and n = 64 for cyan light. Phenotypes were determined 24 hr after illumination.

See also Table S1.

functions. Targeting and activating KillerRed at the plasma membrane is sufficient to inactivate and kill cells. This rapid and lethal effect could be due to the susceptibility of membrane lipids to oxidation. For example, unsaturated lipids are highly susceptible to oxidative stress, resulting in the generation of toxic compounds such as hydroxynonenal and acrolein (Catalá, 2010; Fatokun et al., 2008). In addition to causing loss of membrane fluidity and destruction of the plasma membrane barrier, these toxic compounds react with membrane proteins, resulting in inactivation of critical proteins such as the neuronal glucose transporter, the glutamate transporter, and Na^+/K^+ ATPases (Barnham et al., 2004; Keller et al., 1997; Mark et al., 1995; Smith et al., 2009). In contrast, targeting and activating KillerRed at mitochondria results in the specific disruption (and eventual recovery) of organelle morphology, without killing cells. A potential explanation for the local effect of KillerRed on mitochondria is that ROS are quenched rapidly and thus the effective diffusion rate is very low. Alternatively, it is possible that the TOM20 tag affects KillerRed function, allowing for mitochondrial damage but preventing cell killing. Interestingly, another optogenetic reactive oxygen generator, miniSOG, requires mitochondrial targeting to kill neurons (Qi et al., 2012). miniSOG generates mainly singlet oxygen, whereas KillerRed generates mainly superoxide (Pletnev et al., 2009; Shu et al., 2011; this work). These data suggest that different ROS may affect mitochondria and cell function in different ways. KillerRed thus enables the dissection of local effects of ROS.

ROS are toxic cellular molecules that need to be kept in check for a neuron to function over a long period of time, and ROS accumulation correlates with a variety of neurodegenerative diseases (DiMauro and Schon, 2008; Uttara et al., 2009). Therefore, defining the nature of the cytotoxicity of KillerRed, a generator of ROS, offers a significant opportunity to genetically investigate the mechanisms that regulate cellular responses to ROS. Our findings show that selective neurons, such as AVM, PVM, and AWB, are resistant to damage caused by KillerRed activation and ROS. KillerRed expression is weaker in PVM than in other neurons, so the reduced killing effect could be due to the presence of fewer molecules in the cell. However, AVM and AWB express KillerRed at levels comparable to those observed in other neurons, suggesting that they might have a higher intrinsic capacity to buffer ROS. One such mechanism could be a higher expression of molecules, such as SOD-1, that are able to catabolize ROS into nontoxic elements. Our data demonstrating that a mutation in SOD-1 is able to increase the cytotoxic effect of KillerRed activation in AWB provide support for this idea, although additional mechanisms might also be in place. We expect that the application of KillerRed shown here will provide greater flexibility and control for genetic studies of both neuronal function and ROS-induced neuronal damage in vivo.

EXPERIMENTAL PROCEDURES

Strains and Molecular Biology

Nematodes were cultured using standard methods. All experiments were performed at 22°C except when otherwise noted. A *C. elegans* version of the KillerRed coding sequence was synthesized (GenScript) using worm-optimized codons and synthetic introns (Fire et al., 1990; Stenico et al., 1994). Flanking regions for Multisite Gateway (Invitrogen) were included and the KillerRed construct was placed in pDONR221. tdKillerRed was generated from this monomeric construct using the same linker sequences as tdTomato (Serebrovskaya et al., 2009; Shaner et al., 2004). tdKillerRed was targeted to the plasma membrane through the addition of a myristoylation tag to generate myr-tdKillerRed (Gitai et al., 2003). Promoters were cloned into the [4-1] slot of Multisite Gateway. Final expression constructs were generated with LR clonase into the destination vector pCFJ150 (Frøkjaer-Jensen et al., 2010). For experiments with the mechanosensory neurons, we used the following transgenes and mutations: *zdIs5(Pmec-4::GFP)*, *vdEx405[Pmec-4::KillerRed* (20 ng/μl) + *odr-1::DsRED* (30 ng/μl)], LGIV *ced-3(n717)*, and *vdEx167[Plad-2::mCherry* (25 ng/μl) + *Podr-1::dsRED* (30 ng/μl)]; Neumann et al., 2011). Standard molecular-biology methods were used. The *Pmec-4::KR* construct was generated by cloning a KillerRed cDNA (Evrogen) into a pSM vector

(a derivative of pPD49.26 [Fire et al., 1990], a kind gift from Steve McCarroll and Cori Bargmann) containing *Pmec-4*. KillerRed was amplified with primers containing BamHI restrictions sites and inserted into pSM *Pmec-4* digested with the same enzyme.

DNA constructs were injected into the germline using standard methods (Mello et al., 1991). Expression of KillerRed in the correct cells was verified by fluorescence microscopy.

KillerRed Activation and Imaging

Light from a 200 W mercury bulb (PhotoFluor II; 89 North) was filtered with a 562/20 nm filter. The resulting green light was trained into a 5 mm liquid-light guide. The output from the liquid-light guide was directed through a collimating lens (LA1951-A; Thorlabs) and a focusing lens (LA1027-A). Light intensity was measured with a power meter (PM100A; Thorlabs). Illuminations were done in upside-down PCR tube caps in 30 μl of M9 medium on ice to minimize sample heating. L4 stage transgenic worms were used in all experiments. The animals were allowed to crawl on unseeded plates prior to the experiment to remove excess bacteria. Different neuronal cell types required different illumination protocols to result in optimal killing. Illumination times, light intensities, and transgenic lines carrying myr-tdKillerRed are shown in Table S1. An UltraVIEW VoX (PerkinElmer) spinning disc mounted on a Nikon Ti-E Eclipse inverted microscope and a 60× CFI Plan Apo, NA 1.0 oil objective were used to capture z stacks of nonilluminated and illuminated neurons. Cellular damage in illuminated neurons was documented 18–24 hr after illumination.

Illumination of mechanosensory neurons was performed on animals immobilized on NGM agar plates with tetramisole hydrochloride (0.03%), using a Leica MZ10F fluorescence dissecting microscope with an EtDsRed filter (green light 530–560 nm) and 80× magnification (intensity 3.8 mW/mm^2). Twenty-four hours after irradiation, the animals were mounted on 4% agar pads and visualized by epifluorescence using a Zeiss Axioimager Z1 and a Zeiss Axioimager A1 microscope. A CoolSNAP HQ^2 camera (Photometrics) was used for imaging. Metamorph software was used to analyze the collected images.

Selective illumination was performed using the LCD projector system as previously described (Stirman et al., 2011). GFP fluorescence was used to image the cells and define the location of the soma and axon. A green filter (543–593 nm) was used to activate KR in regions of interest selected after imaging. Typical power densities were 2–3 mW/mm^2. In all experiments performed using this system, the illumination time was 1 hr. The length of the axonal processes that were selectively illuminated was 80 μm in all cases. Extensive degeneration was defined as damage that extended beyond 10% of the illuminated length along the axon.

Acute KillerRed activation using freely swimming worms was performed on a modified version of the COLBERT system (Leifer et al., 2011). Briefly, a freely moving L1 larva was imaged with a 20× microscope objective on an inverted Nikon microscope (TE2000). The fluorescence video was taken with a CoolSNAP CCD camera (Photometrics). A digital micromirror device was used to reflect green laser light to illuminate targeted regions of the worm, inducing KillerRed activation in GABAergic motor neurons.

Activation of miniSOG was performed using the same Photofluor II system employed for KillerRed, but with a filter at the appropriate wavelength (Table S1).

Statistics

Statistical comparisons were made using the two-tailed Fisher's exact test (http://www.graphpad.com/quickcalcs/contingency1/), and 95% confidence intervals were calculated using http://www.graphpad.com/quickcalcs/confInterval1/.

SUPPLEMENTAL INFORMATION

Supplemental Information includes one table and two movies and can be found with this article online at http://dx.doi.org/10.1016/j.celrep.2013.09.023.

ACKNOWLEDGMENTS

We thank Brent Neumann, Rosina Giordano-Santini, and Rowan Tweedale for reading the manuscript, and Luke Hammond for technical assistance.

Work in the Hammarlund lab is supported by the Ellison Medical Foundation and NIH grant R01NS066082 to M.H. Work in the Hilliard lab is supported by NHMRC Project Grants 569500 and 631634, and an ARC Future Fellowship to M.A.H. S.C. was supported by an Australian Postgraduate Award. Work in the Lu lab is supported by grants from the NSF, NIH (R01GM088333, R21EB012803, and R01AG035317), Sloan Foundation, and Human Frontiers Science Program to H.L. Work in the Samuel lab is supported by an NIH Pioneer Award, the NSF, and the Harvard-MIT Joint Research Grants Program. D.C.W. was supported by American Cancer Society grant PF-07-037-01-CSM.

Received: March 26, 2013
Revised: August 1, 2013
Accepted: September 13, 2013
Published: October 24, 2013

REFERENCES

Alfonso, A., Grundahl, K., Duerr, J.S., Han, H.-P., and Rand, J.B. (1993). The Caenorhabditis elegans unc-17 gene: a putative vesicular acetylcholine transporter. Science *261*, 617–619.

Avery, L., and Horvitz, H.R. (1987). A cell that dies during wild-type C. elegans development can function as a neuron in a ced-3 mutant. Cell *51*, 1071–1078.

Avery, L., and Horvitz, H.R. (1989). Pharyngeal pumping continues after laser killing of the pharyngeal nervous system of C. elegans. Neuron *3*, 473–485.

Barnham, K.J., Masters, C.L., and Bush, A.I. (2004). Neurodegenerative diseases and oxidative stress. Nat. Rev. Drug Discov. *3*, 205–214.

Bulina, M.E., Chudakov, D.M., Britanova, O.V., Yanushevich, Y.G., Staroverov, D.B., Chepurnykh, T.V., Merzlyak, E.M., Shkrob, M.A., Lukyanov, S., and Lukyanov, K.A. (2006). A genetically encoded photosensitizer. Nat. Biotechnol. *24*, 95–99.

Campbell, R.E., Tour, O., Palmer, A.E., Steinbach, P.A., Baird, G.S., Zacharias, D.A., and Tsien, R.Y. (2002). A monomeric red fluorescent protein. Proc. Natl. Acad. Sci. USA *99*, 7877–7882.

Carpentier, P., Violot, S., Blanchoin, L., and Bourgeois, D. (2009). Structural basis for the phototoxicity of the fluorescent protein KillerRed. FEBS Lett. *583*, 2839–2842.

Catalá, A. (2010). A synopsis of the process of lipid peroxidation since the discovery of the essential fatty acids. Biochem. Biophys. Res. Commun. *399*, 318–323.

Chow, B.Y., Han, X., Dobry, A.S., Qian, X., Chuong, A.S., Li, M., Henninger, M.A., Belfort, G.M., Lin, Y., Monahan, P.E., and Boyden, E.S. (2010). High-performance genetically targetable optical neural silencing by light-driven proton pumps. Nature *463*, 98–102.

DiMauro, S., and Schon, E.A. (2008). Mitochondrial disorders in the nervous system. Annu. Rev. Neurosci. *31*, 91–123.

Edwards, S.L., Charlie, N.K., Milfort, M.C., Brown, B.S., Gravlin, C.N., Knecht, J.E., and Miller, K.G. (2008). A novel molecular solution for ultraviolet light detection in Caenorhabditis elegans. PLoS Biol. *6*, e198.

Ellis, H.M., and Horvitz, H.R. (1986). Genetic control of programmed cell death in the nematode C. elegans. Cell *44*, 817–829.

Fang-Yen, C., Gabel, C.V., Samuel, A.D.T., Bargmann, C.I., and Avery, L. (2012). Laser microsurgery in Caenorhabditis elegans. Methods Cell Biol. *107*, 177–206.

Fatokun, A.A., Stone, T.W., and Smith, R.A. (2008). Oxidative stress in neurodegeneration and available means of protection. Front. Biosci. *13*, 3288–3311.

Fire, A., Harrison, S.W., and Dixon, D. (1990). A modular set of lacZ fusion vectors for studying gene expression in Caenorhabditis elegans. Gene *93*, 189–198.

Frøkjaer-Jensen, C., Davis, M.W., Hollopeter, G., Taylor, J., Harris, T.W., Nix, P., Lofgren, R., Prestgard-Duke, M., Bastiani, M., Moerman, D.G., and Jorgensen, E.M. (2010). Targeted gene deletions in C. elegans using transposon excision. Nat. Methods *7*, 451–453.

Gitai, Z., Yu, T.W., Lundquist, E.A., Tessier-Lavigne, M., and Bargmann, C.I. (2003). The netrin receptor UNC-40/DCC stimulates axon attraction and outgrowth through enabled and, in parallel, Rac and UNC-115/AbLIM. Neuron *37*, 53–65.

Hall, D.H., Gu, G., García-Añoveros, J., Gong, L., Chalfie, M., and Driscoll, M. (1997). Neuropathology of degenerative cell death in Caenorhabditis elegans. J. Neurosci. *17*, 1033–1045.

Ichishita, R., Tanaka, K., Sugiura, Y., Sayano, T., Mihara, K., and Oka, T. (2008). An RNAi screen for mitochondrial proteins required to maintain the morphology of the organelle in Caenorhabditis elegans. J. Biochem. *143*, 449–454.

Kanaji, S., Iwahashi, J., Kida, Y., Sakaguchi, M., and Mihara, K. (2000). Characterization of the signal that directs Tom20 to the mitochondrial outer membrane. J. Cell Biol. *151*, 277–288.

Keller, J.N., Pang, Z., Geddes, J.W., Begley, J.G., Germeyer, A., Waeg, G., and Mattson, M.P. (1997). Impairment of glucose and glutamate transport and induction of mitochondrial oxidative stress and dysfunction in synaptosomes by amyloid β-peptide: role of the lipid peroxidation product 4-hydroxynonenal. J. Neurochem. *69*, 273–284.

Landis, G.N., and Tower, J. (2005). Superoxide dismutase evolution and life span regulation. Mech. Ageing Dev. *126*, 365–379.

Leifer, A.M., Fang-Yen, C., Gershow, M., Alkema, M.J., and Samuel, A.D.T. (2011). Optogenetic manipulation of neural activity in freely moving Caenorhabditis elegans. Nat. Methods *8*, 147–152.

Liu, Q., Hollopeter, G., and Jorgensen, E.M. (2009). Graded synaptic transmission at the Caenorhabditis elegans neuromuscular junction. Proc. Natl. Acad. Sci. USA *106*, 10823–10828.

Mark, R.J., Hensley, K., Butterfield, D.A., and Mattson, M.P. (1995). Amyloid beta-peptide impairs ion-motive ATPase activities: evidence for a role in loss of neuronal Ca2+ homeostasis and cell death. J. Neurosci. *15*, 6239–6249.

McIntire, S.L., Jorgensen, E., Kaplan, J., and Horvitz, H.R. (1993). The GABAergic nervous system of Caenorhabditis elegans. Nature *364*, 337–341.

McIntire, S.L., Reimer, R.J., Schuske, K., Edwards, R.H., and Jorgensen, E.M. (1997). Identification and characterization of the vesicular GABA transporter. Nature *389*, 870–876.

Mello, C.C., Kramer, J.M., Stinchcomb, D., and Ambros, V. (1991). Efficient gene transfer in C. elegans: extrachromosomal maintenance and integration of transforming sequences. EMBO J. *10*, 3959–3970.

Nagel, G., Brauner, M., Liewald, J.F., Adeishvili, N., Bamberg, E., and Gottschalk, A. (2005). Light activation of channelrhodopsin-2 in excitable cells of Caenorhabditis elegans triggers rapid behavioral responses. Curr. Biol. *15*, 2279–2284.

Neumann, B., Nguyen, K.C.Q., Hall, D.H., Ben-Yakar, A., and Hilliard, M.A. (2011). Axonal regeneration proceeds through specific axonal fusion in transected C. elegans neurons. Dev. Dyn. *240*, 1365–1372.

Okazaki, A., Sudo, Y., and Takagi, S. (2012). Optical silencing of C. elegans cells with arch proton pump. PLoS ONE *7*, e35370.

Pletnev, S., Gurskaya, N.G., Pletneva, N.V., Lukyanov, K.A., Chudakov, D.M., Martynov, V.I., Popov, V.O., Kovalchuk, M.V., Wlodawer, A., Dauter, Z., and Pletnev, V. (2009). Structural basis for phototoxicity of the genetically encoded photosensitizer KillerRed. J. Biol. Chem. *284*, 32028–32039.

Qi, Y.B., Garren, E.J., Shu, X., Tsien, R.Y., and Jin, Y. (2012). Photo-inducible cell ablation in Caenorhabditis elegans using the genetically encoded singlet oxygen generating protein miniSOG. Proc. Natl. Acad. Sci. USA *109*, 7499–7504.

Rand, J.B. (1989). Genetic analysis of the cha-1-unc-17 gene complex in Caenorhabditis. Genetics *122*, 73–80.

Roy, A., Carpentier, P., Bourgeois, D., and Field, M. (2010). Diffusion pathways of oxygen species in the phototoxic fluorescent protein KillerRed. Photochem. Photobiol. Sci. *9*, 1342–1350.

Serebrovskaya, E.O., Edelweiss, E.F., Stremovskiy, O.A., Lukyanov, K.A., Chudakov, D.M., and Deyev, S.M. (2009). Targeting cancer cells by using an antireceptor antibody-photosensitizer fusion protein. Proc. Natl. Acad. Sci. USA *106*, 9221–9225.

Shaner, N.C., Campbell, R.E., Steinbach, P.A., Giepmans, B.N.G., Palmer, A.E., and Tsien, R.Y. (2004). Improved monomeric red, orange and yellow fluorescent proteins derived from Discosoma sp. red fluorescent protein. Nat. Biotechnol. *22*, 1567–1572.

Shu, X., Lev-Ram, V., Deerinck, T.J., Qi, Y., Ramko, E.B., Davidson, M.W., Jin, Y., Ellisman, M.H., and Tsien, R.Y. (2011). A genetically encoded tag for correlated light and electron microscopy of intact cells, tissues, and organisms. PLoS Biol. *9*, e1001041.

Smith, A.J., Smith, R.A., and Stone, T.W. (2009). 5-Hydroxyanthranilic acid, a tryptophan metabolite, generates oxidative stress and neuronal death via p38 activation in cultured cerebellar granule neurones. Neurotox. Res. *15*, 303–310.

Stenico, M., Lloyd, A.T., and Sharp, P.M. (1994). Codon usage in Caenorhabditis elegans: delineation of translational selection and mutational biases. Nucleic Acids Res. *22*, 2437–2446.

Stirman, J.N., Crane, M.M., Husson, S.J., Wabnig, S., Schultheis, C., Gottschalk, A., and Lu, H. (2011). Real-time multimodal optical control of neurons and muscles in freely behaving Caenorhabditis elegans. Nat. Methods *8*, 153–158.

Teh, C., Chudakov, D.M., Poon, K.-L., Mamedov, I.Z., Sek, J.-Y., Shidlovsky, K., Lukyanov, S., and Korzh, V. (2010). Optogenetic in vivo cell manipulation in KillerRed-expressing zebrafish transgenics. BMC Dev. Biol. *10*, 110.

Uttara, B., Singh, A.V., Zamboni, P., and Mahajan, R.T. (2009). Oxidative stress and neurodegenerative diseases: a review of upstream and downstream antioxidant therapeutic options. Curr. Neuropharmacol. *7*, 65–74.

White, J.G., Southgate, E., Thomson, J.N., and Brenner, S. (1986). The structure of the nervous system of the nematode Caenorhabditis elegans. Philos. Trans. R. Soc. Lond. B Biol. Sci. *314*, 1–340.

Zhang, F., Wang, L.-P., Brauner, M., Liewald, J.F., Kay, K., Watzke, N., Wood, P.G., Bamberg, E., Nagel, G., Gottschalk, A., and Deisseroth, K. (2007). Multimodal fast optical interrogation of neural circuitry. Nature *446*, 633–639.

3.3 Supplementary data

Supplemental Table S1. Details of KillerRed transgenes and illumination conditions, related to all Figures.

Figure	Neuron type	Transgene/injection concentration	Intensity	Wavelength	Illumination time
1	GABA	Punc-47 KillerRed	1mW/mm^2	white	2 hours
1	Dopamine (CEP, ADE, PDE)	Pdat-1::myr-tdKillerRed (20ng/µl)	46mW/mm^2	542-582 nm.	15 min.
1	RIA	Pglr-3::myr-tdKillerRed linearized construct (3ng/µl)	46mW/mm^2	542-582 nm.	10 min.
1	Acetylcholine	Punc-17::myr-tdKillerRed (20ng/µl)	46mW/mm^2	542-582 nm.	5 min.
1	Mechanosensory (ALM, PLM, AVM, PVM)	Pmec-4::KillerRed (20ng/µl)	3.8 mW/mm^2	530-560 nm.	30 min.
1	AFD	Pgcy-8::myr-tdKillerRed (50ng/µl)	46mW/mm^2	542-582 nm.	15 min.
1	AWB	Pstr-1::myr-tdKillerRed (30ng/µl)	46mW/mm^2	542-582 nm.	10 min.
2	Acetylcholine	Punc-17::myr-tdKillerRed (20ng/µl)	46mW/mm^2	542-582 nm.	5 min.
2	GABA	Punc-47 KillerRed	40mW/mm^2	542-582 nm.	5 min.
3	AWB	Pstr-1::myr-tdKillerRed (30ng/µl)	46mW/mm^2	542-582 nm.	10 min.
3	Acetylcholine	Punc-17::myr-tdKillerRed (20ng/µl)	46mW/mm^2	542-582 nm.	2 min.
3	Mechanosensory (ALM, PLM,	Pmec-4::KillerRed (20ng/µl)	3.8 mW/mm^2	530-560 nm.	30 min.

	AVM, PVM)				
4	AWB	*Pstr-1::myr-tdKillerRed* (30ng/*µl*)	46mW/mm^2	542-582 nm.	10 min.
4	GABA	*Punc-47::myr-tdKillerRed* (20ng/*µl*)	46mW/mm^2	542-582 nm.	5 min.
5	Mechanosensory (ALM, PLM, AVM, PVM)	*Pmec-4::KillerRed (20ng/µl)*	3.8 mW/mm^2	530-560 nm.	30 min.
5	Mechanosensory (ALM, PLM, AVM, PVM)	*Pmec-4::KillerRed (20ng/µl)* (anterior or posterior illumination)	5.8 mW/mm^2	543-593 nm.	30 min.
5	Mechanosensory (ALM, PLM, AVM, PVM)	*Pmec-4::KillerRed (20ng/µl)* (axon or soma illumination)	52 mW/mm^2	543-593 nm.	1h
6	Muscle (mitochondria)	*Pmyo-3::mito-tdKillerRed* (20ng/*µl*)	46mW/mm^2	542-582 nm.	5 min.
6	Muscle (plasma membrane)	*Pmyo-3::myr-tdKillerRed* (20ng/*µl*)	46mW/mm^2	542-582 nm.	5 min.
7	Acetylcholine	*miniSOG* CZ14527 *Punc-17(beta)-tomm-20-N'55AA::miniSOG(juEx3790)* (Qi et al., 2012)	0.57mW/mm2	461-489	30 min.
7	Acetylcholine	*Punc-17::myr-tdKillerRed* (20ng/*µl*)	0.57mW/mm2	542-582 nm.	30 min.
7	Acetylcholine	*miniSOG* CZ14527 *Punc-17(beta)-tomm-20-N'55AA::miniSOG(juEx3790)* (Qi et al., 2012)	0.57mW/mm2	542-582 nm.	30 min.
7	Acetylcholine	*Punc-17::myr-tdKillerRed* (20ng/*µl*)	0.57mW/mm2	461-489	30 min.
7	Mechanosensory (ALM, PLM, AVM, PVM)	*Pmec-4::KillerRed (20ng/µl)*	0.57mW/mm2	460-500 nm	20 min.
7	Mechanosensory (ALM, PLM, AVM, PVM)	*Pmec-4::KillerRed (20ng/µl)*	0.82mW/mm2	426 -446 nm	20 min.

3.4 Discussion and implications of findings

As demonstrated by the present study (and reviewed in chapter 1), neurons are particularly sensitive to ROS. The generation of ROS is a normal byproduct of mitochondrial respiration, and specific cellular mechanisms of detoxification are in place to protect cells from damage. In the present study ROS were generated cell-specifically in subsets of neurons using the phototoxic molecule KillerRed. The result of this ROS generation was rapid and irreversible neuronal cell death. As an optogenetic tool in *C. elegans* KillerRed has two main applications. The first is as an optogentic method of neuronal ablation; such methods are essential to determine the function of a cell or group of cells. Indeed, until now the simplest method of determining the function of a neuron has been to ablate it with a laser and observe the resulting defect. Although used with great effect in *C. elegans*, this approach carries the intrinsic limitation imposed by the single-cell surgery procedure, which enormously limits the efficiency when a larger number of cells must be eliminated simultaneously. The second application is as a method of subcellular ROS generation to study the effect of ROS accumulation in neurons. ROS accumulation and oxidative damage have been linked to many neurodegenerative diseases, and an increase in ROS has been shown to induce axonal degeneration (reviewed in chapter 1). The present study demonstrates that the activation of KillerRed in specific regions of the axon is sufficient to induce localized axonal degeneration. Although ROS accumulation has been identified as a key risk factor for axonal degeneration, the precise mechanism by which ROS induce axonal degeneration is not known. Therefore, the application of this tool as a method of inducing ROS generation in neurons provides a way to study the mechanisms of ROS-induced neurodegeneration *in vivo*. Chapter 4 examines the mechanisms of protection against ROS-induced neurodegeneration, using KillerRed to induce ROS production.

3.5 Statement of contribution

I performed the experiments presented in Figure 1g, h, i, k, l, Figure 3c, Figure 4e-g. In addition, I contributed substantially to the design and planning of experiments and in the writing of the manuscript. The strategy of using KillerRed to damage neurons was initially developed as an approach for the study of axonal regeneration and degeneration. In this context, this paper represents a novel method of inducing neurodegeneration *in vivo* to identify and study the molecular mechanisms involved.

Chapter 4:
Discovery of molecular mechanisms regulating neuronal degeneration induced by ROS

4.1 Introduction

The study presented in chapter 3 demonstrated that the optogenetic tool KillerRed is able to specifically and rapidly induce neurodegeneration in several classes of *C. elegans* neurons, via the generation of ROS in response to specific light illumination. Neurons are particularly susceptible to ROS, and as such oxidative damage has been linked to many neurodegenerative diseases including Alzheimer's and Parkinson's diseases, ALS and MS (Uttara et al., 2009). Mitochondria have been identified as the primary source of cellular ROS, and mitochondrial dysfunction is a common pathology in many neurodegenerative disorders (Lin and Beal, 2006). However, the molecular mechanisms that link ROS accumulation to neurodegeneration remain mostly unknown.

In the study presented in this chapter, KillerRed is used as a tool to discover the cellular and molecular mechanisms of neurodegeneration induced by ROS in the *C. elegans* mechanosensory neurons. First, ROS is shown to induce neuronal death through a necrotic mechanism rather than apoptosis. Second, KillerRed activation in different neuronal regions (such as the axon, cell body, or specific regions within the axon) is demonstrated to differentially induce neurodegeneration, suggesting that specific regions within a neuron have diverse sensitivities to ROS. Finally, the axonal guidance molecule UNC-6/Netrin is identified as a novel axonal protective molecule against ROS-induced neurodegeneration.

Together these data further characterize ROS-induced neuronal cell death and serve to demonstrate that KillerRed can be used as a tool to discover novel mechanisms of neuronal protection against such degeneration. This work is part of an ongoing international collaboration with the laboratory of Prof. Hang Lu, at the Georgia Institute of Technology, Atlanta, and is being prepared for submission in early 2015.

4.2 Results

KillerRed induces necrosis in neurons

KillerRed can efficiently kill a variety of neurons in *C. elegans*, including sensory neurons, interneurons, and motor neurons (section 3.2). This inducible neuronal ablation approach is strictly cell-autonomous and highly specific. Furthermore KillerRed-induced neuronal damage is independent of the canonical apoptosis pathway, given that animals lacking the CED-3 caspase have a rate of neuronal death upon illumination that is indistinguishable from that of wild-type animals (section 3.2). These results combined with the swollen and vacuolated appearance of the cell bodies in ablated neurons, led to the hypothesis that KillerRed-generated ROS trigger a necrotic cell death pathway. In *C. elegans,* neurodegeneration that proceeds through necrotic cell death has been shown to require the calpain proteases CLP-1 and TRA-3 (Syntichaki et al., 2002). To conclusively determine that a necrotic pathway mediates KillerRed-induced neuronal death, we tested the effect of KillerRed irradiation in animals lacking either the CLP-1 or TRA-3 calpain proteases. A transgenic *C. elegans* strain expressing cytosolic monomeric KillerRed, as well as GFP, specifically in the six mechanosensory neurons using the promoter of the gene *mec-4* (*Pmec-4::KR*; *Pmec-4::GFP*), was crossed with individual mutants in either *clp-1* or *tra-3*. In wild-type animals KillerRed activation caused robust cell death in the ALM and PLM neurons, whereas AVM and PVM were largely refractory to KillerRed-induced damage (Fig 4.1; section 3.2). A strong suppression of KillerRed-induced cell death was observed in both the ALM and PLM neurons of *clp-1* and *tra-3* mutants (Fig 4.1). The requirement of CLP-1 and TRA-3 for efficient KillerRed-induced neuronal death strongly supports the hypothesis that ROS-induced neurodegeneration proceeds through a necrotic cell death mechanism.

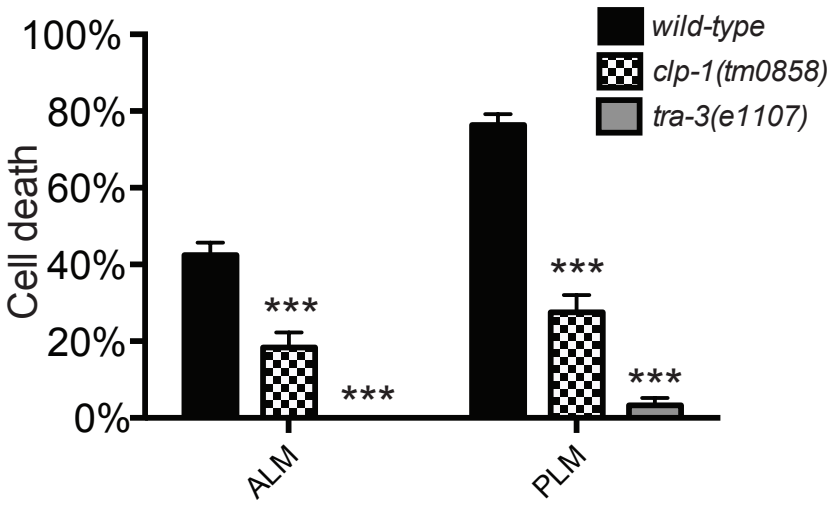

Figure 4.1. KillerRed-induced ROS triggers a necrotic mechanism in mechanosensory neurons. Wild-type, *clp-1(tm0858),* and *tra-3(e1107)* animals expressing KillerRed in the mechanosensory neurons ALM and PLM were observed 24hr following a 30min illumination with green light (530-560nm). *clp-1(tm0858)* and *tra-3(e1107)* mutants show a significant reduction in cell death. n> 98 neurons. ***= P-value<0.001.

ROS activation in specific axonal regions is sufficient to induce neuronal ablation

Selective illumination of the cell soma or axon of ALM neurons expressing KillerRed is sufficient to induce cell death (section 3.2). To determine if individual axonal regions display selective vulnerability to ROS-induced damage this illumination was further restricted to three regions within the axon of ALM: a proximal region close to the soma, a region in the middle of the axon posterior to the synaptic branch, and a distal region at the synaptic branch point (Fig 4.2a). Remarkably, illumination of the proximal or distal region was sufficient to induce cell death in ALM, whereas illumination of the middle region of the ALM axon was unable to kill the neuron (Fig 4.2c). To further examine the spatial requirement of selective illumination of the distal region of the axon, illumination was restricted even further to three regions surrounding the synaptic branch of ALM: one posterior to the branch site, one at the branch site, and one anterior to the branch site (Fig 4.2b). Illumination of the branch point of ALM or the region posterior to it was sufficient to induce cell death, whereas illuminating the region anterior to the synaptic branch was unable to induce cell death (Fig 4.2d). Taken together these results suggest that specific regions within individual neurons exhibit a selective vulnerability to KillerRed-induced ROS damage. Strikingly, this damage is not proportional to the distance from the cell body. In both selective illumination paradigms there were regions that were unable to induce cell death after illumination which were closer to the soma than those capable of inducing cell death. This raises the possibility that distinct subcellular compartments, comprising different distributions of organelles and molecules, are able to provide either increased protection or sensitivity to ROS, in a region-specific manner.

UNC-6/Netrin protects against KR induced neurodegeneration

The ventral mechanosensory neurons AVM and PVM are resistant to KillerRed-induced damage (section 3.2). The increased resistance to ROS-induced damage of these neurons may be mediated by extrinsic or intrinsic factors. Animals lacking UNC-6/Netrin or SLT-1/Slit have anteriorly misrouted AVM and PVM axons that fail to initiate growth towards the ventral nerve cord (Hao et al., 2001). To determine if the local environment surrounding AVM and PVM mediates this protection, we tested the effect of KillerRed illumination in mutants where guidance of the AVM and PVM axon was disrupted was tested (Fig 4.3a). KillerRed irradiation in populations of animals lacking UNC-6 resulted in a strong increase in cell death in the AVM neuron (Fig 4.3b). Conversely, populations of animals lacking SLT-1 were no more sensitive to KillerRed illumination than wild-type controls (Fig 4.3b). Both *unc-6* and *slt-1* mutants have a similar penetrance of misrouted AVM neurons (Hao et al., 2001; Hedgecock et al., 1990). Thus, these data clearly indicate an effect of UNC-6 in protecting the AVM axon from ROS-induced damage; however they

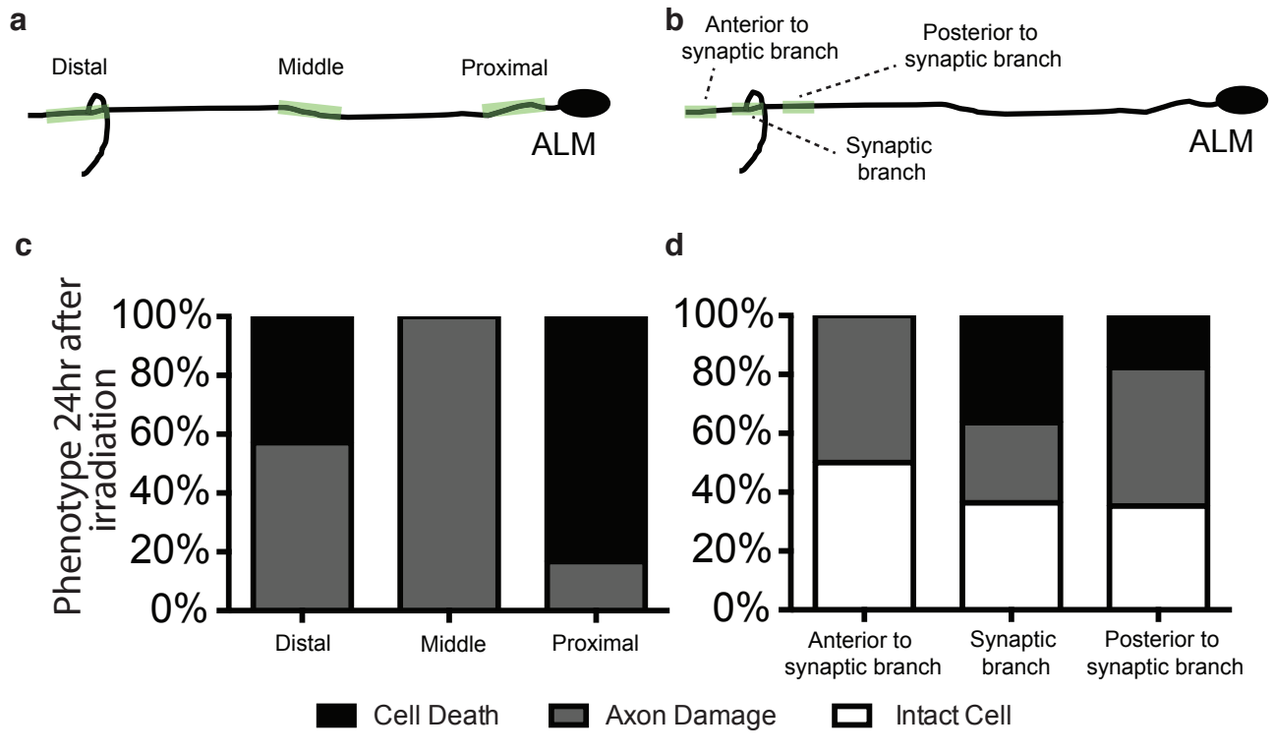

Figure 4.2. Subcellular ROS activation triggers cell death in the ALM neurons. **a**, ALM neurons expressing KillerRed were illuminated with green light (543-593nm) using a selective illumination system in three axonal regions: proximal, middle, and distal. **b**, illumination was reduced to three regions surrounding the synaptic branch of ALM: anterior to, posterior to, and at the synaptic branch point. **c**, phenotype of the ALM neuron 24hr following a 1hr illumination of the regions shown in **a**. Illumination of distal and proximal regions of the ALM axon were sufficient to induce cell death. n> 6 neurons. **d**, phenotype of the ALM neuron 24hr after a 1hr illumination of the regions shown in **b**. Illumination of the synaptic branch or a region posterior to the synaptic branch was sufficient to induce cell death. n> 17 neurons.

also reveal that this effect is not due to the simple aberrant trajectory of the axon but rather to another mechanism.

UNC-6/Netrin acts via UNC-40/DCC and SAX-3/Robo independently of SLT-1/Slit

In *C. elegans* the attractive guidance cue UNC-6 is expressed in ventral regions and acts through its receptor UNC-40 to attract the AVM axon to the ventral nerve cord (Chan et al., 1996; Wadsworth et al., 1996). In parallel, the repulsive guidance cue SLT-1, expressed in dorsal regions, acts through its receptor SAX-3 to repel the AVM axon towards the ventral nerve cord (Hao et al., 2001). To determine the mechanism of UNC-6 protection we performed KillerRed illumination in animals lacking either UNC-40 or SAX-3. As in *unc-6* mutants, *unc-40* mutants had a strong increase in the incidence of AVM cell death following illumination (Fig 4.3b). Animals lacking the repulsive guidance molecule SLT-1 showed no change in their sensitivity to ROS-induced damage. However, in *sax-3* mutants we observed a strong increase in AVM cell death following illumination of KillerRed (Fig 4.3b). These data suggest that UNC-6 acts through its receptor UNC-40 to mediate neuronal protection against ROS and that this pathway may involve a SLT-1-independent role for the receptor SAX-3. A full genetic analysis of these pathways is needed to confirm this hypothesis.

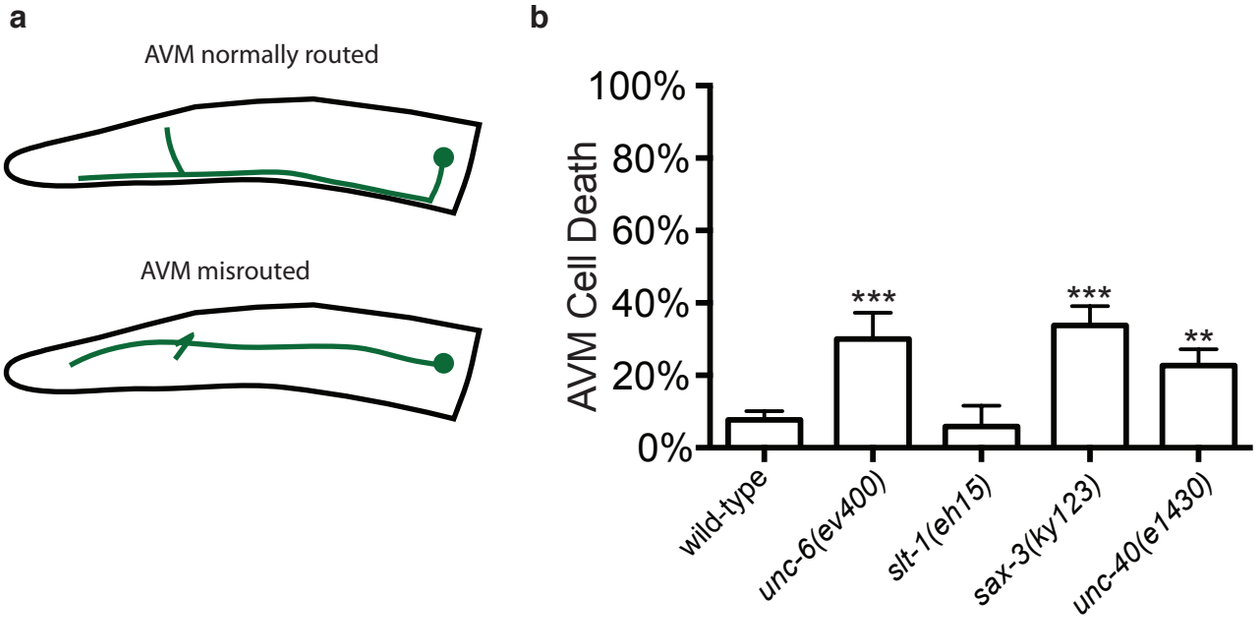

Figure 4.3. UNC-6 protects against KillerRed-induced cell death in the AVM neuron.
a, Schematic examples of normally routed (top) and mis-routed (bottom) AVM axons. **b,** cell death was scored in the AVM neuron 24hr after a 30min illumination with green light (530-560nm) in wild-type and mutant animals lacking molecules required for the correct guidance of the AVM axon. A significant increase in AVM cell death was observed in *unc-6(ev400)*, *sax-3(ky123)*, and *unc-40(e1430)* mutants. n> 17 neurons. **= P-value < 0.01, ***= P-value<0.001.

4.3 Discussion and implications of findings

The present study together with that presented in chapter 3 demonstrates that KillerRed can be used as an optogenetic method of inducing both axonal and neuronal degeneration. This method is suitable for use in both forward and reverse genetic approaches to discover the mechanisms that regulate axonal and neuronal degeneration induced by ROS. As demonstrated in chapter 3, most neuronal classes tested displayed a differential sensitivity to KillerRed-induced death. Selective vulnerability is a common theme in neurodegenerative disorders, whereby specific populations of neurons degenerate while others are spared in response to the same stimulus (Mattson and Magnus, 2006). In this manner, neurons refractory to KillerRed activation provide an excellent model in which to study the mechanisms underlying this selective vulnerability. The present study demonstrates that not only are individual neurons differentially sensitive to ROS, but that regions within the same neuron exhibit differential sensitivity. Synaptic regions of the ALM axon were more sensitive to KillerRed activation than non-synaptic regions. It is not clear from these data if the synapse is more sensitive to ROS, or if the distribution and/or function of organelles, such as mitochondria, within these regions are different.

This study also identified UNC-6/Netrin as a protective factor against KillerRed-induced ROS. Loss of UNC-6/Netrin resulted in a dramatic increase in the rate of neuronal cell death following KillerRed activation in the AVM neuron (a neuron normally resistant to KillerRed-induced damage). Loss of the UNC-6/Netrin receptor, UNC-40/DCC, also increased the rate of KillerRed-induced neuronal degeneration. However, SAX-3/Robo, the receptor for the repulsive guidance cue SLT-1/Slit, protected against neurodegeneration independently of its canonical ligand. A full genetic analysis is needed to determine if these molecules function in the same pathway to protect neurons from ROS-induced degeneration. One potential mechanism of neuronal protection is through the regulation of mitochondria. SAX-3 has been demonstrated to function independently of SLT-1 in regulating the localization, morphology, and function of mitochondria in *C. elegans* muscle (Han et al., 2012). It is possible that, together or in parallel with the UNC-6/UNC-40 pathway, SAX-3 has a similar function in neurons. In addition to its role in guidance, Netrin-DCC signalling has been demonstrated to function as a cellular dependence signal in the nervous system (Furne et al., 2008; Llambi et al., 2001). In this context DCC amplifies caspase-mediated apoptosis in the absence of its ligand Netrin. There is no known role for SAX-3/Robo in this system and it is not known if the increased neuronal cell death observed in *unc-6*, *unc-40*, and *sax-3* mutants, occurs via a necrotic or an apoptotic mechanism.

Taken together the data presented in this chapter provide strong evidence that KillerRed can be used to study the molecular mechanisms of ROS-induced axonal and neuronal degeneration.

4.4 Materials and methods

Strains and molecular biology

Nematodes were cultured using standard methods. All experiments were performed at 20°C. The *Pmec-4::KillerRed* construct was as used in chapter 3.

KillerRed activation and imaging

Animals were immobilized on NGM agar plates using tetramisole hydrochloride (0.03%), and irradiated using a Leica MZ10F fluorescence dissecting microscope with an EtDsRed filter (green light 530-560 nm) with an 80X magnification (intensity 3.8mW/mm^2). 24 hr after irradiation animals were mounted on 4% agar pads, and epifluorescence was used to visualize animals either with a Zeiss Axioimager Z1 or with a Zeiss Axioimager A1 microscope. A Photometrics camera, Cool snap HQ^2, was used for image acquisition, and Metamorph software was used for image analysis. The selective illumination using the LCD projector system is as described in Stirman et al. (2011). GFP fluorescence was used to image the cells and define the location of the soma and axon. A green filter (543-593 nm) was used to activate KillerRed in regions of interest selected after imaging. Typical power intensities were 2-3 mW/mm^2. In all experiments performed using this system illumination time was 1 hr. The length of the axonal processes that were selectively illuminated was 80μm in all cases. Extensive degeneration was defined as damage that extended beyond 10% of the illuminated length along the axon.

Statistical analyses

Statistical analyses were performed using Primer of Biostatistics 3.01. The error of proportions was used to estimate variation within a single population. The Student's *t*-test was used in all cases.

4.5 Statement of contribution

I performed the experiments presented in Figure 4.1 and Figure 4.3. Together with the principal advisor Dr. Massimo Hilliard, I significantly contributed to this project in designing and planning experiments, which are ongoing in collaboration with the lab of Prof. Hang Lu at the Georgia Institute of Technology, Atlanta.

Chapter 5:
Discovery of molecular mechanisms of axonal fusion following regeneration

5.1 Introduction

Chapters 3 and 4 outlined an approach to study axonal degeneration in response to axonal injury in the form of ROS induced by KillerRed. A complementary response to axonal degeneration after injury is that of axonal regeneration (as reviewed in chapter 1). The *C. elegans* mechanosensory neuron PLM is capable of robust axonal regeneration following laser axotomy (Wu et al., 2007). Following formation of a growth cone and axon extension during regeneration, a proportion of regrowing PLM axons reconnect with their separated distal fragment and undergo a membrane fusion event. This protects the distal fragment from degeneration and restores both membrane and cytoplasmic continuity in a process known as axonal fusion (reviewed in chapter 1). This process is highly specific, supporting the notion that there are molecular mechanisms in place that mediate the recognition of the distal axonal fragment by the regrowing proximal fragment.

The study presented in this chapter, identifies a molecular pathway that acts as a 'save-me' signal on the distal axonal fragment and signals via receptors on the regrowing proximal axon to mediate recognition and axonal fusion. This signalling pathway utilizes components of the apoptotic recognition and engulfment pathway and is activated by both laser axotomy and genetically induced axonal damage.

This work is an international collaboration with the laboratory of Ding Xue (University of Colorado), and is currently in revision at the peer-reviewed journal *Nature*. A copy of the reviewed manuscript is presented as section 5.2 of this thesis.

5.2 Axonal fusion during regeneration requires conserved components of the apoptotic pathway

Neumann, B., **Coakley, S.**, Giordano-Santini, R., Linton, C., Zhang, Y., Yang, H., Xue, D. and Hilliard, M.A. (2014) Axonal fusion during regeneration requires conserved components of the apoptotic pathway. *In revision at **Nature**.*

Complete, functional regeneration after nervous system injury requires transected axons to reconnect with their original target tissue; however, how this occurs remains poorly understood. Axonal fusion, a spontaneous regenerative mechanism identified in several different species, provides an efficient means of achieving target reconnection as a regrowing axon is able to contact and fuse with its own separated axon fragment, thereby re-establishing the original axonal tract. Here we report a molecular characterization of this process in *Caenorhabditis elegans*, identifying phosphatidylserine (PS) and the PS receptor (PSR-1) as critical components for successful axonal fusion. PSR-1 functions cell-autonomously in the regrowing neuron and requires both its PS-binding and catalytic domains. Interestingly, instead of acting in the CED-2, CED-5, CED-12 phagocytosis pathway, PSR-1 functions in a parallel phagocytic pathway that is mediated by the transthyretin protein TTR-52, and includes CED-1, CED-7, NRF-5 and CED-6. We show that TTR-52 binds to PS exposed on the injured axon and that its function is sufficient to restore fusion several hours following injury. Thus, conserved components of the apoptotic cell clearance machinery play an unexpected role in mediating reconnection between axon fragments during regeneration of the nervous system. We propose that PS functions in this context as a 'save me' signal for the distal fragment.

Axonal regeneration occurs with the primary objective of re-establishing lost connection between an injured neuron and its original target tissue. Although extensive knowledge has been gained regarding the intrinsic and extrinsic modifiers of axonal regeneration, insight into how a neuron can rejoin with its target is lacking. A highly efficient means to re-establish the connection between an injured neuron and its target tissue occurs spontaneously in several invertebrate species [1-7]. This process, referred to as axonal fusion, occurs when the proximal axon that is still attached to the cell body regrows towards, then reconnects and fuses with its separated distal fragment. Previously, we and others have demonstrated that axonal fusion in the *C. elegans* mechanosensory neurons is a highly specific process that occurs through a fusion event, with both membrane and cytoplasmic continuity re-established [4,7]. However, the genetic components that mediate axonal fusion remain largely unknown, with the nematode-specific fusogen, Epithelial Fusion Failure 1 (EFF-1), the only protein previously found to be involved [4].

We speculated that the process of axonal fusion might resemble that of apoptosis [7], in which the dying cell exposes "eat-me" signals that mediate recognition and engulfment by surrounding phagocytes. During apoptosis, plasma membrane phospholipid asymmetry is lost, causing phosphatidylserine (PS), which is normally restricted to the cytoplasmic leaflet, to be externalized

to the exoplasmic leaflet where it enables recognition by phagocytic cells [8-11]. Two partially redundant genetic pathways regulate the removal of apoptotic cells in *C. elegans*, the first of which is mediated by the PS receptor (PSR-1/jmjd6) that directly binds exposed PS [12,13] and signals through the CED-2/CrkII, CED-5/Dock180, CED-12/ELMO and CED-10/RAC1 GTPase engulfment pathway [14-17]. In the second pathway, the secreted transthyretin-like protein TTR-52 bridges exposed PS on apoptotic cells with the CED-1/LRP1/MEGF10 transmembrane receptor [18,19] in a pathway that includes the LPS-binding/lipid transfer protein NRF-5, CED-7/ABC transporter, and CED-6/GULP [20-23]. These two pathways converge with the downstream activation of CED-10/RAC1 GTPase that triggers the cytoskeleton rearrangements necessary for engulfment [24]. Here we demonstrate that the function of these conserved apoptotic molecules is largely shared between apoptotic cell clearance and axon fusion during regeneration, and suggest that in the context of axonal regeneration PS functions as a 'save me' signal for the distal axonal fragment.

To study axonal fusion we expressed GFP specifically within the six mechanosensory neurons of *C. elegans* (Fig. 1a) and performed laser axotomy of the posterior-lateral mechanosensory (PLM) neurons (Fig. 1b). To specifically study the process of axonal fusion, we analyzed only severed axons that re-established a connection between the regrowing proximal axon and its separated distal fragment. Maintenance, or inhibition of degeneration, was used as evidence of a successful fusion event, while degeneration of the distal axonal fragment after reconnection had occurred was considered proof of an unsuccessful fusion event. In wild-type (WT) animals, 80% of axons that displayed proximal-distal reconnection underwent successful fusion (Fig. 1b, d). EFF-1, which mediates a vast array of fusion events in *C. elegans* [25], was previously found to function in axonal fusion [4]. Animals lacking EFF-1 displayed a strong suppression in the rate of axonal fusion (Fig. 1d and Extended Data Fig. 1a, b). To determine where EFF-1 is required for this process, we expressed a GFP-tagged version of the protein specifically in the mechanosensory neurons. This transgene could rescue the defect in *eff-1* null animals, indicating that EFF-1 functions cell-autonomously for the PLM axonal fusion event (Extended Data Fig. 1b). Following axotomy, we consistently observed EFF-1::GFP on the membrane of regrowing axons (Extended Data Fig. 1c, d). These findings suggest that EFF-1, localized on the membrane of the regenerative growth cone, mediates fusion once contact is re-established with the separated axon fragment.

While axon fusion is conserved across a range of species [1-7], EFF-1 is not [26]. In order to identify other conserved components required for this process, we undertook a candidate screen on molecules previously identified to mediate biological events that we predicted might share components with, or employ similar means as, axonal fusion. From this screen we identified PSR-1 as an important component for axonal fusion. Two different loss-of-function deletions in *psr-1*

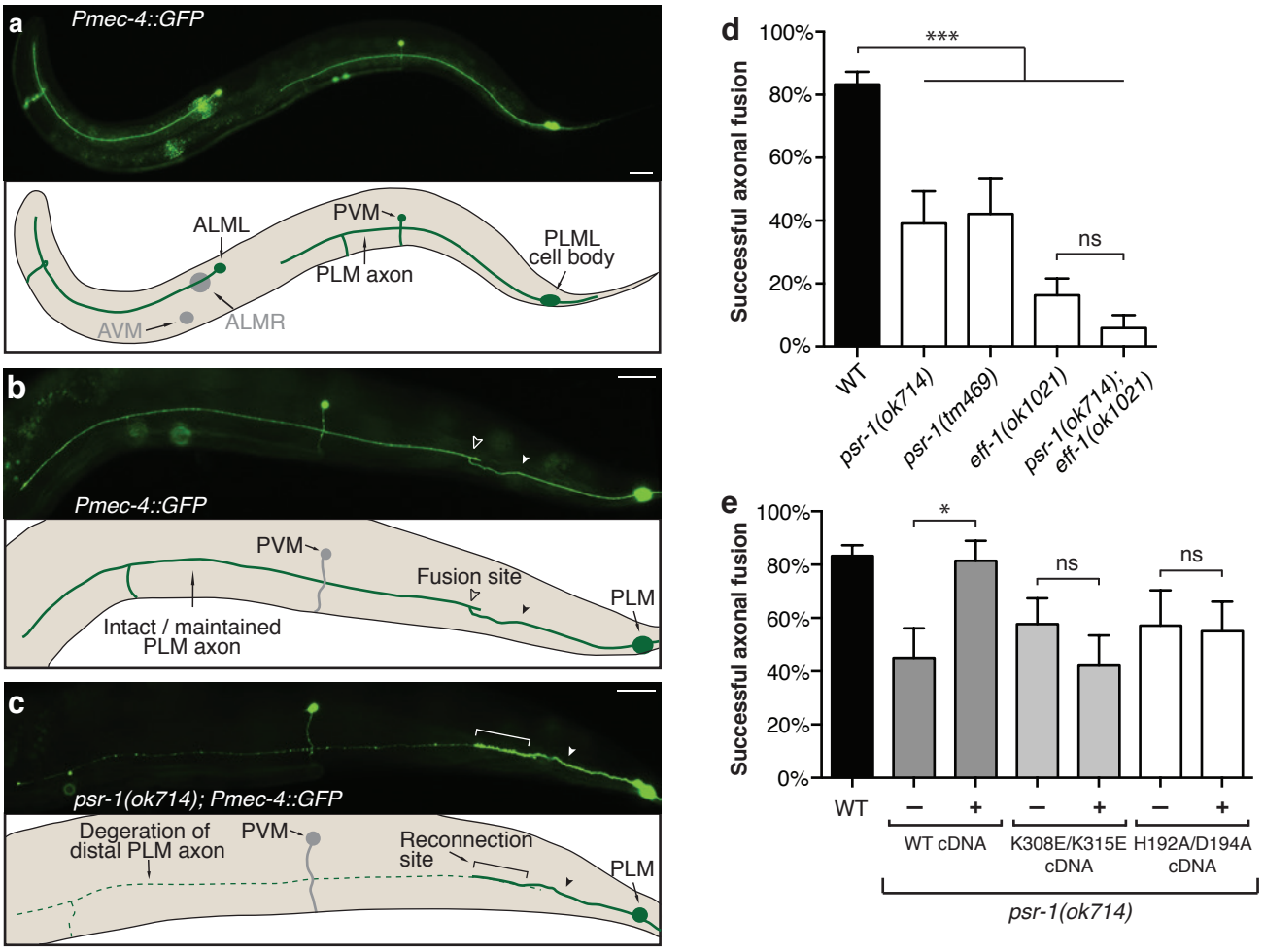

Figure. 1. PSR-1 mediates axonal fusion in a cell-autonomous manner. **a**, A wild-type (WT) *zdIs5(Pmec-4::GFP)* animal with fluorescent PLM mechanosensory neurons. Anterior is left and ventral is down in this and all proceeding images. Out of focus neurons located on the opposite side of the animal (ALMR and AVM) are shown in gray in the schematic; scale bar 25 µm. **b**, Successful axonal fusion in a WT animal, 24 hr post-axotomy. Filled arrowheads point to site of axotomy; open arrowheads show fusion site; scale bar 25 µm. **c**, Unsuccessful fusion in a *psr-1(ok714)* mutant animal, 24 hr after axotomy reconnection has occurred, but fusion has failed, allowing the progression of degeneration in the distal segment. Bracket highlights region of reconnection; scale bar 25 µm. **d**, Quantification of successful fusion events in WT (black bar) and mutant animals (white bars); $n \geq 19$. **e**, Cell-autonomous rescue of the axonal fusion defect in *psr-1(ok714)* animals with expression of WT *psr-1* cDNA. Expression of *psr-1* cDNA carrying mutations that prevent PS binding (K308E/K315E), or that disrupt the Fe(II) binding site in the JmjC domain (H192A/D194A), fail to rescue the defect; representative results from six independent lines tested; $n \geq 14$. Error bars indicate standard error of proportion; * p-value < 0.05; *** < 0.001; ns = not significant.

caused a strong suppression in the rate of axonal fusion (Fig. 1c, d). Furthermore, double mutants between *eff-1* and *psr-1* displayed only a slight decrease (not statistically significant) in the rate of fusion compared with either of the single mutants (Fig. 1d), which may suggest that *psr*-1 and *eff*-1 function in the same genetic pathway.

PSR-1 contains two highly conserved functional domains, an extracellular lysine-rich PS binding domain, and an intracellular JmjC domain that contains various biochemical activities, including histone arginine demethylase activity, lysyl hydroxylase activity, and single-stranded RNA binding activity [27-29]. To investigate the requirement of these domains for axonal fusion, we expressed different versions of the full-length *psr-1* cDNA selectively in the mechanosensory neurons of *psr-1* mutant animals. Expression of WT cDNA restored the rate of axonal fusion to that of WT animals (Fig. 1e), demonstrating that PSR-1 functions cell-autonomously within PLM. Next we expressed *psr-1* cDNA carrying mutations that disrupt its PS binding activity (K308/K315E; unpublished data) and found that it could no longer rescue the defect (Fig. 1e). Similarly, expression of *psr-1* cDNA carrying mutations at the Fe(II) binding site (H192A/D194A) in the JmjC domain failed to rescue the defect caused by loss of PSR-1 (Fig. 1e). Mutation of either of these two sites did not alter the stability of the PSR-1 protein (unpublished data). Thus, these results demonstrate that PSR-1 requires both the extracellular PS binding domain and the intracellular JmjC domain for its cell-autonomous activity in axonal fusion.

PSR-1 functions in a known pathway that includes CED-2/CrkII, CED-5/Dock180, CED-12/ELMO and CED-10/RAC1 to mediate the recognition and removal of apoptotic cells (Fig. 2a). Interestingly, we found that components of this cell corpse engulfment pathway are not required for axonal fusion, as animals carrying mutations in *ced-2*, *ced-5,* or *ced-10* presented a normal rate of axonal fusion (Fig. 2b). Next, we analyzed components of a second, partly redundant cell corpse engulfment pathway, which includes the secreted transthyretin PS binding protein TTR-52/Transthyretin and the lipid binding protein NRF-5, the membrane transporter CED-7/ABC transporter, the transmembrane receptor CED-1/LRP1/MEGF10, and the intracellular adapter CED-6/GULP. Remarkably, we found that TTR-52 was critical for successful axonal fusion (Fig. 2c and Extended Data Fig. 2a). As TTR-52 is normally expressed in and secreted from the intestinal cells to bind PS exposed by apoptotic cells during embryogenesis [19], we asked whether this was also true during axonal fusion. As shown in Figure 2c, WT TTR-52 tagged with mCherry and expressed from a heat-shock promoter completely rescued the axonal fusion defect when induced either at the time of injury, or up to 6 hours after injury. Heat-shock treatment applied to WT animals, or to *ttr-52* mutants not carrying the rescue transgene, did not significantly increase the rate of axonal fusion and did not cause a consistent alteration in the length of regrowth (Extended Data Fig. 2b-f). Thus,

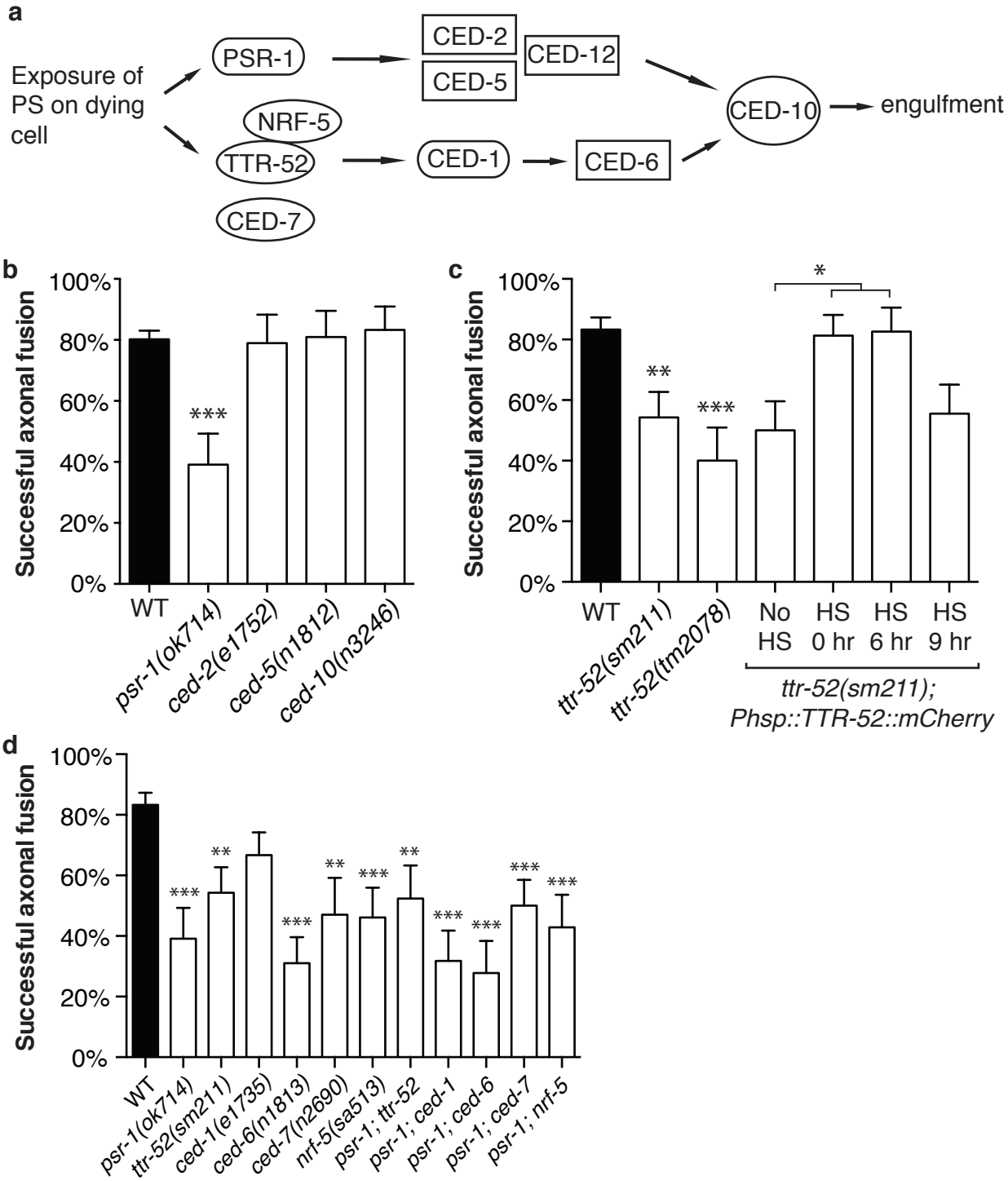

Figure 2. PSR-1 functions in the TTR-52-mediated cell corpse engulfment pathway during axonal fusion. **a**, Recognition and engulfment of apoptotic cells is mediated by two partially redundant parallel pathways. **b**, Animals deficient in *ced-2*, *ced-5* or *ced-10* have normal axonal fusion as in WT animals; n ≥ 19. **c**, TTR-52 is required for successful axonal fusion. Expression of TTR-52::mCherry fully rescues the defect when induced from a heat-shock (HS) promoter immediately after axotomy (0 hr) and up to 6 hr post-axotomy; n ≥ 20. **d**, Loss-of-function mutations in genes acting in the TTR-52 pathway reduce axonal fusion, and the axonal fusion defect in the double mutants with *psr-1* is not worse than that of single mutants; n ≥ 18. Error bars indicate standard error of proportion; p-values: * < 0.05; ** < 0.01; *** < 0.001 compared to WT unless marked on graph.

these findings identify the secreted TTR-52 molecule as functioning after the time of injury to regulate fusion between two axon segments.

We utilized the same transgene to visualize the localization of TTR-52 following axotomy of PLM. Animals were analyzed prior to surgery, and at several time points after surgery. Although we could not detect any localization of TTR-52::mCherry to PLM in WT animals, *ttr-52* mutant animals lacking TTR-52 expression from the endogenous *ttr-52* gene displayed low levels of TTR-52::mCherry binding to PLM (Fig. 3a, b and data not shown). These findings indicate that the endogenous protein was competing with the tagged version for a low level of PS on the surface of the PLM axon. Interestingly, in non-operated adult animals, we observed TTR-52::mCherry localizing to the axon of PLM, as well as that of other neurons; this also occurred in larval stages (Extended Data Fig. 3a-c), but to a lesser extent, suggesting that the neuron's ability to maintain membrane PS asymmetry may decline with aging. Following axotomy, TTR-52 rapidly localized to both the distal and proximal axon segments, with slightly stronger binding observed on the distal axon fragment (Fig. 3a). This localization pattern was maintained for approximately one hour, and then gradually declined to background levels over the four hours following transection (Fig. 3a, b). These results suggest that TTR-52 likely functions as a secreted molecule that binds to the injured neuron and plays an important role in mediating the fusion of the proximal axon with its separated distal counterpart. To further confirm that TTR-52 was indeed binding to PS in this context, we analyzed the localization of a secreted version of Annexin V (sAnxV), a highly efficient and specific calcium-dependent PS binding protein [30-32]. PS was rapidly exposed on the proximal and distal PLM axon segments following axotomy, with sAnxV binding to both segments within 15 minutes after transection (Fig. 3c). Binding of sAnxV::mRFP was strongest to the distal segment, but similar patterns were observed for both the proximal and distal axons, with rapid localization that peaked one hour after axotomy, before gradually declining (Fig. 3d). This localization pattern of sAnxV::mRFP closely matches that of TTR-52::mCherry (Fig. 3a, b), supporting a model in which PS is exposed on the axonal membrane after injury and acts as a 'save-me' signal for TTR-52 to bind and initiate the reconnection and fusion needed to repair the damage. Similar to the localization of TTR-52, we observed more sAnxV binding to the intact PLM axon in adult animals than in larvae (Extended Data Fig. 3d,e), again implying that the preservation of membrane PS asymmetry diminishes with age.

Next we examined the involvement of the other components of the TTR-52 engulfment pathway in axonal fusion. Inactivation of *ced-1* caused a modest deficit in axonal fusion that was not significantly different from that in WT animals (Fig. 2d and Extended Data Table 1). However, animals lacking NRF-5, CED-7 or CED-6 displayed strong reductions in axonal fusion (Fig. 2d and

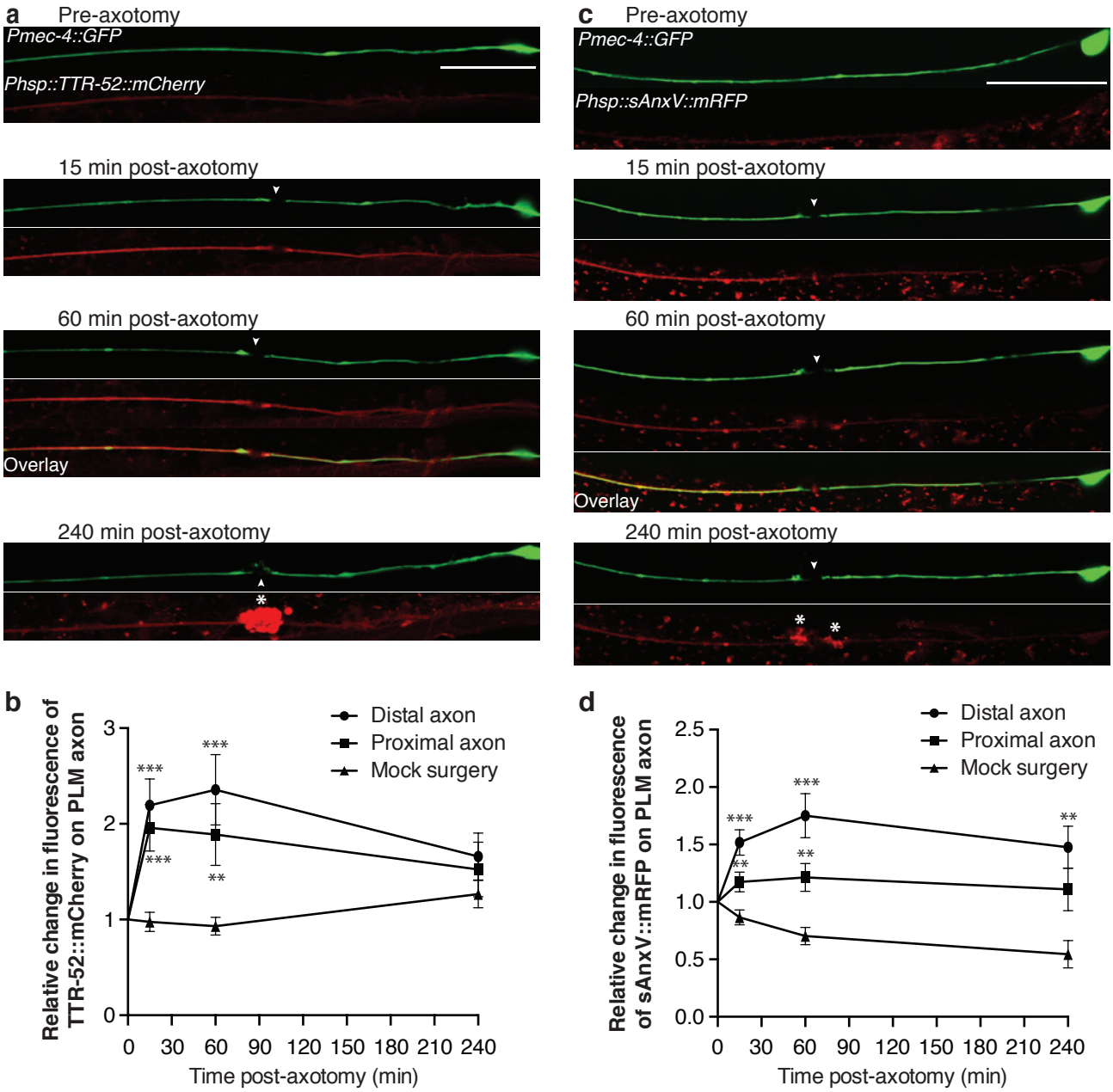

Figure 3. TTR-52 binds to PS exposed on the PLM axon after axotomy. **a**, Localization of TTR-52::mCherry in *ttr-52(sm211); smIs119; zdIs5* animals to the PLM axon prior to axotomy and at several time points after transection. Overlay image is shown for the 60 min time-point; the filled arrowheads point to the site of axotomy; asterisk highlights accumulation of TTR-52::mCherry at the site of injury; scale bar 10 µm. **b**, Quantification of the relative fluorescence levels of TTR-52::mCherry on the PLM distal and proximal axons after axotomy compared to mock surgery conditions. The intensity of TTR-52::mCherry on the distal axon is not significantly different from that on the proximal axon. **c**, Localization of the PS sensor, sAnxV::mRFP, to the axon of PLM prior to axotomy and at several time points after transection. Overlay image is shown for the 60 min time-point; filled arrowhead points to the site of axotomy; asterisks highlight accumulation of sAnxV::mRFP at the site of injury; scale bar 10 µm. **d**, Quantification of the relative fluorescence levels of sAnxV::mRFP on the PLM distal and proximal axon segments after axotomy compared to mock surgery conditions. The intensity of sAnxV::mRFP on the distal axon is significantly stronger than that on the proximal axon at the 15 min and 60 min time-points ($p < 0.05$). Error bars indicate standard error; $n \geq 21$; p-values: ** < 0.01; *** < 0.001 compared to mock surgery.

Extended Data Table 1). Furthermore, we found that double mutants between *psr-1* and either *ttr-52*, *ced-1*, *nrf-5*, *ced-7*, or *ced-6* were no worse than single mutant animals (Fig. 2d and Extended Data Table 1), indicating that unlike apoptosis, PSR-1 functions within this TTR-52-mediated pathway during axonal fusion. Similarly to that seen in *psr-1; eff-1* double mutant animals (Fig. 1d), *ttr-52; eff-1* double mutants did not display a significantly worse defect in axonal fusion than single mutant animals (Extended Data Fig. 2g), indicating that both *psr-1* and *ttr-52* might function in the same genetic pathway as *eff-1*.

To determine if the loss of any of the genes analyzed caused a reduction in the regenerative potential of PLM, we calculated the average length of regrowth 24 hours post-axotomy. Mutations in *psr-1*, *ttr-52*, *ced-7*, *ced-10* and *nrf-5* all caused significantly less regrowth in PLM (Extended Data Table 2 and Extended Data Fig. 4a, b). However, although a reduction in regrowth was evident for several genes, we found no correlation between the average length of regrowth and the rate of axonal fusion. For instance, *ced-10* mutants displayed reduced regrowth, but presented no defect in axonal fusion, while animals that lacked *eff-1* had the strongest defect in axonal fusion, but their regenerative growth was not different from that of WT animals. Moreover, neither the actual percentage of animals displaying regrowth nor the proportion of axons able to extend across the damage site was consistently different from that observed for WT animals (Extended Data Fig. 4c-e).

Previously we demonstrated that, although axonal fusion is a highly specific process, instances of aspecific fusion do occur when a second axon in close proximity to PLM is also severed [7]. The axon of each bilateral PLN neuron fasciculates for much of its length with the axon of the PLM neuron of the ipsilateral side [33] (Fig. 4a). When both fasciculating axons are simultaneously transected, approximately 10% of animals undergo aspecific fusion between these two neurons [7]. Interestingly, we observed a similar phenotype in animals deficient in the *unc-70/β-spectrin* gene, a genetic background in which the axons of *C. elegans* motor neurons lose the capacity to resist physical strain and undergo spontaneous cycles of breaks followed by regeneration [34]. We observed that *unc-70* mutant animals display aberrant morphology of the PLM axons comprising breaks, loop structures, and branching (Extended Data Fig. 5a, b), as well as spontaneous fusion between PLM and PLN neurons visualized through transfer of the GFP fluorophore (Fig. 4b, c). These fusion events were found to be dependent on the EFF-1 fusogen and required DLK-1, a mitogen-activated triple kinase molecule essential for regeneration [35,36] (Extended Data Fig. 5c). Remarkably, we found that loss of *psr-1*, *ttr-52* or *ced-6* caused a strong reduction in the rate of *unc-70*-induced PLM-PLN fusion (Fig. 4c). Similar to our findings for axotomy-induced PLM axonal fusion, loss of *ced-1* led to a modest decrease in the incidence of PLM-PLN fusion (Fig. 4c). Thus, these data

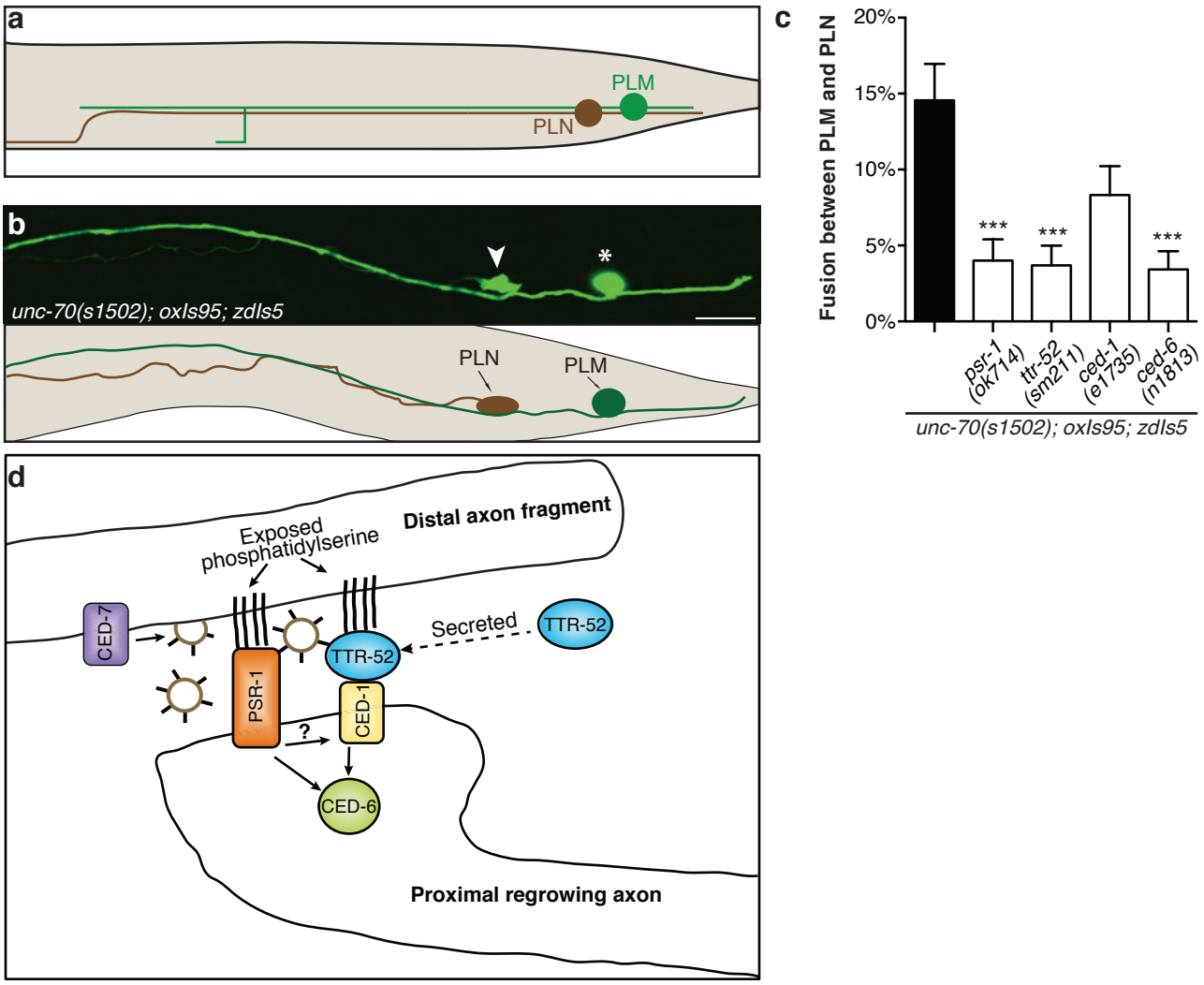

Figure 4. Molecules involved in apoptotic cell clearance mediate aspecific axonal fusion caused by *unc-70* mutation. **a**, The axon of each of the bilateral PLN neurons (brown) fasciculates with the PLM axon (green) on the ipsilateral side. **b**, Loss of *unc-70* causes spontaneous fusion events between PLM (asterisk) and PLN (arrowhead), leading to the appearance of GFP in the cell body and axon of PLN; scale bar 10 µm. **c**, The frequency of aspecific fusion events between PLM and PLN is strongly reduced in animals with mutations in *psr-1*, *ttr-52* and *ced-6*; n ≥ 200; p-values: *** < 0.001 compared to *unc-70(s1502)*. **d**, Proposed schematic model for the role of the apoptotic pathway in axonal fusion. Following injury, PS is exposed on the distal fragment where it acts as a 'save me' signal, and this might be enhanced by CED-7-facilitated secretion of PS coated vesicles. PS is recognized by secreted extracellular bridging protein TTR-52 and by the transmembrane PSR-1 on the proximal axon. The 'save me' signal is transduced intracellularly via CED-6, and possibly also through activation of the TTR-52-interacting CED-1 receptor.

indicate that the conserved molecules involved in apoptotic cell clearance are also required for axonal fusion in a genetic model of neuronal injury.

We have identified a genetic pathway that controls axonal fusion during regeneration. Our data uncover a new role for PSR-1, a molecule previously shown to function as a phagocytic receptor [12,13], a histone arginine demethylase [27], a lysyl hydroxylase [29], a single-stranded RNA binding protein [28], and now a protein required for efficient axonal regeneration. Our study demonstrates that both the extracellular PS-binding domain and the intracellular JmjC domain of PSR-1 are important for its function in mediating axonal fusion after neuronal injuries; our results indicate that PS is exposed on the surface of severed axonal segments, which may underlie the action of PS-binding PSR-1 and the PS-binding extracellular protein TTR-52 by facilitating the interaction and fusion of two separated axonal segments. Thus, exposure of PS might function as a 'save me' signal for the severed distal axon. PSR-1 acts in the same pathway as TTR-52 as well as its partners in cell corpse clearance, CED-7, NRF-5, and CED-6 to promote this axonal healing process (Fig. 4d). Taken together, our results support a model in which recognition of the separated axon fragment by the regrowing axon is achieved by a change in lipid membrane composition and mediated by the same molecules involved in recognizing an apoptotic cell, with EFF-1 acting as the fusogen necessary to restore membrane and cytoplasmic continuity.

Finally, stemming from observations of axonal fusion in invertebrates, highly innovative preclinical paradigms are currently being applied to mammalian systems, in which severed nerve fibers are surgically reconnected in 'end-to-end' or 'end-to-side' operations [37,38]. Together with the application of high molecular weight substances (such as polyethylene glycol) to the injury site that facilitate fusion and restoration of the original nerve tract [39-41], these procedures have generated highly encouraging results with respect to functional recovery. Our results strongly support such efforts, providing a detailed characterization of the molecular mechanisms mediating axonal fusion, knowledge that will facilitate such strategies.

Methods Summary

Standard techniques were used for *C. elegans* maintenance, crosses and other genetic manipulations [42] and all experiments were performed at 22ºC unless otherwise stated. Axotomies were performed as previously described [7], using a MicroPoint Laser System Basic Unit, with axons severed approximately 50 μm anterior to the PLM cell body in L4 or 1 day old adult (for localization of TTR-52 and sAnxV) animals. Animals were analyzed 24 hr post-axotomy for regrowth, reconnection, and fusion, and re-analyzed at 48 and/or 72 hr post-axotomy for clarification of successful fusion. Axons were deemed to be reconnected when the proximal and distal axons were visually connected and within the same focal plane. Axonal regrowth was quantified by measuring the length of the longest neurite beyond the cut site 24 hr post-axotomy; neurons that underwent axonal fusion were excluded from these quantifications. To study the localization of EFF-1::GFP, animals were imaged 16 to 20 hr post-axotomy LSM 510 META confocal microscope and Zen 2009 software. To score for the presence of EFF-1::GFP on the membrane of regrowing axons, fluorescence profiles of line scans at different sections of the regrowing axon tip were generated and EFF-1::GFP was scored as localizing to the membrane if the peak of green intensity (EFF-1::GFP) and the peak of red intensity (cytoplasmic mCherry) were not overlapping. Localization experiments for TTR-52::mCherry and sAnxV::mRFP were performed in 1 day old adult animals (unless stated otherwise) with a LSM 510 META confocal microscope and Zen 2008 software. Expression of TTR-52::mCherry and sAnxV::mRFP were induced 4 hr prior to analysis with incubation at 30°C for 30 min. Changes in fluorescence intensity were calculated with line scans. To control for changes in focus and intensity, mCherry/mRFP expression was normalized to GFP for each image and recorded relative to pre-axotomy levels.

References

1 Bedi, S. S. & Glanzman, D. L. Axonal rejoining inhibits injury-induced long-term changes in *Aplysia* sensory neurons in vitro. *J. Neurosci.* **21**, 9667-9677 (2001).

2 Birse, S. C. & Bittner, G. D. Regeneration of giant axons in earthworms. *Brain Res.* **113**, 575-581 (1976).

3 Deriemer, S. A., Elliott, E. J., Macagno, E. R. & Muller, K. J. Morphological evidence that regenerating axons can fuse with severed axon segments. *Brain Res.* **272**, 157-161 (1983).

4 Ghosh-Roy, A., Wu, Z., Goncharov, A., Jin, Y. & Chisholm, A. D. Calcium and cyclic AMP promote axonal regeneration in *Caenorhabditis elegans* and require DLK-1 kinase. *J. Neurosci.* **30**, 3175-3183 (2010).

5 Hoy, R. R., Bittner, G. D. & Kennedy, D. Regeneration in crustacean motoneurons: evidence for axonal fusion. *Science* **156**, 251-252 (1967).

6 Macagno, E. R., Muller, K. J. & DeRiemer, S. A. Regeneration of axons and synaptic connections by touch sensory neurons in the leech central nervous system. *J. Neurosci.* **5**, 2510-2521 (1985).

7 Neumann, B., Nguyen, K. C., Hall, D. H., Ben-Yakar, A. & Hilliard, M. A. Axonal regeneration proceeds through specific axonal fusion in transected *C. elegans* neurons. *Dev. Dyn.* **240**, 1365-1372 (2011).

8 Fadok, V. A. *et al.* Exposure of phosphatidylserine on the surface of apoptotic lymphocytes triggers specific recognition and removal by macrophages. *J. Immunol.* **148**, 2207-2216 (1992).

9 Martin, S. J. *et al.* Early redistribution of plasma membrane phosphatidylserine is a general feature of apoptosis regardless of the initiating stimulus: inhibition by overexpression of Bcl-2 and Abl. *J. Exp. Med.* **182**, 1545-1556 (1995).

10 Verhoven, B., Schlegel, R. A. & Williamson, P. Mechanisms of phosphatidylserine exposure, a phagocyte recognition signal, on apoptotic T lymphocytes. *J. Exp. Med.* **182**, 1597-1601 (1995).

11 van den Eijnde, S. M. *et al.* Cell surface exposure of phosphatidylserine during apoptosis is phylogenetically conserved. *Apoptosis* **3**, 9-16 (1998).

12 Fadok, V. A. *et al.* A receptor for phosphatidylserine-specific clearance of apoptotic cells. *Nature* **405**, 85-90 (2000).

13 Wang, X. *et al.* Cell corpse engulfment mediated by *C. elegans* phosphatidylserine receptor through CED-5 and CED-12. *Science* **302**, 1563-1566 (2003).

14 Gumienny, T. L. *et al.* CED-12/ELMO, a novel member of the CrkII/Dock180/Rac pathway, is required for phagocytosis and cell migration. *Cell* **107**, 27-41 (2001).

15 Reddien, P. W. & Horvitz, H. R. CED-2/CrkII and CED-10/Rac control phagocytosis and cell migration in *Caenorhabditis elegans*. *Nature Cell Biol.* **2**, 131-136 (2000).

16 Wu, Y. C. & Horvitz, H. R. *C. elegans* phagocytosis and cell-migration protein CED-5 is similar to human DOCK180. *Nature* **392**, 501-504 (1998).

17 Albert, M. L., Kim, J. I. & Birge, R. B. αvβ5 integrin recruits the CrkII-Dock180-rac1 complex for phagocytosis of apoptotic cells. *Nature Cell Biol.* **2**, 899-905 (2000).

18 Zhou, Z., Hartwieg, E. & Horvitz, H. R. CED-1 is a transmembrane receptor that mediates cell corpse engulfment in *C. elegans*. *Cell* **104**, 43-56 (2001).

19 Wang, X. *et al. Caenorhabditis elegans* transthyretin-like protein TTR-52 mediates recognition of apoptotic cells by the CED-1 phagocyte receptor. *Nature Cell Biol.* **12**, 655-664 (2010).

20 Zhang, Y., Wang, H., Kage-Nakadai, E., Mitani, S. & Wang, X. *C. elegans* secreted lipid-binding protein NRF-5 mediates PS appearance on phagocytes for cell corpse engulfment. *Curr. Biol.* **22**, 1276-1284 (2012).

21 Luciani, M. F. & Chimini, G. The ATP binding cassette transporter ABC1, is required for the engulfment of corpses generated by apoptotic cell death. *EMBO J.* **15**, 226-235 (1996).

22 Wu, Y. C. & Horvitz, H. R. The *C. elegans* cell corpse engulfment gene *ced-7* encodes a protein similar to ABC transporters. *Cell* **93**, 951-960 (1998).

23 Liu, Q. A. & Hengartner, M. O. Candidate adaptor protein CED-6 promotes the engulfment of apoptotic cells in *C. elegans*. *Cell* **93**, 961-972 (1998).

24 Reddien, P. W. & Horvitz, H. R. The engulfment process of programmed cell death in caenorhabditis elegans. *Annu. Rev. Cell Dev. Biol.* **20**, 193-221 (2004).

25 Podbilewicz, B. Cell fusion. *WormBook : the online review of C. elegans biology*, 1-32 (2006).

26 Shemer, G. & Podbilewicz, B. The story of cell fusion: big lessons from little worms. *BioEssays* **25**, 672-682 (2003).

27 Chang, B., Chen, Y., Zhao, Y. & Bruick, R. K. JMJD6 is a histone arginine demethylase. *Science* **318** (2007).

28 Hong, X. *et al.* Interaction of JMJD6 with single-stranded RNA. *Proc. Natl. Acad. Sci. U.S.A.* **107**, 14568-14572 (2010).

29 Webby, C. J. *et al.* Jmjd6 catalyses lysyl-hydroxylation of U2AF65, a protein associated with RNA splicing. *Science* **325**, 90-93 (2009).

30 Andree, H. A. *et al.* Binding of vascular anticoagulant α (VACα) to planar phospholipid bilayers. *J. Biol. Chem.* **265**, 4923-4928 (1990).

31 Koopman, G. *et al.* Annexin V for flow cytometric detection of phosphatidylserine expression on B cells undergoing apoptosis. *Blood* **84**, 1415-1420 (1994).

32 Mapes, J. *et al.* CED-1, CED-7, and TTR-52 regulate surface phosphatidylserine expression on apoptotic and phagocytic cells. *Curr. Biol.* **22**, 1267-1275 (2012).

33 White, J. G., Southgate, E., Thomson, J. N. & Brenner, S. The structure of the nervous system of the nematode *Caenorhabditis elegans*. *Philos. Trans. R Soc. Lond. B Biol. Sci.* **314**, 1-340 (1986).

34 Hammarlund, M., Jorgensen, E. M. & Bastiani, M. J. Axons break in animals lacking β-spectrin. *J Cell Biol* **176**, 269-275 (2007).

35 Hammarlund, M., Nix, P., Hauth, L., Jorgensen, E. M. & Bastiani, M. Axon regeneration requires a conserved MAP kinase pathway. *Science* **323**, 802-806 (2009).

36 Yan, D., Wu, Z., Chisholm, A. D. & Jin, Y. The DLK-1 kinase promotes mRNA stability and local translation in *C. elegans* synapses and axon regeneration. *Cell* **138**, 1005-1018 (2009).

37 Dong, C. *et al.* Reconstruction of anorectal function through end-to-side neurorrhaphy by autonomic nerves and somatic nerve in rats. *J. Surg. Res.* **180**, e63-71 (2013).

38 Silva, D. N. *et al.* End-to-side nerve repair using fibrin glue in rats. *Acta Bras. Cir.* **25**, 158-162 (2010).

39 Bittner, G. D. *et al.* Rapid, effective, and long-lasting behavioral recovery produced by microsutures, methylene blue, and polyethylene glycol after completely cutting rat sciatic nerves. *J. Neurosci. Res.* **90**, 967-980 (2012).

40 Spaeth, C. S., Robison, T., Fan, J. D. & Bittner, G. D. Cellular mechanisms of plasmalemmal sealing and axonal repair by polyethylene glycol and methylene blue. *J. Neurosci. Res.* **90**, 955-966 (2012).

41 Britt, J. M. *et al.* Polyethylene glycol rapidly restores axonal integrity and improves the rate of motor behavior recovery after sciatic nerve crush injury. *J. Neurophysiol.* **104**, 695-703 (2010).

42 Brenner, S. The genetics of *Caenorhabditis elegans*. *Genetics* **77**, 71-94 (1974).

5.3 Supplementary data

Methods

Strains and genetics

Standard techniques were used for *C. elegans* maintenance, crosses and other genetic manipulations [1]. All experiments were performed at 22ºC unless otherwise stated and all strains were grown on OP50 bacteria, except for animals carrying the *unc-70(s1502)* mutation, which were grown on HB101 bacteria. The following mutations were used: LGI: *ced-1(e1735)*, *dlk-1(ju476)*; LGII: *eff-1(ok1021)*, *eff-1(hy21)*; LGIII: *ced-6(n1813)*, *ced-7(n2690)*, *ttr-52(sm211)*, *ttr-52(tm2078)*; LGIV: *ced-2(e1752)*, *ced-5(n1812), ced-10(n3246)*, *psr-1(ok714)*, *psr-1(tm469)*; LGV: *nrf-5(sa513)*, *unc-70(s1502)*. Transgenes used were: *smIs119[Phsp16-2::ttr-52::mCherry]* [2], *smIs95[Phsp16-2::sAnxV::mRFP]* [3], *oxIs95[Ppdi-2::unc-70; Pmyo2::GFP]* [4], *vdEx575[Pmec-4::psr-1(c)* (10 ng/µl), *Podr-1::dsRED* (30 ng/µl)*]*, *vdEx663[Pmec-4::EFF-1::GFP* (5 ng/µl)*; Pmec-4::mCherry* (20 ng/µl)*; Podr-1::DsRed* (60 ng/µl)*], vdEx705[Pmec-4::psr-1(c)(H192A/D194A)* (10 ng/µl)*; Podr-1::dsRed* (30 ng/µl)*]*, *vdEx709[Pmec-4::psr-1(c)(K308E K315E)* (10 ng/µl)*; Podr-1::dsRed* (30 ng/µl)*]*, *zdIs5[Pmec-4::GFP]*.

Molecular biology

Standard molecular biology techniques were used. The *Pmec-4::psr-1(c)* plasmid was generated through insertion of a Bam HI/Age I *psr-1* cDNA amplicon in a plasmid between the *mec-4* promoter and the *unc-54* 3`UTR. The following primers were used: fwd primer 5'-tcagtgggatccatgtcattagggcgagatag-3'; rev primer 5'-tcagtgaccggtttaaactagcgagttctgaaaat-3'. QuikChange mutagenesis (Agilent Technologies, Santa Clara, CA) was used to introduce the K308/K315E and H192A/D194A mutations, with the *Pmec-4::psr-1(c)* plasmid used as the template.

To build the *Pmec-4::EFF-1::GFP* plasmid, *eff-1* genomic DNA was amplified (fwd primer 5'-ctagctagcatggaaccgccgtttgagtg-3'; rev primer 5'-gaaccggtttaatgtactggctactgctatag-3`) and cloned into pSM-mCherry plasmid using Nhe I and Age I restriction enzymes, to obtain *pSM EFF-1::mCherry*. The *mec-4* promoter was then cloned from plasmid *pSM Pmec-4::EFF-1* into *pSM EFF-1::mCherry* using Sal I and Sph I restriction enzymes, to obtain *Pmec-4::EFF-1::mCherry*. Finally, an Age I/Apa I fragment from plasmid *pCP.179* [5], a kind gift of Shai Shaham, was cloned into *Pmec-4::EFF-1::mCherry* to obtain *Pmec-4::EFF-1::GFP*.

Laser axotomy and microscopy

Animals were immobilized in 0.05% tetramisole hydrochloride on 4% agar pads. Axotomies were

performed as previously described [6], using a MicroPoint Laser System Basic Unit attached to a Zeiss Axio Imager A1 (Objective EC Plan-Neofluar 100x/1.30 Oil M27). Axons were severed in L4 or 1 day old adult (for localization of TTR-52 and sAnxV) animals approximately 50 μm anterior to the PLM cell body, visualized on a Zeiss Axio Imager Z1 microscope equipped with a Photometrics camera (Cool Snap HQ2; Tucson, AZ) and analyzed with MetaMorph software (Molecular Devices, Sunnyvale, CA). Animals were analyzed 24 hr post-axotomy for regrowth, reconnection, and fusion, and re-analyzed at 48 and/or 72 hr post-axotomy for clarification of successful fusion. Axons were deemed to be reconnected when the proximal and distal axons were visually connected and within the same focal plane. Axonal regrowth was quantified by measuring the length of the longest neurite beyond the cut site 24 hr post-axotomy; neurons that underwent axonal fusion were excluded from these quantifications.

Visualization of EFF-1

To study the localization of EFF-1::GFP in regrowing axons, laser axotomies were performed in animals carrying the *vdEx663* transgene, and individual animals were then imaged 16 to 20 hr later using a LSM 510 META confocal microscope and Zen 2009 software. Green fluorescence was visualized with a 488 nm laser (10% power, with a gain of 750-760 and 8x averaging) and red fluorescence was visualized with a 543 nm laser (15% power, with a gain of 538 and 8x averaging). Image analysis was performed using ImageJ 1.47p. To score for the presence of EFF-1::GFP on the membrane of regrowing axons, fluorescence profiles of line scans at different sections of the regrowing axon tip were obtained using the "Plot Profile" tool in ImageJ. EFF-1::GFP was scored as localizing to the membrane if the peak of green intensity (EFF-1::GFP) and the peak of red intensity (cytoplasmic mCherry) were not overlapping.

Visualization of TTR-52 and Annexin V

Localization experiments for TTR-52::mCherry and sAnxV::mRFP were performed in 1 day old adult animals (unless stated otherwise) with a LSM 510 META confocal microscope and Zen 2008 software. Green fluorescence was analyzed with a 488 nm laser (2.4% power, with a gain of 601 and 8x averaging) and red fluorescence with a 543 nm laser (100% power, with a gain of 1012 and 8x averaging). Expression of TTR-52::mCherry and sAnxV::mRFP were induced 4 hr prior to analysis with incubation at 30°C for 30 min. Changes in fluorescence intensity were calculated with line scans performed using ImageJ 1.46r software. To avoid bright fluorescence associated with collateral laser damage, line scans were recorded ~5 μm from the damage on both the proximal and distal axon segments for a length of ~15 μm. Line scans were recorded along the same region for the 488 nm and 543 nm channels for each image. To control for changes in focus and intensity,

mCherry/mRFP expression was normalized to GFP for each image and recorded relative to pre-axotomy levels. For calculation of fluorescence of intact axons, line scans were performed along the PLM axon for the initial ~100 μm anterior from the cell body. Background fluorescence was calculated with similar line scans performed ~1 μm dorsally from the PLM axon. Ratios were calculated against GFP fluorescence levels.

Statistical analysis

Statistical analysis was performed using Primer of Biostatistics 3.01, GraphPad Prism and Microsoft Excel. Error of proportions was used to assess variation across a single population, two-way comparison was performed using the *t*-test, and ANOVA for more than two groups.

References

1 Brenner, S. The genetics of *Caenorhabditis elegans*. *Genetics* **77**, 71-94 (1974).

2 Wang, X. *et al. Caenorhabditis elegans* transthyretin-like protein TTR-52 mediates recognition of apoptotic cells by the CED-1 phagocyte receptor. *Nature Cell Biol.* **12**, 655-664 (2010).

3 Zou, W. *et al. Caenorhabditis elegans* myotubularin MTM-1 negatively regulates the engulfment of apoptotic cells. *PLoS Genet.* **5**, e1000679 (2009).

4 Hammarlund, M., Jorgensen, E. M. & Bastiani, M. J. Axons break in animals lacking β-spectrin. *J. Cell Biol.* **176**, 269-275 (2007).

5 Procko, C., Lu, Y. & Shaham, S. Glia delimit shape changes of sensory neuron receptive endings in *C. elegans*. *Development* **138**, 1371-1381 (2011).

6 Neumann, B., Nguyen, K. C., Hall, D. H., Ben-Yakar, A. & Hilliard, M. A. Axonal regeneration proceeds through specific axonal fusion in transected *C. elegans* neurons. *Dev. Dyn.* **240**, 1365-1372 (2011).

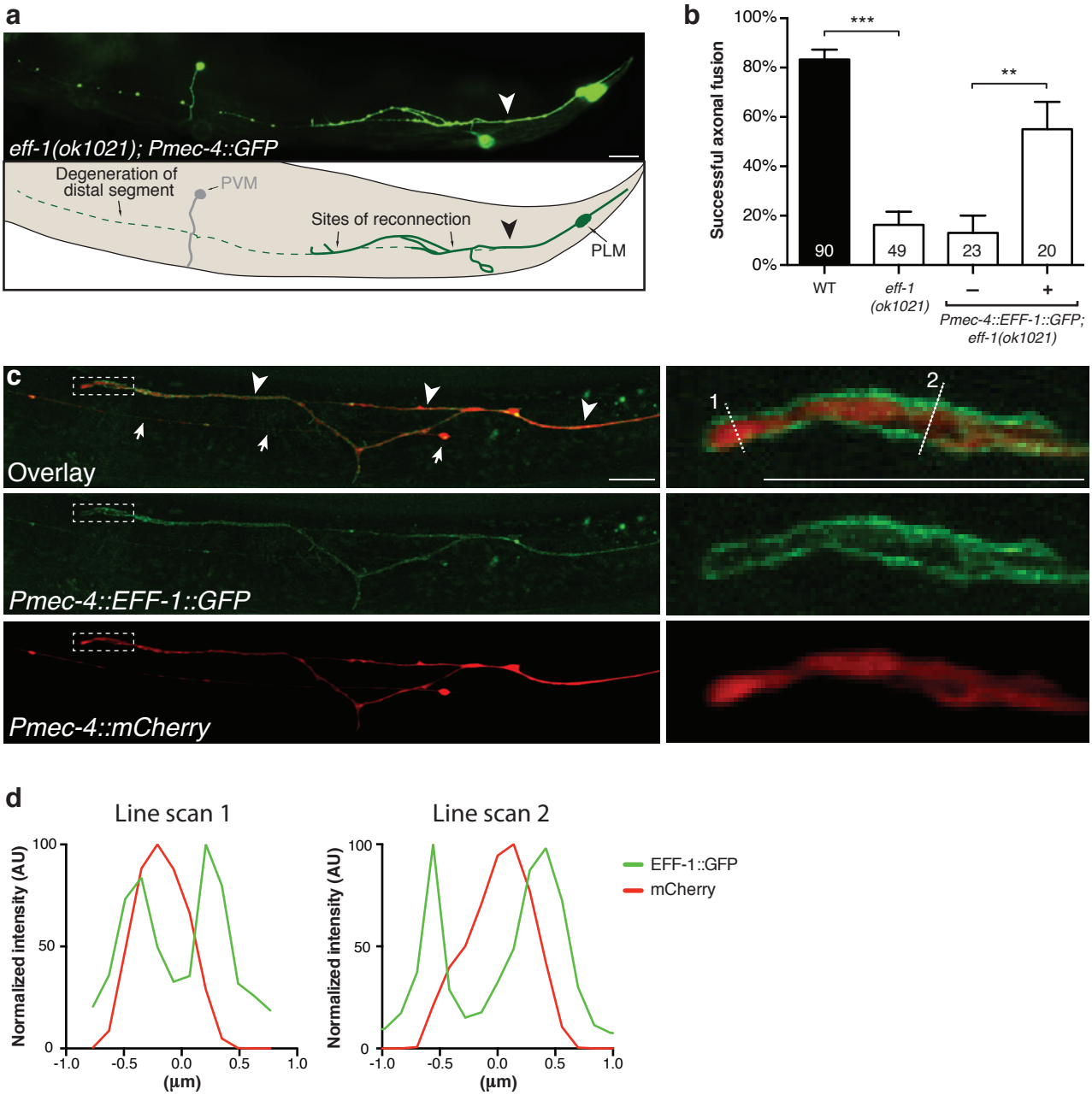

Extended Data Figure 1. EFF-1 functions cell-autonomously in PLM and localizes to the membrane of growth cones. **a**, Defective axonal fusion in an *eff-1(ok1021); zdIs5(Pmec-4::GFP)* animal 48 hr post-axotomy. Arrowhead shows cut site; scale bar 25 µm. **b**, Quantification of axonal fusion in *eff-1(ok1021)* animals compared to WT and cell-autonomous rescue with expression of *Pmec-4::EFF-1::GFP* (one of three transgenic lines tested presenting similar phenotype). Error bars represent standard error of proportion; n values within each bar; p-values: ** < 0.01, *** < 0.001. **c**, EFF-1 localizes to the membrane of regrowing axons. Maximum projections of Z-stack confocal images of a regrowing axon with EFF-1::GFP present all along the regrowing proximal fragment (arrowheads) and at the membrane of the regrowing tip (box and right panel). The distal fragment is indicated by arrows; scale bars 10 µm. **d**, Fluorescence profiles from the line scans shown in the top right panel of panel c illustrate the presence of EFF-1::GFP on the membrane. A total of 12 growth cones (from 8 animals) were analyzed and 8 of these (67%) displayed membrane-localized EFF-1.

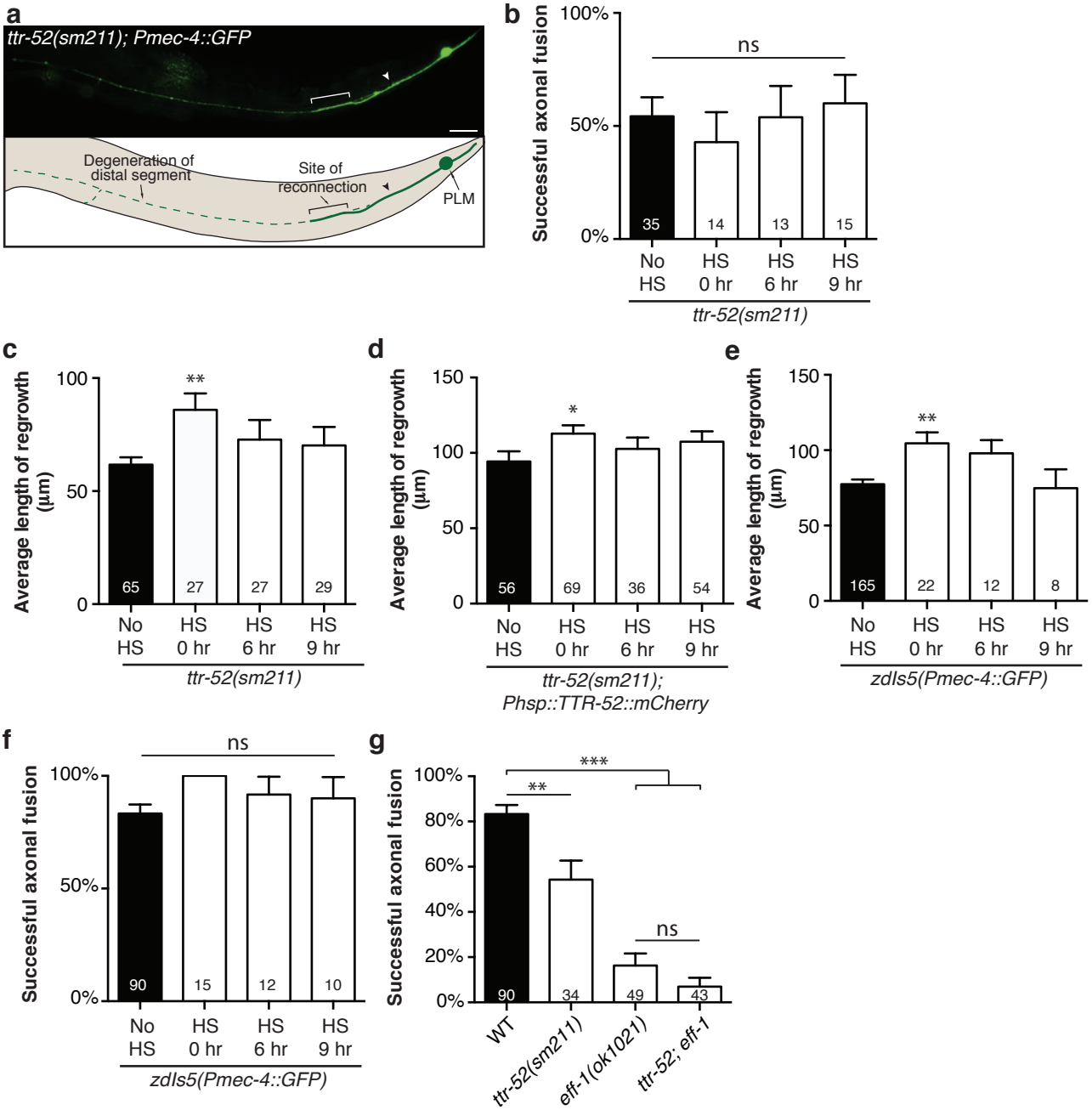

Extended Data Figure 2. Analysis of regeneration after heat-shock treatment and in *ttr-52; eff-1* double mutant animals. **a**, Unsuccessful fusion in a *ttr-52(sm211)* animal. Regrowth has extended from the cut site (arrowhead) and contacted the distal fragment (bracketed region), but degeneration of the distal fragment is proceeding. Scale bar 25 µm. **b**, Rate of successful axonal fusion in *ttr-52(sm211)* animals without or with heat-shock (HS) treatment. c, The average length of regrowth in *ttr-52(sm211)* animals given heat-shock after axotomy compared to those without HS treatment. **d**, Quantification of regrowth in *ttr-52(sm211); Phsp::TTR-52::mCherry* animals without HS treatment compared to those that received HS immediately after axotomy (0 hr), or at 6 or 9 hr post-axotomy. **e**, Comparison of the average length of regrowth in *zdIs5* animals without HS or with HS given at different times after axotomy. **f**, Successful axonal fusion in *zdIs5* animals without HS compared to animals given HS at different times post-axotomy. **g**, Successful axonal fusion in *ttr-52(sm211)* and *eff-1(ok1021)* single mutants compared to *ttr-52; eff-1* double mutant animals. Error bars represent standard error of proportion (**b**, **f**, **g**) and standard error (**c**, **d**, **e**); n values within each bar; p-values: * < 0.05, ** < 0.01, *** < 0.001 compared to WT or no HS (black bars), unless marked otherwise on graph; ns = not significant.

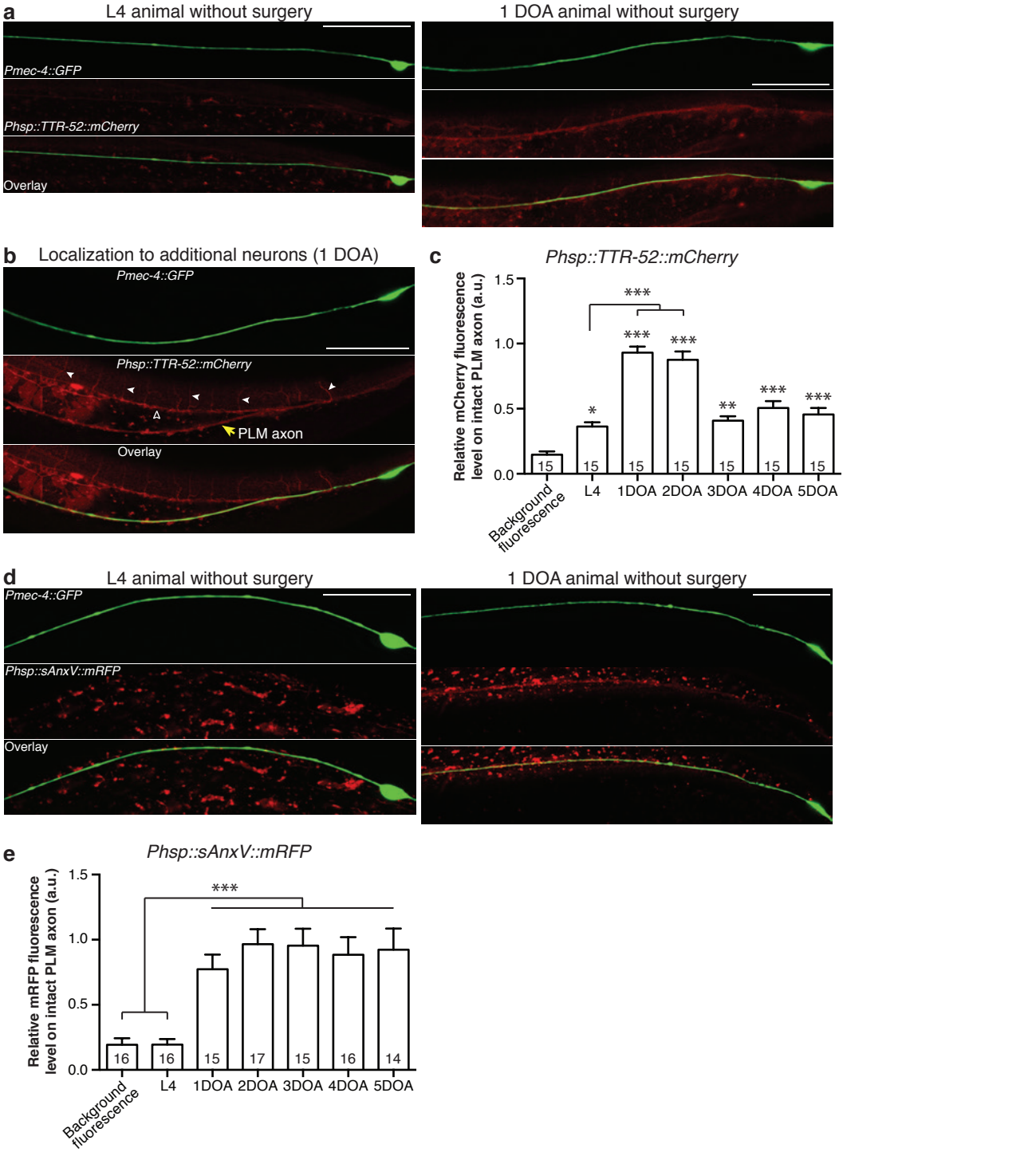

Extended Data Figure 3. PS is exposed on intact axons in adult animals. **a**, Localization of TTR-52::mCherry in a representative larval stage 4 (L4, left panels) and a 1 day old adult (1 DOA, right panels). **b**, Localization of TTR-52::mCherry to additional neuronal processes. The open arrowhead and closed arrowheads highlight additional processes that, based on their morphology, are the primary and secondary branches of the PVD dendrite. **c**, Relative level of TTR-52::mCherry binding to the intact PLM axon in animals of advancing ages compared to background fluorescence levels. **d**, Representative images demonstrating relative fluorescence levels of sAnxV::mRFP in a L4 (left panels) and 1 DOA animal (right panels). **e**, Relative binding of sAnxV::mRFP to the intact PLM axon in L4 and 1-5 DOA animals. Data shown are mRFP fluorescence relative to GFP levels expressed from the Pmec-4::GFP transgene. Scale bars 25 μm; n values within each bar; a.u. = arbitrary units; error bars indicate standard error; p-values: * < 0.05, ** < 0.01, *** < 0.001 compared to background unless marked otherwise.

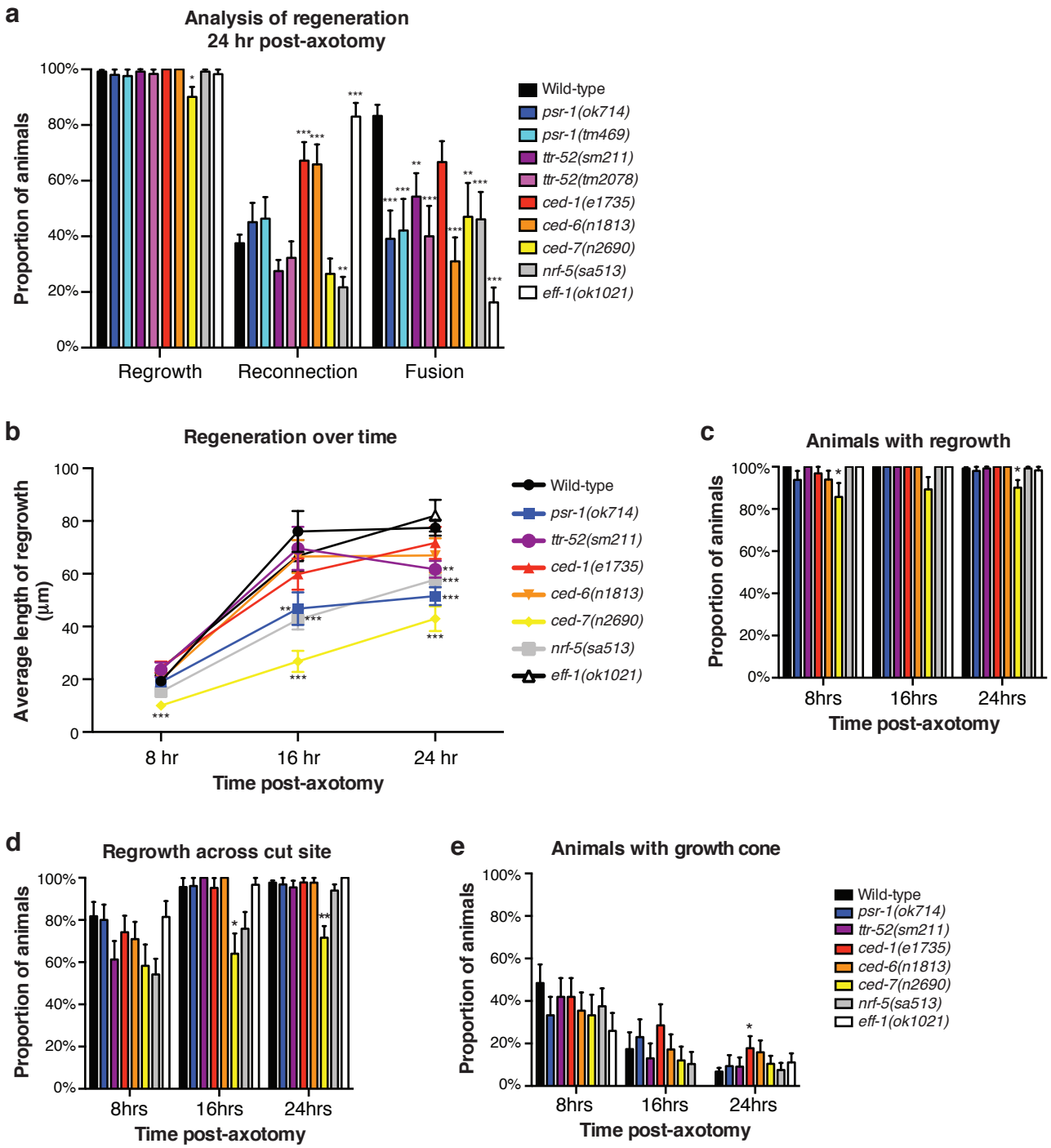

Extended Data Fig. 4. Quantification of regeneration. **a**, Analysis of regrowth, reconnection (as a proportion of regrowing axons), and fusion (as a proportion of reconnecting axons) in WT and single mutant animals. **b**, Average length of regeneration over time in single mutant animals. **c**, The percentage of animals at different times post-axotomy that displayed regrowth. **d**, Average number of axons that regrew across the cut site at different time points after axotomy. **e**, Quantification of the percentage of axons presenting a growth cone at different stages of regeneration. $n \geq 15$; p-values: * < 0.05, ** < 0.01, *** < 0.001.

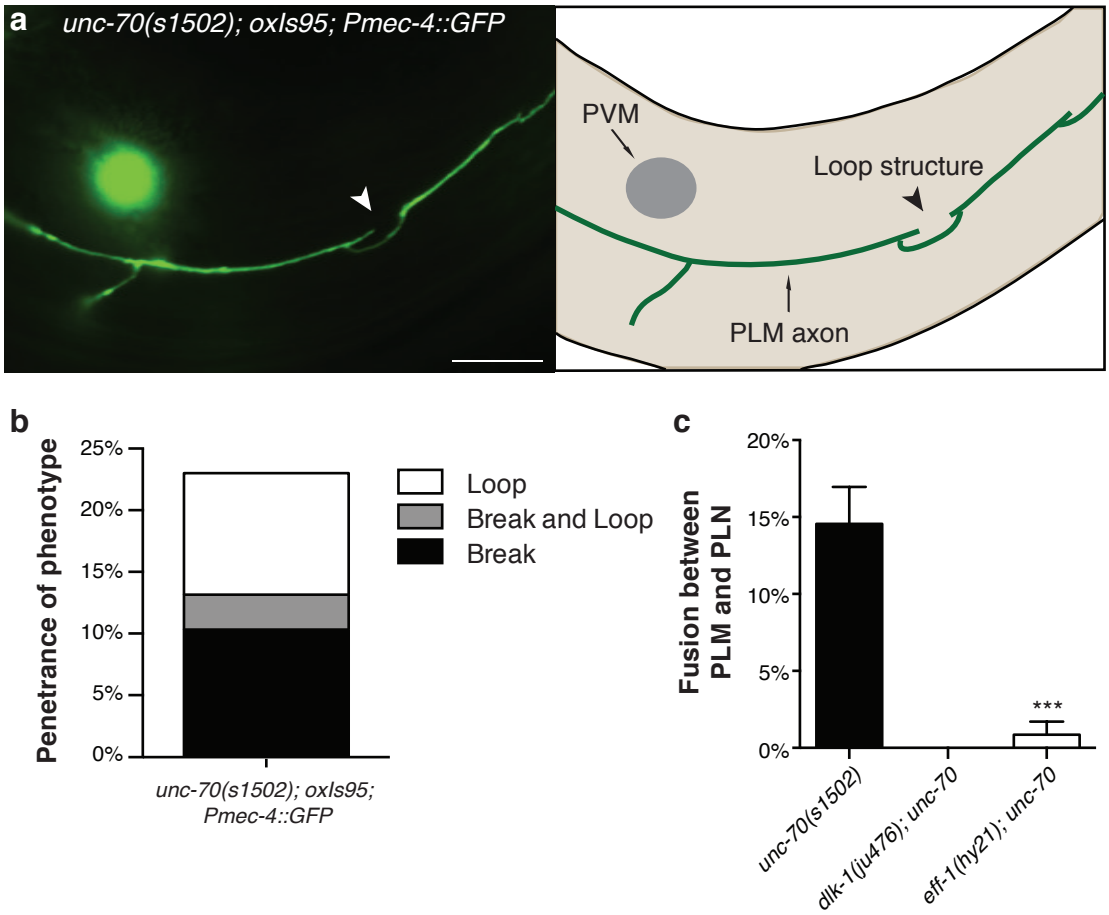

Extended Data Figure 5. Mutation of unc-70 causes axonal defects and PLM-PLN fusion events that are dependent on *eff-1* and *dlk-1*. **a**, In the absence of UNC-70 the PLM mechanosensory neuron develops abnormal morphology with breaks, loop structures (arrowhead) and branching. Scale bar 25 µm. **b**, Quantification of the penetrance of abnormal loop structures as well as axonal breakages; n > 200. **c**, Spontaneous fusion between PLM and PLN is completely abolished in *dlk-1* mutants and shows a large reduction in an *eff-1* mutant background. n > 100; p-value: *** < 0.001.

Extended Data Table 1. Quantification of regeneration in single and double mutant animals.

Genotype	Number of animals	Regrowth	Reconnection	Fusion
zdIs5	242	240 (99%)	90 (38%)	75 (83%)
ced-1(e1735); zdIs5	58	58 (100%)	39 (67%)	26 (67%)
ced-2(e1752); zdIs5	48	48 (100%)	19 (40%)	15 (79%)
ced-5(n1812); zdIs5	33	33 (100%)	21 (63%)	17 (81%)
ced-6(n1813); zdIs5	44	44 (100%)	29 (66%)	9 (31%)
ced-7(n2690); zdIs5	71	64 (90%)	17 (27%)	8 (47%)
ced-10(n3246); zdIs5	54	53 (98%)	24 (45%)	20 (83%)
eff-1(ok1021); zdIs5	60	59 (98%)	49 (83%)	8 (16%)
nrf-5(sa513); zdIs5	121	120 (99%)	26 (22%)	12 (46%)
psr-1(ok714); zdIs5	52	51 (98%)	23 (45%)	9 (39%)
psr-1(tm469); zdIs5	42	41 (98%)	19 (46%)	8 (42%)
ttr-52(sm211); zdIs5	128	127 (99%)	35 (28%)	19 (54%)
ttr-52(tm2078); zdIs5	63	62 (98%)	20 (32%)	8 (40%)
psr-1(ok714); ced-1(e1735); zdIs5	38	38 (100%)	22 (58%)	7 (32%)
psr-1(ok714); ced-6(n1813); zdIs5	37	37 (100%)	18 (49%)	5 (28%)
psr-1(ok714); ced-7(n2690); zdIs5	97	95 (98%)	34 (36%)	17 (50%)
psr-1(ok714); eff-1(ok1021); zdIs5	40	40 (100%)	34 (85%)	2 (6%)
psr-1(ok714); nrf-5(sa513); zdIs5	79	76 (96%)	21 (28%)	9 (43%)
psr-1(ok714); ttr-52(sm211); zdIs5	55	54 (98%)	21 (39%)	11 (52%)
ttr-52(sm211); eff-1(ok1021); zdIs5	56	56 (100%)	43 (77%)	3 (7%)

Extended Data Table 2. Average length of regrowth in single and double mutant animals.

Genotype	Number of animals	Length of regrowth (μm)	p value to *zdIs5*
zdIs5	165	77.49	
ced-1(e1735); zdIs5	32	71.73	0.43
ced-2(e1752); zdIs5	33	89.43	0.11
ced-5(n1812); zdIs5	16	95.74	0.077
ced-6(n1813); zdIs5	35	66.92	0.15
ced-7(n2690); zdIs5	56	42.96	8.06E-09
ced-10(n3246); zdIs5	33	46.72	2.64E-05
eff-1(ok1021); zdIs5	51	82.07	0.56
nrf-5(sa513); zdIs5	108	57.79	1.89E-05
psr-1(ok714); zdIs5	42	51.51	9.35E-05
psr-1(tm469); zdIs5	33	42.40	1.13E-06
ttr-52(sm211); zdIs5	108	61.74	0.0046
ttr-52(tm2078); zdIs5	54	62.18	0.012
psr-1(ok714); ced-1(e1735); zdIs5	31	51.91	0.0013
psr-1(ok714); ced-6(n1813); zdIs5	32	59.83	0.016
psr-1(ok714); ced-7(n2690); zdIs5	78	38.01	1.73E-14
psr-1(ok714); eff-1(ok1021); zdIs5	38	88.63	0.10
psr-1(ok714); nrf-5(sa513); zdIs5	67	49.49	1.56E-07
psr-1(ok714); ttr-52(sm211); zdIs5	43	69.50	0.23
ttr-52(sm211); eff-1(ok1021); zdIs5	56	74.29	0.59

5.4 Discussion and implications of findings

The identification of a molecular pathway that regulates axonal fusion during regeneration is of extreme significance, due to its potential medical implications as well as its importance to the advance of knowledge in a rapidly expanding field of research. Until now the only molecule known to regulate axonal fusion during regeneration was the fusogen EFF-1 (Ghosh-Roy et al., 2010). Axonal fusion represents a rapid and efficient means of restoring neuronal circuitry following damage. The present study identifies a 'save-me' signal in the form of the phospholipid PS, which is triggered on the distal fragment of the injured axon in response to damage. This signal is analogous to the so called 'eat-me' signal presented by apoptotic cells which is recognized by engulfing cells and mediates recognition and engulfment. Previous studies have speculated that such a mechanism may exist (Neumann et al., 2011), but until now none has been identified.

Components of the apoptotic recognition and engulfment pathway have been demonstrated to have a role in clearance of the distal axonal fragment following axonal damage in *Drosophila* and *C. elegans* (reviewed in chapter 1). Awasaki and colleagues (2006) proposed that axonal degeneration resulted in the exposure of an 'eat-me' signal analogous to that of an apoptotic cell. It is not clear if the same signal mediates degeneration of the distal fragment and recognition of the distal fragment during fusion, although this is an attractive hypothesis. Such a mechanism would provide a competition between degenerative and regenerative mechanisms to facilitate rapid axonal repair.

Understanding the mechanisms of axonal fusion allows the possibility of interventions to facilitate axonal fusion during regeneration. The present study demonstrates that genetically induced axonal damage is sufficient to activate similar mechanisms that induce neuronal fusion between two closely associated damaged neurons. The cell-cell fusion between two neurons shares several features of axonal fusion during regeneration, and the present study demonstrates that it can be used as a model of the latter. The study presented in chapter 6 uses this new paradigm to perform a forward genetic screen for axonal fusion mutants.

5.5 Statement of contribution

I performed the experiments presented in Figure 4 and Extended Data Figure 5, as well as did part of the experiments presented in Figure 1d-e, Figure 2b-d, Extended Table 1 and 2. The application of a genetic method of axonal injury to the study of axonal fusion is at the core of my contribution to this project. The paradigm of cell-cell fusion utilized in section 5.2 represents a novel means to study axonal fusion during regeneration, and this is the experimental platform on which the work presented in Chapter 6 of this thesis is based.

Chapter 6:
Designing a genetic method of axonal injury and isolation of novel mutants

6.1 Introduction

A key feature of multicellular organisms is the ability to integrate individual cells into tissue. This requires each cell to precisely maintain its structure and resist the mechanical stresses imposed by an active organism moving freely in its environment. A striking example of this resistance can be seen in the nervous system across phyla. A neuron is often several orders of magnitude longer than it is wide and yet is able to withstand significant strain during development and movement of the organism. In neurons this strain resistance is provided, at least in part, by the membrane cytoskeleton component β-spectrin (Hammarlund et al., 2007), which has been shown to be part of a periodic network with actin, ankyrin, and adducin (Xu et al., 2013). *C. elegans* motor neurons lacking UNC-70 develop normally but are unable to resist the mechanical stress of movement, which generates axon breaks followed by axonal regeneration (Hammarlund et al., 2007). This sensitivity to mechanical strain has been exploited in reverse genetic approaches to discover genes essential for regeneration in motor neurons (Hammarlund et al., 2009; Nix et al., 2014).

The study presented in chapter 5 demonstrated that in the absence of UNC-70 the PLM mechanosensory neuron undergoes a cell-cell fusion event with the nearby PLN neuron. This fusion event shares similarities with axonal fusion during regeneration in that it requires both axonal regeneration and fusion machinery to occur. The study presented in this chapter reveals that the loss of UNC-70 in PLM neurons causes a loss of axonal integrity defined by the formation of axonal breaks, and induces further remodelling visible as axonal loops. Detailed characterization of these defects reveals that axonal remodelling is independent of regeneration, but dependent on axonal fusion machinery. A genetic model of axonal injury enables the use of forward genetic screening as a method of identifying novel mutants with neuronal fusion defects. In the present study, we isolated and characterized three novel mutants, *vd30*, *vd33,* and *vd35,* which modify *unc-70*-induced axonal breaks, remodelling, and neuronal fusion.

6.2 Results

Axonal defects in unc-70/β-spectrin mutants arise in mature neurons

The study presented in chapter 5 demonstrated that the damage induced by loss of UNC-70 is sufficient to induce severe defects in the architecture of the axonal process, and in some cases stimulate neuronal fusion between the mechanosensory neuron PLM and its fasciculating neuron PLN. In GABAergic motor neurons UNC-70 is dispensable for normal axon outgrowth, but these neurons acquire movement-induced axonal defects as the animals age (Hammarlund et al., 2007). To test if the acquisition of the defects we observe in the PLM neuron of *unc-70* mutants is similar to those in GABAergic motor neurons, we studied PLM morphology at different stages of the animal's development (Fig 6.1d-e), using the same transgenic strain expressing GFP under the *Pmec-4* promoter as described in chapter 5. At the first larval stage (L1), the vast majority of PLM neurons displayed a completely wild-type morphology (Fig 6.1d-e) and only very rarely presented axonal defects. This indicates that, as occurs in GABAergic motor neurons, the mechanosensory neurons PLM left and right also present an overall wild-type morphology, with the axon normally guided to its target during development. Axonal breaks and loops (referred to as axonal remodelling) were observed in the fourth larval stage (L4) and in adult animals (Fig 6.1a-b,d-e), indicating that these morphological abnormalities arise in PLM axons after development is completed; thus, these defects are not likely to be the consequence of a defect in initial axonal outgrowth or guidance. In agreement with this interpretation, the appearance of the PLN neuron via neuronal fusion appeared only in adult stages (Fig 6.1c,f). At both L1 and L4 stages we never observed PLM-PLN fusion in *unc-70* mutants (Fig 6.1c,f), whereas in adults ~15% of animals lacking UNC-70 underwent a neuronal fusion event between PLM and PLN (Fig 6.1f). These data support a model in which *unc-70*-induced axonal injury in the PLM mechanosensory neuron proceeds in a similar manner to that observed in GABAergic motor neurons, with defects appearing after the development of the axonal process is completed.

Axonal remodelling does not require regeneration machinery

We never observed the formation of a distinct growth cone in the PLM neurons in response to *unc-70*-induced damage, which is instead a key characteristic of injured GABAergic motor neurons (Hammarlund et al., 2007). The MAP3K DLK-1 is required for axonal regeneration to proceed in multiple *C. elegans* neurons, including PLM (Ghosh-Roy et al., 2010; Hammarlund et al., 2009). The study presented in chapter 5 demonstrated that blocking regeneration using a *dlk-1* mutant is sufficient to prevent the neuronal fusion observed in *unc-70* mutants; these data strongly indicate that axonal regeneration is a major underlying mechanism in *unc-70*-induced neuronal fusion. The

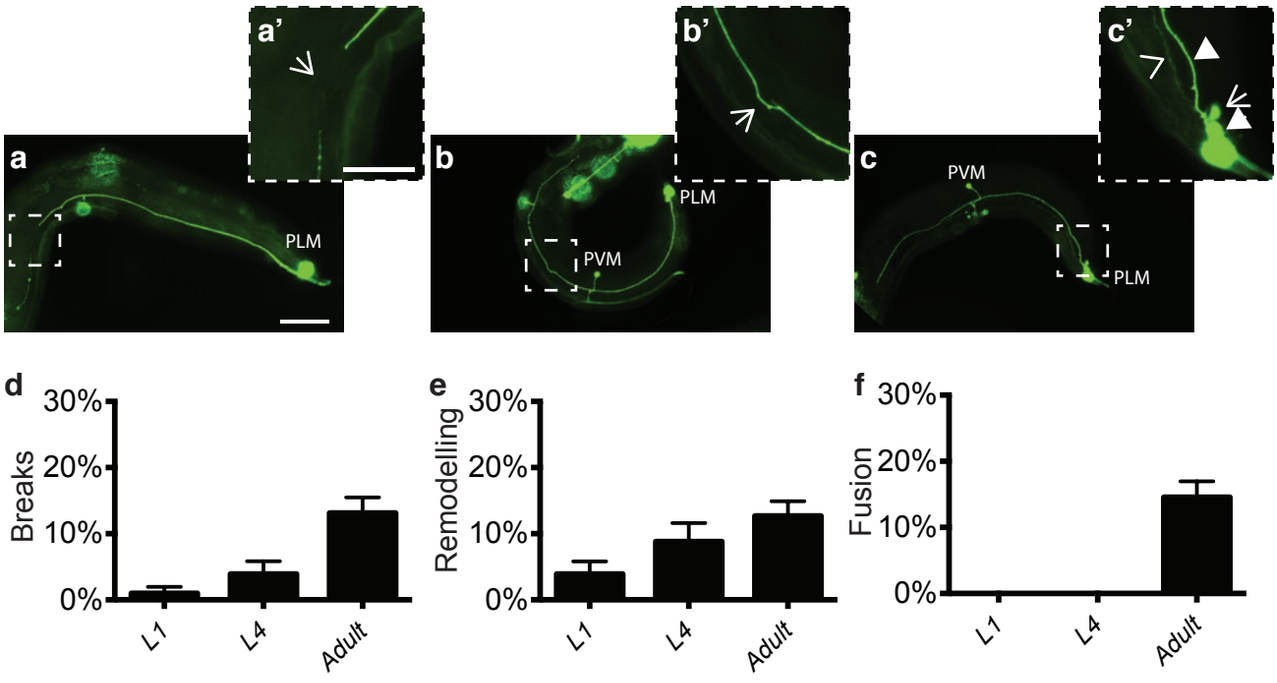

Figure 6.1. Axonal defects in *unc-70/ß-spectrin* mutants arise in mature neurons. **a**, an adult *unc-70(s1502)* mutant with GFP visible in the mechanosensory neuron PLM. Anterior is left and ventral is down in this and all images. Axonal breakage occurs in a proportion of PLM neurons (boxed area and arrow in **a'**). Scale bar in **a** = 50 µm; in **a'**= 25 µm. **b**, axonal remodelling visible as an axonal loop (boxed area and arrow **b'**) in the PLM axon of an *unc-70(s1502)* mutant animal. **c**, an *unc-70(s1502)* animal after a spontaneous fusion event between PLM (closed arrow in **c'**) and PLN (open arrow in **c'**), leading to the appearance of GFP in the cell body (open arrow in **c'**) and axon of PLN (open arrowhead in **c'**). **d**, frequency of axonal breakages in L1, L4 and adult *unc-70(s1502)* mutant animals. **e**, frequency of axonal loops in L1, L4, and adult *unc-70(s1502)* mutant animals. **f**, frequency of neuronal fusion in L1, L4, and adult *unc-70(s1502)* mutant animals. n> 102.

appearance of axonal remodelling phenotypes could in principle be caused by an axonal regeneration process or be independent of any regenerative event. To discriminate between these possibilities we tested the penetrance of this phenotype in animals lacking DLK-1. In *dlk-1; unc-70* double mutants axonal breakages and remodelling phenotypes appeared with the same frequency as in control animals (*unc-70* single mutants), demonstrating that DLK-1, and thus regeneration, is not required for their formation (Fig 6.2a-b). Taken together these data support a model in which, differently from PLM-PLN cell-cell fusion, the formation of axonal breakages and remodelling caused by lack of UNC-70 is not dependent of axonal regeneration.

We next decided to investigate if loss of the neuronal fusion machinery had any effect on the formation of axonal breaks and remodelling. We analysed animals lacking the fusogen EFF-1, which is required cell autonomously to regulate various fusion events in the PLM neuron (chapter 5). *eff-1; unc-70* double mutants presented with a large increase in the frequency of axonal breaks and remodelling (Fig 6.2c-d). EFF-1, a known fusogen and membrane-remodelling molecule, has been shown to inhibit the formation of dendritic branches in the *C. elegans* mechanosensory neuron PVD (Oren-Suissa et al., 2010). One hypothesis is that EFF-1 may inhibit axonal remodelling and facilitate neuronal fusion in the PLM neuron. To test if EFF-1 overexpression was sufficient to increase neuronal fusion, wild-type EFF-1 was overexpressed in the PLM neuron and its effect observed in *unc-70* mutants. Overexpressing wild-type EFF-1 in the mechanosensory neuron PLM in *unc-70* mutants had no effect on the frequency of axonal breaks and remodelling (Fig 6.2e-f); however, these animals presented with a very large increase in the frequency of neuronal fusion between PLM-PLN (Fig 6.2g). Together these data indicate that regeneration is required for neuronal fusion but not axon remodelling, and that EFF-1 acts by facilitating neuronal fusion between PLM-PLN and may also non-cell-autonomously inhibit membrane remodelling. Alternatively, this phenotype may be non-cell-autonomous and result of a developmental defect in the tissue surrounding the axon. At this stage the exact cause of the axonal remodelling phenotype is unknown; it is unclear if these morphological changes are the result of a defect in axonal development or maintenance.

Loss of UNC-70/β-spectrin causes multiple defects in PLN neurons

The axon of each bilateral PLN neuron fasciculates for much of its length with the axon of the PLM neuron of the ipsilateral side (White et al., 1986). To test if the PLN neuron develops similar axonal defects in the absence of UNC-70, mCherry was expressed in the PLN neuron using the *lad-2* promoter and its morphology observed. In adult animals the axon of the PLN neuron developed defects similar to those observed in the PLM axon in *unc-70* mutants (Fig 6.3a-b). Interestingly,

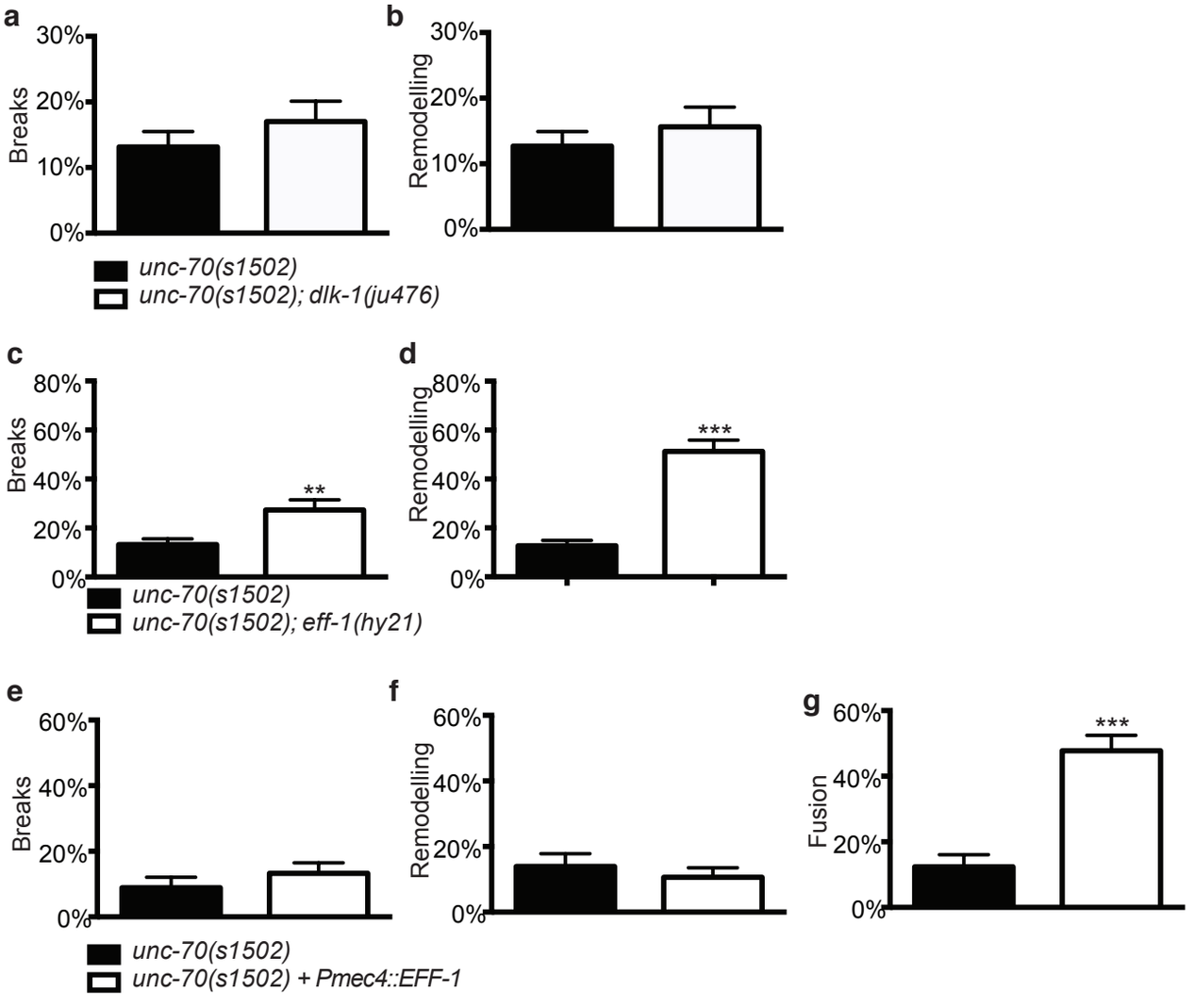

Figure 6.2. Axonal remodelling does not require regeneration. **a**, quantification of rates of axonal breakages in *unc-70* and *unc-70; dlk-1* animals. n>147. **b**, quantification of rates of axon remodelling in *unc-70* and *unc-70; dlk-1* animals. n>147. **c**, quantification of rates of axonal breakages in *unc-70* and *unc-70; eff-1* mutants. n> 117. **d**, quantification of rates of axon remodelling in *unc-70* and *unc-70; eff-1* mutants. n> 117. **e**, quantification of rates of axonal breakages in *unc-70* mutants overexpressing EFF-1 specifically in PLM using the *Pmec-4* promoter. n> 79. **f**, quantification of rates of axon remodelling in unc-70 mutants overexpressing EFF-1 specifically in PLM using the *Pmec-4* promoter. n> 79. **g**, quantification of rates of neuronal fusion between PLM and PLN in *unc-70* mutants overexpressing EFF-1 specifically in PLM using the *Pmec-4* promoter. n> 79. **= P-value<0.01 and ***= P-value<0.001.

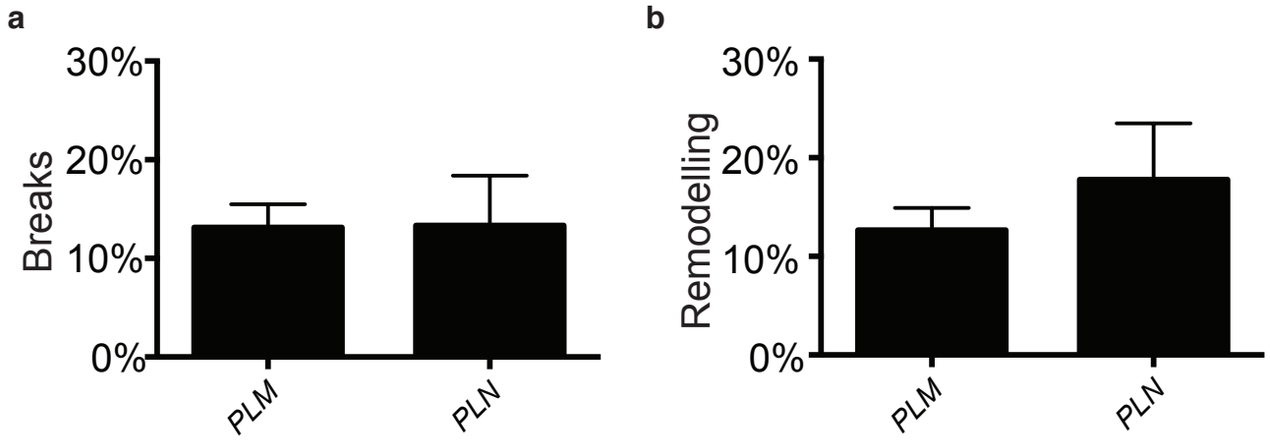

Figure 6.3. Loss of UNC-70/β-spectrin causes multiple defects in PLN neurons. **a**, frequency of axonal breakages in the PLM and PLN neurons in adult *unc-70(s1502)* mutants. **b**, frequency of axonal loops in the PLM and PLN neurons in adult *unc-70(s1502)* mutants. n>35.

similar defects were also observed in the axon of the ALN neuron (Fig S6.1), which fasciculates for some of its length with the axon of the mechanosensory neuron ALM (White et al., 1986). The ALM neuron displayed branching defects but breaks and axonal remodelling were rarely observed (Fig S6.1). Consistent with the phenotypes observed in the PLM and PLN neurons, some cases of neuronal fusion between ALM-ALN were observed in *unc-70* mutants (Fig S6.1). These data support a model in which, following *unc-70*-induced damage, two closely associated neurons are able to undergo a regeneration-dependent neuronal fusion event.

Dynamics of unc-70/β-spectrin induced neuronal fusion

To investigate the temporal dynamics of *unc-70*-induced damage time-lapse imaging was performed. As above, PLM-PLN fusion was detected by the appearance of the fluorophore GFP (expressed in PLM) diffusing into the PLN neuron. We found that GFP appeared first in the process of PLN, where it transitioned from faint to bright (Fig 6.4a-i); the GFP signal became brighter in the PLN process over time, gradually appearing in regions more proximal to the PLN cell body, until eventually reaching the cell body itself (Fig 6.4d). This result supports a model in which GFP first enters the PLN neuron at the site of PLM-PLN fusion, and then proceeds to diffuse in a retrograde fashion towards the PLN cell body.

Forward genetic screen for mutants with defects in axonal maintenance and neuronal fusion

Components of the apoptotic engulfment pathway, PSR-1, TTR-52, and CED-6, mediate PLM-PLN neuronal fusion in *unc-70* mutants (chapter 5). The fusogen EFF-1 mediates not only neuronal fusion in this model, but also modifies the formation of axonal breaks and membrane remodelling in *unc-70* mutants. These data suggest that molecules involved in membrane remodelling and neuronal fusion can present deficits in an *unc-70* sensitized background. To identify other molecules involved in the axonal breaks, loops, and neuronal fusion in an unbiased way, a pilot forward genetic screen was performed using ethyl methanosulfonate (EMS) in an *unc-70* sensitized background. From this screen we identified three novel mutants: *vd30, vd33,* and *vd35* (Fig 6.5a-c). These mutants affected the phenotypes of axonal breakage, remodelling, and neuronal fusion to different extents.

The mutant *vd30* was the most severe, presenting highly penetrant axonal breaks, remodelling, and PLM-PLN fusion phenotypes. Almost 50% of PLM axons in *vd30; unc-70* mutants contained axonal breaks, and approximately 73% of PLM axons displayed some form of axonal looping (Fig 6.5a-b). Importantly, the frequency of PLM-PLN neuronal fusion was almost double that of the *unc-70* mutant (Fig 6.5c). *vd33* mutants presented a large increase in axonal breaks and remodelling but no alteration to the frequency of neuronal fusion (Fig 6.5a-c). This indicates that

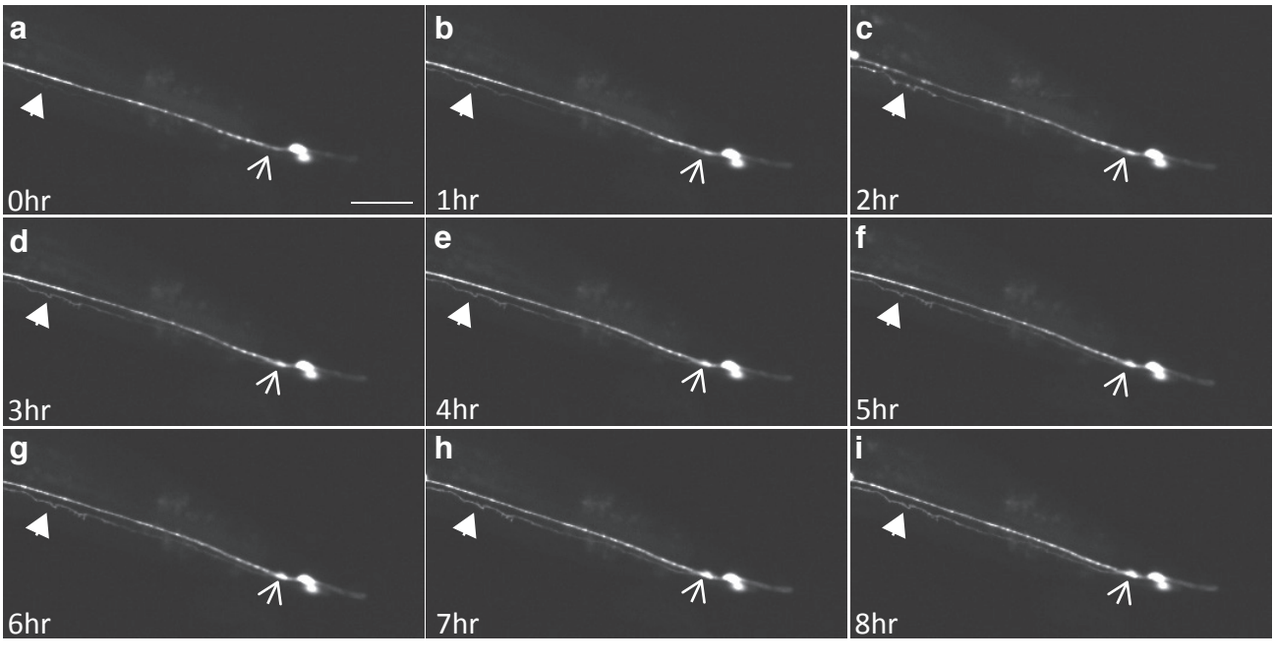

Figure 6.4. Dynamics of *unc-70/β-spectrin*-induced neuronal fusion. **a-i**, time-lapse images of a neuronal fusion event occurring between the PLM and PLN neuron, *in vivo*, in the *unc-70(s1502)* mutant. Filled arrowhead indicates the site of initial GFP transfer first visible at 0hr (**a**). Open arrowhead indicates site of eventual PLN cell body appearance, which occurs after GFP is visible in the axonal process (**b-i**). Scale bar = 50 μm.

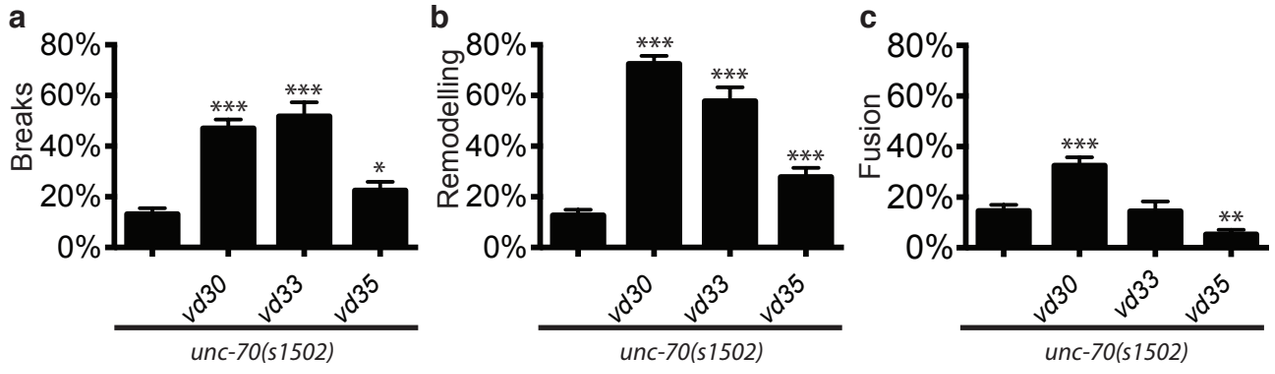

Figure 6.5. Novel mutants with defects in axonal maintenance and neuronal fusion.
a, frequency of axonal breakages in the PLM neuron of novel mutants *vd30*, *vd33,* and *vd35* in an *unc-70(s1502)* mutant background, compared to *unc-70(s1502)* mutants. **b**, frequency of axonal loops in the PLM neuron of novel mutants *vd30*, *vd33,* and *vd35* in an *unc-70(s1502)* mutant background, compared to *unc-70(s1502)* mutants. **c**, frequency of neuronal fusion between the PLM and PLN neurons of novel mutants *vd30*, *vd33,* and *vd35* in an *unc-70(s1502)* mutant background, compared to *unc-70(s1502)* mutants. n>83.

vd33 affects axonal maintenance but is dispensable for neuronal fusion. The *vd35* mutation increased both the penetrance of axonal breaks and remodelling in PLM (Fig 6.5a-b), but reduced the frequency of PLM-PLN neuronal fusion to less than half that of the background strain (Fig 6.5c). Therefore these three mutants support the notion that axonal maintenance, including breakage and remodelling, is a biological event that can be genetically separated from PLM-PLN neuronal fusion, and that these two processes are thus likely mediated by at least partially different molecular machinery.

Novel mutant vd30 has severe defects in axonal maintenance and neuronal fusion

vd30 impacts all aspects of *unc-70*-induced damage. To test if the defects observed in *vd30; unc-70* mutants proceeded similarly to those in *unc-70* single mutants, we analysed the developmental timing of these defects and their dependence on regeneration, as well as their real-time dynamics using time-lapse microscopy. The acquisition of defects over time in *vd30; unc-70* double mutants was very similar to that of *unc-70* mutants although the defects occurred more frequently (Fig 6.6a-c). Although *vd30* increased the frequency, and in some cases the severity of these defects, they occurred at approximately the same developmental stage as in *unc-70* animals. The requirement of regeneration for the development of axonal defects in *vd30; unc-70* double mutants was also tested by blocking regeneration in a *dlk-1* mutant. This experimental condition abolished PLM-PLN neuronal fusion in these animals (Fig 6.6d). Therefore, neuronal fusion in *vd30; unc-70* mutants also requires regeneration to proceed. Finally, time-lapse microscopy was performed to visualize the dynamics of these defects and to compare them with those in *unc-70* mutants. GFP was first observed in the process of the PLN neuron, after which it diffused in a retrograde direction towards the soma of PLN (Fig 6.7a-f). Although this occurred more frequently in *vd30; unc-70* mutants, there were no obvious differences in the dynamics of this process compared tour observations in *unc-70* mutants. Interestingly, in some instances the PLN neuron became brighter than normally observed in *unc-70* animals, suggesting that the fusion process in *vd30* mutants may be more efficient (data not shown). These results demonstrate that the development and acquisition of axonal defects in *vd30; unc-70* mutants proceeds in the same manner as in *unc-70* mutants, albeit at a higher frequency and possibly at a higher efficiency.

vd30 is required for axonal fusion during regeneration

A highly efficient method to repair an injured neuron occurs spontaneously in several invertebrate species (Bedi and Glanzman, 2001; Birse and Bittner, 1976; Deriemer et al., 1983; Ghosh-Roy et al., 2010; Hoy et al., 1967; Macagno et al., 1985; Neumann et al., 2011). This process, referred to as axonal fusion, occurs when the proximal axon that is still attached to the cell body regrows

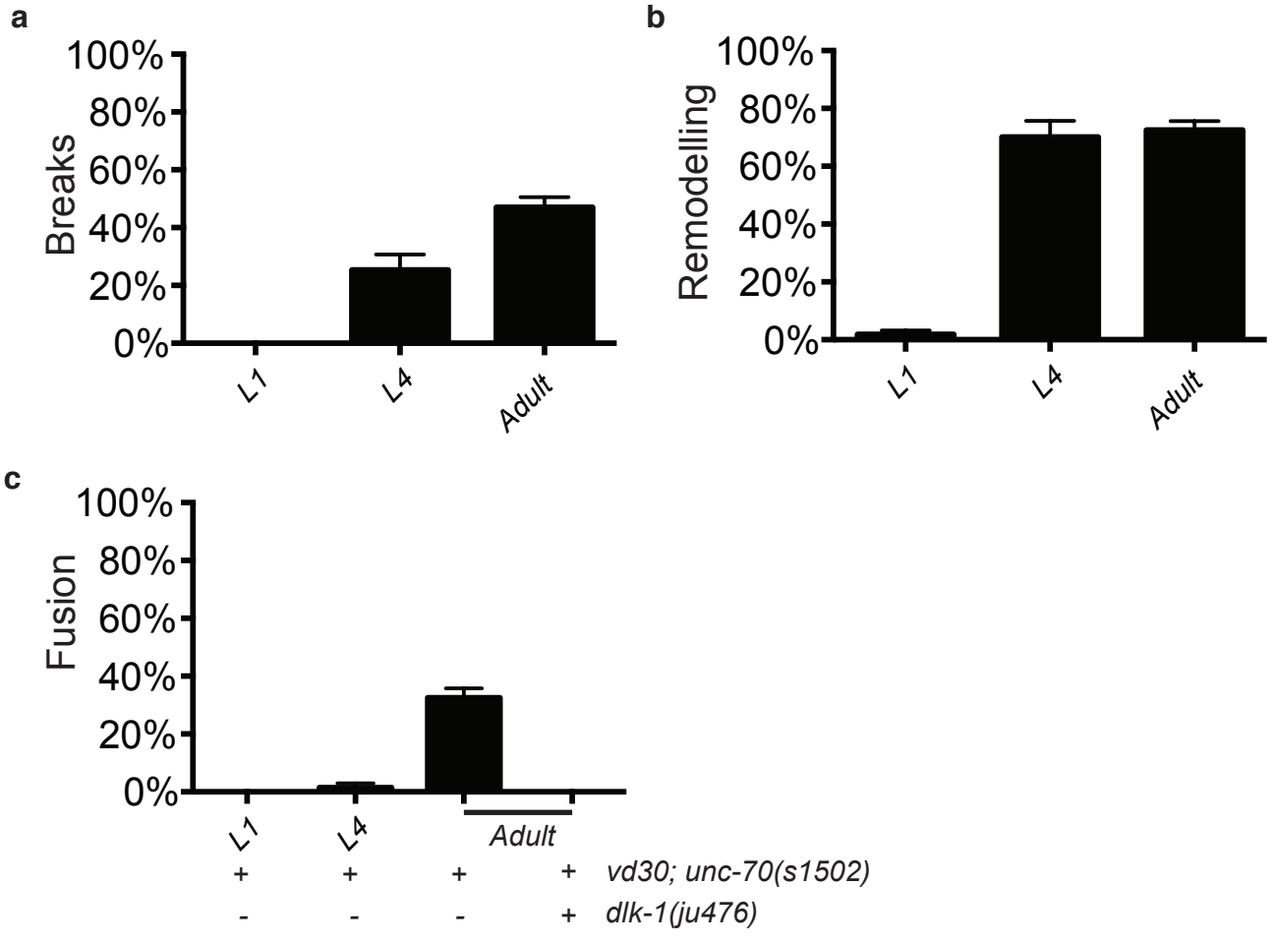

Figure 6.6. Defects in *vd30* mutants accumulate over time, and increase neuronal fusion in a regeneration-dependent fashion. **a**, frequency of axonal breakages in L1, L4, and adult *vd30; unc-70(s1502)* mutant animals. n> 267. **b**, frequency of axonal remodelling in L1, L4, and adult *vd30; unc-70(s1502)* mutant animals. n> 267. **c**, frequency of neuronal fusion in L1, L4, and adult *vd30; unc-70(s1502)* and *dlk-1(ju476); unc-70(s1502)* mutant animals. n>147.

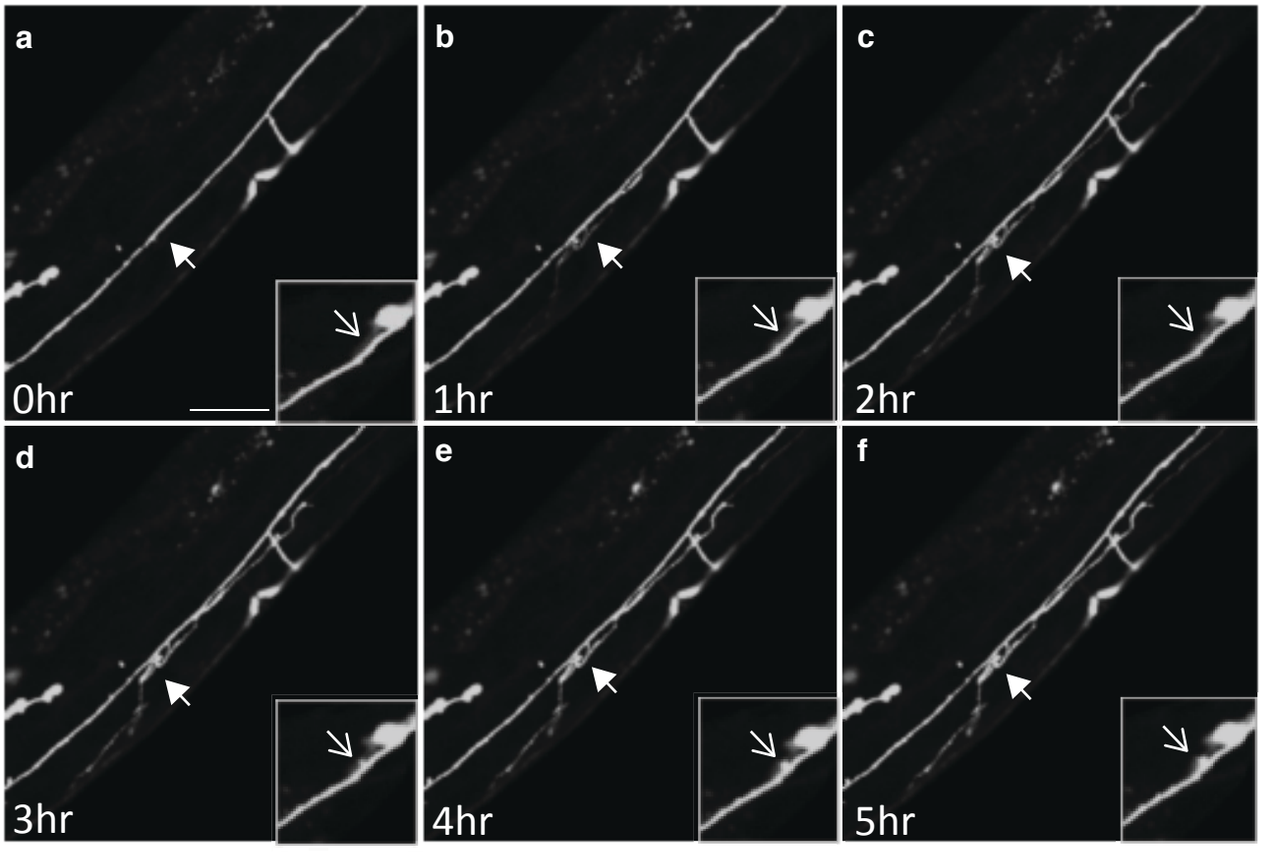

Figure 6.7. Dynamics of neuronal fusion in *vd30* novel mutant. a-f, *in vivo* time-lapse images of a neuronal fusion event occurring between the PLM and PLN neuron in the novel mutant *vd30; unc-70(s1502)*. Filled arrowhead indicates the site of initial GFP transfer first visible at 0hr (**a**). Inset (**a-f**) is a view of the PLM cell body with the site of eventual PLN cell body appearance labelled (open arrowhead). Scale bar = 50 μm.

towards, then reconnects and fuses with its separated distal fragment. Axonal fusion in the *C. elegans* mechanosensory neurons is a highly specific process that occurs through a fusion event, with both membrane and cytoplasmic continuity re-established (Ghosh-Roy et al., 2010; Neumann et al., 2011). Axonal fusion is mediated by the fusogen EFF-1 (Ghosh-Roy et al., 2010) and requires the components of the apoptotic recognition and engulfment pathway including PSR-1, TTR-52, and downstream components of the TTR-52 pathway (chapter 5). This molecular machinery is also required for neuronal fusion between PLM-PLN in *unc-70* mutants (chapter 5). To test if *vd30* also enhances axonal fusion during regeneration, laser axotomy was performed on the PLM axon in *vd30* animals in a wild-type background. To specifically study the process of axonal fusion, only severed axons that re-established a connection between the regrowing proximal axon and its separated distal fragment were analysed. As previously described (Neumann et al., 2011), successful fusion was considered as the maintenance, or inhibition of degeneration of the distal axonal fragment after reconnection; on the contrary, degeneration of the distal fragment following reconnection was considered as unsuccessful fusion. In wild-type animals 78% of animals that displayed proximal-distal reconnection underwent successful fusion (Fig 6.8a,c). *vd30* mutants showed a reduction in successful axonal fusion following reconnection with the distal fragment after regeneration (Fig 6.8b-c). Furthermore, the defect in axonal fusion was found to be specific for PLM, as axonal fusion was unaffected in the ALM neuron (Fig S6.2). The mechanosensory neurons in *vd30* animals displayed no morphological defects in a wild-type background, indicating that the defects in axonal maintenance are only present in the sensitized *unc-70* background (data not shown). These findings demonstrate a role for *vd30* in the regulation of axonal fusion during regeneration as well as PLM-PLN neuronal fusion in the *unc-70* background.

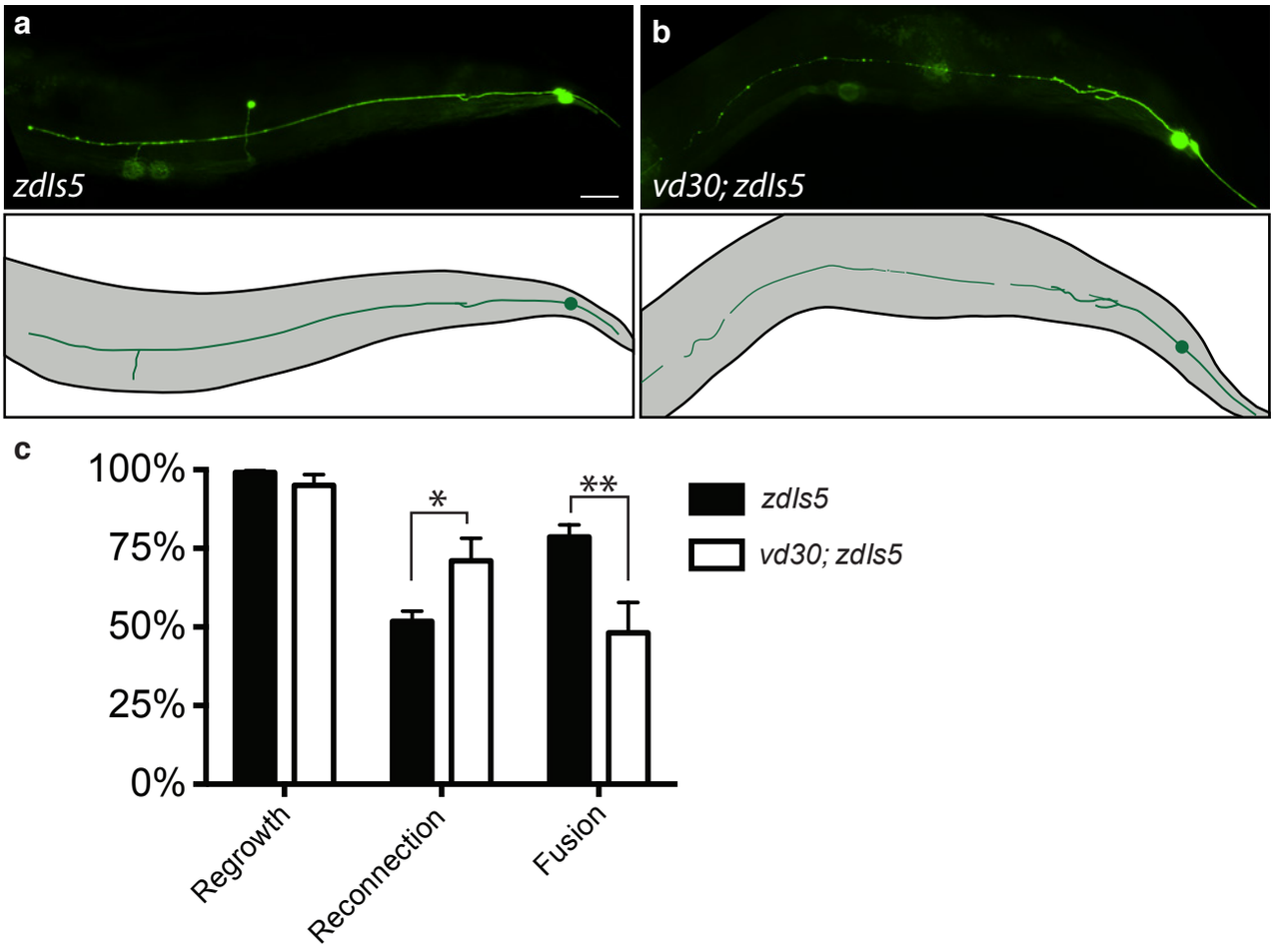

Figure 6.8. Axonal fusion during regeneration is reduced in *vd30* mutants. **a**, successful axonal fusion in a wild-type animal, 24hr post-axotomy. Scale bar = 25 µm. **b**, following regeneration and reconnection with the distal fragment, axonal fusion has failed to occur in a *vd30* mutant animal and the distal fragment has proceeded to degenerate. **c**, quantification of rates of regeneration, reconnection and axonal fusion in wild-type (*zdIs5*) and *vd30* mutant animals. n> 27.
*= P-value<0.05, **= P-value<0.01. Error bars indicate SEM.

6.3 Supplementary data

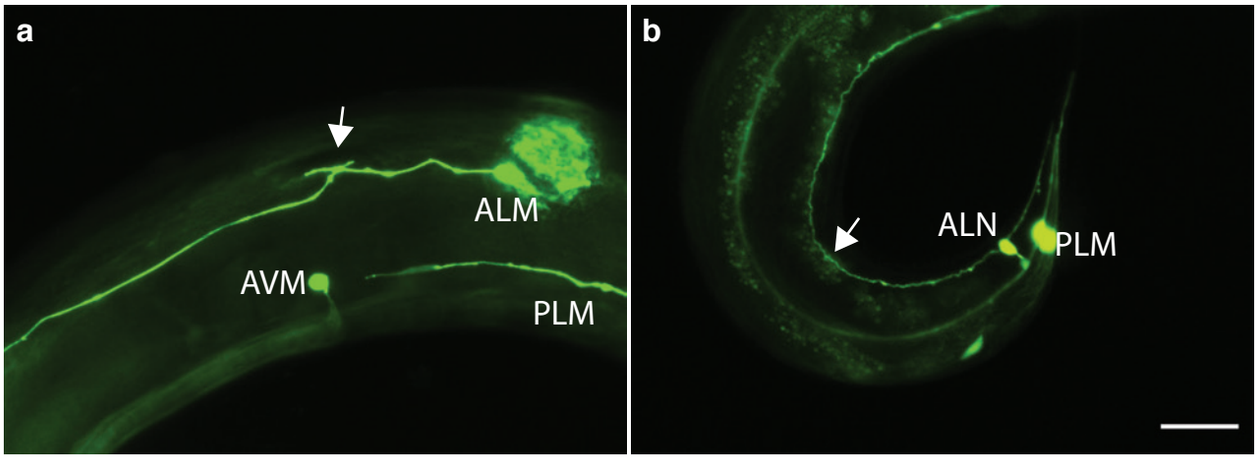

Supplementary Figure 6.1. Axonal defects in ALM and ALN neuronal fusion. **a**, ALM axons present with branched axonal processes. Breaks and axonal looping as observed in PLM were rarely seen (data not shown). **b**, on rare occasions fusion occurred between ALM and the ALN neuron resulting in GFP transfer into the cell body and axon of ALN (arrow). Scale bar = 25µm.

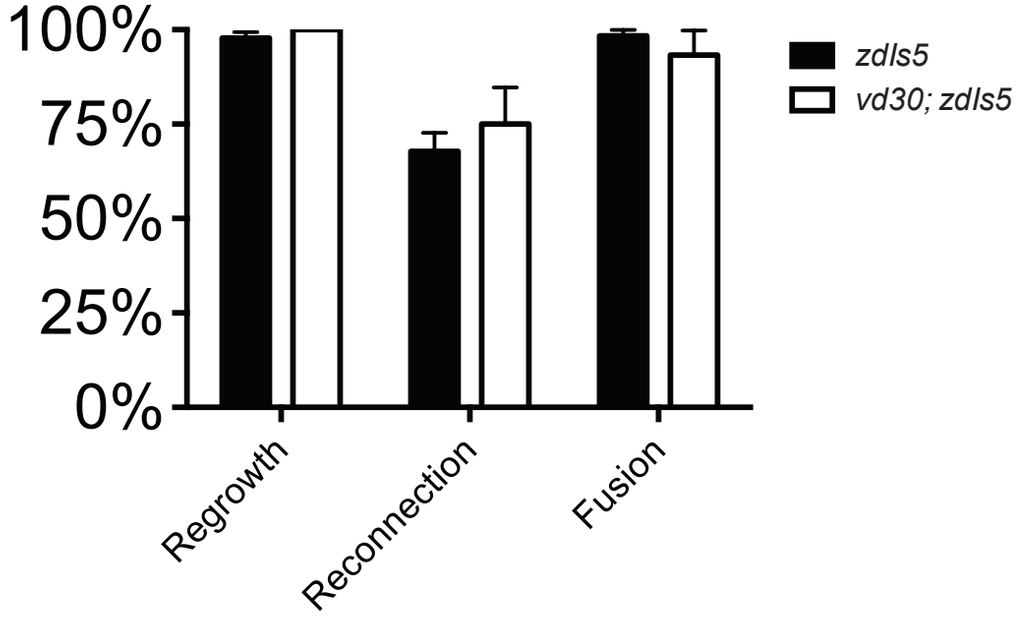

Supplementary Figure 6.2. ALM regenerates normally in *vd30* mutant animals. Quantification of rates of regeneration, reconnection and axonal fusion in the ALM neuron in *vd30* mutants in a *zdIs5(Pmec-4::GFP)* wild-type background compared to *zdIs5* animals. n> 15.

6.4 Discussion and implications of findings

The lack of the membrane cytoskeletal protein UNC-70 induces defects in axonal integrity in *C. elegans* mechanosensory neurons, distinct from spontaneous axonal breakage and regeneration seen in motor neurons. This damage induces axonal breakages without generating growth cones, as well as the formation of novel looped structures along the axonal process. We defined axonal looping as remodeling based on the observation that this phenotype is independent of *dlk-1*, the key axonal regeneration gene, and is dependent on the fusogen/membrane-remodeling gene *eff-1*. However, the exact nature of this phenotype is currently unknown and under investigation. These axonal abnormalities are acquired over time and are not the result of axon outgrowth defects. As both the mechanosensory neurons and GABAergic neurons are capable of generating growth cones following laser-induced axonal damage (Wu et al., 2007; Yanik et al., 2004), it is likely that the differences seen here are caused by differences in the injury itself rather than the regenerative capacity of the neurons. The mechanosensory neurons extend along the anterior-posterior axis of the animal, whereas the GABAergic motor neurons extend commissures across the ventral-dorsal axis (White et al., 1986). The location of these processes, and their interactions with the surrounding tissue, may be the reason behind the observed difference. It is possible that the axons of the GABAergic motor neurons, which extend circumferentially around the animal's body, experience more tensile force than the mechanosensory neurons, which extend along the longitudinal axis of the animal. As a consequence, the GABAergic motorneurons may suffer a more acute injury than the mechanosensory neurons. Furthermore, during development of the animal the PLM axon becomes embedded in the surrounding hypodermis (Chalfie and Sulston, 1981), which could possibly buffer some of the tensile force of the neuron. These defects may arise during the growth of the animal following axon guidance and extension, and may be the result of strain caused by a mis-match in the rate of elongation of the animal's body and the axonal process of PLM. The PLM neuron has evolved to detect external mechanical force, and as such the nature of its surrounding tissue, in combination with intrinsic mechanisms, may act as an additional mechanism to protect the axon from damage.

In addition to defects in the axons of mechanosensory neurons in animals lacking UNC-70, neuronal fusion events between the PLM mechanosensory neuron and the nearby neuron PLN were also observed as previously described in chapter 5. In the present study this phenomenon has been characterized in real time, revealing the sequence of events that starts with rapid uptake of GFP into the axon of PLN before diffusion of the fluorophore in a retrograde manner toward the cell body. GABAergic motor neurons in *unc-70* mutants have been shown to form spontaneous growth cones

on intact regions of their axons, suggesting that mechanical stresses on the animal that are insufficient to transect the axon are able to induce growth cone formation (Nix et al., 2014). It is possible that similar localized damage events occurring on both the PLM and PLN axons in regions of close apposition are sufficient to induce a regenerative event triggering neuronal fusion. This is supported by the observation that the axons of PLN and PLM simultaneously acquire axonal breaks and remodelling. Similar defects were also observed in the ALM and ALN neurons and some cases of ALM-ALN neuronal fusion. Following transection of both the PLM and PLN axons with a UV-laser, cell-cell fusion has been observed between the PLM and PLN neurons in small percentage of animals (Neumann et al., 2011). An attractive hypothesis is that neuronal fusion is the result of a regenerative event triggered by Ca^{2+} influx as a consequence of *unc-70*-induced axonal injury. The requirement of the DLK-1 MAP3K, essential for regeneration, supports this hypothesis.

In addition to DLK-1, neuronal fusion between PLM and PLN requires the fusogen EFF-1, as well as components of the apoptotic machinery, PSR-1, TTR-52, and CED-6 (section 5.2). The present study isolated three novel mutants that affect various aspects of *unc-70*-induced axonal damage as well as neuronal fusion. Analysis of these mutants revealed individual differences that are of profound biological significance. Comparison of these three mutants with animals lacking or overexpressing the fusogen EFF-1 suggests that axonal maintenance, including breakage and remodelling, are biological events that can be genetically separated from PLM-PLN neuronal fusion, and are thus likely mediated by at least partially different molecular machinery. The genetic lesions of the three novel mutants are currently being determined by traditional single nucleotide polymorphism (SNP) mapping (Davis et al., 2005; Wicks et al., 2001) combined with whole genome sequencing (Zuryn et al., 2010). The identification of these lesions will reveal the molecular elements and cellular mechanisms underpinning the different axonal phenotypes discovered, as well as the molecular basis of the cell-cell fusion.

The maintenance of axonal integrity and structure is critical to the correct function and organization of the nervous system in any organism. Defects in axonal integrity and structure, such as breaks, sprouting, branching, and varicosities, are associated with axonal degeneration and ageing phenotypes (Neumann and Hilliard, 2014; Pan et al., 2011; Tank et al., 2011; Toth et al., 2012). The complete set of genes required to maintain an axon for the lifetime of an animal and in response to injury remain unknown. The present study demonstrates that using a sensitized *C. elegans* strain with defects in axonal maintenance, both forward and reverse genetic approaches can be used in order to discover the molecules that regulate axonal fusion following injury.

6.5 Materials and methods

Strains and molecular biology

Nematodes were cultured under standard conditions (Brenner, 1974). All experiments were performed at 22°C. The wild-type strain N2 Bristol and the *zdIs5[Pmec-4::GFP]* and *oxIs95[Ppdi-2::unc-70]* transgenes were used. The *zdIs5* and *oxIs95* strains were a kind gift of Scott Clark and Erik Jorgensen, respectively. Standard molecular biology techniques were used (Sambrook et al., 1989).

Isolation of mutants

Animals of genotype *unc-70(s1502); oxIs95; zdIs5* were mutagenized using 50 mM ethyl methanesulfonate (Sigma) for 4 hr. The *vd30, vd33* and *vd35* mutations were isolated from a non-clonal visual screen of approximately 25,000 F2 progeny.

Laser axotomy

Axotomies were performed as previously described (Neumann et al., 2011). A MicroPoint Laser System Basic Unit, with axons severed approximately 50 μm anterior to the PLM or ALM cell body in L4 animals. Animals were analysed 24 hr post-axotomy for regrowth, reconnection, and fusion, and re-analyzed at 48 and/or 72 hr post-axotomy for clarification of successful fusion. Axons were deemed to be reconnected when the proximal and distal axons were visually connected and within the same focal plane with a 63x objective.

Statistical analysis

Statistical analyses were performed using Primer of Biostatistics 3.01 software. Error of proportions was used to assess variation across a single population. Two-way comparison was performed using the Students *t*-test.

Microscopy

Animals were immobilized in 0.05% tetramisole hydrochloride on 4% agar pads and visualized using Zeiss Axioimager Z1 and Zeiss Axioimager A1 microscopes. Images were taken using a Photometrics camera (Cool Snap HQ^2) and analysed with Metamorph software. For time-lapse microscopy animals were immobilized in 0.05% tetramisole hydrochloride on 10% agar pads sealed with vaseline and visualized using a Zeiss Inverted Spinning Disk confocal microscope equipped with a Yokogawa W1 disk head and a Piezo z-drive. Images were captured with a Hamamatsu Flash4.0 scientific CMOS camera using Slidebook 5.0 software.

6.6 Statement of contribution

I performed and significantly participated in the design and planning of all experiments. This work represents the primary focus of my PhD thesis aimed at discovering the molecular mechanisms that regulate membrane fusion in neurons.

Chapter 7:
Discussion

7.1 Overview

Axonal injury can be induced by a wide variety of insults, which trigger active mechanisms of axonal degeneration and regeneration in their respective compartments (reviewed in chapter 1). Although a large body of work from multiple model systems has uncovered critical components of these pathways, a complete picture of the molecular mechanisms by which axons are destroyed or repaired following injury is still lacking. The intersection of several technological advances has allowed these biological events to be studied and approached genetically in the nematode *C. elegans*. The development of genetically encoded fluorescent molecules, UV- and femtosecond-laser axotomy techniques, and the rise of next generation sequencing technology, have enabled the study of axonal degeneration and regeneration to be performed at single axon resolution, at the genomic scale.

The goal of this thesis was to develop paradigms in which specific aspects of axonal degeneration and regeneration could be studied with both forward and reverse genetic approaches in *C. elegans* neurons, and to use them to discover molecules that regulate these processes. The main findings of this work include: (i) identification of mutations in *mec-7/β-tubulin* that stabilize MTs, which promotes axon formation and reduces axonal regeneration rates (chapter 2); (ii) development of an optogenetic method of inducing cell ablation and neurodegeneration using the genetically encoded photosensitizer KillerRed (chapter 3); (iii) discovery of a role for the conserved guidance factor UNC-6/Netrin in protection against ROS-induced degeneration using genetically encoded KillerRed (chapter 4); (iv) identification of conserved components of the apoptotic recognition and engulfment pathway that regulate axonal fusion during regeneration (chapter 5); and (v) discovery of novel mutants with defects in axonal fusion during regeneration, using a genetically induced axonal injury model and forward genetics (chapter 6).

Together these findings provide two new paradigms in which axonal degeneration and regeneration via axonal fusion can be studied using forward and reverse genetic approaches. Furthermore, they provide critical new insights into how axons are protected from axonal degeneration induced by ROS, as well as an entirely novel function for conserved molecules in regulating axonal fusion during regeneration.

7.2 Developmental control of axonal morphology and regeneration

The development of a neuron requires regulated MT dynamics to correctly specify neurite identity and initiate axon outgrowth (Jiang et al., 2005; Kishi et al., 2005; Maniar et al., 2012; Yoshimura et al., 2005). More recently, MTs themselves have been implicated as instructive cues in the process of axonal specification (Baas, 2002; Hoogenraad and Bradke, 2009; Stiess and Bradke, 2011; Witte et al., 2008). The transformation of a mature stable axon into a regrowing axon following injury requires changes to MT dynamics (reviewed in chapter 1). The findings presented in chapter 2 demonstrate that normal MT dynamics are required for axon specification during development and axonal regeneration following injury.

The hyperstable microtubules present in animals with mutations in the gene *mec-7/β-tubulin* result in ectopic neurite formation with axon-like properties. This is the first time that MTs have been demonstrated to have an instructive role in the regulation of the number of neurites the neuron extends. During ALM development in *mec-7/β-tubulin* mutant animals, both the primary and ectopic neurites are able to extend over long distances. However, following laser-induced transection axon regrowth is reduced in both neurites. This supports a model in which axonal regeneration is distinct from axon outgrowth during development.

The defects in axonal regeneration seen in *mec-7/β-tubulin* mutants may be a direct result of MT stability, or due to secondary axonal transport defects. Wu et al. (2007) demonstrated that axonal regeneration in *C. elegans* mechanosensory neurons only occurred when the synaptic connection was disrupted. Interestingly, the localization of synaptic machinery is disrupted in *mec-7/β-tubulin* mutants. It is possible that the mislocalized synaptic machinery may prevent the neuron from detecting the loss of the neuron's primary synapse after axotomy, thus reducing regeneration. Alternatively, the defects in axonal transport observed in *mec-7/β-tubulin* mutants could itself be the primary cause of both synaptic defects and disrupted axonal regeneration. Finally, another possible explanation is a defect in injury signalling in *mec-7/β-tubulin* mutants. Recently, loss of microtubule stability has been demonstrated to trigger axonal outgrowth in a DLK-1-dependent manner (Marcette et al., 2014; Richardson et al., 2014). Microtubule destabilization is a critical event in axonal injury signalling. It is possible that the hyperstable microtubules of *mec-7/β-tubulin* mutants disrupt axonal injury signalling, resulting in a reduction in axonal regeneration. Further study is needed to determine which of these mechanisms are responsible for the reduced axonal regeneration observed in *mec-7/β-tubulin* mutants.

7.3 Molecular mechanisms of axonal and neuronal degeneration induced by ROS

In addition to triggering regeneration in the proximal axonal fragment, injury to an axon causes degeneration of the distal fragment, which occurs via an active mechanism. Although much is now known about several of the components involved in this process, a full picture is far from complete. Mitochondrial function is essential for the maintenance of a healthy axon. Altered mitochondrial transport, mitochondrial dysfunction, and the accumulation of ROS are all able to cause axonal degeneration. The study presented in chapter 3 demonstrates the ability of the optogenetic tool KillerRed to ablate *C. elegans* neurons *in vivo* via the generation of ROS. In addition to its function as a cell ablation tool, KillerRed is capable of triggering localized degeneration of *C. elegans* mechanosensory neurons when it is selectively activated in the axon. The mechanism by which ROS induces axonal degeneration in neurons is unknown. These findings provided an opportunity to study the effects of ROS accumulation *in vivo* in the context of axonal and neuronal degeneration.

Axonal injury can trigger axonal regeneration, axonal degeneration, and in some cases neuronal death. Many neurodegenerative diseases have axonal degeneration pathologies in combination with neuronal death. In both animal and disease models cell death and Wallerian degeneration function via distinct mechanisms (Coleman, 2005). The nature of KillerRed-induced ROS accumulation provided a platform to study both localized axonal degeneration and the pathology of ROS-induced neuronal death. Remarkably, the effect of KillerRed was not universal, with some neurons highly vulnerable to KillerRed-generated ROS, and others more refractory. Selective vulnerability is a common theme in neurodegenerative disorders, with specific populations of neurons degenerating while others are resistant to the same stimulus (Mattson and Magnus, 2006). The study presented in chapter 4 utilized this differential sensitivity to ROS to identify molecules that function to protect cells from KillerRed-induced ROS degeneration. Through a candidate gene approach, the conserved guidance molecule UNC-6/Netrin was identified as a neuroprotective factor.

It is not clear from these results is by which mechanism UNC-6/Netrin confers protection against ROS-induced degeneration. Predictably, loss of the UNC-6/Netrin receptor, UNC-40/DCC, increased the rate of KillerRed-induced neuronal degeneration. However, SAX-3/Robo, the receptor for the repulsive guidance cue SLT-1/Slit, also protected against neurodegeneration independently of its canonical ligand. A full genetic analysis is needed to determine if these molecules function in the same pathway to protect neurons from ROS-induced degeneration.

7.4 Molecular mechanisms of axonal fusion during regeneration

Invertebrate neurons have been observed to regenerate and reconnect with their separated distal axonal fragments via axonal fusion. In *C. elegans* mechanosensory neurons this is a highly specific process that requires the fusogen EFF-1. Prior to the study presented in chapter 5, no other molecules involved in mediating axonal fusion had been identified. Previous studies from our laboratory had challenged regrowing proximal axonal fragments with multiple distal fragments and observed a high degree of specificity in the axonal fusion process, suggesting that there is a recognition mechanism involving the participation of the distal fragment (Neumann et al., 2011). Using a candidate gene approach, the study presented in chapter 5 uncovered a novel role for conserved members of the apoptotic recognition and engulfment pathways in mediating axonal fusion during regeneration. In this model, injury to the axon triggers the exposure of a 'save-me' signal on the distal axonal fragment in the form of the membrane phospholipid PS. This signal is recognized by PS-binding protein PSR-1 on the proximal fragment and the secreted molecule TTR-52. These two bridging molecules act via the intracellular adapter CED-6 in the proximal axonal fragment to facilitate EFF-1-dependent axonal fusion.

Fascinatingly, as discussed in chapter 1 this process once again involves the intersection of axonal degeneration and axonal regeneration machinery. The transmembrane receptor Draper/CED-1 and CED-6 have been demonstrated to mediate clearance of the distal axonal fragment in *Drosophila* following injury (Awasaki et al., 2006; MacDonald et al., 2006). In addition, unpublished data from our laboratory suggest that CED-1- and CED-6-mediated clearance is conserved in *C. elegans* and reduces axonal clearance following injury (Annika Nichols and Massimo Hilliard, *personal communication*). This raises the possibility that axonal degeneration triggers a universal external injury signal that competes as an 'eat-me' signal or 'save-me' signal in the separated distal fragment (Fig 7.1). In the event of proximal fragment regrowth and reconnection this signal is able to facilitate axonal fusion, and in the event of non-reconnection this signal is able to mediate engulfment and clearance by phagocytic cells.

In addition to studying axonal fusion during regeneration triggered by axotomy, the study in chapter 5 provides an alternative paradigm in which to study injury-triggered neuronal fusion using spontaneous axonal damage induced by the loss of UNC-70. This injury model generates cell-cell fusion between two closely associated neurons following axonal damage in both cells. *unc-70*-induced neuronal fusion requires regeneration and shares the machinery required for axonal fusion. Therefore, the experimental paradigm developed in chapter 5 allows the discovery of novel

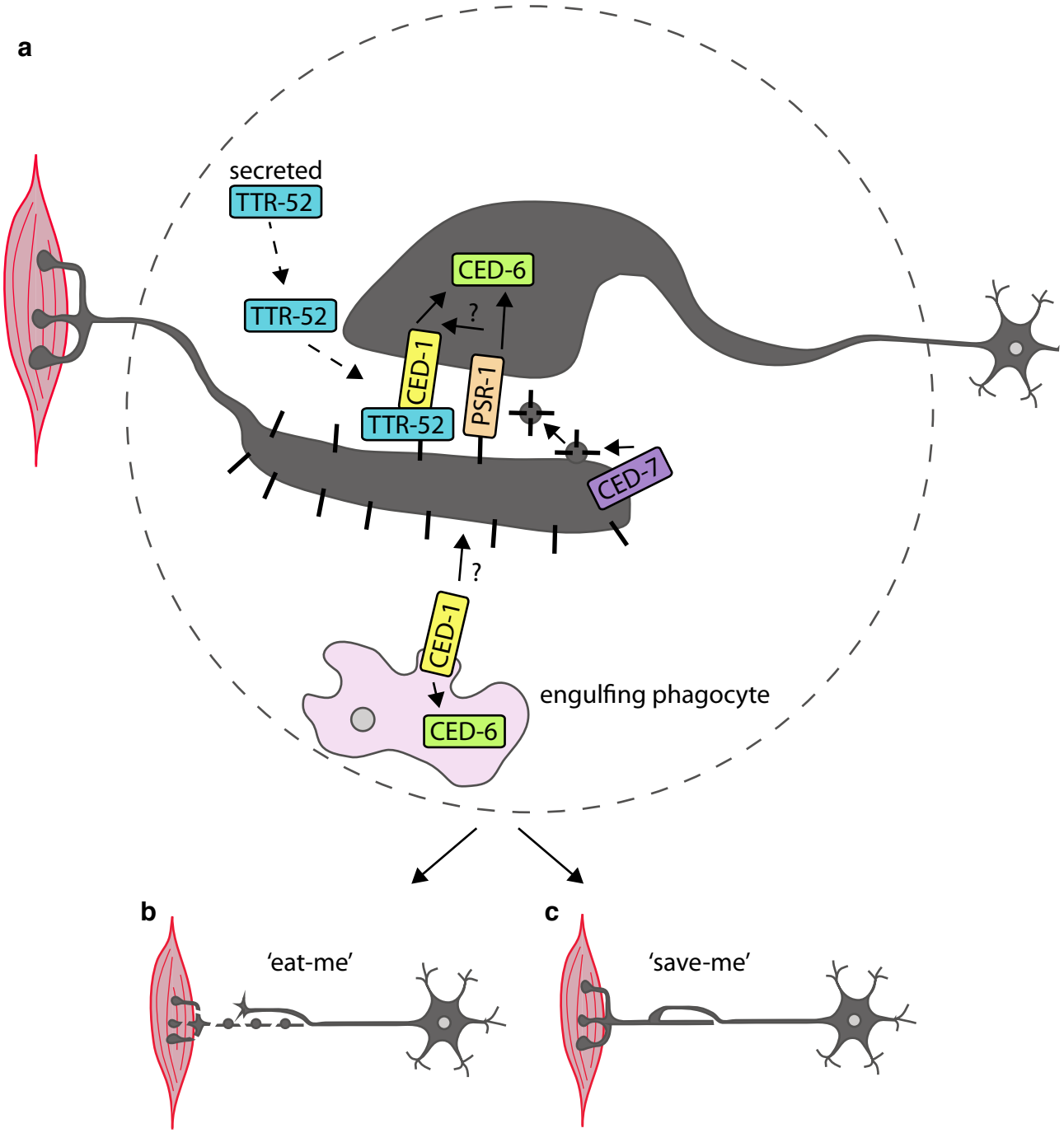

Figure 7.1. Conserved components of apoptotic recognition machinery regulate axonal fusion and axonal degeneration. Proposed schematic model for the recognition of the distal axonal fragment by the regrowing proximal axonal fragment during axonal regeneration via axonal fusion. **a**, following injury, PS is exposed on the distal fragment where it acts as a 'save me' signal, and this might be enhanced by CED-7-facilitated secretion of PS-coated vesicles. PS is recognized by secreted extracellular bridging protein TTR-52, and by the transmembrane PSR-1 on the proximal axon. The 'save me' signal is transduced intracellularly via CED-6, and possibly also through activation of the TTR-52-interacting CED-1 receptor. CED-1 and CED-6 also mediate clearance of the degenerating distal axonal fragment in cases where the regrowing proximal fragment does not reach the distal fragment. In this context, the distal fragment is hypothesized to present an unknown 'eat-me' signal (**b**) which may compete with the 'save-me' signal (**c**) to facilitate circuit repair.

molecules required for both neuronal and axonal fusion. This finding provided the basis for the study presented in chapter 6, where *unc-70*-induced axonal damage and neuronal fusion was used in a forward genetic screen to identify novel mutants.

Thus, the body of work presented here provides the first example in which a forward genetic approach has been used to study any aspect of axonal regeneration in any system. Typically axonal injury is induced by UV- or femtosecond-laser axotomy, which although highly specific imposes time constraints as each animal requires an individual surgery. Using this approach, the study presented in chapter 6 identified two novel mutants with defects in *unc-70*-induced neuronal fusion. This paradigm has paved the way to a more extensive use of forward genetic screens to discover novel molecules required for axonal fusion during regeneration.

7.5 Conclusions

In summary, this thesis provides a substantial contribution to the understanding of the molecular mechanisms of both axonal degeneration and regeneration. In addition to the identification of novel roles for conserved molecules in axonal fusion during regeneration, these studies provide two new paradigms that allow future investigations to utilize the full power of *C. elegans* genetics to dissect these biological processes.

References

Abe, N., and Cavalli, V. (2008). Nerve injury signaling. Curr Opin Neurobiol *18*, 276-283.

Amiri, M., and Hollenbeck, P.J. (2008). Mitochondrial biogenesis in the axons of vertebrate peripheral neurons. Dev Neurobiol *68*, 1348-1361.

Andersen, P.M., and Al-Chalabi, A. (2011). Clinical genetics of amyotrophic lateral sclerosis: what do we really know? Nat Rev Neurol *7*, 603-615.

Awasaki, T., Tatsumi, R., Takahashi, K., Arai, K., Nakanishi, Y., Ueda, R., and Ito, K. (2006). Essential role of the apoptotic cell engulfment genes draper and ced-6 in programmed axon pruning during Drosophila metamorphosis. Neuron *50*, 855-867.

Baas, P.W. (2002). Neuronal polarity: microtubules strike back. Nat Cell Biol *4*, E194-195.

Bartosz, G. (2009). Reactive oxygen species: destroyers or messengers? Biochem Pharmacol *77*, 1303-1315.

Baxter, R.V., Ben Othmane, K., Rochelle, J.M., Stajich, J.E., Hulette, C., Dew-Knight, S., Hentati, F., Ben Hamida, M., Bel, S., Stenger, J.E.*, et al.* (2002). Ganglioside-induced differentiation-associated protein-1 is mutant in Charcot-Marie-Tooth disease type 4A/8q21. Nat Genet *30*, 21-22.

Bedi, S.S., and Glanzman, D.L. (2001). Axonal rejoining inhibits injury-induced long-term changes in Aplysia sensory neurons in vitro. J Neurosci *21*, 9667-9677.

Bhatt, D.H., Otto, S.J., Depoister, B., and Fetcho, J.R. (2004). Cyclic AMP-induced repair of zebrafish spinal circuits. Science *305*, 254-258.

Billger, M., Wallin, M., and Karlsson, J.O. (1988). Proteolysis of tubulin and microtubule-associated proteins 1 and 2 by calpain I and II. Difference in sensitivity of assembled and disassembled microtubules. Cell Calcium *9*, 33-44.

Birse, S.C., and Bittner, G.D. (1976). Regeneration of giant axons in earthworms. Brain Res *113*, 575-581.

Bisby, M.A., and Chen, S. (1990). Delayed wallerian degeneration in sciatic nerves of C57BL/Ola mice is associated with impaired regeneration of sensory axons. Brain Res *530*, 117-120.

Bittner, G.D., Keating, C.P., Kane, J.R., Britt, J.M., Spaeth, C.S., Fan, J.D., Zuzek, A., Wilcott, R.W., Thayer, W.P., Winograd, J.M.*, et al.* (2012). Rapid, effective, and long-lasting behavioral recovery produced by microsutures, methylene blue, and polyethylene glycol after completely cutting rat sciatic nerves. J Neurosci Res *90*, 967-980.

Britt, J.M., Kane, J.R., Spaeth, C.S., Zuzek, A., Robinson, G.L., Gbanaglo, M.Y., Estler, C.J., Boydston, E.A., Schallert, T., and Bittner, G.D. (2010). Polyethylene glycol rapidly restores axonal integrity and improves the rate of motor behavior recovery after sciatic nerve crush injury. J Neurophysiol *104*, 695-703.

Brown, M.C., Lunn, E.R., and Perry, V.H. (1992). Consequences of slow Wallerian degeneration for regenerating motor and sensory axons. J Neurobiol *23*, 521-536.
Brown, M.C., Perry, V.H., Hunt, S.P., and Lapper, S.R. (1994). Further studies on motor and sensory nerve regeneration in mice with delayed Wallerian degeneration. Eur J Neurosci *6*, 420-428.
Bulina, M.E., Lukyanov, K.A., Britanova, O.V., Onichtchouk, D., Lukyanov, S., and Chudakov, D.M. (2006). Chromophore-assisted light inactivation (CALI) using the phototoxic fluorescent protein KillerRed. Nat Protoc *1*, 947-953.
Byrne, A.B., Walradt, T., Gardner, K.E., Hubbert, A., Reinke, V., and Hammarlund, M. (2014). Insulin/IGF1 signaling inhibits age-dependent axon regeneration. Neuron *81*, 561-573.
Calkins, M.J., and Reddy, P.H. (2011). Assessment of newly synthesized mitochondrial DNA using BrdU labeling in primary neurons from Alzheimer's disease mice: Implications for impaired mitochondrial biogenesis and synaptic damage. Biochim Biophys Acta *1812*, 1182-1189.
Chalfie, M., and Sulston, J. (1981). Developmental genetics of the mechanosensory neurons of Caenorhabditis elegans. Dev Biol *82*, 358-370.
Chalfie, M., Sulston, J.E., White, J.G., Southgate, E., Thomson, J.N., and Brenner, S. (1985). The neural circuit for touch sensitivity in Caenorhabditis elegans. J Neurosci *5*, 956-964.
Chan, S.S., Zheng, H., Su, M.W., Wilk, R., Killeen, M.T., Hedgecock, E.M., and Culotti, J.G. (1996). UNC-40, a C. elegans homolog of DCC (Deleted in Colorectal Cancer), is required in motile cells responding to UNC-6 netrin cues. Cell *87*, 187-195.
Chen, H., Detmer, S.A., Ewald, A.J., Griffin, E.E., Fraser, S.E., and Chan, D.C. (2003). Mitofusins Mfn1 and Mfn2 coordinately regulate mitochondrial fusion and are essential for embryonic development. J Cell Biol *160*, 189-200.
Chen, L., Wang, Z., Ghosh-Roy, A., Hubert, T., Yan, D., O'Rourke, S., Bowerman, B., Wu, Z., Jin, Y., and Chisholm, A.D. (2011). Axon regeneration pathways identified by systematic genetic screening in C. elegans. Neuron *71*, 1043-1057.
Chen, X.J., Levedakou, E.N., Millen, K.J., Wollmann, R.L., Soliven, B., and Popko, B. (2007). Proprioceptive sensory neuropathy in mice with a mutation in the cytoplasmic Dynein heavy chain 1 gene. J Neurosci *27*, 14515-14524.
Chisholm, A.D. (2013). Cytoskeletal dynamics in Caenorhabditis elegans axon regeneration. Annu Rev Cell Dev Biol *29*, 271-297.
Chow, B.Y., Han, X., Dobry, A.S., Qian, X., Chuong, A.S., Li, M., Henninger, M.A., Belfort, G.M., Lin, Y., Monahan, P.E.*, et al.* (2010). High-performance genetically targetable optical neural silencing by light-driven proton pumps. Nature *463*, 98-102.

Coleman, M. (2005). Axon degeneration mechanisms: commonality amid diversity. Nat Rev Neurosci *6*, 889-898.
Conforti, L., Adalbert, R., and Coleman, M.P. (2007). Neuronal death: where does the end begin? Trends Neurosci *30*, 159-166.
Corcoran, A., and Cotter, T.G. (2013). Redox regulation of protein kinases. FEBS J *280*, 1944-1965.
Court, F.A., and Coleman, M.P. (2012). Mitochondria as a central sensor for axonal degenerative stimuli. Trends Neurosci *35*, 364-372.
Davis, M.W., Hammarlund, M., Harrach, T., Hullett, P., Olsen, S., and Jorgensen, E.M. (2005). Rapid single nucleotide polymorphism mapping in C. elegans. BMC Genomics *6*, 118.
Deriemer, S.A., Elliott, E.J., Macagno, E.R., and Muller, K.J. (1983). Morphological evidence that regenerating axons can fuse with severed axon segments. Brain Res *272*, 157-161.
DiMauro, S., and Schon, E.A. (2008). Mitochondrial disorders in the nervous system. Annu Rev Neurosci *31*, 91-123.
Dong, C., Gao, W., Jia, R., Li, S., Shen, Z., and Li, B. (2013). Reconstruction of anorectal function through end-to-side neurorrhaphy by autonomic nerves and somatic nerve in rats. J Surg Res *180*, e63-71.
Erez, H., and Spira, M.E. (2008). Local self-assembly mechanisms underlie the differential transformation of the proximal and distal cut axonal ends into functional and aberrant growth cones. J Comp Neurol *507*, 1019-1030.
Fang, Y., Soares, L., Teng, X., Geary, M., and Bonini, N.M. (2012). A novel Drosophila model of nerve injury reveals an essential role of Nmnat in maintaining axonal integrity. Curr Biol *22*, 590-595.
Ferri, A., Sanes, J.R., Coleman, M.P., Cunningham, J.M., and Kato, A.C. (2003). Inhibiting axon degeneration and synapse loss attenuates apoptosis and disease progression in a mouse model of motoneuron disease. Curr Biol *13*, 669-673.
Fischer, L.R., and Glass, J.D. (2010). Oxidative stress induced by loss of Cu,Zn-superoxide dismutase (SOD1) or superoxide-generating herbicides causes axonal degeneration in mouse DRG cultures. Acta Neuropathol *119*, 249-259.
Furne, C., Rama, N., Corset, V., Chedotal, A., and Mehlen, P. (2008). Netrin-1 is a survival factor during commissural neuron navigation. Proc Natl Acad Sci U S A *105*, 14465-14470.
Gabel, C.V., Antoine, F., Chuang, C.F., Samuel, A.D., and Chang, C. (2008). Distinct cellular and molecular mechanisms mediate initial axon development and adult-stage axon regeneration in C. elegans. Development *135*, 1129-1136.

Ghosh, A.S., Wang, B., Pozniak, C.D., Chen, M., Watts, R.J., and Lewcock, J.W. (2011). DLK induces developmental neuronal degeneration via selective regulation of proapoptotic JNK activity. J Cell Biol *194*, 751-764.

Ghosh-Roy, A., Goncharov, A., Jin, Y., and Chisholm, A.D. (2012). Kinesin-13 and tubulin posttranslational modifications regulate microtubule growth in axon regeneration. Dev Cell *23*, 716-728.

Ghosh-Roy, A., Wu, Z., Goncharov, A., Jin, Y., and Chisholm, A.D. (2010). Calcium and cyclic AMP promote axonal regeneration in Caenorhabditis elegans and require DLK-1 kinase. J Neurosci *30*, 3175-3183.

Gitler, D., and Spira, M.E. (1998). Real time imaging of calcium-induced localized proteolytic activity after axotomy and its relation to growth cone formation. Neuron *20*, 1123-1135.

Hafezparast, M., Klocke, R., Ruhrberg, C., Marquardt, A., Ahmad-Annuar, A., Bowen, S., Lalli, G., Witherden, A.S., Hummerich, H., Nicholson, S.*, et al.* (2003). Mutations in dynein link motor neuron degeneration to defects in retrograde transport. Science *300*, 808-812.

Hammarlund, M., Jorgensen, E.M., and Bastiani, M.J. (2007). Axons break in animals lacking beta-spectrin. J Cell Biol *176*, 269-275.

Hammarlund, M., Nix, P., Hauth, L., Jorgensen, E.M., and Bastiani, M. (2009). Axon regeneration requires a conserved MAP kinase pathway. Science *323*, 802-806.

Han, S.M., Tsuda, H., Yang, Y., Vibbert, J., Cottee, P., Lee, S.J., Winek, J., Haueter, C., Bellen, H.J., and Miller, M.A. (2012). Secreted VAPB/ALS8 major sperm protein domains modulate mitochondrial localization and morphology via growth cone guidance receptors. Dev Cell *22*, 348-362.

Hao, J.C., Yu, T.W., Fujisawa, K., Culotti, J.G., Gengyo-Ando, K., Mitani, S., Moulder, G., Barstead, R., Tessier-Lavigne, M., and Bargmann, C.I. (2001). C. elegans slit acts in midline, dorsal-ventral, and anterior-posterior guidance via the SAX-3/Robo receptor. Neuron *32*, 25-38.

Harel, N.Y., and Strittmatter, S.M. (2006). Can regenerating axons recapitulate developmental guidance during recovery from spinal cord injury? Nat Rev Neurosci *7*, 603-616.

Hedgecock, E.M., Culotti, J.G., and Hall, D.H. (1990). The unc-5, unc-6, and unc-40 genes guide circumferential migrations of pioneer axons and mesodermal cells on the epidermis in C. elegans. Neuron *4*, 61-85.

Hoogenraad, C.C., and Bradke, F. (2009). Control of neuronal polarity and plasticity--a renaissance for microtubules? Trends Cell Biol *19*, 669-676.

Hoy, R.R., Bittner, G.D., and Kennedy, D. (1967). Regeneration in crustacean motoneurons: evidence for axonal fusion. Science *156*, 251-252.

Itoh, A., Horiuchi, M., Bannerman, P., Pleasure, D., and Itoh, T. (2009). Impaired regenerative response of primary sensory neurons in ZPK/DLK gene-trap mice. Biochem Biophys Res Commun *383*, 258-262.
Jiang, H., Guo, W., Liang, X., and Rao, Y. (2005). Both the establishment and the maintenance of neuronal polarity require active mechanisms: critical roles of GSK-3beta and its upstream regulators. Cell *120*, 123-135.
Johnson, G.V., Litersky, J.M., and Jope, R.S. (1991). Degradation of microtubule-associated protein 2 and brain spectrin by calpain: a comparative study. J Neurochem *56*, 1630-1638.
Kerschensteiner, M., Schwab, M.E., Lichtman, J.W., and Misgeld, T. (2005). In vivo imaging of axonal degeneration and regeneration in the injured spinal cord. Nat Med *11*, 572-577.
Kishi, M., Pan, Y.A., Crump, J.G., and Sanes, J.R. (2005). Mammalian SAD kinases are required for neuronal polarization. Science *307*, 929-932.
Knoferle, J., Koch, J.C., Ostendorf, T., Michel, U., Planchamp, V., Vutova, P., Tonges, L., Stadelmann, C., Bruck, W., Bahr, M.*, et al.* (2010). Mechanisms of acute axonal degeneration in the optic nerve in vivo. Proc Natl Acad Sci U S A *107*, 6064-6069.
Kulbatski, I., Cook, D.J., and Tator, C.H. (2004). Calcium entry through L-type calcium channels is essential for neurite regeneration in cultured sympathetic neurons. J Neurotrauma *21*, 357-374.
LaMonte, B.H., Wallace, K.E., Holloway, B.A., Shelly, S.S., Ascano, J., Tokito, M., Van Winkle, T., Howland, D.S., and Holzbaur, E.L. (2002). Disruption of dynein/dynactin inhibits axonal transport in motor neurons causing late-onset progressive degeneration. Neuron *34*, 715-727.
Lin, M.T., and Beal, M.F. (2006). Mitochondrial dysfunction and oxidative stress in neurodegenerative diseases. Nature *443*, 787-795.
Liu, K., Tedeschi, A., Park, K.K., and He, Z. (2011). Neuronal intrinsic mechanisms of axon regeneration. Annu Rev Neurosci *34*, 131-152.
Llambi, F., Causeret, F., Bloch-Gallego, E., and Mehlen, P. (2001). Netrin-1 acts as a survival factor via its receptors UNC5H and DCC. EMBO J *20*, 2715-2722.
Lunn, E.R., Perry, V.H., Brown, M.C., Rosen, H., and Gordon, S. (1989). Absence of Wallerian degeneration does not hinder regeneration in peripheral nerve. Eur J Neurosci *1*, 27-33.
Macagno, E.R., Muller, K.J., and DeRiemer, S.A. (1985). Regeneration of axons and synaptic connections by touch sensory neurons in the leech central nervous system. J Neurosci *5*, 2510-2521.
MacDonald, J.M., Beach, M.G., Porpiglia, E., Sheehan, A.E., Watts, R.J., and Freeman, M.R. (2006). The Drosophila cell corpse engulfment receptor Draper mediates glial clearance of severed axons. Neuron *50*, 869-881.

Maniar, T.A., Kaplan, M., Wang, G.J., Shen, K., Wei, L., Shaw, J.E., Koushika, S.P., and Bargmann, C.I. (2012). UNC-33 (CRMP) and ankyrin organize microtubules and localize kinesin to polarize axon-dendrite sorting. Nat Neurosci *15*, 48-56.

Marcette, J.D., Chen, J.J., and Nonet, M.L. (2014). The Caenorhabditis elegans microtubule minus-end binding homolog PTRN-1 stabilizes synapses and neurites. Elife *3*, e01637.

Mattson, M.P., and Magnus, T. (2006). Ageing and neuronal vulnerability. Nat Rev Neurosci *7*, 278-294.

Mi, W., Beirowski, B., Gillingwater, T.H., Adalbert, R., Wagner, D., Grumme, D., Osaka, H., Conforti, L., Arnhold, S., Addicks, K.*, et al.* (2005). The slow Wallerian degeneration gene, WldS, inhibits axonal spheroid pathology in gracile axonal dystrophy mice. Brain *128*, 405-416.

Miller, B.R., Press, C., Daniels, R.W., Sasaki, Y., Milbrandt, J., and DiAntonio, A. (2009). A dual leucine kinase-dependent axon self-destruction program promotes Wallerian degeneration. Nat Neurosci *12*, 387-389.

Misgeld, T., Kerschensteiner, M., Bareyre, F.M., Burgess, R.W., and Lichtman, J.W. (2007). Imaging axonal transport of mitochondria in vivo. Nat Methods *4*, 559-561.

Morfini, G.A., Burns, M., Binder, L.I., Kanaan, N.M., LaPointe, N., Bosco, D.A., Brown, R.H., Jr., Brown, H., Tiwari, A., Hayward, L.*, et al.* (2009). Axonal transport defects in neurodegenerative diseases. J Neurosci *29*, 12776-12786.

Neumann, B., and Hilliard, M.A. (2014). Loss of MEC-17 Leads to Microtubule Instability and Axonal Degeneration. Cell Rep *6*, 93-103.

Neumann, B., Nguyen, K.C., Hall, D.H., Ben-Yakar, A., and Hilliard, M.A. (2011). Axonal regeneration proceeds through specific axonal fusion in transected C. elegans neurons. Dev Dyn, 1365-1372.

Neumann, S., Bradke, F., Tessier-Lavigne, M., and Basbaum, A.I. (2002). Regeneration of sensory axons within the injured spinal cord induced by intraganglionic cAMP elevation. Neuron *34*, 885-893.

Niemann, A., Ruegg, M., La Padula, V., Schenone, A., and Suter, U. (2005). Ganglioside-induced differentiation associated protein 1 is a regulator of the mitochondrial network: new implications for Charcot-Marie-Tooth disease. J Cell Biol *170*, 1067-1078.

Nix, P., Hammarlund, M., Hauth, L., Lachnit, M., Jorgensen, E.M., and Bastiani, M. (2014). Axon Regeneration Genes Identified by RNAi Screening in C. elegans. J Neurosci *34*, 629-645.

Nix, P., Hisamoto, N., Matsumoto, K., and Bastiani, M. (2011). Axon regeneration requires coordinate activation of p38 and JNK MAPK pathways. Proc Natl Acad Sci U S A *108*, 10738-10743.

Okazaki, A., Sudo, Y., and Takagi, S. (2012). Optical silencing of C. elegans cells with arch proton pump. PLoS One *7*, e35370.

Oren-Suissa, M., Hall, D.H., Treinin, M., Shemer, G., and Podbilewicz, B. (2010). The fusogen EFF-1 controls sculpting of mechanosensory dendrites. Science *328*, 1285-1288.

Osterloh, J.M., Yang, J., Rooney, T.M., Fox, A.N., Adalbert, R., Powell, E.H., Sheehan, A.E., Avery, M.A., Hackett, R., Logan, M.A.*, et al.* (2012). dSarm/Sarm1 is required for activation of an injury-induced axon death pathway. Science *337*, 481-484.

Pan, C.L., Peng, C.Y., Chen, C.H., and McIntire, S. (2011). Genetic analysis of age-dependent defects of the Caenorhabditis elegans touch receptor neurons. Proc Natl Acad Sci U S A *108*, 9274-9279.

Perlson, E., Hanz, S., Ben-Yaakov, K., Segal-Ruder, Y., Seger, R., and Fainzilber, M. (2005). Vimentin-dependent spatial translocation of an activated MAP kinase in injured nerve. Neuron *45*, 715-726.

Perlson, E., Maday, S., Fu, M.M., Moughamian, A.J., and Holzbaur, E.L. (2010). Retrograde axonal transport: pathways to cell death? Trends Neurosci *33*, 335-344.

Pestronk, A., Drachman, D.B., and Griffin, J.W. (1980). Effects of aging on nerve sprouting and regeneration. Exp Neurol *70*, 65-82.

Pichichero, M., Beer, B., and Clody, D.E. (1973). Effects of dibutyryl cyclic AMP on restoration of function of damaged sciatic nerve in rats. Science *182*, 724-725.

Polleux, F., and Snider, W. (2010). Initiating and growing an axon. Cold Spring Harb Perspect Biol *2*, a001925.

Press, C., and Milbrandt, J. (2008). Nmnat delays axonal degeneration caused by mitochondrial and oxidative stress. J Neurosci *28*, 4861-4871.

Rawson, R.L., Yam, L., Weimer, R.M., Bend, E.G., Hartwieg, E., Horvitz, H.R., Clark, S.G., and Jorgensen, E.M. (2014). Axons degenerate in the absence of mitochondria in C. elegans. Curr Biol *24*, 760-765.

Reid, E., Kloos, M., Ashley-Koch, A., Hughes, L., Bevan, S., Svenson, I.K., Graham, F.L., Gaskell, P.C., Dearlove, A., Pericak-Vance, M.A.*, et al.* (2002). A kinesin heavy chain (KIF5A) mutation in hereditary spastic paraplegia (SPG10). Am J Hum Genet *71*, 1189-1194.

Richardson, C.E., Spilker, K.A., Cueva, J.G., Perrino, J., Goodman, M.B., and Shen, K. (2014). PTRN-1, a microtubule minus end-binding CAMSAP homolog, promotes microtubule function in Caenorhabditis elegans neurons. Elife *3*, e01498.

Rosen, D.R. (1993). Mutations in Cu/Zn superoxide dismutase gene are associated with familial amyotrophic lateral sclerosis. Nature *364*, 362.

Rugarli, E.I., and Langer, T. (2012). Mitochondrial quality control: a matter of life and death for neurons. EMBO J *31*, 1336-1349.
Sagot, Y., Dubois-Dauphin, M., Tan, S.A., de Bilbao, F., Aebischer, P., Martinou, J.C., and Kato, A.C. (1995). Bcl-2 overexpression prevents motoneuron cell body loss but not axonal degeneration in a mouse model of a neurodegenerative disease. J Neurosci *15*, 7727-7733.
Sambrook, J., Fritsch, E.F., and Maniatis, T. (1989). Molecular Cloning: A Laboratory Manual (Cold Spring Harbour, NY: Cold Spring Harbour Laboratory Press).
Samsam, M., Mi, W., Wessig, C., Zielasek, J., Toyka, K.V., Coleman, M.P., and Martini, R. (2003). The Wlds mutation delays robust loss of motor and sensory axons in a genetic model for myelin-related axonopathy. J Neurosci *23*, 2833-2839.
Silva, D.N., Coelho, J., Frazilio Fde, O., Odashiro, A.N., Carvalho Pde, T., Pontes, E.R., Vargas, A.F., Rosseto, M., and Silva, A.B. (2010). End-to-side nerve repair using fibrin glue in rats. Acta Cir Bras *25*, 158-162.
Singer, M., Flinker, D., and Sidman, R.L. (1956). Nerve destruction by colchicine resulting in suppression of limb regeneration in adult triturus. J Exp Zool *131*, 267-300.
Spaeth, C.S., Robison, T., Fan, J.D., and Bittner, G.D. (2012). Cellular mechanisms of plasmalemmal sealing and axonal repair by polyethylene glycol and methylene blue. J Neurosci Res *90*, 955-966.
Spira, M.E., Oren, R., Dormann, A., and Gitler, D. (2003). Critical calpain-dependent ultrastructural alterations underlie the transformation of an axonal segment into a growth cone after axotomy of cultured Aplysia neurons. J Comp Neurol *457*, 293-312.
Stiess, M., and Bradke, F. (2011). Neuronal polarization: the cytoskeleton leads the way. Dev Neurobiol *71*, 430-444.
Stirman, J.N., Crane, M.M., Husson, S.J., Wabnig, S., Schultheis, C., Gottschalk, A., and Lu, H. (2011). Real-time multimodal optical control of neurons and muscles in freely behaving Caenorhabditis elegans. Nat Methods *8*, 153-158.
Stone, M.C., Nguyen, M.M., Tao, J., Allender, D.L., and Rolls, M.M. (2010). Global up-regulation of microtubule dynamics and polarity reversal during regeneration of an axon from a dendrite. Mol Biol Cell *21*, 767-777.
Syntichaki, P., Xu, K.L., Driscoll, M., and Tavernarakis, N. (2002). Specific aspartyl and calpain proteases are required for neurodegeneration in C-elegans. Nature *419*, 939-944.
Tanaka, K., Zhang, Q.L., and Webster, H.D. (1992). Myelinated fiber regeneration after sciatic nerve crush: morphometric observations in young adult and aging mice and the effects of macrophage suppression and conditioning lesions. Exp Neurol *118*, 53-61.

Tank, E.M., Rodgers, K.E., and Kenyon, C. (2011). Spontaneous age-related neurite branching in Caenorhabditis elegans. J Neurosci *31*, 9279-9288.
Tedeschi, A., and Bradke, F. (2013). The DLK signalling pathway--a double-edged sword in neural development and regeneration. EMBO Rep *14*, 605-614.
Toth, M.L., Melentijevic, I., Shah, L., Bhatia, A., Lu, K., Talwar, A., Naji, H., Ibanez-Ventoso, C., Ghose, P., Jevince, A.*, et al.* (2012). Neurite sprouting and synapse deterioration in the aging Caenorhabditis elegans nervous system. J Neurosci *32*, 8778-8790.
Uttara, B., Singh, A.V., Zamboni, P., and Mahajan, R.T. (2009). Oxidative stress and neurodegenerative diseases: a review of upstream and downstream antioxidant therapeutic options. Curr Neuropharmacol *7*, 65-74.
Verdu, E., Buti, M., and Navarro, X. (1995). The effect of aging on efferent nerve fibers regeneration in mice. Brain Res *696*, 76-82.
Verdu, E., Ceballos, D., Vilches, J.J., and Navarro, X. (2000). Influence of aging on peripheral nerve function and regeneration. J Peripher Nerv Syst *5*, 191-208.
Wadsworth, W.G., Bhatt, H., and Hedgecock, E.M. (1996). Neuroglia and pioneer neurons express UNC-6 to provide global and local netrin cues for guiding migrations in C. elegans. Neuron *16*, 35-46.
Waller, A. (1850). Experiments on the section of glossopharyngeal and hypoglossal nerves of the frog and observations of the alternatives produced thereby in the structure of their primitive fibres. Phil Trans R Soc Lond B *140*, 423-429.
Wang, M.S., Wu, Y., Culver, D.G., and Glass, J.D. (2000). Pathogenesis of axonal degeneration: parallels between Wallerian degeneration and vincristine neuropathy. J Neuropathol Exp Neurol *59*, 599-606.
Westermann, B. (2010). Mitochondrial fusion and fission in cell life and death. Nat Rev Mol Cell Biol *11*, 872-884.
White, J.G., Southgate, E., Thomson, J.N., and Brenner, S. (1986). The structure of the nervous system of the nematode Caenorhabditis elegans. Philos Trans R Soc Lond B Biol Sci *314*, 1-340.
Wicks, S.R., Yeh, R.T., Gish, W.R., Waterston, R.H., and Plasterk, R.H. (2001). Rapid gene mapping in Caenorhabditis elegans using a high density polymorphism map. Nat Genet *28*, 160-164.
Witte, H., Neukirchen, D., and Bradke, F. (2008). Microtubule stabilization specifies initial neuronal polarization. J Cell Biol *180*, 619-632.
Wu, Z., Ghosh-Roy, A., Yanik, M.F., Zhang, J.Z., Jin, Y., and Chisholm, A.D. (2007). Caenorhabditis elegans neuronal regeneration is influenced by life stage, ephrin signaling, and synaptic branching. Proc Natl Acad Sci U S A *104*, 15132-15137.

Xiong, X., Wang, X., Ewanek, R., Bhat, P., Diantonio, A., and Collins, C.A. (2010). Protein turnover of the Wallenda/DLK kinase regulates a retrograde response to axonal injury. J Cell Biol *191*, 211-223.
Xu, K., Zhong, G., and Zhuang, X. (2013). Actin, spectrin, and associated proteins form a periodic cytoskeletal structure in axons. Science *339*, 452-456.
Yan, D., Wu, Z., Chisholm, A.D., and Jin, Y. (2009). The DLK-1 kinase promotes mRNA stability and local translation in C. elegans synapses and axon regeneration. Cell *138*, 1005-1018.
Yanik, M.F., Cinar, H., Cinar, H.N., Chisholm, A.D., Jin, Y., and Ben-Yakar, A. (2004). Neurosurgery: functional regeneration after laser axotomy. Nature *432*, 822.
Yiu, G., and He, Z. (2006). Glial inhibition of CNS axon regeneration. Nat Rev Neurosci *7*, 617-627.
Yoshimura, T., Kawano, Y., Arimura, N., Kawabata, S., Kikuchi, A., and Kaibuchi, K. (2005). GSK-3beta regulates phosphorylation of CRMP-2 and neuronal polarity. Cell *120*, 137-149.
Zhang, F., Wang, L.P., Brauner, M., Liewald, J.F., Kay, K., Watzke, N., Wood, P.G., Bamberg, E., Nagel, G., Gottschalk, A.*, et al.* (2007). Multimodal fast optical interrogation of neural circuitry. Nature *446*, 633-639.
Zhao, C., Takita, J., Tanaka, Y., Setou, M., Nakagawa, T., Takeda, S., Yang, H.W., Terada, S., Nakata, T., Takei, Y.*, et al.* (2001). Charcot-Marie-Tooth disease type 2A caused by mutation in a microtubule motor KIF1Bbeta. Cell *105*, 587-597.
Ziv, N.E., and Spira, M.E. (1993). Spatiotemporal distribution of Ca2+ following axotomy and throughout the recovery process of cultured Aplysia neurons. Eur J Neurosci *5*, 657-668.
Ziv, N.E., and Spira, M.E. (1995). Axotomy induces a transient and localized elevation of the free intracellular calcium concentration to the millimolar range. J Neurophysiol *74*, 2625-2637.
Zou, Y., Chiu, H., Zinovyeva, A., Ambros, V., Chuang, C.F., and Chang, C. (2013). Developmental decline in neuronal regeneration by the progressive change of two intrinsic timers. Science *340*, 372-376.
Zuchner, S., Mersiyanova, I.V., Muglia, M., Bissar-Tadmouri, N., Rochelle, J., Dadali, E.L., Zappia, M., Nelis, E., Patitucci, A., Senderek, J.*, et al.* (2004). Mutations in the mitochondrial GTPase mitofusin 2 cause Charcot-Marie-Tooth neuropathy type 2A. Nat Genet *36*, 449-451.
Zuryn, S., Le Gras, S., Jamet, K., and Jarriault, S. (2010). A strategy for direct mapping and identification of mutations by whole-genome sequencing. Genetics *186*, 427-430.